KAVEH AZIZIAN

OPTIMUM-SYNTHESIS METHODS FOR CABLE-DRIVEN PARALLEL MECHANISMS

Thèse présentée
à la Faculté des études supérieures et postdoctorales de l'Université Laval
dans le cadre du programme de doctorat en génie mécanique
pour l'obtention du grade de Philosophiæ Doctor (Ph.D.)

FACULTÉ DES SCIENCES ET DE GÉNIE
UNIVERSITÉ LAVAL
QUÉBEC

2012

Abstract

Cable-driven parallel mechanisms are a special kind of parallel mechanisms in which the rigid links are replaced by cables. These mechanisms include a moving platform and a fixed base which are connected by several cables. Controlling the lengths of the cables provides the desired motion of the moving platform. These mechanisms have the potential of providing large workspaces compared to conventional parallel and serial mechanisms, as cables can be wound onto reels over long lengths. However, this characteristic is restricted by the nature of the cables, which must be kept in tension in order to provide the desired motion for the main platform.

The main objective of this dissertation is to devise efficient methods for the optimum dimensional synthesis of the redundantly constrained cable-driven parallel mechanisms i.e., those mechanisms for which the number of cables exceeds the number of degrees of freedom. More precisely, we wish to obtain the geometry of a cable-driven parallel mechanism whose wrench-closure workspace includes a prescribed workspaces. The wrench-closure workspace (WCW) of a parallel cable-driven mechanism is the set of end effector poses for which all applied wrenches are feasible. An applied wrench is said to be feasible if it can be produced by a set of a non-negative cable tensions. Once the dimensional synthesis problem is solved, we can apply the solution repeatedly to various numbers of cables to perform the structural synthesis.

This thesis is divided into three main parts. First, the wrench-closure workspace of planar cable-driven parallel mechanisms (PCDPMs) and characteristics of their boundaries are investigated. This study uncovers the unseen relationships between the constant orientation wrench-closure workspace (COWCW) of PCDPMs and the oriented

areas. A graphical algorithm is proposed to determine the type of conic sections forming the boundaries of COWCWs. Then, based on the obtained mathematical expressions, a methodology is proposed to solve the dimensional synthesis problem of PCDPMs for discrete orientations ,i.e., translations. The method is based on convex relaxation techniques, which allow us to formulate the dimensional synthesis as a nonlinear program. The idea is to maximize the size of multiple boxes which represent an approximation of a prescribed workspace while constraining them inside the WCW of the PCDPM during the solution procedure. A multiple-box approximation of the prescribed workspace is obtained via the interval analysis method.

The resulting algorithm is extended to the continous orientation case or a given range of orientation angles as well. In fact, we introduce a nonlinear program through which the PCDPM geometry is changed while maximizing the scaling factor of the prescribed set of boxes. When the locally optimum scaling factor is greater or equal to one, the WCW of the resulting PCDPM contains the set of boxes. Otherwise, the obtained WCW generally offers a good coverage of the prescribed one. Finally, based on the results obtained for planar parallel cable-driven mechanisms, an algorithm is proposed to solve the dimensional synthesis of spatial parallel cable-driven mechanisms. Alike the planar case, we propose a large-scale nonlinear program whose optimum solutions can provide geometries of PCDMs for a prescribed workspace within a given range of orientation angles. The efficiency of these methods is demonstrated by solving various case studies using a developed piece of computer code. Therefore, this thesis is expected to provide an effective tool for the designers of parallel cable-driven robots.

Résumé

Les mécanismes parallèles entraînés par câbles sont une classe spéciale de mécanismes parallèles pour lesquels les liaisons rigides sont remplacées par des câbles. Ces mécanismes comprennent une plateforme mobile et une base fixe, qui sont reliées par plusieurs câbles. Le contrôle des longueurs des câbles produit le mouvement désiré de la plateforme mobile. Ces mécanismes ont le potentiel de fournir des espaces de travail à grande échelle comparativement aux mécanismes parallèles conventionnels car les câbles peuvent être enroulés sur des bobines sur de grandes longueurs. Cependant, cette caractéristique est limitée par la nature des câbles, qui doivent demeurer en tension afin de produire un mouvement désiré de la plateforme principale.

L'objectif principal de cette thèse est de concevoir des méthodes efficaces pour la synthèse dimensionelle optimale des mécanismes parallèles entraînés par câbles surcontraints, c'est-à-dire, des mécanismes pour lesquels le nombre de câbles excède le nombre de degrés de liberté. Plus précisément, nous souhaitons obtenir la géométrie des mécanismes parallèles entraînés par câbles dont l'espace des poses polyvalente (EPP) comprend des espaces de travail prescrits. L'espace des poses polyvalentes d'un mécanisme parallèle entraîné par câbles est l'ensemble des poses (les positions et les orientations) de l'organe terminal pour lesquelles tous les torseurs appliqués sont réalisables. Un torseur appliqué est dit réalisable, s'il peut être produit par un ensemble de câbles dont les tensions sont non-négatives. Une fois le problème de la synthèse dimensionnelle résolu, nous pouvons appliquer la solution à plusieurs reprises pour différents nombres de câbles afin d'effectuer la synthèse de la structure.

Cette thèse est divisée en trois parties principales. Tout d'abord, l'espace des poses

polyvalentes des mécanismes parallèles plans entraînés par câbles et les caractéristiques de leurs frontières sont étudiés. Cette étude révèle les relations jusqu'ici inconnues entre l'EPP à orientation constante (EPPOC) et les aires orientées. Un algorithme graphique est proposé afin de déterminer les types de sections coniques formant les frontières de l'EPPOC . Puis, sur la base des expressions mathématiques obtenues, une méthodologie est proposée pour résoudre le problème de la synthèse dimensionnelle des mécanismes parallèles plans entraînés par câbles pour les orientations discrètes c'est-à-dire, les translations. L'algorithme est basé sur des techniques de relaxation convexe qui nous amènent à formuler la synthèse dimensionnelle comme un programme non linéaire. L'idée est de maximiser la taille de plusieurs boîtes qui représentent une approximation d'un espace de travail prescrit, tout en essayant de les garder à l'intérieur de l'EPP du mécanisme parallèle plan entraîné par câbles pendant la procédure d' optimisation. Une telle approximation de l'espace de travail prescrit est obtenue via la méthode d'analyse par intervalles. L'algorithme obtenu est étendu au cas de l'orientation en continu pour un intervalle donné d'angles d'orientation. En fait, nous introduisons un programme non linéaire permettant de varier la géométrie du mècanisme parallèle plan entraîné par câbles et maximiser le facteur d'échelle de l'ensemble prescrit de boîtes. Lorsque le facteur d'échelle optimal est supérieur ou égal à un, l'EPP du mécanismes parallèle plan entraîné par câbles résultant contient l'ensemble des boîtes prescrit. Sinon, l'EPP obtenu offre généralement une bonne couverture des boîtes prescrites. Enfin, sur la base des résultats obtenus pour des mécanismes parallèles plans entraînés par câbles, un algorithme est proposé pour résoudre la synthèse dimensionelle de mécanismes parallèles spatiaux entraînés par câbles. Comme pour le cas plan, nous proposons un programme non linéaire à grande échelle dont les solutions optimales peuvent fournir des géométries de mécanismes parallèles spatiaux entraînés par câbles pour un espace de travail prescrit dans une plage donnée des angles d'orientation. L'efficacité de ces méthodes est démontrée par plusieurs exemples en utilisant un logiciel développé. En outre, cette thèse fournit un outil efficace pour les concepteurs de robots parallèles entraînés par câbles.

Foreword

I appreciate my research supervisor, Dr. Philippe Cardou for his continual support and providing good directions during the program. With his interest on the subject and leadership capabilities, he was a source of ideas for this research.

I would like to express my gratitude to Prof. Gosselin of whom I enjoyed being a student during the Ph.D program and I was working in the labroatory founded by him.

Special thanks to the members of Robotics Labroatory of Laval University for creating a pleasing and friendly working environment.

I wish to thank the thesis committee members especially, Prof. Lang and Prof. Bonev whose detailed remarks and comments improved the quality of this manuscript.

Finally, I would like to thank my parents to whom I owe all success I have achieved in my life.

Yet Freedom! yet thy banner torn but flying,

Streams like the thunder storm against the wind [1].

Dedicated to the honorable people of South Azerbaijan whom Iran is obliged his existence to their dedication and patriotism but they are even refused from their absolute right of writing and studying in their own language!

---

[1] Agianst the Wind (TV Series 1978) by George Miller and Simon Wincer

Contents

List of Tables

List of Figures

Chapter 1

Introduction

1.1 Cable-Driven Parallel Mechanisms

A parallel robot consists of an end effector and a fixed base that are connected by at least two independent kinematic chains. The payload is distributed among the legs, so that each leg supports only a fraction of the total load. For this reason, parallel manipulators have a larger payload-to-weight ratio, higher stiffness and a better positioning accuracy than do serial manipulators. It is also possible to reduce the weight of the moving parts by fixing the actuators on the base of the manipulator. This condition gives good inertial properties to parallel manipulators and allows to move the end effector at high velocities. As a drawback, in general, parallel manipulators have a smaller workspace than do serial manipulators of the same size. A special kind of parallel manipulators are cable driven, an example of which are shown in Fig. 1.1. The mechanical structure

(a)   (b)
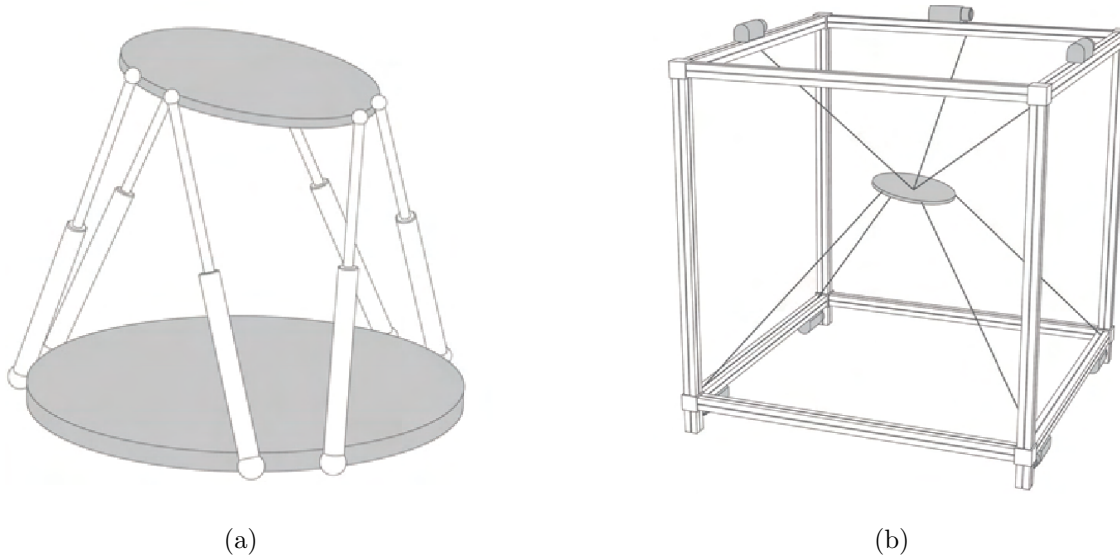
Figure 1.1: (a) conventional and (b) cable-driven parallel manipulators [1].

of a cable-driven parallel manipulator consists of a moving platform (MP) and a fixed base, which are connected to one another by multiple cables. Cable-driven parallel manipulators are structurally similar to traditional parallel ones. The end effector is moved by extending and retracting cables, the joint variables being the cable lengths. In general, each cable is wound around an actuated reel fixed to the base and attached to the moving platform at its other end. Forces on the end effector are obtained by pulling the cables. Since cables can be wound onto reels over long lengths, the reachable workspaces of cable-driven mechanisms can be larger than those of conventional parallel mechanisms. However, it is not possible for the platform to reach every pose of this workspace, because unlike the links of a conventional parallel mechanism, cables can only pull. Indeed, there generally exist many poses inside this workspace for which the cables cannot balance all applied wrenches because at least one of them would have to push on the platform.

Cable-driven parallel manipulators offer some other advantages over conventional parallel mechanisms. They have few moving parts, with only small masses, which gives them good inertial properties and make them suitable for applications that require high velocities and accelerations. Other characteristics include high payload-to-weight ratios, transportability, and low cost. Notice that it is also possible to easily reconfigure these mechanisms by relocating their cable attachment points. They also offer some other advantages, as described in [3], including the remote location of motors and controls, rapid deployability, high load capacity, and reliability. The main drawbacks

of cable-driven parallel manipulators are due to the cables, which can only pull and not push. Consequently, they must be maintained in tension during operation. Assuming no limits on the strength of the cables and the torques delivered by the actuators, the relationship between the pose and the feasible wrenches at the platform appears as a fundamental issue for the cable-driven parallel mechanisms design. In the spatial case, the interferences between cables, which must generally be avoided, form another problem.

1.1.1 Applications

Robots have had a great influence on industrial manufacturing and assembly. However, for some applications such as the inspection and repair in shipyards and airplane hangars, classical industrial robots are inefficient. Generally speaking, the workspace provided by conventional serial and parallel manipulators is not large enough for such applications. Cable-driven parallel mechanisms have the potential of providing such large workspaces and other unique characteristics mentioned in section 1.1. These manipulators have been used in several kinds of applications in a recent past. Because of their high payload to weight ratio, they have been studied for load lifting and positioning, [4], as shown in Fig. 1.2(a). In this field, very high loads must be moved and high stiffness and stability are requested for the employed devices. Cable-driven parallel manipulators can have a large workspace and reach high velocities. Because of these characteristics, they can be used in sports recording, as in the case of the Skycam [8]. This device, shown in Fig. 1.2(b), has been developed as a parallel cable-driven mechanism moving a camera for use in stadiums and indoor arenas. Their modularity and low inertia give them good characteristics for operation in remote or unreachable locations [6] (see Fig. 1.2(c)). Rapid deployability and large workspace of cable-driven parallel mechanisms make them ideal for the handling of hazardous materials and disaster search and rescue efforts [7](see Fig. 1.2(d)).

Recently, these robots have demonstrated their capabilities in actuated sensing [9] and [10] aquatic applications as well. If many applications involve spatial cable-driven robots, there is also an interest for planar cable-driven robots in several applications [10–12].
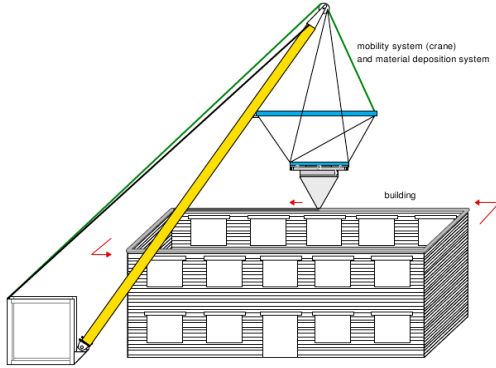
(a) Automated construction system including a cable-driven mechanism [4]

(b) The Skycam, a sport recording device [5]
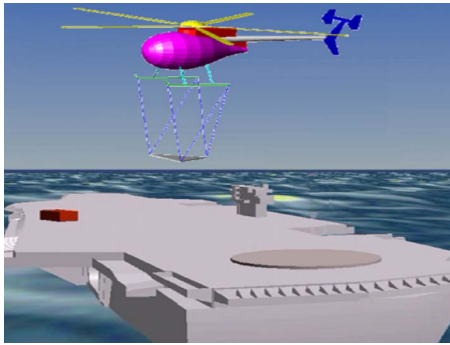
(c) A helicopter operation for a ship replenishment in midsea using a cable-driven manipulator [6]
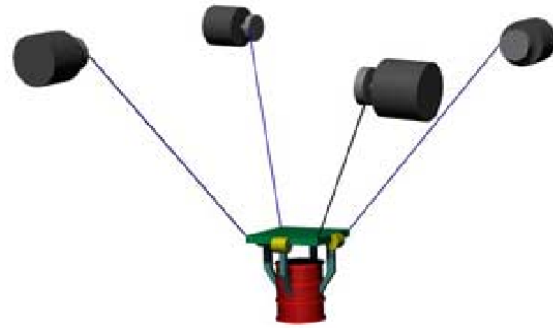
(d) A spatial cable-driven mechanism handling potentially hazardous material [7]

Figure 1.2: Various applications of cable-driven parallel mechanisms.

Evidently, for such applications, the available workspaces of these robots have a great impact on their performances. Hence, the study and determination of the workspace of this kinds of manipulators has recieved attentions.

1.1.2 Classification of Cable-Driven Parallel Mechanisms

A classification of cable-driven parallel mechanisms can be obtained by considering the number of degrees of freedom of the end effector n and the number of cables m.

- If $m < n + 1$, then the manipulator is said to be under constrained, and cables cannot balance all applied wrenches unless an external force such as gravity is applied to the end-effector.

- If $m = n + 1$, then the manipulator is said to be completely constrained. The movement of the end effector can be fully controlled with this minimum number of cables.

- If $m > n + 1$, then the number of cables exceeds the number of degrees of freedom by more than one, and the manipulator is said to be redundantly constrained.

For redundant cable-driven parallel mechanisms, whose dimensional synthesis is the main concern of this work, the motion of the end effector can be completely controlled and the additional cables can be used in order to avoid singular configurations in the performed trajectory. For these manipulators a drawback can be the increased risk of cable interferences.

1.1.3   Synthesis and Analysis

According to Norton [13], in engineering, the word analysis means to decompose, to take apart, to resolve into its constituent parts. "This is quite necessary and requires a thorough understanding of both the mathematical techniques and fundamental physics of the function of the system. Since a system must exist before it can be analyzed, the first step in any engineering design is synthesis. Hence, synthesis actually means design and bringing an engineering system into existence."

In the mechanical design of industrial robots the kinematic structure is often selected and designed on the basis of previous experiences. Synthesis can help to design new types of robots to achieve a desired goal and application. Evidently, the shape and size of the workspace of a robot are among its most important properties, which must be investigated in the design procedure. While workspace analysis examines the properties of an already defined manipulator, robot design describes the opposite task of finding the optimal robot for a given task such as a given workspace. To identify the optimal robot, usually different designs have to be compared with respect to the desired

properties which generally makes the design process a computationally intensive task. Finally, one or more designs turn out as most favorable.

According to Merlet [14], the design (or synthesis) task can be divided into two separate subtasks:

1. Structural synthesis: This step includes the determination of the topology of the mechanical structure. In particular, the number and types of degrees of freedom of the joints and their interconnections are identified.

2. Dimensional synthesis: Here, the positions and orientations of the joints as well as the link lengths are specified.

For the special case of a cable-driven robot, the link topology is fixed and the structure synthesis only consists in choosing the number of cables. Once the structure synthesis is completed, a dimensional synthesis can be performed. For a cable-driven parallel robot, this is nothing but the identification of the cable attachment points on the base and on the end effector or, more briefly, the geometry of the robot.

1.2   Background and Objectives of the Thesis

The wrench-closure workspace (WCW) of parallel cable-driven mechanisms is the set of poses for which all applied wrenches are feasible. An applied wrench is said to be feasible if it can be balanced by a set of non-negative cable tensions. This is a special case of the wrench-feasible workspace (WFW), which is the set of poses of the moving platform for which the cables can balance any wrench of a given set of wrenches, such that the tension in each cable remains within a prescribed range. The WCW of cable-driven parallel mechanisms has been studied in several research works. A necessary condition for the WCW to be non empty is that the number of cables be greater than the number of degrees of freedom of the moving platform [15, 16]. We refer to these mechanisms as fully-constrained, as opposed to under constrained cable-driven mechanisms, which use the weight of the platform to control its motion, while keeping the cables in tension [17]. For fully-constrained cable driven mechanisms, the WCW

depends only on the geometry of the mechanism, i.e, on the locations of the attachment points on the fixed frame and on the moving platform.

A large body of literature is already available for determining the workspace of parallel cable-driven robots due to the unilateral nature of the forces applied by the cables on the mobile platform. Most of the available methods allow to determine the workspace of these robots, by means of a symbolic method [2] or by a discretization method [18]. Fattah and Agrawal [19] proposed a methodology to calculate the workspace of redundant and non redundant planar cable driven robots by means of a discretization method. In their method, tensions in the cables are calculated and conditions are obtained to verify whether a reference point on the moving platform is reachable with positive tensions. Riechel and Ebert-Uphoff [20] present a means of analytically deriving the WFW for the case of a point-mass end-effector and analyze the characteristics and trends of the WFW. Some authors apply the antipodal theorem to calculate the WCW of PPCDMs [21]. All these works pertain to the analysis of the workspace of cable-driven parallel mechanisms. Very few of them tackle the difficult design problem of finding a parallel cable-driven mechanism from a prescribed workspace, i.e., the synthesis problem.

Gouttefarde et al. [22] propose an interval-analysis based approach to find boxes guaranteed to be fully inside or fully outside of the WFW. The proposed approach can be applied to verify whether a given prescribed workspace is fully included in the WFW of a given cable-driven mechanism. This is a valuable tool for the dimensional synthesis of cable driven robots, but because of its computational cost, we do not know that it has been already applied to such problems.

Agrawal et al. [23] deal with the mechanical design of a 6-6 cable-suspended parallel robot. They use the global conditioning index (GCI) and the volume of the workspace as performance indices for the design optimization of a 6-DOF cable-suspended robot driven by six cables. The main objective of the design problem is to determine which cable-suspended parallel robot is able to orient itself perpendicular to the surface in question with the largest workspace volume and the maximum GCI. In their approach, they consider different possible designs and calculate the volume of workspace and GCI by discretizing the surface into several points while considering the orientations of MP constant. Based on the obtained results, they choose the mechanism with the largest workspace as well as the highest GCI. The proposed method may be an effective

tool when designing similar cable suspended parallel robot, but does not deal with the synthesis problem of CDPMs.

To the knowledge of the authors, Hay and Snyman [24] were the first and only researchers to report directly on the synthesis of parallel cable-driven manipulators. They defined the dexterous workspace of a PCDPM as the intersection of all constant orientation workspaces in a given set of rotation angles, while cable tensions are constrained to lie within a given set and cable lengths are greater than a given minimum. Their main goal is to maximize the area of the dexterous workspace for a given range of rotation angles by finding the locations of fixed points of the robot along a fixed rectangular frame. They begin with a randomly chosen PPCDM design and maximize the area of its dexterous workspace by varying its geometry. In this manner, they find a locally optimum configuration of the fixed points of the robot, while the locations of the attachment points on the platform have already been assumed. It was observed by some researchers [25] that the locations of the attachment points on the moving platform tend to have more effect on the WCW than the locations of the attachment points on the fixed frame. Therefore, this locally-optimum robot design corresponds to a dexterous workspace of maximum area, but not for a *prescribed workspace*.

The principal goal of this thesis is to find effective algorithms for the dimensional synthesis of cable-driven parallel mechanisms. In other words, we aim at devising algorithms leading to the geometry of a CDPM whose wrench-closure workspace includes a *prescribed workspace*. In trying to find such algorithms, we uncover some hidden properties of the WCW of planar cable-driven parallel mechanisms (PCDPM) as well.

Devising a methodology for the optimum design of cable-driven parallel mechanisms for a desired workspace enables us to prepare a series of computer codes, which prove the efficiency of these methods while we solve various case studies. It is hoped that the algorithms and corresponding computer codes will provide an efficient tool for the designers of cable-driven parallel mechanisms.

1.3   Overview of the Thesis

Before attempting to find the required geometry of a cable-driven parallel mechanism
for a prescribed wrench-closure workspace, we have to set up a standard mathematical
description and investigate the characteristics of the wrench-closure workspace of such
robots. This means that we must begin with the analysis of cable-driven parallel
mechanisms before attempting their synthesis. In the next chapter we recall the kineto-
static equations of planar cable-driven parallel mechanisms and formally define the
WCW of such mechanisms. We present the relationships between the oriented areas
concept and the boundaries of WCW of these mechanisms. Finally, we introduce a
graphical algorithm to determine the types of conic sections forming the boundaries of
the constant orientation WCW (COWCW) of PCDPMs.

The kinetostatic equations obtained in Chapter 2 are the starting point of our
approach to the dimensional synthesis of CDPMs. In Chapter 3, we investigate the
dimensional synthesis of PCDPMs for a constant orientation. We introduce a linear
program to verify whether a given box lies inside the COWCW of a PCDPM. The
approach is based on convex relaxation techniques and leads to the contracted COWCW
concept. We then introduce a scaling factor to maximize the size of the prescribed box,
while considering the geometic parameters of the PCDPM as unknowns. This leads
to a nonlinear program whose solution provides us optimum geometries of different
PCDPMs. The COWCW of these PCDPMs includes the scaled box. Evidently, if the
corresponding scaling factor at the optimum point is greater than or equal to one then
the COWCW of the obtained PCDPM is guaranteed to include the prescribed box.
Integrating multiple boxes in this nonlinear program allows for the representation of an
irregular prescribed workspace. The local optima provide geometries of PCDPM whose
COWCWs include the prescribed workspace. We use the interval analysis method to
approximate the prescribed workspace by multiple boxes. The results obtained for
discrete orientations of the end effector are extended to the continuous orientation
case, i.e., to ranges of orientation angles, at the end of chapter 3. The introduced
approach is again based on convex relaxation techniques and the final solutions of
the corresponding nonlinear programs provides geometries of PCDPMs whose WCWs
within the given range of orientations include the prescribed workspace.

Finally, based on the results obtained for planar CDPMs, we introduce an algorithm

for the dimensional synthesis of spatial CDPMs in Chapter 4. Alike for the planar case, the convex relaxation technique is applied to a linear program to verify whether a given six-dimensional box, i.e., bounded orientations and positions, is inside the WCW of a given CDPM. This leads to a nonlinear program whose optima represent CDPM geometries whose WCW includes a prescribed workspace within a given range of orientation angles. The introduced nonlinear program may easily become a large scale problem, depending on the number of three-dimensional boxes representing the prescribed workspace, and solving such problems can be challenging. We resolve this issue using a custom tailored sequential linear program. The efficiency of the introduced algorithms is illustrated by several examples throughout the Chapters 3 and 4. Finally, conclusions are drawn and future work is suggested in Chapter 5.

Chapter 2

Kinetostatics and Wrench-Closure Workspace of Planar Cable-Driven Parallel Mechanisms

This chapter provides the basic framework required for the analysis and synthesis of planar cable-driven parallel mechanisms (PCDPMs). First, we recall the kinetostatic of the PCDMs and formally define the WCW of these robots. Then, we introduce a linear program to calculate the wrench-closure workspace of the PCDPMs. We demonstrate the analogy between the 3-R$\underline{P}$R planar parallel robots and PCDPMs with three cables. We investigate the boundaries of COWCWs of PCDPMs and uncover their relationships with oriented-area concepts. Finally, we propose a graphical algorithm for the determination of the types of conic sections that compose the boundary segments of the COWCWs.

2.1 Introduction

A planar cable-driven parallel mechanism (PCDPM) consists of a moving platform (MP) and a fixed frame, which are connected with multiple cables, as shown in Fig. 2.1. The cables and the moving platform are assumed to be contained in the same plane. The moving-platform pose in this plane is controlled by winding and unwinding the cables. Each cable is wound around an actuated reel fixed to the base and attached to the moving platform at its other end. Forces on the moving platform are obtained by pulling on the cables with the servo-controlled reels. Since the cables can be wound onto reels over long lengths, the workspace of a cable-driven mechanism can be larger than that of a conventional parallel mechanism. However, this is only a potential advantage, since the workspace of a PCDPM is further limited by the inability of cables to push on the moving platform. Indeed, there generally exist many poses inside this workspace for which the cables cannot balance all applied wrenches, because at least one of them would have to push on the platform.
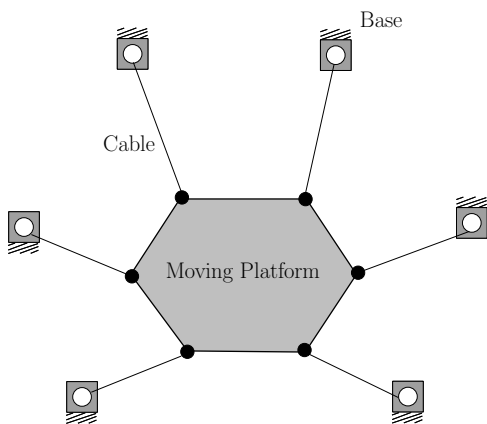
(a) Schematic of a planar parallel cable-driven mechanism with six cables
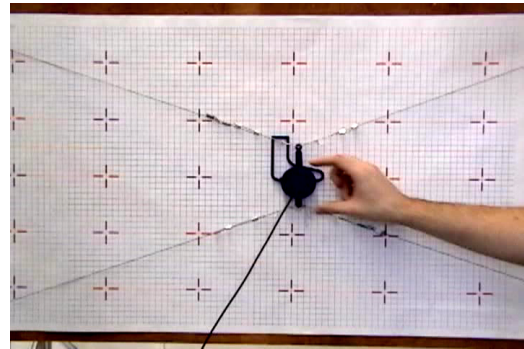
(b) A prototype of planar parallel cable-driven mechanism with four cables at Robotics Laboratory of Université Laval [11]

Figure 2.1: Planar parallel cable-driven mechanism.

Many existing works deal with the limitation of the workspace of cable-driven parallel robots induced by the unilateral nature of the forces applied by the cables on the mobile platform. Most of them propose methods allowing to determine the workspace of these robots, for instance, by means of discretization [18] or of symbolic calculations [2].

In the discretization method, a superset of the workspace is first discretized. This gives a set of poses, which are then tested one by one to see whether each of them lies in the WCW. Unlike the discretization method, the symbolic method consists in computing the boundaries of the WCW and determining which side of each boundary corresponds to the WCW. Evidently, this method is more reliable than the discretization method, which can be considered as an estimation method, because there may exist some points between validated mesh points that lie outside the WCW. Moreover, because symbolic expressions of the WCW boundaries are readily available, the symbolic method is generally significantly faster than the discretization method.

Several research works can be found about the symbolic method. Stump and Kumar [2] derive limiting conditions that lead to symbolic expressions for the boundary of the wrench-closure workspace. They apply Farka's lemma to provide the necessary and sufficient condition to evaluate the reachable workspace of a cable-driven parallel mechanism. They present an algebraic procedure to find a hyperplane that separates the convex hull formed by the cable wrench vectors and the wrench of external forces. Then, they extend the method to find the sufficient condition for ensuring that the platform of the mechanism can resist any arbitrary applied wrench. Gouttefarde and Gosselin [26] – [27] present a detailed analysis of the constant-orientation wrench-closure workspace (COWCW) of planar parallel mechanisms and propose theorems that characterize the poses of the WCW of a planar cable-driven mechanism. They show that the boundary of this workspace is composed of conic sections. Apparently, these conic sections can be any of the three types, i.e., hyperbola, parabola or ellipse.

The main goal of this chapter is to set up mathematical equations for the analysis of PCDPMs and shed light on the relationship between the geometry of a PCDPM and the types of conic sections forming the boundary of its COWCW. In particular, we shall provide a graphical method, which allows to determine the types of each conic section forming the boundary without any calculations. Since the proposed method involves some geometric constructions, we also provide sufficient conditions that can be assessed from mere inspection in many instances of PCDPMs.

These results may be used by the designer of a PCDPM to quickly analyze various geometries. Moreover, the analysis being completely general, these results are regarded as a contribution to the theory of parallel cable-driven mechanisms. Finally, the facts presented in this chapter can be equally applied to find the singularity loci of 3-R$\underline{P}$R

parallel manipulators [28] and [29]. This significantly extends the reach of the proposed graphical method.

2.2 Kinetostatic Model

The first step to the analysis of the boundaries of the WCW of a planar cable-driven parallel mechanism is the definition of its kinetostatic model. Such a planar cable-driven mechanism is schematically shown in Fig. 2.2. It consists of a moving platform (MP) that is connected by m cables to m fixed points A_i, $i = 1, \ldots, m$. Cable i is attached to the MP at B_i, and winds at A_i around an actuated reel. In order to analyze the motion
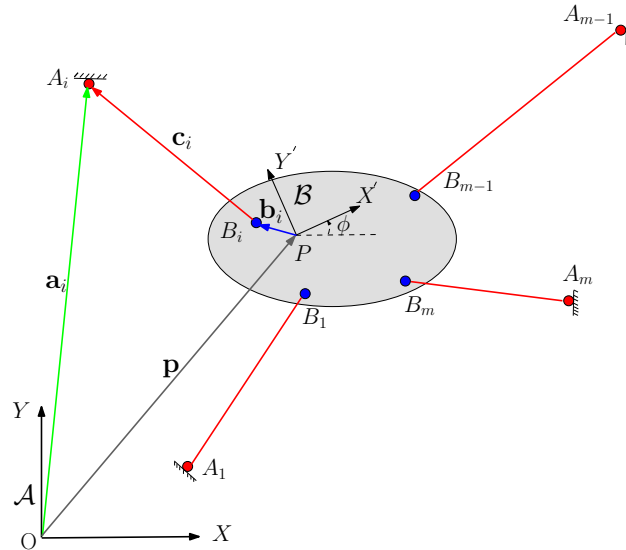
Figure 2.2: Sketch of a planar cable-driven mechanism with m cables.

of the MP, we have to consider two frames: the reference frame $\mathcal{A}$, which is fixed to the base at point O, and the moving frame $\mathcal{B}$, which is attached to the MP at reference point P. The moving platform can be transformed to the reference frame by a rotation of angle ϕ. The cables and the moving platform are assumed to lie in parallel planes. In this sense, they are said to be coplanar. The ith cable connects points A_i and B_i. We use the following notation for the analysis of a generic PCDPM:

- Vector $\mathbf{a}_i \in \mathbb{R}^2$ represents the position of the actuated reel A_i in the fixed frame $\mathcal{A}$;

- Vector $\mathbf{b}_i \in \mathbb{R}^2$ is a constant vector and represents the position of the attachment point B_i of the ith cable in frame $\mathcal{B}$;

- Vector $\mathbf{p} \in \mathbb{R}^2$, which is expressed in $\mathcal{A}$, represents the position of the point P with respect to point O;

- Vector $\mathbf{c}_i$ points from B_i to A_i, and its magnitude represents the length of the ith cable;

- ϕ is the angle between the fixed axis X and the moving axis X'.

Vector $\mathbf{c}_i$ representing the ith cable is obtained as

$$\mathbf{c}_i = \mathbf{a}_i - \mathbf{p} - \mathbf{Q}\mathbf{b}_i. \tag{2.1}$$

where $\mathbf{Q}$ is the rotation matrix taking the fixed frame onto the moving frame, and can be expressed as

$$\mathbf{Q} = \mathbf{1}_{2\times2} \cos\phi + \mathbf{E} \sin\phi, \tag{2.2}$$

where, $\mathbf{E} = \begin{bmatrix} 0 & -1 \\ 1 & 0 \end{bmatrix}$ and $\mathbf{1}_{2\times2} \in \mathbb{R}^{2\times2}$ is the 2×2 identity matrix. The wrench applied by the ith cable at P, the origin of the moving frame, is

$$\mathbf{v}_i = [\ \mathbf{f}_i^T \quad n_i\ ]^T, \tag{2.3}$$

where $\mathbf{f}_i$ and n_i are the force and moment about P produced by the ith cable. Since the exerted force is parallel to its corresponding cable and its related moment is perpendicular to the plane, their mathematical expressions are

$$\mathbf{f}_i = \frac{t_i}{l_i}\mathbf{c}_i, \quad n_i = \det([\mathbf{Q}\mathbf{b}_i \quad \frac{t_i}{l_i}\mathbf{c}_i]). \tag{2.4}$$

where l_i and t_i are the length and tension of cable i, respectively. If we assume that points A_i and B_i do not coincide, then the wrench applied to the platform by cable i is $\frac{t_i}{l_i}\mathbf{w}_i$, with $\mathbf{w}_i$ defined as

$$\mathbf{w}_i = \begin{bmatrix} \mathbf{c}_i^T & \mathbf{c}_i^T\mathbf{E}\mathbf{Q}\mathbf{b}_i \end{bmatrix}^T. \tag{2.5}$$

Equation (2.5) shows that $\mathbf{w}_i$ is a function of the geometric parameters of the mechanism and the orientation angle of the moving platform. We define the wrench matrix and tension vector of the mechanism as

$$\mathbf{W} = \begin{bmatrix} \mathbf{w}_1 & \mathbf{w}_2 & \cdots & \mathbf{w}_m \end{bmatrix} \text{ and } \mathbf{t} = \begin{bmatrix} \frac{t_1}{l_1} & \frac{t_2}{l_2} & \cdots & \frac{t_m}{l_m} \end{bmatrix}^T, \tag{2.6}$$

respectively. The static equilibrium of the moving platform may be expressed as

$$\mathbf{W}\mathbf{t} + \mathbf{w}_P = \mathbf{0}_3, \tag{2.7}$$

where $\mathbf{0}_3$ is the three-dimensional zero vector and $\mathbf{w}_P$ is the wrench applied on the MP at P, and is equivalent to the system of external forces and moments. These external loads may include gravity forces, for example.

2.2.1 The Wrench-Closure Workspace and Its boundaries

Now we can define the wrench-closure workspace of planar cable-driven parallel mechanisms as follows.

Definition 1 *The Wrench-Closure Workspace (WCW)*

The WCW of planar parallel cable-driven mechanisms is formally defined as the set of poses for which

$$\forall \mathbf{w}_P \in \mathbb{R}^3, \exists\, \mathbf{t} \in \mathbb{R}^m \mid \mathbf{t} \succeq \mathbf{0}_m \text{ and } \mathbf{W}\mathbf{t} + \mathbf{w}_P = \mathbf{0}_3,$$

where the symbol $\succeq$ denotes the componentwise inequality.

2.2.1.1 A Linear Program to Verify Whether a Pose Lies in the WCW of a PCDPM

In order to find a valid tension vector $\mathbf{t}$ for a given pose, we need to solve the linear system of equations given by eq. (2.7). From linear algebra, we know that the vector sum of any solution of eq. (2.7) with a vector in the null space of $\mathbf{W}$ is again a solution to eq. (2.7) [30]. In other words, if we consider $\mathbf{t}^\star$ and $\mathbf{t}^\perp$ as a solution of eq. (2.7) and a vector in the null space of $\mathbf{W}$, respectively, then

$$\mathbf{t} = \mathbf{t}^\star + \lambda \mathbf{t}^\perp, \lambda \in \mathbb{R}^+, \tag{2.8}$$

is also a solution of eq. (2.7).

For $\mathbf{t}^\perp$ whose components are all (strictly) positive, we can add a sufficiently large scalar multiple λ of this vector to any particular solution $\mathbf{t}^\star$ of eq. (2.7) to obtain a cable-tension vector $\mathbf{t}$ with positive components. Therefore, in order to determine whether a given pose is inside the WCW of the mechanism, we need to determine whether there exists a set of positive tensions such that

$$\mathbf{Wt} = \mathbf{0}_3, \tag{2.9}$$

where $\mathbf{0}_3$ is the three-dimensional zero vector. In other words, we need to solve the following feasibility problem for each pose of the MP:

$$\mathbf{Wt} = \mathbf{0}_3,$$
$$\mathbf{t} \succ \mathbf{0}_m. \tag{2.10}$$

Therefore, the WCW of a PCDPM is the set of poses for which eq. (2.10) is satisfied. We can use this equation in a linear program to calculate the wrench-closure workspace of planar parallel cable-driven robots as follows.

In order to verify whether a given pose lies within the wrench-closure workspace of a PCDPM, we introduce the following linear programming (LP) problem:

$$\begin{aligned}
r = \text{maximize} \quad & d, \\
\text{subject to} \quad & \mathbf{t} \succeq d\mathbf{1}_m, \\
& \mathbf{Wt} = \mathbf{0}_3, \\
& d \leq 1, \\
\text{over } d \text{ and } \mathbf{t}, &
\end{aligned} \tag{2.11}$$

where d is a dummy variable, and $\mathbf{1}_m = [1 \quad 1 \quad \cdots \quad 1]^T \in \mathbb{R}^m$. When solving this LP, the solver pushes d in the positive direction as much as it can. Since d is equal or smaller than all the components of vector $\mathbf{t}$ and is being maximized, it remains equal to the smallest component of vector $\mathbf{t}$. But the solver can also vary the components of $\mathbf{t}$, since they are also optimization variables. Therefore, when solving the LP, the solver always increases the smallest component of vector $\mathbf{t}$ in order to allow d to increase further. If d becomes greater than zero, then this means that the smallest component of vector $\mathbf{t}$ is also greater than zero, which means that all the components of $\mathbf{t}$ are greater than zero. This, in turn, means that the given pose lies in the WCW.

If d cannot be made greater than zero, that means there is no strictly positive $\mathbf{t}$, and the pose is outside the WCW. For poses outside the WCW, notice that d will always

end up equal to zero, since $s = 0$ and $\mathbf{t} = \mathbf{0}_m$ is always a feasible point of this LP (i.e., it satisfies all the constraints). Therefore, for this LP, we have

$$r = \begin{cases} 1 & \text{if the pose lies in the WCW,} \\ 0 & \text{otherwise.} \end{cases} \tag{2.12}$$

We can calculate the constant orientation wrench-closure workspace (COWCW) of PCDPMs using this linear program and discretizing the plane to several points. We illustrate this with the following example.

2.2.1.2 Example: WCW of a Planar Cable-Driven Parallel Mechanism

Figure 2.3 shows a sample PCDPM drawn from Stump and Kumar [2]. The parameters of the considered PCDPM are given in Table 2.1.

Table 2.1: Geometric parameters of the assumed PCDPM.

i	$\mathbf{a}_i^T$	$\mathbf{b}_i^T$
1	$[0 \quad 0]$	$[-.5 \quad 0]$
2	$[6 \quad 0]$	$[.5 \quad 0]$
3	$[6 \quad 5]$	$[.5 \quad .5]$
4	$[0 \quad 5]$	$[-.5 \quad .5]$
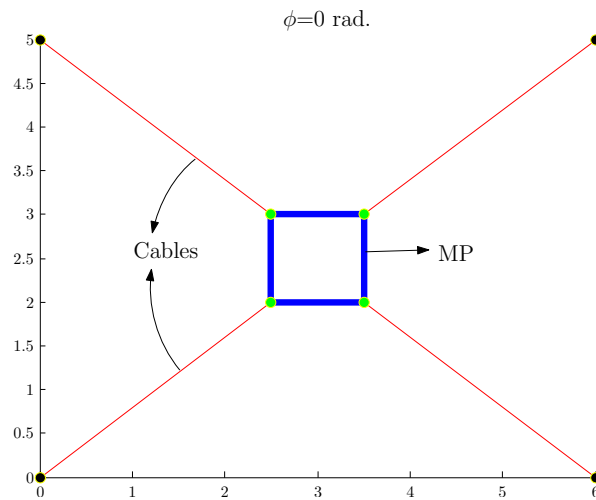
Figure 2.3: A PCDPM with four cables.

Discretizing the xy plane and the ϕ axis provides us with a set of poses whose inclusion in the WCW is to be verified, based on the introduced linear program. Figure

2.4 shows the resulting COWCWs, each corresponding to a different orientation angle.
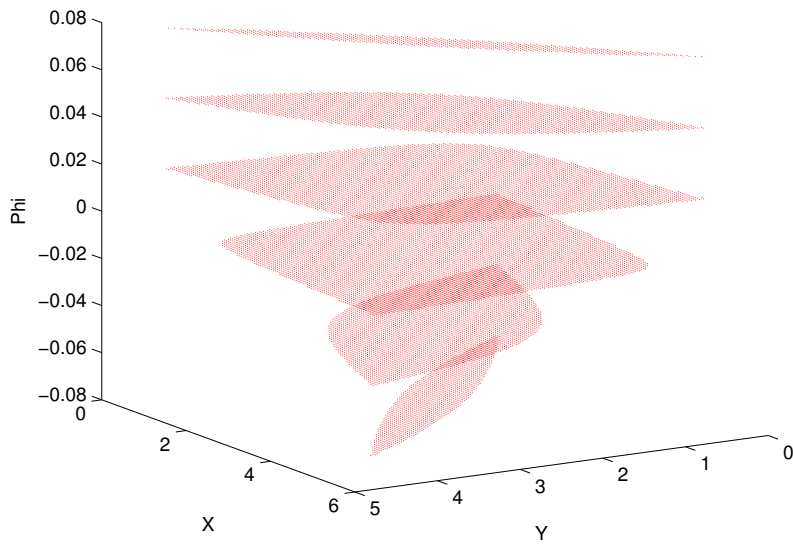
Figure 2.4: COWCWs of the robot depicted in Fig. 2.3 for different orientations.

2.2.1.3   The Boundaries of the Constant-Orientation WCW

Gouttefarde and Gosselin [26] proved that the boundary of the constant-orientation WCW (COWCW) of a PCDPM is composed of segments of conic sections. The mathematical expressions of these conic sections, are obtained in terms of $\mathbf{p}$ by computing the determinant of each 3×3 matrix obtained by choosing three distinct columns of the wrench matrix $\mathbf{W}$. If we call the selected columns p, q and r, then the related conic section equation is given by

$$\det\left(\begin{bmatrix} \mathbf{w}_p & \mathbf{w}_q & \mathbf{w}_r \end{bmatrix}\right) = 0. \tag{2.13}$$

2.3 Singularities of 3-R<u>P</u>R Planar Parallel Mechanisms

One of the simplest parallel robots is the 3-R<u>P</u>R planar robot, where R and P stand for revolute and prismatic joints, respectively and the underlined joints are actuated. It is composed of three identical legs connecting the fixed base to the end effector, as shown in Fig. 2.5. Each leg is of RPR design, with two passive revolute joints and an active prismatic joint in between. Using the notation already introduced in section 2.2,
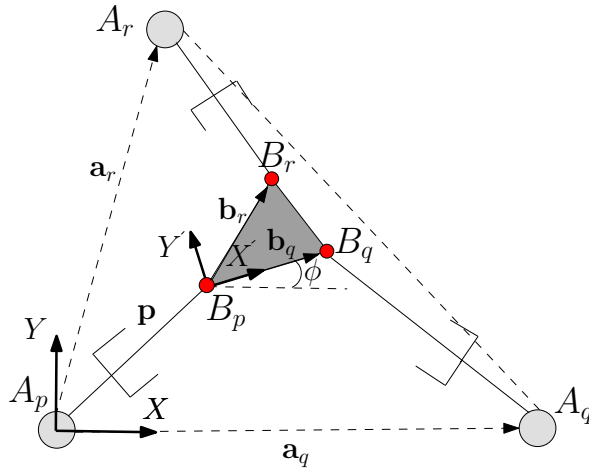
Figure 2.5: A 3 RPR planar parallel mechanism.

we obtain the following expression for the length of the ith prismatic joint of this type of robots

$$l_i^2 = (\mathbf{a}_i - \mathbf{p} - \mathbf{Q}\mathbf{b}_i)^T (\mathbf{a}_i - \mathbf{p} - \mathbf{Q}\mathbf{b}_i). \tag{2.14}$$

The differentiation of eq. (2.14) gives

$$\dot{l}_i = \frac{1}{l_i}(\mathbf{a}_i - \mathbf{p} - \mathbf{Q}\mathbf{b}_i)^T (\dot{\mathbf{p}} + \dot{\phi}\mathbf{E}\mathbf{Q}\mathbf{b}_i). \tag{2.15}$$

Let $\dot{\mathbf{l}} = \begin{bmatrix} \dot{l}_1 & \dot{l}_2 & \dot{l}_3 \end{bmatrix}^T$ and $\dot{\mathbf{s}} = \begin{bmatrix} \dot{\mathbf{p}} & \dot{\phi} \end{bmatrix}^T$, so that

$$\dot{\mathbf{l}} = \mathbf{J}\dot{\mathbf{s}}, \tag{2.16}$$

where

$$\mathbf{J} = \begin{bmatrix} \mathbf{u}_1^T & \mathbf{u}_1^T \mathbf{E}\mathbf{Q}\mathbf{b}_1 \\ \mathbf{u}_2^T & \mathbf{u}_2^T \mathbf{E}\mathbf{Q}\mathbf{b}_2 \\ \mathbf{u}_3^T & \mathbf{u}_3^T \mathbf{E}\mathbf{Q}\mathbf{b}_3 \end{bmatrix} \tag{2.17}$$

is the Jacobian matrix of the robot and $\mathbf{u}_i$ represents the unit vector along the ith link, i.e., $\mathbf{u}_i = \dfrac{\mathbf{c}_i}{l_i}$. Substituting eq. (2.5) in eq. (2.17) gives

$$\mathbf{J} = \begin{bmatrix} \dfrac{\mathbf{w}_1}{l_1} & \dfrac{\mathbf{w}_2}{l_2} & \dfrac{\mathbf{w}_3}{l_3} \end{bmatrix}^T. \tag{2.18}$$

In order to find the singularities of these robots, we need to solve the equation

$$\det(\mathbf{J}) = 0. \tag{2.19}$$

Assuming that the lengths of the rigid links are greater than zero, equation (2.19) is analogous to the equation of the conic sections forming the boundary of the COWCW as it was presented in section 2.2.1.3. The quadratic nature of the singularity loci of these mechanisms was revealed in [31]. While the geometric loci are the same, the physical phenomena they represent are distinct. One represents possible boundaries of the COWCW, and the other, the singularities of the robot. Hence, the proposed method in this thesis can be applied to 3-R$\underline{\text{P}}$R planar robots to find their singularities as we explain in the next section.

2.4 Conditions for Determining the Types of Conic Sections of the Boundaries of the COWCW

Expanding eqs. (2.13) and (2.19) and rewriting them in matrix form leads to

$$\frac{1}{2}\mathbf{p}^T \mathbf{D}_{pqr} \mathbf{p} + \mathbf{h}_{pqr}^T \mathbf{p} + f_{pqr} = 0, \tag{2.20}$$

where $\mathbf{D}_{pqr} \in \mathbb{R}^{2\times 2}$ is symmetric indefinite, $\mathbf{h}_{pqr} \in \mathbb{R}^2$, and $f_{pqr} \in \mathbb{R}$. Notice that all the elements of $\mathbf{D}_{pqr}$, $\mathbf{h}_{pqr}$ and also scalar f_{pqr}, are functions of ϕ and the geometric parameters of the given mechanism, $\mathbf{a}_i$ and $\mathbf{b}_i$, $i = 1, \ldots, m$.

From calculus, we know that the type of a conic section is recognized by the sign of its discriminant, $\det(\mathbf{D}_{pqr})$. Therefore, the following relations allow us to recognize the type of the conic section:

$$\begin{cases} \text{ellipse} & \text{if } \det(\mathbf{D}_{pqr}) > 0, \\ \text{parabola} & \text{if } \det(\mathbf{D}_{pqr}) = 0, \\ \text{hyperbola} & \text{if } \det(\mathbf{D}_{pqr}) < 0. \end{cases} \tag{2.21}$$

Notice that for some values of $\mathbf{D}_{pqr}$, $\mathbf{h}_{pqr}$ and f_{pqr}, these conic sections can degenerate into lines. Matrix $\mathbf{D}_{pqr}$ is obtained by expanding eq. (2.13) and considering the second-order terms. In other words we need to expand the following equation

$$\det\left(\begin{bmatrix} \mathbf{c}_p & \mathbf{c}_q & \mathbf{c}_r \\ \mathbf{b}_p^T\mathbf{Q}^T\mathbf{E}^T\mathbf{c}_p & \mathbf{b}_q^T\mathbf{Q}^T\mathbf{E}^T\mathbf{c}_q & \mathbf{b}_r^T\mathbf{Q}^T\mathbf{E}^T\mathbf{c}_r \end{bmatrix}\right) = 0, \tag{2.22}$$

Expanding eq. (2.22) leads to

$$0 = \mathbf{b}_p^T\mathbf{Q}^T\mathbf{E}^T\mathbf{u}_p\det([\mathbf{c}_q\ \mathbf{c}_r]) + \mathbf{b}_q^T\mathbf{Q}^T\mathbf{E}^T\mathbf{c}_q\det([\mathbf{c}_r\ \mathbf{c}_p]) + \mathbf{b}_r^T\mathbf{Q}^T\mathbf{E}^T\mathbf{c}_r\det([\mathbf{c}_p\ \mathbf{c}_q]), \tag{2.23}$$

which, in turn gives

$$0 = \mathbf{b}_p^T\mathbf{Q}^T\mathbf{E}^T\mathbf{c}_p\mathbf{c}_q^T\mathbf{E}\mathbf{c}_r + \mathbf{b}_q^T\mathbf{Q}^T\mathbf{E}^T\mathbf{c}_q\mathbf{c}_r^T\mathbf{E}\mathbf{c}_p + \mathbf{b}_r^T\mathbf{Q}^T\mathbf{E}^T\mathbf{c}_r\mathbf{c}_p^T\mathbf{E}\mathbf{c}_q. \tag{2.24}$$

Substituting eq. (2.1) into eq. (2.24) leads to

$$\mathbf{p}^T\mathbf{E}^T\mathbf{F}_{pqr}\mathbf{E}\mathbf{p} + \text{first-and zero-order terms in } \mathbf{p} = 0, \tag{2.25}$$

where

$$\mathbf{F}_{pqr} = \mathbf{Q}(-\mathbf{b}_p\mathbf{b}_q^T\mathbf{Q}^T + \mathbf{b}_p\mathbf{a}_q^T - \mathbf{b}_p\mathbf{a}_r^T + \mathbf{b}_p\mathbf{b}_r^T\mathbf{Q}^T + \mathbf{b}_q\mathbf{a}_r^T - \mathbf{b}_q\mathbf{b}_r^T\mathbf{Q}^T - \mathbf{b}_q\mathbf{a}_p^T + \mathbf{b}_q\mathbf{b}_p^T\mathbf{Q}^T$$
$$+ \mathbf{b}_r\mathbf{a}_p^T - \mathbf{b}_r\mathbf{b}_p^T\mathbf{Q}^T - \mathbf{b}_r\mathbf{a}_q^T + \mathbf{b}_r\mathbf{b}_q^T\mathbf{Q}^T).$$

Since $\mathbf{p}^T\mathbf{E}^T\mathbf{F}_{pqr}\mathbf{E}\mathbf{p} = \dfrac{1}{2}\mathbf{p}^T\mathbf{E}^T(\mathbf{F}_{pqr} + \mathbf{F}_{pqr}^T)\mathbf{E}\mathbf{p}$, matrix $\mathbf{D}_{pqr}$ is given by

$$\mathbf{D}_{pqr} = \mathbf{F}_{pqr} + \mathbf{F}_{pqr}^T. \tag{2.26}$$

Hence, for a constant end-effector orientation, matrix $\mathbf{D}_{pqr}$ is expressed as [1]

$$\mathbf{D}_{pqr} = \mathbf{b}_p(\mathbf{a}_q - \mathbf{a}_r)^T + \mathbf{b}_q(\mathbf{a}_r - \mathbf{a}_p)^T + \mathbf{b}_r(\mathbf{a}_p - \mathbf{a}_q)^T + \tag{2.27}$$
$$(\mathbf{a}_q - \mathbf{a}_r)\mathbf{b}_p^T + (\mathbf{a}_r - \mathbf{a}_p)\mathbf{b}_q^T + (\mathbf{a}_p - \mathbf{a}_q)\mathbf{b}_r^T$$

in which vectors $\mathbf{b}_p$, $\mathbf{b}_q$ and $\mathbf{b}_r$ are expressed in the reference frame $\mathcal{A}$. Hence, the discriminant of eq. (2.20) is given by

$$\det(\mathbf{D}_{pqr}) = -(\gamma^2 - 4\alpha\beta), \tag{2.28}$$

where

$$\alpha = \mathbf{a}_p^T\,\mathbf{E}^T\mathbf{a}_q + \mathbf{a}_q^T\,\mathbf{E}^T\mathbf{a}_r + \mathbf{a}_r^T\,\mathbf{E}^T\mathbf{a}_p,$$
$$\beta = \mathbf{b}_p^T\,\mathbf{E}^T\mathbf{b}_q + \mathbf{b}_q^T\,\mathbf{E}^T\mathbf{b}_r + \mathbf{b}_r^T\,\mathbf{E}^T\mathbf{b}_p, \tag{2.29}$$
$$\gamma = \mathbf{a}_p^T\,\mathbf{E}^T\mathbf{b}_q + \mathbf{b}_p^T\,\mathbf{E}^T\mathbf{a}_q + \mathbf{a}_q^T\,\mathbf{E}^T\mathbf{b}_r + \mathbf{b}_q^T\,\mathbf{E}^T\mathbf{a}_r + \mathbf{a}_r^T\,\mathbf{E}^T\mathbf{b}_p + \mathbf{b}_r^T\,\mathbf{E}^T\mathbf{a}_p.$$

---

[1]For a constant orientation matrix $\mathbf{Q}$ is a constant, and we can remove it from the formula if we express the coordinates of $\mathbf{b}_p, \mathbf{b}_q$ and $\mathbf{b}_r$ in the fixed frame $\mathcal{A}$.

One can verify that variables α and β represent twice the oriented areas [32] of the triangles A and B formed by the vertices A_p, A_q, A_r and B_p, B_q, B_r, respectively. As
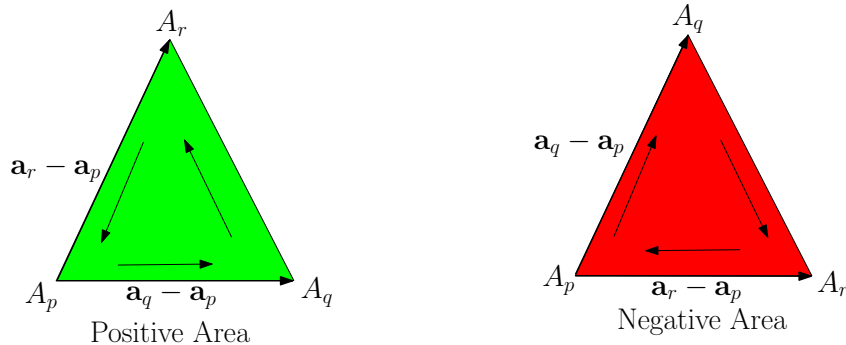
Figure 2.6: Oriented area of the triangle formed by three selected fixed points, A_p, A_q and A_r, of a given PCDPM.

depicted in Fig. 2.6, the oriented area is positive if the sequence A_p, A_q and A_r is in the counter clockwise order, and negative otherwise.

The expression of γ in eq. (2.29) represents a combined area of the two triangles. It is different from the Minkowski mixed area [32] of the triangles, but it can be considered as the mixed area of the triangle obtained by linearly combining the vectors of the corresponding vertices of the triangles A and B. Equation (2.29) leads to the definition of the function taking as inputs the coordinates of the vertices of a triangle, and returning its oriented area times two, namely,

$$\text{area}(\mathbf{p}_1, \mathbf{p}_2, \mathbf{p}_3) = \det\left(\begin{bmatrix} 1 & 1 & 1 \\ \mathbf{p}_1 & \mathbf{p}_2 & \mathbf{p}_3 \end{bmatrix}\right), \tag{2.30}$$

Using eq. (2.30), the expressions of the variables defined in eq. (2.29) can be rewritten as

$$\begin{aligned} \alpha &= \text{area}(\mathbf{a}_p, \mathbf{a}_q, \mathbf{a}_r), \\ \beta &= \text{area}(\mathbf{b}_p, \mathbf{b}_q, \mathbf{b}_r), \\ \gamma &= \text{area}(\mathbf{a}_p, \mathbf{b}_q - \mathbf{b}_r, \mathbf{0}) + \text{area}(\mathbf{a}_q, \mathbf{b}_r - \mathbf{b}_p, \mathbf{0}) + \text{area}(\mathbf{a}_r, \mathbf{b}_p - \mathbf{b}_q, \mathbf{0}). \end{aligned} \tag{2.31}$$

Note that γ in eq. (2.31) can be written in different forms, the one making use of the oriented-area function being preferred here.

2.5 Equivalent Conditions for Determining the Types of Conic Sections

An investigation of eq. (2.28) shows that the discriminant has a direct relation with the orientations of the triangles, i.e, the signs of α and β. As a result, we reach the following lemmas.

Lemma 1 *If triangles A and B have opposite orderings, then the conic section is a hyperbola.*

Proof. When triangles A and B have opposite orderings, then α and β have opposite signs, and $\alpha\beta < 0$, so that the discriminant is positive. Therefore, in such a case, the associated conic section is always a hyperbola.□

Lemma 2 *If one or both of the triangles A and B degenerate into a line, then the conic section is a hyperbola or a parabola. If one of these triangles degenerates to a point, then the conic section is a parabola.*

Proof. When one or both triangles degenerate into a line, we have $\alpha\beta = 0$. Consequently, the discriminant is non-negative, and the boundary is either a parabola or a hyperbola. If one of the triangles degenerates into a point, which means that the three corresponding attachment points coincide, then $\alpha\beta = \gamma = 0$, and the discriminant is zero, and the shape of the COWCW boundary is that of a parabola.□

Lemma 3 *If all the edges of triangle A are parallel to their corresponding edges on triangle B, then the conic section is a parabola.*

Proof. When all the edges of triangles A and B are parallel, which does not imply that they are similar, we have $\mathbf{a}_j - \mathbf{a}_p = \lambda\,(\mathbf{b}_j - \mathbf{b}_p)$, $j=\{q,r\}$ where $\lambda \in \mathbb{R}$ is a real number. Substituting these relations in eq. (2.29) gives $\alpha = \lambda\beta$ and $\gamma = 2\lambda\beta$. Consequently, from eq. (2.28), the discriminant is zero and the corresponding boundary segment is a parabola.□

For the case in which two triangles have the same orientation, $\alpha\beta > 0$, additional work is required in order to recognize the sign of the discriminant in eq. (2.21). For such cases, we define the triangle $C_pC_qC_r$ obtained through the homotopy of $A_pA_q\ A_r$ onto $B_pB_qB_r$. Hence the vertices of this triangle are obtainable by the following equations.

$$
\begin{aligned}
\mathbf{c}_p &= \mu\mathbf{a}_p + (1-\mu)\mathbf{b}_p, \\
\mathbf{c}_q &= \mu\mathbf{a}_q + (1-\mu)\mathbf{b}_q, \\
\mathbf{c}_r &= \mu\mathbf{a}_r + (1-\mu)\mathbf{b}_r.
\end{aligned}
\tag{2.32}
$$

where μ is a free parameter.

Notice that the variables defined in eq. (2.29) are translation invariant. Consequently, shifting the origins of these frames to A_p and B_p has no effect on these variables. Therefore, we can consider the origins of the reference and moving frames to coincide with vertices A_p and B_p, which, in turn, means that

$$
\mathbf{a}_p = \mathbf{b}_p = \mathbf{0}_2.
\tag{2.33}
$$

Figure 2.7 shows the triangles A, B, whose vertices A_p and B_p coincide at the origin. One of their linear combinations C is also shown, which corresponds to $\mu = 0.4$. In
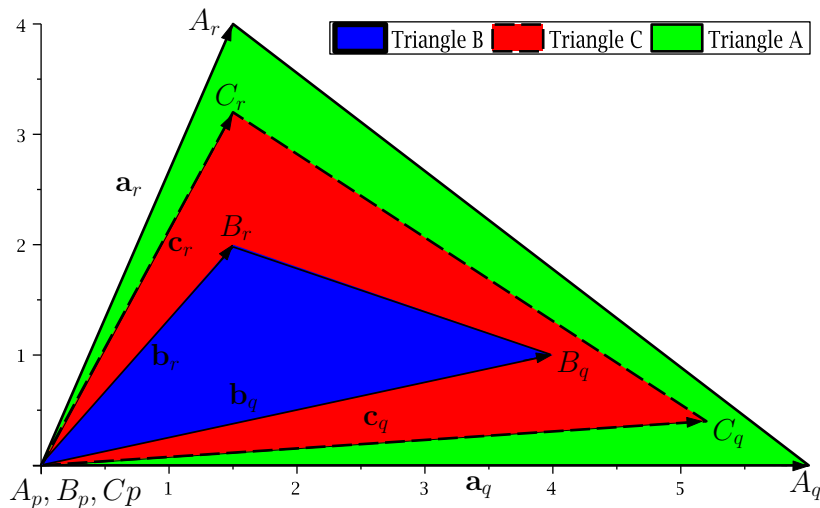
Figure 2.7: Triangles A and B and one of their possible linear combinations C.

general, the area of triangle C can be given by the following equations

$$
2A_C = \mathrm{area}(\mathbf{c}_p, \mathbf{c}_q, \mathbf{c}_r),
\tag{2.34}
$$

Substituting eq. (2.32) into eq. (2.34) and expanding it according to the function defined in eq. (2.30) leads to

$$2A_C = \mu^2(\alpha + \beta - \gamma) + \mu(\gamma - 2\beta) + \beta, \tag{2.35}$$

which is quadratic in the variable μ. Interestingly, the discriminant of eq. (2.35) is the negative of that of the conic section equation given in eq. (2.28). As a result the conditions in eq. (2.21) can be rewritten as a function of the number of real roots of eq. (2.35) when set to zero, namely,

$$\begin{cases} \text{ellipse} & \text{no real root,} \\ \text{parabola} & \text{one real double root,} \\ \text{hyperbola} & \text{two real roots.} \end{cases} \tag{2.36}$$

Therefore, in order to determine the types of the conic sections forming the boundary, we must find out how many times $A_C = 0$, that is, how many times the triangle C degenerates into a line segment.

In order to obtain graphical conditions equivalent to those of eq. (2.36), we define the following function:

$$2A(\mathbf{p}) \equiv \text{area}(\mathbf{p}, \mathbf{c}_q, \mathbf{c}_r). \tag{2.37}$$

Notice that we have the relation $A(\mathbf{c}_p) = A_C$, so that $A(\mathbf{p})$ may be regarded as the area of triangle C, where we left the position of vertex C_p as a free variable. Since $\mathbf{c}_q$ and $\mathbf{c}_r$ are linear in μ, $A(\mathbf{p})$ is a quadratic equation in this parameter. Using the defined *area* function and expanding eq. (2.37) leads to

$$2A(\mathbf{p}) = \delta\mu^2 + (\gamma(\mathbf{p}) - 2\beta(\mathbf{p}))\mu + \beta(\mathbf{p}), \tag{2.38}$$

where $\alpha(\mathbf{p}), \beta(\mathbf{p})$ and $\gamma(\mathbf{p})$ are affine functions of $\mathbf{p}$ and are given by

$$\begin{aligned} \alpha(\mathbf{p}) &= \text{area}(\mathbf{p}, \mathbf{a}_q, \mathbf{a}_r), \\ \beta(\mathbf{p}) &= \text{area}(\mathbf{p}, \mathbf{b}_q, \mathbf{b}_r), \\ \gamma(\mathbf{p}) &= \alpha(\mathbf{p}) + \beta(\mathbf{p}) - \delta, \\ \delta &= \text{area}(\mathbf{a}_q, \mathbf{a}_r, \mathbf{b}_q) + \text{area}(\mathbf{b}_q, \mathbf{b}_r, \mathbf{a}_q). \end{aligned} \tag{2.39}$$

The discriminant of eq. (2.38) is given by

$$\Delta(\mathbf{p}) = \gamma(\mathbf{p})^2 - 4\alpha(\mathbf{p})\beta(\mathbf{p}), \tag{2.40}$$

Equation (2.40) is a quadratic function of $\mathbf{p}$. Hence $\Delta(\mathbf{p}) = 0$ represents a conic section. Substituting eq. (2.39) into eq. (2.40) leads to

$$(\alpha(\mathbf{p}) - \beta(\mathbf{p}))^2 - 2(\alpha(\mathbf{p}) + \beta(\mathbf{p}))\delta + \delta^2 = 0. \qquad (2.41)$$

Letting α and β be the independent variables in eq. (2.41), one may rewrite the quadratic term as $(\boldsymbol{\kappa}^T \mathbf{e})^2 = \boldsymbol{\kappa}^T \mathbf{e}\mathbf{e}^T \boldsymbol{\kappa}$, where $\boldsymbol{\kappa} = [\alpha \quad \beta]^T$ and $\mathbf{e} \equiv [1 \quad -1]^T$. Clearly, the matrix $\mathbf{e}\mathbf{e}^T$ of quadratic coefficients is singular, and, therefore, eq. (2.41) represents a parabola in α and β. Because $\boldsymbol{\kappa}$ is affinely related to $\mathbf{p}$, eq. (2.41) also represents a parabola in $\mathbf{p}$. This leads to the following lemma.

Lemma 4 *The type of conic section composing the boundary of the COWCW can be determined from the following conditions:*

$$\begin{cases} \text{ellipse} & C_p \text{ is inside of the parabola} & (\Delta(\mathbf{c}_p) < 0), \\ \text{parabola} & C_p \text{ is on the parabola} & (\Delta(\mathbf{c}_p) = 0), \\ \text{hyperbola} & C_p \text{ is outside of the parabola} & (\Delta(\mathbf{c}_p) > 0). \end{cases} \qquad (2.42)$$
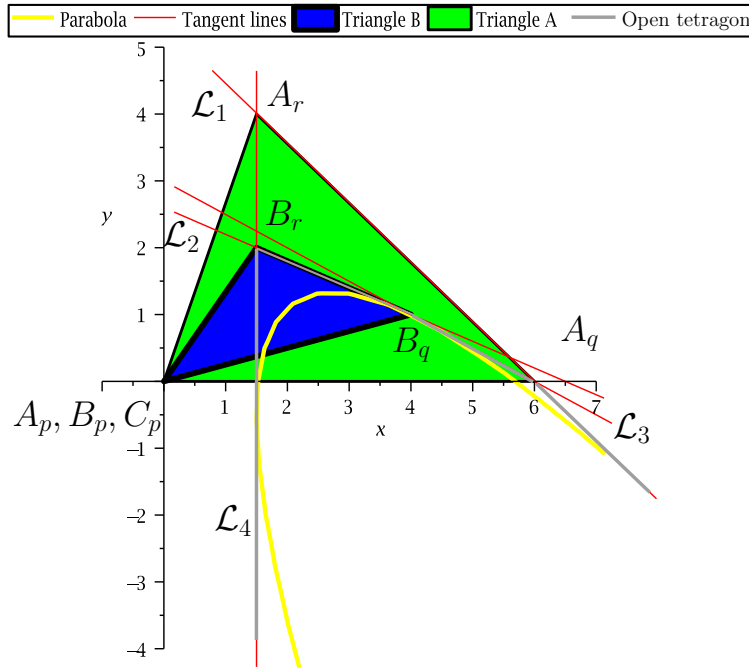
Figure 2.8: Two triangles of a selected set of base and moving-platform points, with their corresponding parabola.

To clarify what is meant by the outside and the inside of the parabola, notice that when there are two possible tangent lines to the parabola passing through C_p, then it is outside, when there is only one, then it is on the parabola, and otherwise, it is inside.

Figure 2.8 shows the triangles A and B depicted in Fig. 2.7 with their corresponding parabola $\Delta(\mathbf{p}) = 0$. In this case C_p is located outside the parabola, and the conic section corresponding to the two triangles is a hyperbola.

Figure 2.8 leads to the following intuitive reasoning. Since the area inside the parabola is generally smaller than the area outside the parabola, although both of them extend to infinity, the most probable type of boundary of a random PCDPM geometry should be the hyperbola, and the least probable type, the parabola. In practice, this conjecture seems to be verified.

From a computational standpoint, the conditions of Lemma 4 do not bring any improvement over those of eq. (2.21). Nevertheless, these new conditions can be exploited in order to obtain a graphical solution to the problem, as we show in the following section.

2.6 Graphically Determining the Types of Conic Sections

Let us call the lines passing through vertices $\{A_r, A_q\}$, $\{B_r, B_q\}$, $\{A_r, B_r\}$ and $\{A_q, B_q\}$, $\mathcal{L}_1$, $\mathcal{L}_2$, $\mathcal{L}_3$ and $\mathcal{L}_4$ respectively, as depicted in Fig. 2.8. Consider the following lemma:

Lemma 5 *All lines $\mathcal{L}_i$, $i = 1, \ldots, 4$ are tangent to the parabola, $\Delta(\mathbf{p}) = 0$.*

Proof. In order to prove this lemma, we first need to find the number of the intersection points between each of these lines and the parabola. Let us begin with line $\mathcal{L}_1$, which is the set of points whose positions can be expressed as $\mathbf{p} = \lambda \mathbf{a}_q + (1 - \lambda)\mathbf{a}_r$. The intersection points of this line with the parabola can be found by solving the following equation for λ:

$$\Delta(\lambda \mathbf{a}_q + (1 - \lambda)\mathbf{a}_r) = 0. \tag{2.43}$$

Substituting $\mathbf{p} = \lambda\mathbf{a}_q + (1 - \lambda)\mathbf{a}_r$ in eq. (2.39) leads to $\alpha(\mathbf{p}) = 0$. Hence, we have $\Delta(\mathbf{p}) = \gamma^2(\mathbf{p})$. Substituting this in eq. (2.43) yields $\gamma(\lambda\mathbf{a}_q + (1 - \lambda)\mathbf{a}_r) = 0$. Since this is an affine function of λ, we are bound to have exactly one solution. The same approach can be used to prove that line $\mathcal{L}_2$ intersects the parabola in only one point. In this case, however, we have $\beta(\mathbf{p}) = 0$.

In the case of line $\mathcal{L}_3$, substituting the corresponding equation $\mathbf{p} = \lambda\mathbf{a}_r + (1 - \lambda)\mathbf{b}_r$ in eq. (2.39) gives the following results:

$$
\begin{aligned}
\alpha(\mathbf{p}) &= (1 - \lambda)a, \\
\beta(\mathbf{p}) &= \lambda b, \\
\delta &= a + b, \\
\gamma(\mathbf{p}) &= -(\lambda a + (1 - \lambda)b).
\end{aligned}
\tag{2.44}
$$

where $a = \mathrm{area}(\mathbf{a}_q, \mathbf{a}_r, \mathbf{b}_r)$ and $b = \mathrm{area}(\mathbf{a}_r, \mathbf{b}_q, \mathbf{b}_r)$. Substituting eq.(2.44) into eq.(2.40) gives

$$
\Delta(\mathbf{p}) = (a + b)^2\lambda^2 - 2b(a + b)\lambda + b^2 = ((a + b)\lambda - b)^2.
\tag{2.45}
$$

Clearly the only (double) root of eq. (2.45) is $\lambda = \dfrac{b}{a + b}$, which means that line $\mathcal{L}_3$ and the parabola have only one common intersection point. With the same approach, we can prove that $\mathcal{L}_4$ and the parabola have only one intersection point as well.

In order to ascertain that these lines are not parallel to the symmetry axis of the parabola we need to show that the following equation is satisfied at the intersection points:

$$
(\partial\Delta/\partial\mathbf{p})^T\mathbf{d}_i = 0, \quad i = 1\ldots 4,
\tag{2.46}
$$

where $\mathbf{d}_i$ is the direction vector of line $\mathcal{L}_i$. In order to calculate $\partial\Delta/\partial\mathbf{p}$, we first need to calculate $\partial(\mathrm{area}(\mathbf{p}, \mathbf{a}_q, \mathbf{a}_r))/\partial\mathbf{p}$. From the definition of the *area* function given in eq. (2.30), one can verify that

$$
\partial(\mathrm{area}(\mathbf{p}, \mathbf{a}, \mathbf{b}))/\partial\mathbf{p} = \mathbf{E}(\mathbf{a} - \mathbf{b}).
\tag{2.47}
$$

Hence, taking the derivatives of both sides of eqs. (2.39) gives

$$
\begin{aligned}
\partial\alpha/\partial\mathbf{p} &= \mathbf{E}(\mathbf{a}_q - \mathbf{a}_r), \\
\partial\beta/\partial\mathbf{p} &= \mathbf{E}(\mathbf{b}_q - \mathbf{b}_r), \\
\partial\gamma/\partial\mathbf{p} &= (\partial\alpha/\partial\mathbf{p} + \partial\beta/\partial\mathbf{p}) = \mathbf{E}(\mathbf{a}_q - \mathbf{a}_r + \mathbf{b}_q - \mathbf{b}_r).
\end{aligned}
\tag{2.48}
$$

From eq. (2.40), we also know that

$$\partial\Delta/\partial\mathbf{p} = 2\gamma(\mathbf{p})\partial\gamma/\partial\mathbf{p} - 4[\beta(\mathbf{p})\partial\alpha/\partial\mathbf{p} + \alpha(\mathbf{p})\partial\beta/\partial\mathbf{p}]. \tag{2.49}$$

Hence, we can calculate $\partial\Delta/\partial\mathbf{p}$ at each intersection point $\mathbf{p}$ by substituting eq. (2.48) into eq. (2.49). Remembering that for line $\mathcal{L}_1$, $\alpha = 0$, and $\gamma = 0$ at an intersection point, we obtain

$$\partial\Delta/\partial\mathbf{p} = -4\beta\mathbf{E}(\mathbf{a}_q - \mathbf{a}_r), \tag{2.50}$$

The direction vector of $\mathcal{L}_1$ is given by

$$\mathbf{d}_1 = (\mathbf{a}_q - \mathbf{a}_r)/||\mathbf{a}_q - \mathbf{a}_r||, \tag{2.51}$$

which gives

$$(\partial\Delta/\partial\mathbf{p})^T\mathbf{d}_1 = -4\beta(\mathbf{a}_q - \mathbf{a}_r)^T\mathbf{E}^T(\mathbf{a}_q - \mathbf{a}_r)/||\mathbf{a}_q - \mathbf{a}_r|| = 0. \tag{2.52}$$

Since $\mathcal{L}_1$ has only one intersection point with the parabola and satisfies eq. (2.46), it is a tangent line of the parabola. Using the same approach for line $\mathcal{L}_3$, we substitute eq. (2.44) and eq. (2.48) into eq. (2.49) which leads to

$$\partial\Delta/\partial(\mathbf{p}) = -2\mathbf{E}(c(\mathbf{a}_q - \mathbf{a}_r) + d(\mathbf{b}_q - \mathbf{b}_r)), \tag{2.53}$$

where $c = \lambda a + (\lambda + 1)b$ and $d = (2 - \lambda)a + (1 - \lambda)b$.

The direction vector of line $\mathcal{L}_3$ is given by

$$\mathbf{d}_3 = (\mathbf{a}_r - \mathbf{b}_r)/||\mathbf{a}_r - \mathbf{b}_r||. \tag{2.54}$$

and hence,

$$(\partial\Delta/\partial\mathbf{p})^T\mathbf{d}_3 = -2(c(\mathbf{a}_q - \mathbf{a}_r) + d(\mathbf{b}_q - \mathbf{b}_r))^T\mathbf{E}^T(\mathbf{a}_r - \mathbf{b}_r)/||\mathbf{a}_r - \mathbf{b}_r|| =$$
$$- 2(ac - bd)/||\mathbf{a}_r - \mathbf{b}_r|| = -2(\lambda(a + b) - b)(a + b)/||\mathbf{a}_r - \mathbf{b}_r||. \tag{2.55}$$

We already proved that $\lambda = \dfrac{b}{a + b}$ at the intersection point of line $\mathcal{L}_3$ and the parabola, . Substituting this value for λ in eq. (2.55) leads to

$$(\partial\Delta/\partial\mathbf{p})^T\mathbf{d}_3 = 0, \tag{2.56}$$

which implies that line $\mathcal{L}_3$ is not parallel to the symmetry axis of parabola as well.

With the same approach we can prove that lines $\mathcal{L}_2$ and $\mathcal{L}_4$ are also tangent to the parabola, which completes the proof. $\square$

Now we can propose the following theorem:
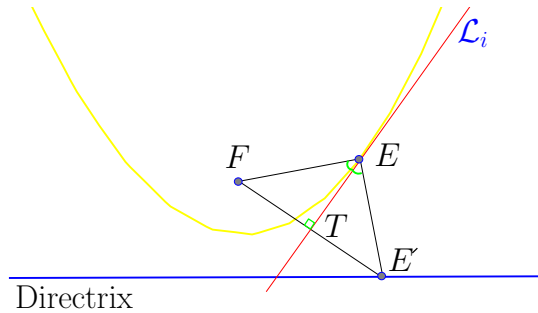
Figure 2.9: A line segment between the focus point and the directrix of a parabola equally divided by a perpendicular tangent line.

Theorem 1 *The circumcircle of a triangle formed by three tangents to a parabola passes through the focus point of the parabola.*

For the proof, see Lambert's theorem [33], p.206–208.

Hence, if we consider the triangles made by lines $\mathcal{L}_1$, $\mathcal{L}_2$, $\mathcal{L}_3$ and $\mathcal{L}_1$, $\mathcal{L}_2$, $\mathcal{L}_4$, their corresponding circumcircles intersect in two points, one of which is the intersection of lines $\mathcal{L}_1$ and $\mathcal{L}_2$, and the other being the focus point of the parabola. Because of the geometric properties of the parabola, when a line segment between the focus point and the directrix line is perpendicular to a given tangent line, it is divided into two line segments of equal lengths by this tangent line [34]. As depicted in Fig. 2.9, the line segment FE' is divided into two line segments FT and TE' of equal lengths by the tangent line $\mathcal{L}_i$. This, in turn, means that the intersection point of line FE' and the directrix is the image of the focus point reflected about the tangent line. Since lines $\mathcal{L}_1$ and $\mathcal{L}_2$ are tangent lines, we can find two points of the directrix from this property, and find the directrix. Also, since a parabola is the locus of the points that are equidistant to the focus point and the directrix, we can verify whether a point lies inside or outside the parabola by comparing its distances to the focus and the directrix, respectively. Hence, if the chosen origin C_p is outside the parabola, its distance from the focus point is greater than its distance from the directrix line. From lemma 4, we then conclude that the corresponding boundary is a hyperbola.

We now summarize the proposed method as a graphical algorithm for determining the types of the conic segments that form the boundary of the COWCW for a selected set of fixed and moving attachment points of a PCDPM.

1. Draw the triangles A and B with their vertices A_p and B_p coinciding at the origin O.

2. Draw the four lines through $A_r A_q$, $B_r B_q$, $A_r B_r$ and $A_q B_q$.

3. Draw the circle through A_r, B_r and the common intersection of $A_r A_q$ and $B_r B_q$. Call this circle $\mathcal{C}_1$.

4. Draw the circle through A_q, B_q and the common intersection of $A_r A_q$ and $B_r B_q$. Call this circle $\mathcal{C}_2$.

5. The parabola focus point F is one of the two intersection points of $\mathcal{C}_1$ and $\mathcal{C}_2$. The other is the intersection point of lines $A_r A_q$ and $B_r B_q$.

6. Reflect F about lines $A_r A_q$ and $B_r B_q$, respectively, to obtain points F_A and F_B.

7. Trace the parabola directrix, which is the line through F_A and F_B.

8. If the origin O is closer to the directrix than to the focus point, then the corresponding conic section is a hyperbola. If the origin O is at equal distances from the focus point and the directrix, then the conic section is a parabola. If the origin O is closer to the focus point F than the directrix, then it is an ellipse.

It is often possible to determine the type of conic section just by a mere inspection, according to eq. (2.42). If C_p is outside of the open tetragon formed by tangent lines and contains the parabola, then the type of conic section is a hyperbola. If C_p is inside, then the corresponding conic section is an ellipse. For the depicted example in Fig. 2.8, this open tetragon passes through B_r, B_q and A_q, and does not contain C_p, so that the type of conic section for this example is a hyperbola.

Notice that some special cases such as those where edges $A_r A_q$ and $B_r B_q$ are parallel or line $\mathcal{L}_2$ passes through A_q, the parabola degenerates into a line, one or both of the circles is undetermined and the proposed method cannot be applied. In the following, section the proposed method is illustrated by two examples.

2.7 Examples

Let us first consider a simple planar parallel cable-driven mechanism, and then a 3-R$\underline{\text{P}}$R mechanism.

2.7.1 A Planar Cable-Driven Parallel Mechanism
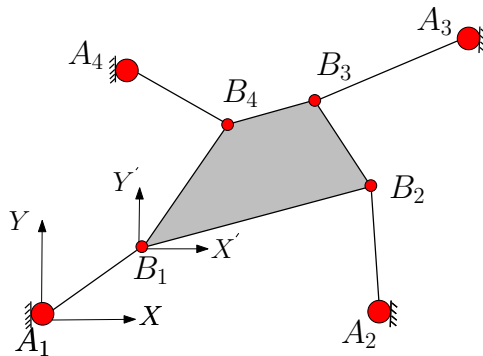
Figure 2.10: A planar parallel cable-driven robot with four cables.

In this section, we apply the proposed method to find the type of a conic section composing a portion of the boundary of the PCDPM with four cables and a trapezoidal moving platform, as shown in Fig. 2.10. The locations of the fixed and moving attachment points are chosen as $\mathbf{a}_1 = \mathbf{0}_2$, $\mathbf{a}_2 = \begin{bmatrix} 6 & 0 \end{bmatrix}^T$, $\mathbf{a}_3 = \begin{bmatrix} 7 & 5 \end{bmatrix}^T$, $\mathbf{a}_4 = \begin{bmatrix} 1.5 & 4 \end{bmatrix}^T$, $\mathbf{b}_1 = \mathbf{0}_2$, $\mathbf{b}_2 = \begin{bmatrix} 4 & 1 \end{bmatrix}^T$, $\mathbf{b}_3 = \begin{bmatrix} 2.5 & 2.25 \end{bmatrix}^T$ and $\mathbf{b}_4 = \begin{bmatrix} 1.5 & 2 \end{bmatrix}^T$.

For this case, we have $\binom{4}{3} = 4$ possible combinations of three cables, each corresponding to one conic section. We consider the cables 1, 2 and 4 in order to illustrate the proposed algorithm, i.e., we choose $p = 1$, $q = 2$, and $r = 4$. As can be seen from Fig. 2.10, the ordering of $A_1 A_2 A_4$ and their corresponding attachment points on the moving platform $B_1 B_2 B_4$ are both in the counter clockwise direction. Hence both of these triangles have the same orientation. Figure 2.8 shows the corresponding parabola and tangent lines defined in section 2.5 for the selected attachment points. The application of the proposed algorithm is depicted in Fig. 2.11. First, we draw the triangles A and B with their vertices A_1 and B_1 coinciding at the origin O. For the second step, we draw lines $\mathcal{L}_i$, $i = 1, \ldots, 4$, defined in section 2.6. Lines $\mathcal{L}_1$ and $\mathcal{L}_2$ intersect at point P_{AB}. In the third step, we draw the circles $\mathcal{C}_1$ passing through A_4, B_4, P_{AB}, and $\mathcal{C}_2$, passing through A_2, B_2, P_{AB}. These circles intersect in two points. One of them is P_{AB}, and the other is the focus point F of the parabola. The next step is to find the points F_A and F_B which are the reflected points of F about lines $\mathcal{L}_1$ and $\mathcal{L}_2$, respectively. The line passing through these two points is the directrix of the parabola. The last step is to find the distances from the origin to the directrix line and focus point. These distances are represented by d_D and d_F, respectively. Apparently, $d_D < d_F$, and the corresponding conic section for this example is a hyperbola. The equation of this
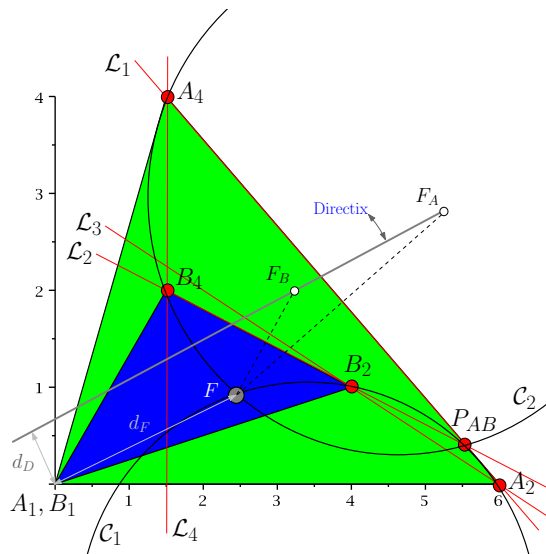
Figure 2.11: Graphical algorithm applied to determine the type of conic section of two triangles depicted in Fig. 2.8.

hyperbola can be obtained directly from eq. (2.13):

$$9.0\,x - 6.0\,y + 5.5\,xy + 3.0\,y^2 - 4\,x^2 = 0.$$

Notice that we could have reached this conclusion even more quickly by noticing that A_1 lies outside of the open tetragon $B_4B_2A_2$, which contains the parabola $\Delta(\mathbf{p})$. This fact is sufficient to conclude that A, is outside the parabola and, hence, the type of conic section is a hyperbola.

2.7.2 A 3-RPR Parallel Mechanism

In this subsection, we illustrate the proposed algorithm by finding the type of singularity curve of a 3-RPR mechanism with a constant orientation of its end effector, shown in Fig. 2.12. The exact geometry of this mechanism is as follows:
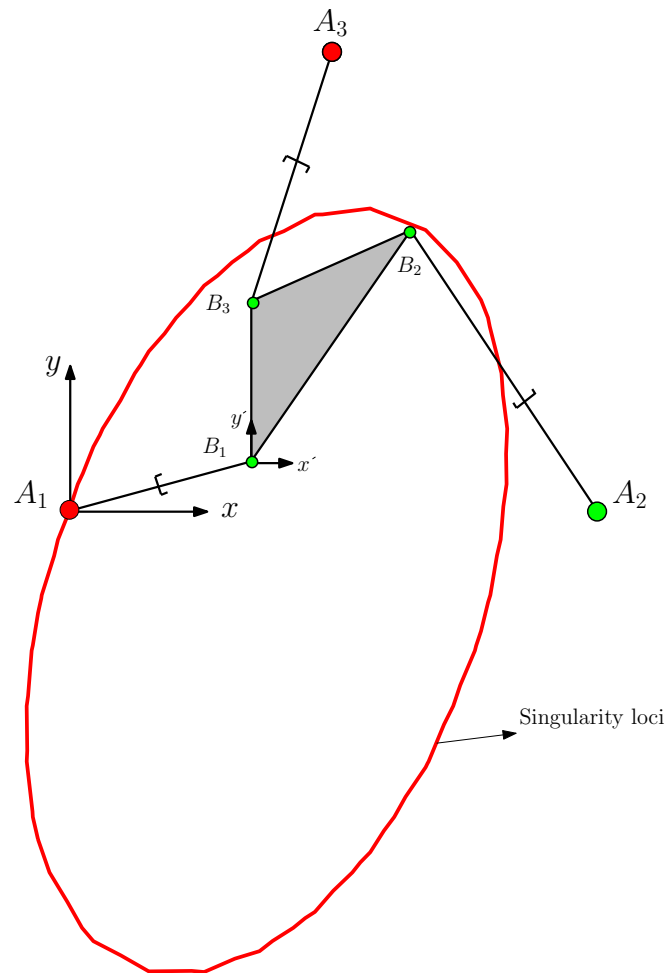
Figure 2.12: A 3-RPR planar parallel mechanism with a constant orientation of its end effector and corresponding singularity loci.

$\mathbf{a}_1 = \mathbf{0}_2$, $\mathbf{a}_2 = \begin{bmatrix} 10 & 0 \end{bmatrix}^T$, $\mathbf{a}_3 = \begin{bmatrix} 5 & 5\sqrt{3} \end{bmatrix}^T$, $\mathbf{b}_1 = \mathbf{0}_2$, $\mathbf{b}_2 = \begin{bmatrix} 3 & 5\sqrt{3}/2 \end{bmatrix}^T$ and $\mathbf{b}_3 = \begin{bmatrix} 0 & 3 \end{bmatrix}^T$.

As we can see from Fig. 2.12, the triangles $A_1 A_2 A_3$ and $B_1 B_2 B_3$ both follow a counterclockwise order. Figure 2.13 shows the application of the developed algorithm for this mechanism in order to find the type of conic section of its singularity curve.
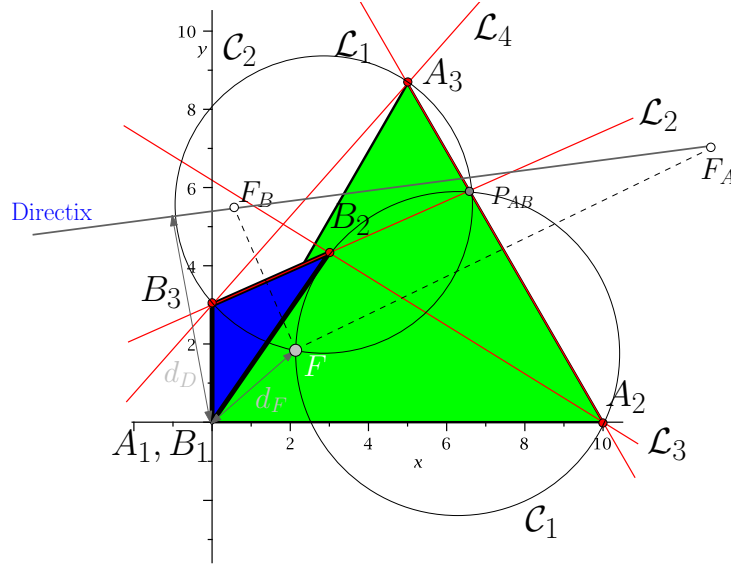
Figure 2.13: Application of the proposed graphical algorithm to find the type of singularity curve of a 3-R$\underline{\text{P}}$R mechanism.

The process is the same as in the previous example. First, we draw the triangles A and B with their vertices A_1 and B_1 coinciding at the origin. Then, we draw the lines $\mathcal{L}_1, \mathcal{L}_2, \mathcal{L}_3$ and $\mathcal{L}_4$ passing through vertices A_2A_3, B_2B_3, A_2B_2 and A_3B_3, respectively. The next step consists in drawing the circles $\mathcal{C}_2$ and $\mathcal{C}_1$ according to the steps 3 and 4 of the algorithm. Circle $\mathcal{C}_1$ passes through $A_2\,B_2$ and the intersection of lines $\mathcal{L}_1$ and $\mathcal{L}_2$, while circle $\mathcal{C}_2$ passes through A_3, B_3 and the intersection of lines $\mathcal{L}_1$ and $\mathcal{L}_2$. One of the two intersection points of these circles is the focus point F, while the other one, P_{AB}, is the intersection of lines $\mathcal{L}_1$ and $\mathcal{L}_2$. Reflecting the focus point about lines $\mathcal{L}_1$ and $\mathcal{L}_2$ gives the points F_A and F_B, respectively. The line passing through these points is the directrix of the parabola. In the last step we find the distance from the focus point to the directrix d_D and the origin d_F. As we can see from this figure, the distance between the focus point F and the origin is less than the distance from the directrix to the origin $(d_F < d_D)$. Hence, the corresponding conic section is an ellipse which is depicted in Fig. 2.12.

The equation of this ellipse can be obtained directly from eq. (2.19):

$$375.0\,x + 105\,y + 27.5\,x\sqrt{3}y - 37.5\,x\sqrt{3} - 125.0\,y\sqrt{3} - 30\,yx - 37.5\,x^2 - 15\,y^2 = 0.$$

2.8   Conclusions

A linear program was introduced to calculate the wrench closure workspace of PCDPMs via a discretization method. A relationship between the boundaries of the constant orientation wrench closure workspace (COWCW) and the geometry of the planar cable-driven parallel mechanisms also was unveiled. A graphical method was proposed to determine the types of conic sections forming the boundary of the constant orientation wrench-closure workspace of a planar parallel cable-driven mechanism. This may be regarded as a contribution to the theory of these mechanisms. It was also shown that these conic sections have a direct relation with the geometry and ordering of the fixed and moving attached points. In fact, the proposed method provides a quick and effective tool to determine the types of conic sections forming the boundary of the constant-orientation wrench-closure workspace of planar cable driven parallel mechanisms. This can prove useful when verifying the validity of the computed WCW for a given geometry, for example. This method can also be applied to find the singularities of 3-R$\underline{P}$R planar parallel robots because of the analogy between the Jacobian matrix of these robots and the wrench matrix of planar cable-driven parallel mechanisms. It is hoped that the results reported here can lead to the development of a graphical method for tracing the boundaries of the constant orientation wrench-closure workspace of a given planar parallel mechanism. However, because of the intricate equations involved, this task appears to be extremely challenging.

Chapter 3

The Dimensional Synthesis Of Planar Cable-Driven Parallel Mechanisms

In this chapter, we tackle the dimensional synthesis problem of finding a geometry for a planar cable-driven parallel mechanism (PCDPM) whose WCW contains a prescribed workspace. To this end, we first introduce a linear program to verify whether a given pose is inside or outside the WCW of a given PCDPM. The relaxation of this linear program over a box leads to a nonlinear feasibility problem that can only be satisfied when this box is completely inside the WCW. We extend this feasibility problem to find a PCDPM geometry whose WCW includes a given set of boxes. These multiple boxes may represent an estimate of the prescribed workspace, which may be obtained through interval analysis. Finally, we introduce a nonlinear program through which the PCDPM geometry is changed while maximizing the scaling factor of the prescribed set of boxes. When the optimum scaling factor is greater or equal to one, the WCW of the resulting PCDPM contains the set of boxes. Otherwise, the WCW generally offers a good coverage of the set of boxes.

3.1 Verifying Whether a Pose Lies in the WCW of a PCDPM

In the previous chapter we developed the kinetostatic equations of PCDPMs and formally defined the wrench-closure workspace concept. In order to devise a formulation for the synthesis problem of PCDPMs, we define the following vector and matrices

$$
\begin{aligned}
\mathbf{A} &\equiv \begin{bmatrix} \mathbf{a}_1 & \cdots & \mathbf{a}_m \end{bmatrix} \in \mathbb{R}^{2\times m}, \\
\mathbf{B} &\equiv \begin{bmatrix} \mathbf{b}_1 & \cdots & \mathbf{b}_m \end{bmatrix} \in \mathbb{R}^{2\times m}, \\
\mathbf{f} &\equiv \begin{bmatrix} \mathbf{b}_1^T \mathbf{Q}^T \mathbf{E}^T \mathbf{a}_1 & \cdots & \mathbf{b}_m^T \mathbf{Q}^T \mathbf{E}^T \mathbf{a}_m \end{bmatrix}^T \in \mathbb{R}^m,
\end{aligned}
\tag{3.1}
$$

which let us rewrite the wrench matrix $\mathbf{W}$ as

$$
\mathbf{W} \equiv \begin{bmatrix} \mathbf{A} - \mathbf{QB} - \mathbf{p1}_m^T \\ \mathbf{f}^T - \mathbf{p}^T \mathbf{EQB} \end{bmatrix} \in \mathbb{R}^{3\times m}
\tag{3.2}
$$

In section 2.2.1.1, we introduced the feasibility problem 2.10 to verify that a given pose is inside or outside of the WCW of a PCDPM. However, we may as well use Stiemke's theorem [35] to verify whether a given pose is inside or outside the WCW. We recall this theorem as follows.

Theorem 2 (Stiemke's Theorem) *Dual WCW Membership Condition [2]*
A pose is outside the WCW of a PCDPM if and only if there exists a small-displacement screw $\boldsymbol{\lambda} \in \mathbb{R}^3$ *such that*

$$
\begin{aligned}
\mathbf{W}^T \boldsymbol{\lambda} &\succeq \boldsymbol{0}_m, \\
\mathbf{W}^T \boldsymbol{\lambda} &\neq \boldsymbol{0}_m.
\end{aligned}
\tag{3.3}
$$

A geometric interpretation of Stiemke's theorem may be obtained by considering $\boldsymbol{\lambda}$ as the normal of a supporting hyperplane, meaning that the convex cone formed by wrench vectors $\mathbf{x} : \mathbf{W}^T \mathbf{x} \succeq \boldsymbol{0}_m$, lies entirely on one side of the plane, as depicted in Fig.3.1. In order to give a physical interpretation to Stiemke's theorem, we may consider the vector $\boldsymbol{\lambda}$ as a small displacement screw [2]. In this case, the quantity $\mathbf{w}_i^T \boldsymbol{\lambda}$ represents the work done by the wrench i over the displacement represented by the screw $\boldsymbol{\lambda}$. Hence, the inequalities $\mathbf{W}^T \boldsymbol{\lambda} \succeq \boldsymbol{0}_m$ imply that there is a motion described by screw $\boldsymbol{\lambda}$, such that the work done by each of the cables is non-negative. The equality $\mathbf{W}^T \boldsymbol{\lambda} \neq \boldsymbol{0}_m$ further
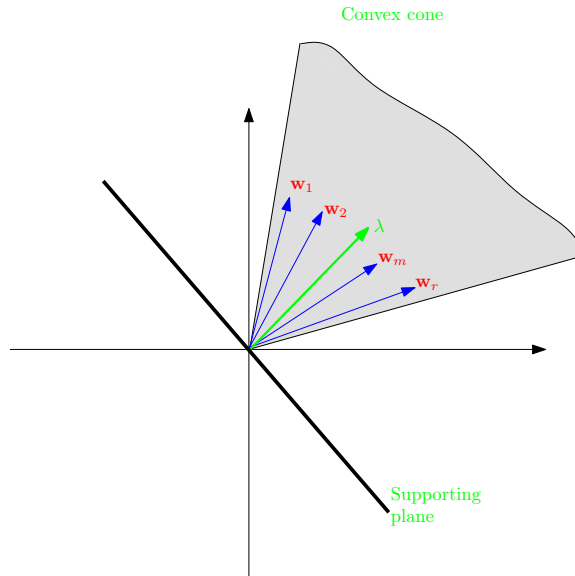
Figure 3.1: Geometric interpretation of Stiemke's theorem.

requires that at least one of the wrenches does strictly positive work. Therefore, the physical interpretation of Stiemke's theorem is that there is a motion for which the system of wrenches does positive work, while none of the cables does negative work.

We can now introduce the following feasibility problem to calculate the WCW of a PCDPM:

$$\mathbf{W}^T\boldsymbol{\lambda} \succeq \mathbf{0}_m,$$
$$\mathbf{1}_m^T\mathbf{W}^T\boldsymbol{\lambda} = 1. \tag{3.4}$$

This problem yields 0 whenever the given pose is outside of the corresponding WCW, and is infeasible otherwise. In other words, the given pose is outside of the WCW if the problem admits a feasible solution, and inside if it does not. Hence, this equation can be used to estimate the WCW of a given PCDPM by discretizing the examined region. This linear feasibility problem is to serve as the corner stone to the proposed formulation of the dimensional synthesis of PCDPMs.

3.2 Verifying Whether a Box Lies Inside the COWCW

We wish to determine whether a given small box lies completely inside the constant-orientation WCW of a given PCDPM. To this end, notice that the problem (3.4) can be turned into a phase-one problem as per the following Lemma.

Lemma 6 *Linear Program WCW Membership Condition*
Consider the linear program

$$
\begin{aligned}
\delta^* = \text{maximize} \quad & \delta, \\
\text{subject to} \quad & \mathbf{W}^T \boldsymbol{\lambda} \succeq \mathbf{0}_m, \\
& \mathbf{1}_m^T \mathbf{W}^T \boldsymbol{\lambda} \geq \delta, \\
\text{over} \quad & \boldsymbol{\lambda} \text{ and } \delta.
\end{aligned}
\tag{3.5}
$$

Then, we have

$$
\delta^* = \begin{cases} +\infty & \text{if the pose lies outside the WCW,} \\ 0 & \text{otherwise.} \end{cases}
\tag{3.6}
$$

Proof. First consider the case where the MP (Moving Platform) pose lies outside the WCW. From eq. (3.4), we then have a $\boldsymbol{\lambda}$ such that $\mathbf{W}^T \boldsymbol{\lambda} \succeq \mathbf{0}_m$ and $\mathbf{1}_m^T \mathbf{W}^T \boldsymbol{\lambda} = 1$. Thus, the point $(\boldsymbol{\lambda}, \delta) = (\boldsymbol{\lambda}, 1)$ lies in the feasible set of problem (3.5), and so do the points $(k\boldsymbol{\lambda}, k)$, where $k \geq 0$. In this latter case, the objective to be maximized is k, which can be chosen arbitrarily large, so that the optimization problem (3.5) becomes unbounded.

Second, we treat the case where the MP pose lies inside the WCW. Then, from Theorem 2, there exists no $\boldsymbol{\lambda}$ such that $\mathbf{W}^T \boldsymbol{\lambda} \succeq \mathbf{0}_m$ and $\mathbf{W}^T \boldsymbol{\lambda} \neq \mathbf{0}_m$. Conversely, any $\boldsymbol{\lambda} \in \mathbb{R}^3$ satisfying $\mathbf{W}^T \boldsymbol{\lambda} \succeq \mathbf{0}_m$ also satisfies $\mathbf{W}^T \boldsymbol{\lambda} = \mathbf{0}_m$. Substituting these results in eq. (3.5) inevitably leads to $\delta = 0$, provided that there exists a feasible $\boldsymbol{\lambda}$. Notice that $(\boldsymbol{\lambda}, \delta) = (\mathbf{0}_3, 0)$ is always a feasible point of problem (3.5), so that its optimum be always 0 when the pose lies inside the WCW. $\square$

Consider now a box $\mathcal{B}$ with the lower-left and upper-right corners $\underline{\mathbf{p}}$ and $\overline{\mathbf{p}}$, respectively, i.e., $\mathcal{B} = \{\mathbf{p} \in \mathbb{R}^2 : \underline{\mathbf{p}} \preceq \mathbf{p} \preceq \overline{\mathbf{p}}\}$. In order to find a necessary condition for $\mathcal{B}$ to

be outside of the COWCW, we substitute eq. (4.11) in problem (3.5),and we let $\mathbf{p}$ be a decision variables of the problem, while constraining it inside $\mathcal{B}$. This leads to

maximize $\quad \delta,$

subject to $\quad \mathbf{0}_m \preceq \mathbf{A}^T \boldsymbol{\mu} - \mathbf{Q}^T \mathbf{B}^T \boldsymbol{\mu} - \mathbf{1}_m \mathbf{p}^T \boldsymbol{\mu} + \mathbf{f} \mu_0 - \mathbf{B}^T \mathbf{Q}^T \mathbf{E}^T \mathbf{p} \mu_0,$

$$\delta \leq \mathbf{1}_m^T \mathbf{A}^T \boldsymbol{\mu} - \mathbf{1}_m^T \mathbf{Q}^T \mathbf{B}^T \boldsymbol{\mu} - m \mathbf{p}^T \boldsymbol{\mu} + \mathbf{1}_m^T \mathbf{f} \mu_0 - \mathbf{1}_m^T \mathbf{B}^T \mathbf{Q}^T \mathbf{E}^T \mathbf{p} \mu_0, \quad (3.7)$$

$$\underline{\mathbf{p}} \preceq \mathbf{p} \preceq \overline{\mathbf{p}},$$

over $\quad \mathbf{p}, \ \boldsymbol{\lambda} \equiv [\boldsymbol{\mu}^T \quad \mu_0]^T \text{ and } \delta.$

Considering $\mathbf{p}$, the operation-point position as an optimization variable, while the MP orientation ϕ remains constant, we obtain a nonlinear optimization problem which includes bilinear terms. This problem provides us a tool to find a necessary condition for a box to be outside of the COWCW, i.e., a condition that is necessarily met by any box $\mathcal{B}$ outside the WCW, but that may also be met by some boxes that are partly or completely inside this workspace. The approach consists in relaxing the constraints of problem (3.7), which makes it easier for a pose to be excluded from the COWCW.

To this end, let us define the variables

$$\boldsymbol{\nu} \equiv \mu_0 \mathbf{p} \qquad \text{and} \qquad \boldsymbol{\eta} \equiv \text{diag}(\boldsymbol{\mu}) \mathbf{p}, \qquad (3.8)$$

which represent the bilinear terms in eq. (3.7), when considering $\mathbf{p}$, $\boldsymbol{\mu}$ and μ_0 as optimization variables. While $\mathbf{p}$ is bounded, i.e.,

$$\underline{\mathbf{p}} \preceq \mathbf{p} \preceq \overline{\mathbf{p}}, \qquad (3.9)$$

the variables μ_0 and $\boldsymbol{\mu}$ remain unbounded. For the sake of this analysis, let us assume that the signs of μ_0 and $\boldsymbol{\mu}$ are known in advance, and label them

$$\sigma_0 \equiv \text{sgn}(\mu_0) \qquad \text{and} \qquad \boldsymbol{\sigma} \equiv \text{sgn}(\boldsymbol{\mu}), \qquad (3.10)$$

where sgn() represents the signum function. Knowing the signs of μ_0 and $\boldsymbol{\mu}$, we can generate the following bounds on $\boldsymbol{\nu}$ and $\boldsymbol{\eta}$:

$$\sigma_0 \underline{\mathbf{p}} \mu_0 \preceq \sigma_0 \boldsymbol{\nu} \preceq \sigma_0 \overline{\mathbf{p}} \mu_0,$$

$$\text{diag}(\boldsymbol{\sigma}) \text{diag}(\underline{\mathbf{p}}) \boldsymbol{\mu} \preceq \text{diag}(\boldsymbol{\sigma}) \boldsymbol{\eta} \preceq \text{diag}(\boldsymbol{\sigma}) \text{diag}(\overline{\mathbf{p}}) \boldsymbol{\mu}. \qquad (3.11)$$

When treating σ_0 and $\boldsymbol{\sigma}$ as constants, the set formed by eq. (3.11) represents a convex polyhedron, which approximates the non-convex surfaces of eq. (3.8). Therefore,

replacing the latter with the former, we obtain a *convex relaxation* of eq. (3.8). This approximation converges to the exact relationship as the size of box $\mathcal{B}$ becomes infinitesimal. This approach is called the reformulation-linearization technique (RLT), and was originally proposed by Sherali and Tuncbilek [36]. Hence, the relaxed form of problem (3.7) is

$$
\begin{aligned}
\text{maximize} \quad & \delta, \\
\text{subject to} \quad & \mathbf{A}^T \boldsymbol{\mu} - \mathbf{Q}^T \mathbf{B}^T \boldsymbol{\mu} - \mathbf{1}_m \mathbf{1}_2^T \boldsymbol{\eta} + \mathbf{f}\mu_0 - \mathbf{B}^T \mathbf{Q}^T \mathbf{E}^T \boldsymbol{\nu} \succeq \mathbf{0}_m, \\
& \mathbf{1}_m^T \mathbf{A}^T \boldsymbol{\mu} - \mathbf{1}_m \mathbf{Q}^T \mathbf{B}^T \boldsymbol{\mu} - m \mathbf{1}_2^T \boldsymbol{\eta} + \mathbf{1}_m^T \mathbf{f}\mu_0 - \mathbf{1}_m^T \mathbf{B}^T \mathbf{Q}^T \mathbf{E}^T \boldsymbol{\nu} \geq \delta, \\
& \sigma_0 \underline{\mathbf{p}}\mu_0 \preceq \sigma_0 \boldsymbol{\nu} \preceq \sigma_0 \overline{\mathbf{p}}\mu_0, \\
& \text{diag}(\boldsymbol{\sigma})\text{diag}(\underline{\mathbf{p}})\boldsymbol{\mu} \preceq \text{diag}(\boldsymbol{\sigma})\boldsymbol{\eta} \preceq \text{diag}(\boldsymbol{\sigma})\text{diag}(\overline{\mathbf{p}})\boldsymbol{\mu}, \\
& \sigma_0 = \text{sgn}(\mu_0), \quad \boldsymbol{\sigma} = \text{sgn}(\boldsymbol{\mu}).
\end{aligned}
\tag{3.12}
$$

The only non-convex constraints in problem (3.12) are the last two equalities. However, these equalities yield exactly eight possible combinations of σ_0 and $\boldsymbol{\sigma}$, which are the solutions to

$$
\sigma_0^2 = 1 \qquad \text{and} \qquad \text{diag}(\boldsymbol{\sigma})^2 = \mathbf{1}_{2\times 2}.
\tag{3.13}
$$

Let us label these solutions $\sigma_{0,j}$ and $\boldsymbol{\sigma}_j$, $j = 1, \ldots, 8$. As a result, the solution to problem (3.12) is the maximum of the outcomes of the eight resulting linear programs. This leads to following Lemma.

Lemma 7 *Linear Sufficient Conditions for a Box to Lie Inside the WCW*
Consider the eight distinct linear programs

$$
\begin{aligned}
\text{maximize} \quad & \delta_j, \\
\text{subject to} \quad & \mathbf{G}_j \boldsymbol{\xi}_j \preceq \mathbf{0}_{m+9}, \\
& j = 1, \ldots, 8.
\end{aligned}
\tag{3.14}
$$

where $\mathbf{G}_j \equiv \begin{bmatrix} \mathbf{g}^T & 1 \\ \mathbf{R}_j^T & \mathbf{0}_{m+24} \end{bmatrix} \in \mathbb{R}^{(m+9)\times 8}$,

$$\mathbf{g} \equiv \begin{bmatrix} -\mathbf{1}_m^T(\mathbf{A}-\mathbf{QB})^T & -\mathbf{1}_m^T\mathbf{f} & \mathbf{1}_m^T\mathbf{B}^T\mathbf{Q}^T\mathbf{E}^T & m\mathbf{1}_2^T \end{bmatrix}^T \in \mathbb{R}^7,$$

$$\mathbf{R}_j \equiv \begin{bmatrix} -(\mathbf{A}-\mathbf{QB})^T & -\mathbf{f} & \mathbf{B}^T\mathbf{Q}^T\mathbf{E}^T & \mathbf{1}_m\mathbf{1}_2^T \\ \mathbf{0}_{2\times2} & \sigma_{0,j}\underline{\mathbf{p}} & -\sigma_{0,j}\mathbf{1}_{2\times2} & \mathbf{0}_2 \\ \mathbf{0}_{2\times2} & -\sigma_{0,j}\overline{\mathbf{p}} & \sigma_{0,j}\mathbf{1}_{2\times2} & \mathbf{0}_2 \\ diag(\boldsymbol{\sigma}_j)diag(\underline{\mathbf{p}}) & \mathbf{0}_2 & \mathbf{0}_{2\times2} & -diag(\boldsymbol{\sigma}_j) \\ -diag(\boldsymbol{\sigma}_j)diag(\overline{\mathbf{p}}) & \mathbf{0}_2 & \mathbf{0}_{2\times2} & diag(\boldsymbol{\sigma}_j) \end{bmatrix}^T \in \mathbb{R}^{7\times(m+8)},$$

and $\boldsymbol{\xi}_j = \begin{bmatrix} \boldsymbol{\mu}_j^T & \mu_{0,j} & \boldsymbol{\nu}_j^T & \boldsymbol{\eta}_j^T & \delta_j \end{bmatrix}^T \in \mathbb{R}^8.$

Then the given box $\mathcal{B} = \{\mathbf{p} \in \mathbb{R}^2 : \underline{\mathbf{p}} \preceq \mathbf{p} \preceq \overline{\mathbf{p}}\}$ *is fully inside the WCW if all of the problems (3.14), $j = 1,\ldots,8$, yield zero.*

Proof. First consider a box which is outside of the OWCW. According to Lemma 6, for all positions $\mathbf{p}$ inside this box, problem (3.7) is unbounded. Since this is a maximization problem, the solution of its relaxed form in eq. (3.12) provides a upper bound to the true solution. This means that problem (3.12) is also unbounded whenever the box is outside the COWCW. On the other hand, the solution to problem (3.7) is the maximum outcome of the eight linear programs of problem (3.14). Hence, at least one of the eight distinct linear programs in eq. (3.14) is unbounded whenever the box is outside of the COWCW. Second, $\begin{bmatrix} \boldsymbol{\mu}^T & \mu & \boldsymbol{\nu}^T & \boldsymbol{\eta}^T & \delta \end{bmatrix}^T = \mathbf{0}_8$ is always feasible for problem (3.12), which implies that whenever all positions $\mathbf{p}$ of the given box are inside the WCW, problem (3.12) yields zero. Since the solution to problem (3.12) is the maximum outcome of the eight distinct LPs of eq. (3.14), and because $\boldsymbol{\xi}_j = \mathbf{0}_8$, $j = 1,\ldots,8$, is always feasible, a given box is completely inside the COWCW whenever all these LPs yield zero. $\square$

Figure 3.2 shows an example of the effect of the proposed convex relaxation on the estimated COWCW. The considered PCDPM is the same as in Fig. 2.3, and the corresponding geometry appears in the foreground of Fig 3.11. We calculate the real-constant orientation wrench-closure workspace (COWCW) of this mechanism for $\phi = .02$ rad. by discretizing the examined region into several points and solving problem (3.4) for each of them. Upon partitioning the plane into boxes instead of points and solving the relaxed problem (3.14) for each box, we obtain a contracted COWCW. In this figure the real COWCW is represented by a cloud of points, while the contracted

COWCW is the negative of the area covered with boxes. As can be seen from this figure, relaxing the constraints results in an underestimation of the corresponding COWCW. In this example, we used square boxes with edge lengths of 0.1. Smaller boxes would have led to a better estimate of the COWCW, as the convex relaxation (3.11) then forms a tighter approximation of (3.8). As they were obtained in problem (3.14), the
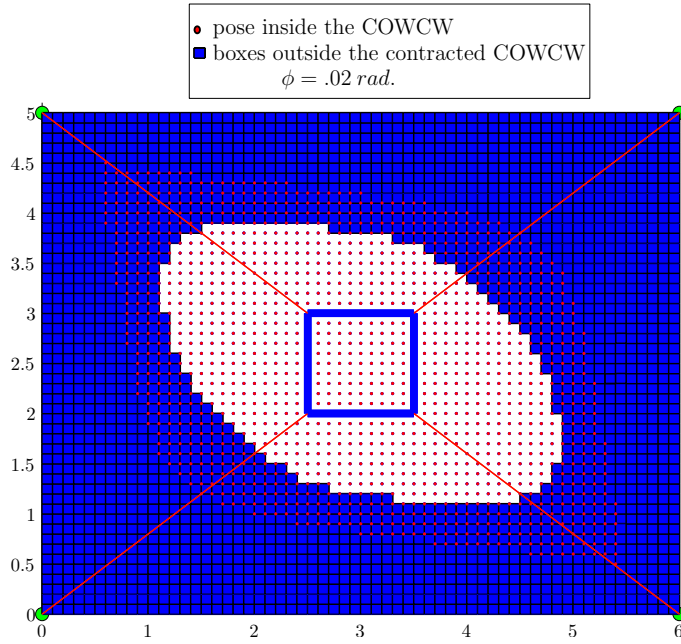
Figure 3.2: Contracted and real COWCW of a PCDPM.

inequality constraints can always be satisfied by choosing $\boldsymbol{\xi}_j = \mathbf{0}_8$. For the purpose of later assembling them, we would like these constraints to be feasible only if a given box is fully inside the WCW. To this end, we compute the Lagrange dual [37] of problem (3.14). In the case of linear programs, recall that either of the following cases may occur [38]:

1. The primal problem admits a feasible solution and has an unbounded objective value, in which case the dual problem is infeasible;

2. The dual problem admits a feasible solution and has an unbounded objective value, in which case the primal problem is infeasible;

3. Both problems admit feasible solutions, in which case both problems have equal optimal values;

4. Both problems are infeasible.

In order to obtain its Lagrange dual, let us start by writing the Lagrangian of problem (3.14),

$$L(\mathbf{x}_j, \boldsymbol{\xi}_j) = \mathbf{x}_j^T \mathbf{G}_j \boldsymbol{\xi}_j - \delta_j, \tag{3.15}$$

where $\mathbf{x}_j \in \mathbb{R}_+^{m+9}$ is the vector of Lagrange multipliers and $\mathbb{R}_+$ represents the non-negative real numbers. Hence, the Lagrange dual problem 3.14is that of maximizing $\theta(\mathbf{x}_j)$, where

$$\theta(\mathbf{x}_j) = \inf_{\boldsymbol{\xi}_j} \ L(\mathbf{x}_j, \boldsymbol{\xi}_j), \quad j = 1, \ldots, 8. \tag{3.16}$$

Recalling that $\delta_j = \mathbf{e}_8^T \boldsymbol{\xi}_j$, where $\mathbf{e}_8 \equiv [\mathbf{0}_7^T \quad 1]^T \in \mathbb{R}^8$, and substituting eq. (3.15) into eq. (3.16) gives

$$\theta(\mathbf{x}_j) = \inf_{\boldsymbol{\xi}_j} (\mathbf{x}_j^T \mathbf{G}_j - \mathbf{e}_8^T) \boldsymbol{\xi}_j. \tag{3.17}$$

where inf refers to the infimum of its argument. Clearly,

$$\theta(\mathbf{x}_j) = \begin{cases} 0 & \text{if } \mathbf{G}_j^T \mathbf{x}_j = \mathbf{e}_8, \\ -\infty & \text{otherwise.} \end{cases} \tag{3.18}$$

Hence, the dual of problem (3.14) can be stated as the feasibility problem

$$\begin{aligned} \text{maximize} \quad & 0, \\ \text{subject to} \quad & \mathbf{G}_j^T \mathbf{x}_j - \mathbf{e}_8 = \mathbf{0}_8, \\ & \mathbf{x}_j \succeq \mathbf{0}_{m+9}, \end{aligned} \tag{3.19}$$

for a given value of $j = 1, \ldots, 8$. The last equality constraint of this program implies that $\mathbf{x}_{j,1} - 1 = 0$. Substituting this in eq. (3.19) eliminates $\mathbf{x}_{j,1}$ as a variable and reduces the number of equality constraints from eight to seven. Therefore, for given $\sigma_{0,j}$ and $\boldsymbol{\sigma}_j$, the corresponding dual problem is

$$\begin{aligned} \text{maximize} \quad & 0, \\ \text{subject to} \quad & \mathbf{R}_j \mathbf{y}_j + \mathbf{g} = \mathbf{0}_7, \\ & \mathbf{y}_j \succeq \mathbf{0}_{m+8}, \\ \text{over} \quad & \mathbf{y}_j, \end{aligned} \tag{3.20}$$

where $\mathbf{y}_j \in \mathbb{R}_+^{m+8}$ represents the vector of Lagrange multipliers.

Problem (3.20) is equivalent to its primal problems (3.14) but is feasible when all problems (3.14) yield zero and is infeasible when any of them is unbounded. These correspond to cases 3. and 1., respectively, of the primal-dual relationships enumerated

above. We may combine all of these distinct linear programs into one in order to verify whether a given box $[\underline{\mathbf{p}} \ \overline{\mathbf{p}}]$ is inside the WCW of a given PCDPM. This can be done by summing the objective values of these problems while considering their constraints all together as follows:

$$
\begin{aligned}
\text{maximize} \quad & 0, \\
\text{subject to} \quad & \mathbf{R}_j \mathbf{y}_j + \mathbf{g} = \mathbf{0}_7, \ \ j = 1, \dots, 8, \\
\text{over} \quad & \mathbf{y}_j \succeq \mathbf{0}_{m+8}, \ \ j = 1, \dots, 8.
\end{aligned}
\tag{3.21}
$$

Notice that eq. (3.20) represents eight distinct linear programs while eq. (3.21) represents only one, with eight times more constraint equations and variables. Equation (3.21) may now be regarded as a single feasibility problem of 56 linear equations into $8m + 64$ non-negative decision variables. This linear program yields the same results as its primal problems, to the difference that it is feasible only when the corresponding box is completely inside the WCW. Having this information, we can now turn our attention to the synthesis problem.

3.3 A Formulation for the Problem of Synthesizing a PCDPM for Constant Orientations

Problem (3.21) serves as a building brick to formulate the dimensional synthesis of PCDPMs. Suppose we are interested in finding a PCDPM geometry whose constant-orientation WCW contains a given box $\mathcal{B}$. In order to solve this problem, we introduce the nonlinear feasibility problem

$$
\begin{aligned}
& \mathbf{R}_j \mathbf{y}_j + \mathbf{g} = \mathbf{0}_7, \\
& \mathbf{y}_j \succeq \mathbf{0}_{m+8}, \ \ j = 1, \dots, 8, \\
& \underline{\mathbf{a}} \preceq \mathbf{a}_i \preceq \overline{\mathbf{a}}, \ \ \underline{\mathbf{b}} \preceq \mathbf{b}_i \preceq \overline{\mathbf{b}}, \ \ i = 1, \dots, m, \\
& \text{over } \mathbf{y}_j \in \mathbb{R}_+^{m+8}, \ \ \mathbf{a}_i \in \mathbb{R}^2, \ \ \mathbf{b}_i \in \mathbb{R}^2.
\end{aligned}
\tag{3.22}
$$

Here, $\underline{\mathbf{a}}$, $\overline{\mathbf{a}}$, $\underline{\mathbf{b}}$ and $\overline{\mathbf{b}}$ are lower and upper bounds on the positions of the base and MP attachments points, which would otherwise be drawn to infinity during the solution process. Problem (3.22) is a nonlinear feasibility problem with $12m + 64$ variables and 56 equality constraints. If it exists, the associated solution yields a PCDPM geometry

whose COWCW is guaranteed to include the prescribed box $\mathcal{B}$. On the other hand, the absence of a solution to this problem does not imply that there is no possible PCDPM geometry containing $\mathcal{B}$. Hence, this method lacks practicality, since failing to obtain a feasible solution does not provide any information regarding a *good* but *not perfect* geometry. For this reason introducing an objective function is thought to be more attractive to the designers. This is the object of the following section.

3.3.1   Introducing an Objective Function

Suppose we want to find the geometry of a PCDPM whose COWCW includes a given box for a given orientation angle ϕ. Evidently, if we use a scaled version of this box in problem (3.22) and can find a geometry of a PCDPM whose COWCW allows for a scaling factor above one, then the original problem is solved. Quite naturally, the idea is to consider the scaling factor as an objective function to be maximized. If, at the optimum point, this factor is smaller than one, then the designer is left with the best infeasible solution.

This scaling process is depicted in Fig. 3.3 for a prescribed box. The box $\mathcal{B}'$ with dashed lines in blue is the scaled image of the smaller one with solid lines in red. The scaling factor is s and the scaling point is C. From this figure, we obtain the lower-left
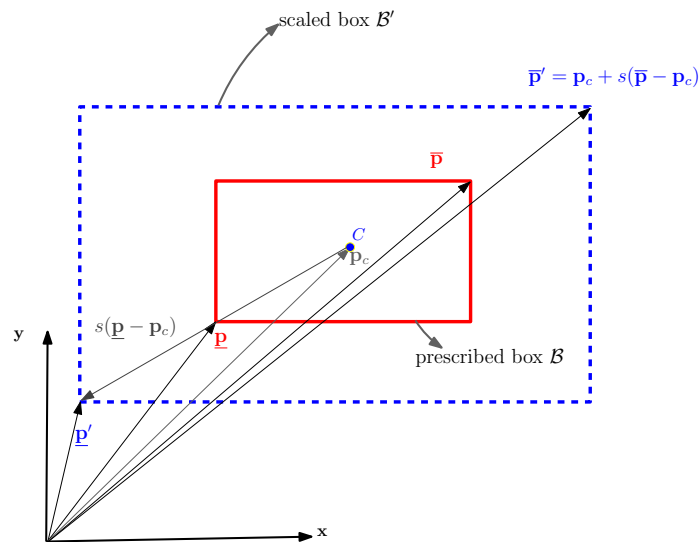
Figure 3.3: An scaled-up box and its corresponding parameters.

and upper-right coordinates of the scaled box $\mathcal{B}'$ as

$$\underline{\mathbf{p}}' = \mathbf{p}_c + s(\underline{\mathbf{p}} - \mathbf{p}_c) \text{ and } \overline{\mathbf{p}}' = \mathbf{p}_c + s(\overline{\mathbf{p}} - \mathbf{p}_c), \tag{3.23}$$

respectively. Vector $\mathbf{p}_c$ and scalar s represent the position of the homothetic center C and the scaling factor, respectively. If we consider the centroid of the box as the scaling point, then $\mathbf{p}_c = \frac{1}{2}(\overline{\mathbf{p}} + \underline{\mathbf{p}})$. Introducing this objective function enables us to develop a nonlinear program for the dimensional synthesis of PCDPMs.

3.3.2 A Nonlinear Program for the Dimensional Synthesis of PCDPMs in Translation

We now turn the feasibility problem (3.22) into a nonlinear program where $\mathbf{R}'_j$ is obtained by substituting $\overline{\mathbf{p}}'$ and $\underline{\mathbf{p}}'$ for $\overline{\mathbf{p}}$ and $\underline{\mathbf{p}}$, respectively, in the expression of $\mathbf{R}_j$ given in problem (3.14). Moreover, to ensure that $\underline{\mathbf{p}}'$ and $\overline{\mathbf{p}}'$ remain the lower left and upper-right corners of the scaled box, we constrain the scaling factor s to the non-negative real numbers.

$$
\begin{aligned}
\text{maximize} \quad & s \\
\text{subject to} \quad & \mathbf{R}'_j \mathbf{y}_j + \mathbf{g} = \mathbf{0}_7, \\
& \underline{\mathbf{p}}' - \mathbf{p}_c - s(\underline{\mathbf{p}} - \mathbf{p}_c) = \mathbf{0}_2, \\
& \overline{\mathbf{p}}' - \mathbf{p}_c - s(\overline{\mathbf{p}} - \mathbf{p}_c) = \mathbf{0}_2, \\
& \underline{\mathbf{a}} \preceq \mathbf{a}_i \preceq \overline{\mathbf{a}}, \ \ \underline{\mathbf{b}} \preceq \mathbf{b}_i \preceq \overline{\mathbf{b}}, \ \ i = 1, \dots, m, \\
& \mathbf{y}_j \succeq \mathbf{0}_{m+8}, \ \ j = 1, \dots, 8, \\
& s \ \geq 0, \\
\text{over} \quad & \mathbf{y}_j \in \mathbb{R}_+^{m+8}, \ \ \mathbf{a}_i \in \mathbb{R}^2, \ \ \mathbf{b}_i \in \mathbb{R}^2, \ \ s \in \mathbb{R}.
\end{aligned} \tag{3.24}
$$

As the problem is non-convex, the geometry obtained by finding a local maximum of problem (3.24) highly depends on the chosen initial guess. We illustrate this with a synthesis example in the following section.

Example 3.1 Constant Orientation WCW for a Given Box

Figure 3.4 shows an illustrative example of the results obtained through the formulation of eq. (3.24). The assumed upper and lower bounds for the geometry of the

mechanism and the lower-left and upper-right coordinates of the given box that need to be inside of the constant orientation WCW for the rotation angle $\phi = 0$ are given in Table 3.1. The number of cables is set to $m = 4$, which is the minimum necessary for a WCW to exist. In order to solve the problem, we need to begin with an initial guess on the decision variables. The initial guess of the geometry is reported in Table 3.2, while we choose $\mathbf{y}_{j,0} = \mathbf{0}_{m+8}$, $j = 1, \ldots, 8$, and $s_0 = 0$ for the remaining variables. The prescribed box appears in solid black lines and the resulting scaled box is in dashed red lines. The resulting robot geometry is also shown in Fig. 3.4, which is obtained by applying a descent method to the problem (3.24). The precise numerical values of the obtained geometry are listed in Table 3.3.

This PCDPM design was computed by resorting to the *fmincon* function of Matlab 7.6.0 *R2008a*, with its default *active-set* algorithm. This algorithm solves nonlinear programs by sequential quadratic programming (SQP). For this example, it takes 12.52 seconds to obtain the result by using a desktop computer equipped with an Intel(R) Core(TM)2 CPU 6400 @ 2.13GHz, and 4GB RAM. Figures 3.5 and 3.6 show respectively the evolutions of the scaling factor and the geometry of the robot from the initial guess to the final local optimum.
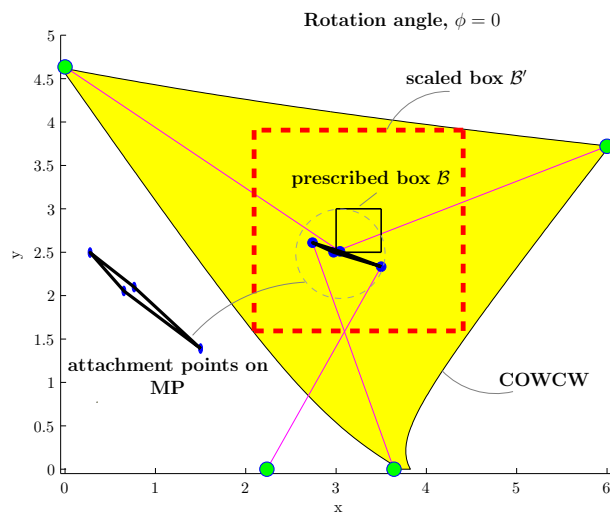
Figure 3.4: Geometry obtained for a PCDPM with four cables and constant orientation for a given box.

The optimum value of the scaling factor is $s^* = 4.6298 \geq 1$, which means that the scaled box and the original box are both inside the resulting COWCW. Notice that we applied the method proposed in [2] with the algorithm proposed in [39] in order to
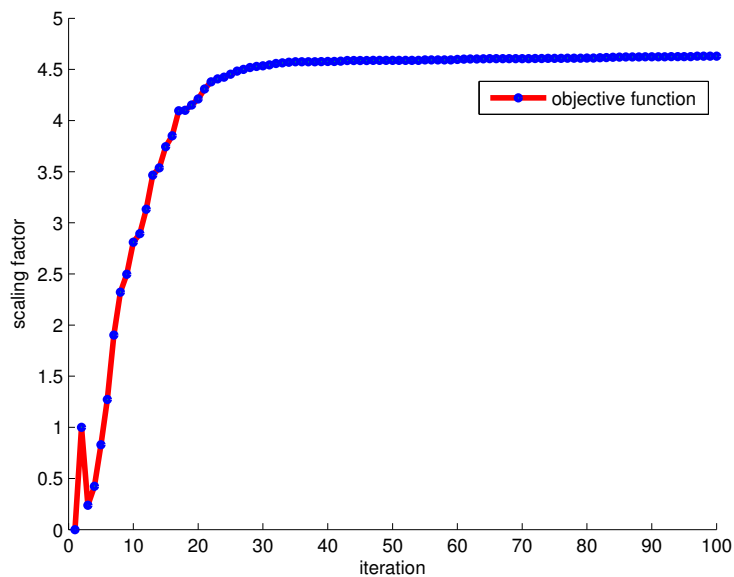
Figure 3.5: Evolutions of the scaling factor during the solution procedure.
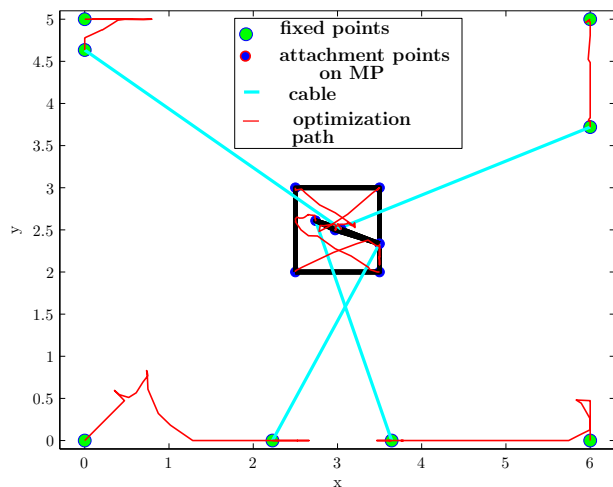
Figure 3.6: Variations of the geometry of the robot from the initial guess to the final solution.

calculate the WCW, which is represented by the yellow region in Fig. (3.4). This figure confirms that the scaled box, and, consequently, the prescribed box, are both located inside of the constant orientation WCW.

Let us now change the initial guess only by modifying $\mathbf{a}_{i,0}$ to $3\mathbf{a}_{i,0}$, $\mathbf{b}_{i,0}$ to $3\mathbf{b}_{i,0}$, $i = 1, \ldots, 4$, while setting $s_0 = 1$ and leaving the other variables as they were before.

Table 3.1: Assumed parameters for example 3.1.

$\underline{\mathbf{a}}^T$	$\overline{\mathbf{a}}^T$	$\underline{\mathbf{b}}^T$	$\overline{\mathbf{b}}^T$	$\underline{\mathbf{p}}_k^T$	$\overline{\mathbf{p}}_k^T$
[0 0]	[6 5]	[−.5 − .5]	[.5 .5]	[3 2.5]	[3.5 3]

Table 3.2: Initial geometry of example 3.1.

i	$\mathbf{a}_{i,0}^T$	$\mathbf{b}_{i,0}^T$
1	[0 0]	[−.5 − .5]
2	[6 0]	[.5 − .5]
3	[6 5]	[.5 .5]
4	[0 5]	[−.5 .5]

Solving the problem with this modified initial guess yields $s^* = 4.6683$, a slightly better result, and the geometry shown in Fig. 3.3.2. Notice that we obtained two completely different geometries for the same box, only by changing the initial guess. The detailed values of the resulting geometry for the modified initial guess are reported in Table 3.4. This example confirms that the initial guess can have a great effect on the obtained geometry.

Table 3.3: Obtained geometry of example 3.1.

i	$\mathbf{a}_i^T$	$\mathbf{b}_i^T$
1	[2.2339 0.0000]	[0.5000 − 0.1669]
2	[3.6406 0.0000]	[−0.2600 0.1097]
3	[6.0000 3.7216]	[−0.0277 − 0.0008]
4	[0.0000 4.6358]	[0.0434 0.0102]

In the foregoing examples, we assumed a constant orientation angle to solve the dimensional synthesis of PCDPMs. Although one may think of applications, e.g., in haptics [11], where the MP should undergo pure translations while being able to apply moments, in general, the MP is required to rotate and translate in the plane. Therefore, we have to investigate the synthesis problem for different orientations as well. This is the topic of the next section.

Table 3.4: Obtained geometry with modified initial guess of example 3.1.

i	$\mathbf{a}_i^T$	$\mathbf{b}_i^T$
1	$[0.1014 \quad 0.0000]$	$[0.4335 \quad -0.1433]$
2	$[5.9631 \quad 0.0000]$	$[-0.5000 \quad 0.1379]$
3	$[6.0000 \quad 4.8535]$	$[-0.2416 \quad -0.0782]$
4	$[0.0000 \quad 4.9203]$	$[0.1015 \quad 0.1668]$
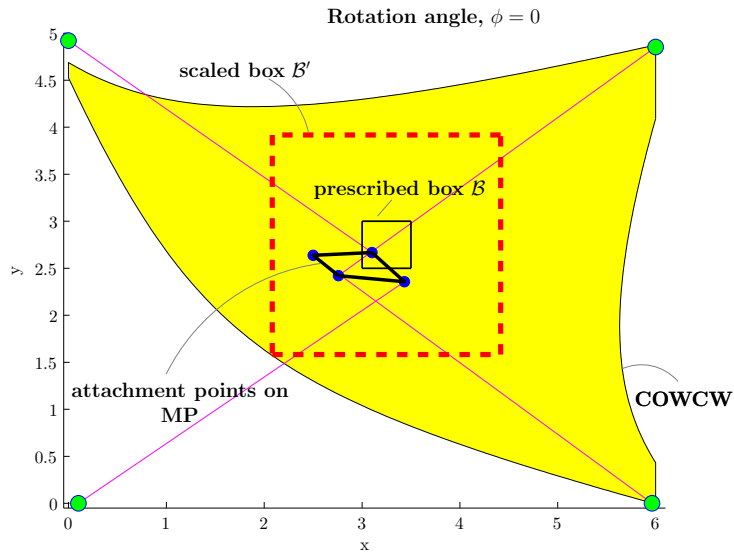
3.3.3 The Dimensional Synthesis of PCDPMs for Different MP Distinct Orientations

We show that formulation (3.24) can be developed to find the geometry of a PCDPM whose COWCWs includes a given box including several orientation angles. In order to solve such a problem, we discretize along the ϕ axis, i.e., we combine the nonlinear programs of (3.24) defined for a set of fixed orientation angles. Evidently, this increases the numbers of constraints and variables. More precisely, if the number of fixed orientation

angles is n, then the nonlinear program to solve the dimensional synthesis problem is

$$
\begin{aligned}
\text{maximize} \quad & s \\
\text{subject to} \quad & \mathbf{R}_{k,j}\mathbf{y}_{k,j} + \mathbf{g}_k = \mathbf{0}_7, \qquad\qquad\qquad\qquad (3.25)\\
& \underline{\mathbf{p}}'_k - \mathbf{p}_c - s(\underline{\mathbf{p}}_k - \mathbf{p}_c) = \mathbf{0}_2, \\
& \overline{\mathbf{p}}'_k - \mathbf{p}_c - s(\overline{\mathbf{p}}_k - \mathbf{p}_c) = \mathbf{0}_2, \\
& \underline{\mathbf{a}} \preceq \mathbf{a}_i \preceq \overline{\mathbf{a}}, \ \ \underline{\mathbf{b}} \preceq \mathbf{b}_i \preceq \overline{\mathbf{b}}, \ \ i = 1,\ldots,m, \\
& s \geq 0, \\
& \mathbf{y}_{k,j} \succeq \mathbf{0}_{m+8}, \ \ j = 1,\ldots,8, \ \ k = 1,\ldots,n, \\
\text{over} \quad & \mathbf{y}_{k,j} \in \mathbb{R}^{m+8}, \ \ \mathbf{a}_i \in \mathbb{R}^2, \ \ \mathbf{b}_i \in \mathbb{R}^2, s \in \mathbb{R}.
\end{aligned}
$$

Notice that constructing the matrix $\mathbf{R}_{k,j}$ and vector $\mathbf{g}_k$ requires substituting the corresponding orientation angle ϕ_k in eq. (3.14). Problem (3.25) is a nonlinear non-convex program with $(8m + 64)n + 4m + 1$ variables, $60n$ equality, and $(8m + 64)n + 8m + 1$ inequality constraints. We illustrate this approach with the following example.

Example 3.2 A Prescribed Box at Different Orientations

Suppose we have a given box with the same coordinates as in example 3.1. We seek a PCDPM whose constant-orientation WCWs include the prescribed box for three different orientations: $\phi_1 = -\frac{\pi}{6}, \phi_2 = 0$ and $\phi_3 = \frac{\pi}{6}$. We set the lower and upper bounds on the geometry to the values given in Table 3.7, and the initial guess is the same as the one displayed in Fig. 3.4. We use the "trust-region-reflective" algorithm of Matlab to solve the problem (3.25), which is called through the *fmincon* command. This method is based on the gradients, which generally accelerates the calculations when these gradiants are specified by the user. The symbolic expressions of the gradients of problem (3.25) are reported in Appendix A. Using the machine mentioned in example 3.1, *fmincon* yields $s^* = 4.3568$, and the obtained geometry is shown in Table 3.5, after a computation time of 161.3 seconds.

This geometry and the corresponding constant orientation WCW for $\phi = 0$ is depicted in Fig. 3.7. Figure 3.8 shows the COWCWs corresponding to the chosen values of ϕ, the prescribed boxes, and their scaled version all together. One can easily verify that all of these COWCWs include the scaled version of the given box.

In this section and the previous one, we developed formulations to find the geometry

Table 3.5: Obtained geometry for three prescribed orientation angles.

i	$\mathbf{a}_i^T$	$\mathbf{b}_i^T$
1	$[0.0000 \quad 0.0000]$	$[0.3729 \quad -0.5000]$
2	$[5.1281 \quad 0.0000]$	$[-0.2570 \quad -0.1436]$
3	$[6.0000 \quad 5.0000]$	$[-0.1238 \quad -0.1244]$
4	$[0.0000 \quad 5.0000]$	$[0.1690 \quad 0.3179]$
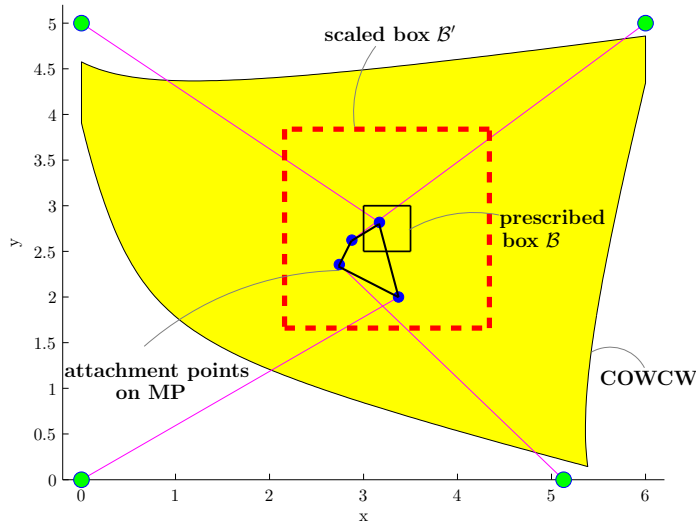
Figure 3.7: Geometry obtained for a PCDPM with four cables for the prescribed box and orientation angle $\phi = 0$.

of a PCDPM whose COWCW includes a given box. In the next section, we show that the proposed approach can be used to synthesize PCDPMs for prescribed workspaces that are non-rectangular.

3.3.4 The Constant-Orientation Dimensional Synthesis of PCDPMs for Non-Rectangular Prescribed Workspaces

Since the main challenge of the synthesis problem consists in finding a PCDPM whose WCW contains a prescribed workspace with an irregular shape, we may estimate such a shape by multiple boxes. To this end, we use interval analysis [40] as a tool to over-estimate the prescribed workspace with a set of boxes. The procedure consists
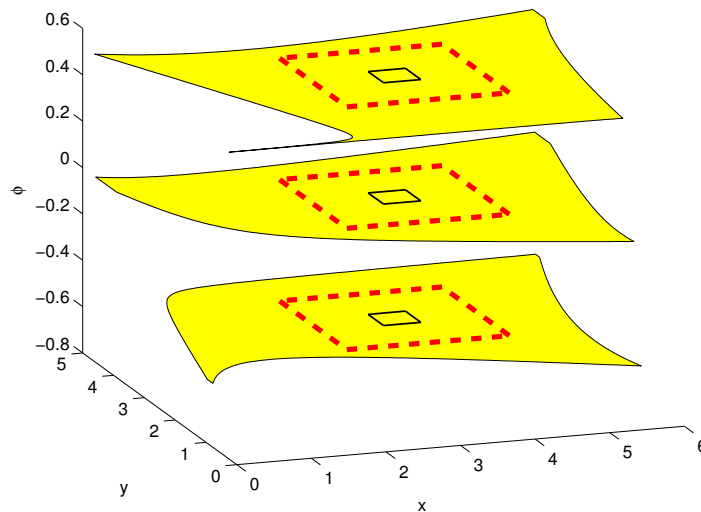
Figure 3.8: Constant orientation WCWs of the obtained geometry with the prescribed and the resulting scaled boxes.

in considering a large rectangle that includes the prescribed workspace. Dividing this large rectangle along its longer edge into smaller boxes, provides two new boxes which are examined to verify whether they are inside or outside the prescribed workspace. When a box is found to be completely inside or outside of the prescribed workspace, then it is marked as a certain box and put aside. Otherwise, the box remains uncertain box and must be divided into two smaller boxes. Again, we examine these new boxes to verify whether they are completely inside or outside the prescribed workspace. The procedure ends whenever the total number of certain and uncertain boxes reaches a given maximum number of boxes. Evidently, larger numbers of boxes provide more precise estimates of the prescribed workspace.

In order to solve the dimensional synthesis problem for a prescribed workspace composed of multiple boxes, we reuse (3.25), which can already accommodate an arbitrary number of boxes. Recall that this is a nonlinear program with $n(8m + 64) + 4m + 1$ variables, $60n$ equality, and $(8m + 64)n + 8m + 1$ inequality constraints. Evidently, depending on the number of boxes required, this problem can become a medium or even large-scale nonlinear program. Problem (3.25) provides us with a tool to find a PCDPM whose single or multiple COWCWs include a prescribed workspace. We illustrate formulation (3.25) for a constant-orientation synthesis example in the following section.

Example 3.3 Synthesis of a PCDPM for a Non-Rectangular Prescribed Constant-Orientation Workspace

Suppose we want to find the geometry of a PCDPM whose constant-orientation WCW at $\phi = 0$, includes the unit disk $(x - 3)^2 + (y - 2)^2 \leq 1$. In order to ensure that the entirety of the disk is covered with boxes, we may keep both the certainly-inside boxes and the uncertain boxes provided by an interval analysis method. But this approach will unnecessarily increase the number of boxes which may lead to longer calculation time and memory error. To avoid this, we may overestimate this disk by approximating a slightly larger disk $\mathcal{C}_s$, $(x - 3)^2 + (y - 2)^2 \leq 1.2^2$ whose certainly inside boxes cover the entire unit disk. We approximate disk $\mathcal{C}_s$, by means of interval analysis, as depicted in Fig. 3.9. As seen in this figure, the certainly-inside boxes of
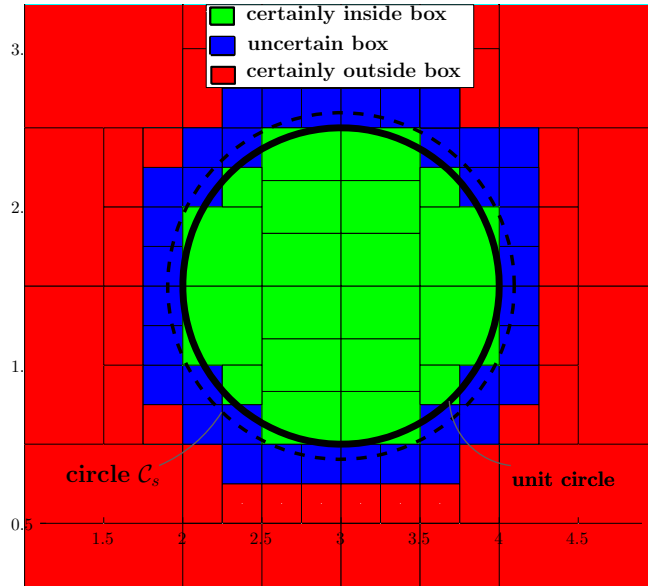
Figure 3.9: Approximating a unit disk with multiple boxes.

disk $\mathcal{C}_s$, which are depicted in green, cover the entire unit disk.

For this estimation we have $n = 20$ prescribed boxes, and the parameters are the same as in Example 3.1, to the difference that the initial guess is $\mathbf{y}_{j,0} = \mathbf{1}_{m+8}$, $j = 1, \ldots, 8$, and $s_0 = 0.1$. We use the same algorithm as for Example 3.2 to solve problem (3.25). With the assumed parameters, the optimum solution is $s^* = 1.2317$, and the detailed values of the obtained geometry are reported in Table 3.6. Since s^* is greater than one, the prescribed workspace is located inside the constant-orientation WCW. Fig. 3.10 shows the obtained geometry and the corresponding COWCW for this

Table 3.6: Obtained geometry for the estimated prescribed workspace with multiple boxes depicted in of example 3.3.

i	$\mathbf{a}_i^T$	$\mathbf{b}_i^T$
1	$[0.3392 \quad 0.0000]$	$[0.4991 \quad 0.0219]$
2	$[6.0000 \quad 0.0000]$	$[-0.1651 \quad -0.1187]$
3	$[6.0000 \quad 2.2082]$	$[-0.1581 \quad 0.5000]$
4	$[1.9459 \quad 4.9996]$	$[0.4933 \quad -0.1746]$
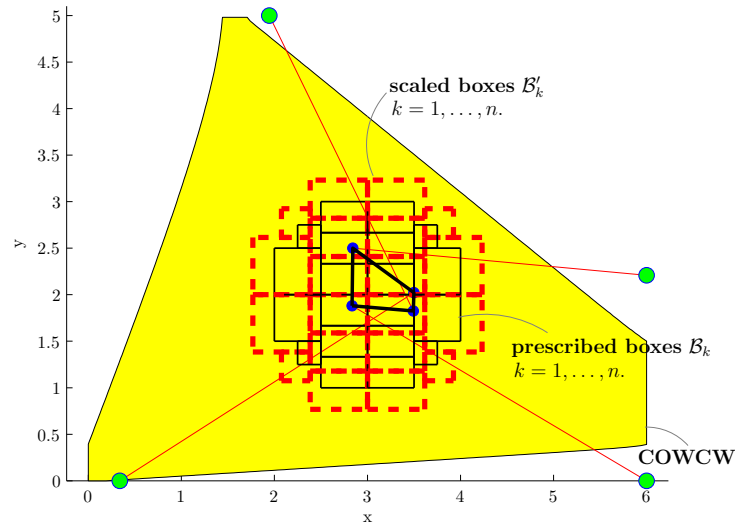
Figure 3.10: Four-cable PCDPM obtained for an irregularly shaped workspace estimated with multiple boxes.

example. In this figure, the boxes in solid black represent the approximated prescribed workspace, while their scaled versions is depicted in red dashed lines. Interestingly, the geometries obtained for this example and the Example 3.2 are somewhat similar to those obtained in Figs. 1.2 and 2.23 of [25].

3.4 Synthesis of a PCDPM for a Prescribed WCW Including a Range of Orientations

In this section we extend the formulation developed in the previous sections for constant-orientations to a continous range of orientations. In other words, we look for a PCDPM whose WCW includes a prescribed workspace covering a given range of orientations. For this purpose, we must explicit the relationship between the wrench matrix $\mathbf{W}$ and the orientation angle ϕ. Therefore, we substitute eq. (2.2) in eq. (4.10) which, leads to

$$\mathbf{f} = \cos\phi\mathbf{u} + \sin\phi\mathbf{v}, \tag{3.26}$$

where $\mathbf{u} \equiv \begin{bmatrix} \mathbf{b}_1^T\mathbf{E}^T\mathbf{a}_1 & \cdots & \mathbf{b}_m^T\mathbf{E}^T\mathbf{a}_m \end{bmatrix}^T \in \mathbb{R}^m$, $\mathbf{v} \equiv -\begin{bmatrix} \mathbf{b}_1^T\mathbf{a}_1 & \cdots & \mathbf{b}_m^T\mathbf{a}_m \end{bmatrix}^T \in \mathbb{R}^m$, and, consequently, the wrench matrix can be rewritten as

$$\mathbf{W} = \mathbf{W}_0 + \mathbf{W}_1\cos\phi + \mathbf{W}_2\sin\phi, \tag{3.27}$$

where $\mathbf{W}_0 = \begin{bmatrix} \mathbf{A}^T - \mathbf{1}_m\mathbf{p}^T & \mathbf{0}_m \end{bmatrix}^T \in \mathbb{R}^{3\times m}$, $\mathbf{W}_1 = \begin{bmatrix} -\mathbf{B}^T & \mathbf{u} - \mathbf{B}^T\mathbf{E}^T\mathbf{p} \end{bmatrix}^T \in \mathbb{R}^{3\times m}$, $\mathbf{W}_2 = \begin{bmatrix} -\mathbf{B}^T\mathbf{E}^T & \mathbf{v} + \mathbf{B}^T\mathbf{E}^T\mathbf{p} \end{bmatrix}^T \in \mathbb{R}^{3\times m}$.

Consider now a box $\mathcal{B}$ with the lower-left and upper-right corners $(\underline{\phi}, \underline{\mathbf{p}})$ and $(\overline{\phi}, \overline{\mathbf{p}})$, respectively, i.e., $\mathcal{B}_\phi = \{(\phi, \mathbf{p}) \in \mathbb{R} \times \mathbb{R}^2 : \underline{\phi} \leq \phi \leq \overline{\phi}, \ \underline{\mathbf{p}} \preceq \mathbf{p} \preceq \overline{\mathbf{p}}\}$. In order to find a necessary condition for $\mathcal{B}_\phi$ to be outside of the WCW, we substitute eq. (3.27) in problem (3.5), we let $\mathbf{p}$ in the decision variables of the problem, while confining it to $\mathcal{B}_\phi$. This leads to

$$
\begin{aligned}
\text{maximize} \quad & \delta, \\
\text{subject to} \quad & \mathbf{0}_m \preceq (\mathbf{A}^T - \mathbf{1}_m\mathbf{p}^T - \mathbf{B}^T\cos\phi - \mathbf{B}^T\mathbf{E}^T\sin\phi)\boldsymbol{\mu} \\
& \quad + (\mathbf{u}\cos\phi + \mathbf{v}\sin\phi - \mathbf{B}^T\mathbf{E}^T\mathbf{p}\cos\phi + \mathbf{B}^T\mathbf{p}\sin\phi)\mu_0, \\
\delta \ \leq \ & \mathbf{1}_m^T((\mathbf{A}^T - \mathbf{1}_m\mathbf{p}^T - \mathbf{B}^T\cos\phi - \mathbf{B}^T\mathbf{E}^T\sin\phi)\boldsymbol{\mu} \\
& \quad + (\mathbf{u}\cos\phi + \mathbf{v}\sin\phi - \mathbf{B}^T\mathbf{E}^T\mathbf{p}\cos\phi + \mathbf{B}^T\mathbf{p}\sin\phi)\mu_0), \\
& \underline{\phi} \leq \phi \leq \overline{\phi}, \ \underline{\mathbf{p}} \preceq \mathbf{p} \preceq \overline{\mathbf{p}},
\end{aligned}
\tag{3.28}
$$

where $\boldsymbol{\lambda} \equiv [\boldsymbol{\mu}^T \quad \mu_0]^T$.

Considering $\mathbf{p}$, the operation-point position, and ϕ, the MP orientation, as optimization variables, we obtain a nonlinear optimization problem. If one were able to

solve this complex problem, then it would be possible to determine whether there is at least one pose of $\mathcal{B}_\phi$ that is not inside the WCW. Conversely, if the global optimum of (3.28) is $\delta^\star = 0$, then box $\mathcal{B}_\phi$ is completely inside the WCW. This global optimum, however, is very difficult to compute in general. Instead, we resort to convex relaxations, whereby we relax the non convex constrains of (3.28) into convex ones, over the box $\mathcal{B}_\phi$. To this end, let us consider the trilinear terms of eq. (3.28), i.e., $\mathbf{p}\cos\phi\mu_0$ and $\mathbf{p}\sin\phi\mu_0$, and define the new variables

$$\boldsymbol{\alpha} \equiv \mathbf{p}\cos\phi \qquad \text{and} \qquad \boldsymbol{\beta} \equiv \mathbf{p}\sin\phi. \qquad (3.29)$$

Substituting these new variables in eq. (3.28) leads to

$$
\begin{aligned}
\text{maximize} \quad & \delta, \\
\text{subject to} \quad & \mathbf{0}_m \preceq (\mathbf{A}^T - \mathbf{1}_m\mathbf{p}^T - \mathbf{B}^T\cos\phi - \mathbf{B}^T\mathbf{E}^T\sin\phi)\boldsymbol{\mu} \\
& \quad + (\mathbf{u}\cos\phi + \mathbf{v}\sin\phi)\mu_0 - \mathbf{B}^T\mathbf{E}^T\boldsymbol{\alpha} + \mathbf{B}^T\boldsymbol{\beta}, \\
& \delta \leq \mathbf{1}_m^T((\mathbf{A}^T - \mathbf{1}_m\mathbf{p}^T - \mathbf{B}^T\cos\phi - \mathbf{B}^T\mathbf{E}^T\sin\phi)\boldsymbol{\mu} \\
& \quad + (\mathbf{u}\cos\phi + \mathbf{v}\sin\phi)\mu_0 - \mathbf{B}^T\mathbf{E}^T\boldsymbol{\alpha} + \mathbf{B}^T\boldsymbol{\beta}), \\
& \underline{\phi} \leq \phi \leq \overline{\phi}, \ \ \underline{\mathbf{p}} \preceq \mathbf{p} \preceq \overline{\mathbf{p}}, \\
& \boldsymbol{\alpha} = \mathbf{p}\cos\phi, \ \ \boldsymbol{\beta} = \mathbf{p}\sin\phi,
\end{aligned}
\qquad (3.30)
$$

which reduces the degree of the constraints to two, while adding four equality constraints. For the given box $\mathcal{B}_\phi$, we can obtain upper and lower bonds on these new variables $\boldsymbol{\alpha}$ and $\boldsymbol{\beta}$, as they are the multiplications of the interval variables [40] $\mathbf{p}, \cos\phi$ and $\sin\phi$. For a given interval of orientation angles, $\underline{\phi} \leq \phi \leq \overline{\phi}$ we have

$$\underline{c} \leq \cos\phi \leq \overline{c} \qquad \text{and} \qquad \underline{s} \leq \sin\phi \leq \overline{s}, \qquad (3.31)$$

where $\underline{c} = \min(\cos\underline{\phi}, \cos\overline{\phi}), \overline{c} = \max(\cos\underline{\phi}, \cos\overline{\phi}), \underline{s} = \min(\sin\underline{\phi}, \sin\overline{\phi})$ and $\overline{s} = \max(\sin\underline{\phi}, \sin\overline{\phi})$, respectively. Thus we obtain

$$\underline{\boldsymbol{\alpha}} \preceq \boldsymbol{\alpha} \preceq \overline{\boldsymbol{\alpha}} \qquad \text{and} \qquad \underline{\boldsymbol{\beta}} \preceq \boldsymbol{\beta} \preceq \overline{\boldsymbol{\beta}}, \qquad (3.32)$$

where $\underline{\boldsymbol{\alpha}} = \min(\mathbf{S}_\alpha), \overline{\boldsymbol{\alpha}} = \max(\mathbf{S}_\alpha)$, and $\underline{\boldsymbol{\beta}} = \min(\mathbf{S}_\beta), \overline{\boldsymbol{\beta}} = \max(\mathbf{S}_\beta)$, and $\mathbf{S}_\alpha = \begin{bmatrix} \underline{\mathbf{p}}\underline{c} & \underline{\mathbf{p}}\overline{c} & \overline{\mathbf{p}}\underline{c} & \overline{\mathbf{p}}\,\overline{c} \end{bmatrix} \in \mathbb{R}^{2\times4}$, $\mathbf{S}_\beta = \begin{bmatrix} \underline{\mathbf{p}}\underline{s} & \underline{\mathbf{p}}\overline{s} & \overline{\mathbf{p}}\underline{s} & \overline{\mathbf{p}}\,\overline{s} \end{bmatrix} \in \mathbb{R}^{2\times4}$. Let us now separate the bilinear terms appearing in eq. (3.30) when considering $\boldsymbol{\mu}, \mu_0, \mathbf{p}, \boldsymbol{\alpha}, \boldsymbol{\beta}, \cos\phi$ and $\sin\phi$ as optimization variables, and define the following variables

$$
\begin{aligned}
& \boldsymbol{\eta} \equiv \text{diag}(\boldsymbol{\mu})\mathbf{p}, \ \ \boldsymbol{\rho} \equiv \boldsymbol{\mu}\cos\phi, \ \ \boldsymbol{\tau} \equiv \boldsymbol{\mu}\sin\phi, \ \ \boldsymbol{\chi} \equiv \boldsymbol{\alpha}\mu_0, \\
& \boldsymbol{\psi} \equiv \boldsymbol{\beta}\mu_0, \ \ \rho_0 \equiv \mu_0\cos\phi \ \ \text{and} \ \ \tau_0 \equiv \mu_0\sin\phi.
\end{aligned}
\qquad (3.33)
$$

While the variables $\mathbf{p}, \boldsymbol{\alpha}, \boldsymbol{\beta}, \cos\phi$ and $\sin\phi$ are bounded, the variables μ_0 and $\boldsymbol{\mu}$ remain unbounded. Alike for the constant orientation case, let us assume that the signs of μ_0 and $\boldsymbol{\mu}$ are known in advance, and label them as in eq. (4.27). Knowing the signs of μ_0 and $\boldsymbol{\mu}$ enables us to generate the following bounds on the newly defined variables of eq. (3.33):

$$\text{diag}(\boldsymbol{\sigma})\text{diag}(\underline{\mathbf{p}})\boldsymbol{\mu} \preceq \text{diag}(\boldsymbol{\sigma})\boldsymbol{\eta} \preceq \text{diag}(\boldsymbol{\sigma})\text{diag}(\overline{\mathbf{p}})\boldsymbol{\mu},$$
$$\underline{c}\,\text{diag}(\boldsymbol{\sigma})\boldsymbol{\mu} \preceq \text{diag}(\boldsymbol{\sigma})\boldsymbol{\rho} \preceq \overline{c}\,\text{diag}(\boldsymbol{\sigma})\boldsymbol{\mu},$$
$$\underline{s}\,\text{diag}(\boldsymbol{\sigma})\boldsymbol{\mu} \preceq \text{diag}(\boldsymbol{\sigma})\boldsymbol{\tau} \preceq \overline{s}\,\text{diag}(\boldsymbol{\sigma})\boldsymbol{\mu}, \qquad (3.34)$$
$$\sigma_0\mu_0\underline{\boldsymbol{\alpha}} \preceq \sigma_0\boldsymbol{\chi} \preceq \sigma_0\mu_0\overline{\boldsymbol{\alpha}},$$
$$\sigma_0\mu_0\underline{\boldsymbol{\beta}} \preceq \sigma_0\boldsymbol{\psi} \preceq \sigma_0\mu_0\overline{\boldsymbol{\beta}},$$
$$\underline{c}\,\sigma_0\mu_0 \leq \sigma_0\rho_0 \leq \overline{c}\,\sigma_0\mu_0,$$
$$\underline{s}\,\sigma_0\mu_0 \leq \sigma_0\tau_0 \leq \overline{s}\,\sigma_0\mu_0.$$

When treating σ_0 and $\boldsymbol{\sigma}$ as constants, the set formed by eq. (3.34) represents a convex polyhedron, which approximates the non-convex surfaces of eq. (3.33). Therefore, replacing the latter with the former, we obtain a *convex relaxation* of eq. (3.33). Hence, the relaxed form of problem (3.28) is

$$\text{maximize} \quad \delta,$$
$$\text{subject to} \quad \mathbf{0}_m \preceq \mathbf{A}^T\boldsymbol{\mu} - \mathbf{1}_m\mathbf{1}_2^T\boldsymbol{\eta} - \mathbf{B}^T\boldsymbol{\rho} - \mathbf{B}^T\mathbf{E}^T\boldsymbol{\tau} + \rho_0\mathbf{u} + \tau_0\mathbf{v}$$
$$- \mathbf{B}^T\mathbf{E}^T\boldsymbol{\chi} + \mathbf{B}^T\boldsymbol{\psi},$$
$$\delta \leq \mathbf{1}_m^T\mathbf{A}^T\boldsymbol{\mu} - m\mathbf{1}_2^T\boldsymbol{\eta} - \mathbf{1}_m^T\mathbf{B}^T\boldsymbol{\rho} - \mathbf{1}_m^T\mathbf{B}^T\mathbf{E}^T\boldsymbol{\tau}$$
$$+ \rho_0\mathbf{1}_m^T\mathbf{u} + \tau_0\mathbf{1}_m^T\mathbf{v} - \mathbf{1}_m^T\mathbf{B}^T\mathbf{E}^T\boldsymbol{\chi} + \mathbf{1}_m^T\mathbf{B}^T\boldsymbol{\psi},$$
$$\text{diag}(\boldsymbol{\sigma})\text{diag}(\underline{\mathbf{p}})\boldsymbol{\mu} \preceq \text{diag}(\boldsymbol{\sigma})\boldsymbol{\eta} \preceq \text{diag}(\boldsymbol{\sigma})\text{diag}(\overline{\mathbf{p}})\boldsymbol{\mu},$$
$$\underline{c}\,\text{diag}(\boldsymbol{\sigma})\boldsymbol{\mu} \preceq \text{diag}(\boldsymbol{\sigma})\boldsymbol{\rho} \preceq \overline{c}\,\text{diag}(\boldsymbol{\sigma})\boldsymbol{\mu},$$
$$\underline{s}\,\text{diag}(\boldsymbol{\sigma})\boldsymbol{\mu} \preceq \text{diag}(\boldsymbol{\sigma})\boldsymbol{\tau} \preceq \overline{s}\,\text{diag}(\boldsymbol{\sigma})\boldsymbol{\mu}, \qquad (3.35)$$
$$\sigma_0\mu_0\underline{\boldsymbol{\alpha}} \preceq \sigma_0\boldsymbol{\chi} \preceq \sigma_0\mu_0\overline{\boldsymbol{\alpha}},$$
$$\sigma_0\mu_0\underline{\boldsymbol{\beta}} \preceq \sigma_0\boldsymbol{\psi} \preceq \sigma_0\mu_0\overline{\boldsymbol{\beta}},$$
$$\underline{c}\,\sigma_0\mu_0 \leq \sigma_0\rho_0 \leq \overline{c}\,\sigma_0\mu_0,$$
$$\underline{s}\,\sigma_0\mu_0 \leq \sigma_0\tau_0 \leq \overline{s}\,\sigma_0\mu_0,$$
$$\sigma_0 = \text{sgn}(\mu_0), \; \boldsymbol{\sigma} = \text{sgn}(\boldsymbol{\mu}).$$

Alike for problem (3.12), the only non-convex constraints in problem (3.35) are the latter two equations, which yield exactly eight possible combinations of σ_0 and $\boldsymbol{\sigma}$, i.e.,

the solutions to the eq. (4.30). Labeling these solutions as $\sigma_{0,j}$ and $\boldsymbol{\sigma}_j$, $j = 1, \ldots, 8$, the solution to problem (3.35) is the maximum of the outcomes of the eight resulting linear programs. This leads to the following Lemma.

Lemma 8 *Sufficient Condition for a Box to Lie Inside the WCW within a Given Range of Orientation Angles*
Consider the eight distinct linear programs

$$
\begin{aligned}
maximize \quad & \delta_j, \\
subject\ to \quad & \mathbf{H}_j \boldsymbol{\omega}_j \preceq \mathbf{0}_{m+25}, \\
& j = 1, \ldots, 8,
\end{aligned}
\tag{3.36}
$$

where $\boldsymbol{\omega}_j = \begin{bmatrix} \mu_{0,j} & \rho_{0,j} & \tau_{0,j} & \boldsymbol{\mu}_j^T & \boldsymbol{\eta}_j^T & \boldsymbol{\rho}_j^T & \boldsymbol{\tau}_j^T & \boldsymbol{\chi}_j^T & \boldsymbol{\psi}_j^T & \delta_j \end{bmatrix}^T \in \mathbb{R}^{16}$,

$$
\mathbf{H}_j \equiv \begin{bmatrix} \mathbf{h}^T & 1 \\ \mathbf{U}_j^T & \mathbf{0}_{m+24} \end{bmatrix} \in \mathbb{R}^{(m+25) \times 16} \text{ and vector } \mathbf{h} \text{ and matrix } \mathbf{U}_j \text{ are given in Appendix}
$$

B. Then, the given box $\mathcal{B}_\phi = \{(\phi, \mathbf{p}) \in \mathbb{R} \times \mathbb{R}^2 : \underline{\phi} \leq \phi \leq \overline{\phi}, \ \underline{\mathbf{p}} \preceq \mathbf{p} \preceq \overline{\mathbf{p}}\}$ *is fully inside the WCW if all of the problems (3.14), $j = 1, \ldots, 8$, yield zero.*

Proof. The proof is similar to that of lemma 7, and, for the sake of conciseness is omitted. $\square$

Hence, problem (3.36) provides a sufficient condition for a box to lie completely inside the WCW within a given range of orientation angles. This condition may be used to compute a *contracted* WCW, namely, a subset of the Cartesian workspace that is guaranteed to lie inside the WCW. Let us consider the mechanism depicted in Fig. 2.3 again. We divide the Cartesian space into boxes that cover the interval -0.03 rad $\leq \phi \leq 0.03$ rad along the ϕ axis, and that have edges of length 0.1 m along the x and y axes. We solve problem (3.36) for each of these boxes, and keep only those for which the maximum is 0. We obtain the contracted WCW, which is shown in Fig. 3.11, along with cross-sections of the exact WCW. Evidently, this contracted WCW is the intersection of the constant orientation WCWs (COWCWs) corresponding to all orientations within the given range. Smaller boxes would have led to a closer estimate of the WCW, as the convex relaxation (3.34) then forms a tighter approximation of (3.33).
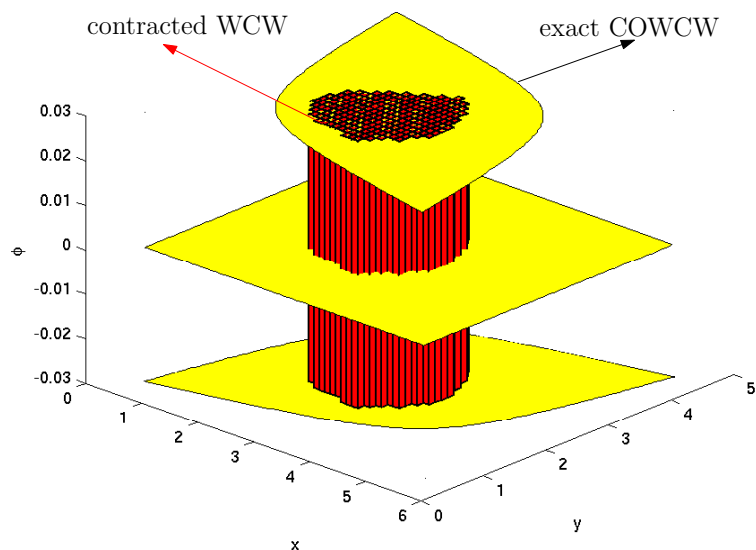
(a) 3D view
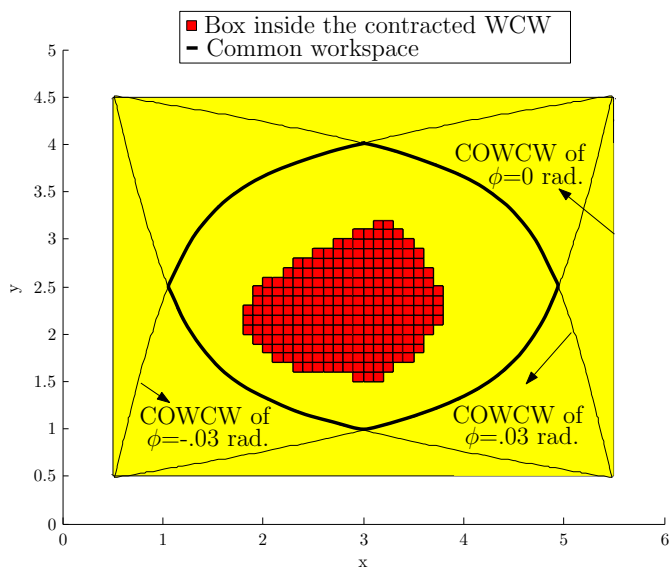
(b) Top view

Figure 3.11: Contracted WCW and cross sections of the exact WCW of the PCDPM geometry found in [2].

notice that the inequality constraints in problem (3.36) can always be satisfied by choosing $\boldsymbol{\omega}_j = \mathbf{0}_{16}$. Alike for the constant orientation synthesis problem, we would like these constraints to be feasible only if a given box were fully inside the WCW within a given range of orientation angles. Hence, we compute the Lagrange dual of problem

(3.36). Let us start by writing the Lagrangian of problem (3.14),

$$L(\mathbf{x}_j, \boldsymbol{\omega}_j) = \mathbf{x}_j^T(\mathbf{H}_j\boldsymbol{\omega}_j) - \delta_j, \tag{3.37}$$

where $\mathbf{x}_j \in \mathbb{R}_+^{m+25}$ is the vector of Lagrange multipliers. Hence, the Lagrange dual of our problem is that of maximizing $\theta(\mathbf{x}_j)$, where

$$\theta_j(\mathbf{x}_j) = \inf_{\boldsymbol{\omega}_j} L(\mathbf{x}_j, \boldsymbol{\omega}_j), \quad j = 1, \ldots, 8. \tag{3.38}$$

Considering $\delta_j = \mathbf{e}_{16}^T\boldsymbol{\omega}_j$, where $\mathbf{e}_{16} = [\mathbf{0}_{15}^T \quad 1]^T \in \mathbb{R}^{16}$, and substituting eq. (4.33) into eq. (4.34) gives

$$\theta_j(\mathbf{x}_j) = \inf_{\boldsymbol{\omega}_j}(\mathbf{x}_j^T\mathbf{H}_j - \mathbf{e}_{16}^T)\boldsymbol{\omega}_j. \tag{3.39}$$

Evidently,

$$\theta_j(\mathbf{x}_j) = \begin{cases} 0 & \text{if } \mathbf{H}_j^T\mathbf{x}_j = \mathbf{e}_{16}, \\ -\infty & \text{otherwise.} \end{cases} \tag{3.40}$$

Hence, the dual problem of problem (3.36) can be stated as the following feasibility problem:

$$\begin{aligned} &\text{maximize} \quad 0, \\ &\text{subject to} \quad \mathbf{H}_j^T\mathbf{x}_j - \mathbf{e}_{16} = \mathbf{0}_{16}, \\ &\qquad\qquad\quad \mathbf{x}_j \succeq \mathbf{0}_{m+25}, \quad j = 1, \ldots, 8. \\ &\text{over} \qquad \mathbf{x}_j. \end{aligned} \tag{3.41}$$

The last equality constraint of this linear program implies $x_{j,1} = 1$, $j = 1, \ldots, 8$, where $x_{j,1}$ represents the first element of the Lagrange multiplier $\mathbf{x}_j$. Substituting this in eq. (3.41) eliminates $\mathbf{x}_{j,1}$ as a variable and reduces the number of the equality constraints from 16 to 15 which yields

$$\begin{aligned} &\text{maximize} \quad 0, \\ &\text{subject to} \quad \mathbf{U}_j\mathbf{y}_j + \mathbf{h} = \mathbf{0}_{15}, \\ &\qquad\qquad\quad \mathbf{y}_j \succeq \mathbf{0}_{m+24}, \quad j = 1, \ldots, 8. \\ &\text{over} \qquad \mathbf{y}_j, \end{aligned} \tag{3.42}$$

where $\mathbf{y}_j \in \mathbb{R}_+^{m+24}$ represents the vector of Lagrange multipliers after eliminating the last equality constraint of eq. (3.41).

Problem (3.42) is equivalent to its primal problems (3.36) but it is feasible when all problems (3.36) yield zero, and infeasible when any of those problems is unbounded.

Like in the constant-orientation case these correspond to cases 3 and 1, respectively, of the primal-dual relationships. We may combine all of these problems into a single one in order to verify whether a given box $\mathcal{B}_\phi$ is inside the WCW of a given PCDPM for a given continous range of orientation angles. This can be done by summing the objective values of these problems while considering all of their constraints together as follows:

$$
\begin{aligned}
\text{maximize} \quad & 0, \\
\text{subject to} \quad & \mathbf{U}_j \mathbf{y}_j + \mathbf{h} = \mathbf{0}_{15}, \quad j = 1, \ldots, 8, \\
& \mathbf{y}_j \succeq \mathbf{0}_{m+24}, \quad j = 1, \ldots, 8, \\
\text{over} \quad & \mathbf{y}_j, \quad j = 1, \ldots, 8.
\end{aligned}
\tag{3.43}
$$

Notice that eq. (3.42) represents eight distinct linear programs while eq. (3.43) represents only one. Equation (3.43) may now be regarded as a single feasibility problem of 120 equality constraints and $8m + 192$ non-negative variables. If there is a feasible solution to this problem then the given box $\mathcal{B}_\phi$ is inside the WCW. Having this information, we can now turn our attention to the synthesis problem.

3.5 A Formulation for the Problem of Synthesizing a PCDPM

Problem (3.43) provides a tool to solve the dimensional synthesis of PCDPMs. Suppose we are interested in finding a PCDPM geometry whose WCW contains a given box $\mathcal{B}_\phi$ within a given range of orientation angles. In order to solve this problem we introduce the nonlinear feasibility problem

$$
\begin{aligned}
\text{satisfy} \quad & \mathbf{U}_j \mathbf{y}_j + \mathbf{h} = \mathbf{0}_{15}, \quad j = 1, \ldots, 8, \\
& \mathbf{y}_j \succeq \mathbf{0}_{m+24}, \quad j = 1, \ldots, 8, \\
& \underline{\mathbf{a}} \preceq \mathbf{a}_i \preceq \overline{\mathbf{a}}, \quad \underline{\mathbf{b}} \preceq \mathbf{b}_i \preceq \overline{\mathbf{b}}, \quad i = 1, \ldots, m, \\
\text{over} \quad & \mathbf{y}_j \in \mathbb{R}^{m+24}, \quad \mathbf{a}_i \in \mathbb{R}^2, \quad \mathbf{b}_i \in \mathbb{R}^2,
\end{aligned}
\tag{3.44}
$$

where, $\underline{\mathbf{a}}$, $\overline{\mathbf{a}}$, $\underline{\mathbf{b}}$ and $\overline{\mathbf{b}}$ are lower and upper bounds on the positions of the base and MP attachments points. If it exists, the associated solution of problem (3.44) yields a PCDPM geometry whose WCW is guaranteed to include the prescribed box $\mathcal{B}_\phi$. On

the other hand, the absence of a solution to this problem does not imply that there is no possible PCDPM geometry containing $\mathcal{B}_\phi$. Hence, this method lacks practicality, since failing to obtain a feasible solution does not provide any information regarding a *good* but *not perfect* geometry. For this reason, we add the objective function defined in section (3.3.1) over the constraints.

3.5.1 A Nonlinear Program for the Dimensional Synthesis of PCDPMs

We now turn the feasibility problem (3.44) into a nonlinear program where $\mathbf{U}'_j$ is obtained by substituting $\overline{\mathbf{p}}'$ and $\underline{\mathbf{p}}'$ for $\overline{\mathbf{p}}$ and $\underline{\mathbf{p}}$, respectively, in the expression of $\mathbf{U}_j$ given in problem (3.36). Hence, the nonlinear program corresponding to the synthesis of PCDPMs for a prescribed box is

$$
\begin{aligned}
\text{maximize} \quad & s \\
\text{subject to} \quad & \mathbf{U}'_j \mathbf{y}_j + \mathbf{h} = \mathbf{0}_{15}, \\
& \underline{\mathbf{p}}' - \mathbf{p}_c - s(\underline{\mathbf{p}} - \mathbf{p}_c) = \mathbf{0}_2, \\
& \overline{\mathbf{p}}' - \mathbf{p}_c - s(\overline{\mathbf{p}} - \mathbf{p}_c) = \mathbf{0}_2, \\
& \underline{\mathbf{a}} \preceq \mathbf{a}_i \preceq \overline{\mathbf{a}}, \ \ \underline{\mathbf{b}} \preceq \mathbf{b}_i \preceq \overline{\mathbf{b}}, \ \ i = 1, \dots, m, \\
& \mathbf{y}_j \succeq \mathbf{0}_{m+24}, \ \ j = 1, \dots, 8, \\
& s \geq 0, \\
\text{over} \quad & \mathbf{y}_j \in \mathbb{R}^{m+24}_+, \ \ \mathbf{a}_i \in \mathbb{R}^2, \ \ \mathbf{b}_i \in \mathbb{R}^2, \ \ s \in \mathbb{R}_+.
\end{aligned}
\tag{3.45}
$$

As in section 3.3.4, for a prescribed workspace with an irregular shape, we may use interval analysis as a tool to over-estimate this workspace with a set of boxes. Also, notice that it may prove useful to divide even a rectangular prescribed WCW into smaller boxes, since the proposed convex relaxations are tighter over smaller boxes, and may thus lead to a larger maximum value of the scaling factor.

In order to solve the dimensional synthesis problem for a prescribed workspace composed of multiple boxes, the formulation (3.45) can be developed to include several boxes. This is done by considering the constraints corresponding to each box while attempting to maximize a common scaling factor s with respect to a common scaling

point, which may be the centroid of the approximated WCW. Symbolically, we obtain

$$\text{maximize} \quad s$$

$$\text{subject to} \quad \mathbf{U}'_{k,j}\mathbf{y}_{k,j} + \mathbf{h} = \mathbf{0}_{15}, \tag{3.46}$$

$$\underline{\mathbf{p}}'_k - \mathbf{p}_c - s(\underline{\mathbf{p}}_k - \mathbf{p}_c) = \mathbf{0}_2,$$

$$\overline{\mathbf{p}}'_k - \mathbf{p}_c - s(\overline{\mathbf{p}}_k - \mathbf{p}_c) = \mathbf{0}_2,$$

$$\underline{\mathbf{a}} \preceq \mathbf{a}_i \preceq \overline{\mathbf{a}}, \ \ \underline{\mathbf{b}} \preceq \mathbf{b}_i \preceq \overline{\mathbf{b}}, \ \ i = 1, \dots, m,$$

$$s \geq 0,$$

$$\mathbf{y}_{k,j} \succeq \mathbf{0}_{m+24}, \ \ j = 1, \dots, 8, \ \ k = 1 \dots n,$$

$$\text{over} \quad \mathbf{y}_{k,j} \in \mathbb{R}^{m+24}_+, \ \ \mathbf{a}_i \in \mathbb{R}^2, \ \ \mathbf{b}_i \in \mathbb{R}^2, \ s \in \mathbb{R}_+.$$

where n is the number of boxes. Notice that we must consider the lower-left corner $\underline{\mathbf{p}}'_k$ and upper-right corner $\overline{\mathbf{p}}'_k$ of each scaled box to construct the matrix $\mathbf{U}'_{k,j}$. This forms a nonlinear program with $8n(m+24)+4m+1$ variables, $120n$ equality constraints, and $8n(m+24)+8m+1$ inequality constraints. Evidently, depending on the number of boxes required, this problem can become a large-scale nonlinear program. Nevertheless, problem (3.46) provides us with a tool to find a PCDPM whose WCW includes a prescribed workspace within a given range of orientations. As the problem (3.46) is non-convex, the geometry it yields depends on the chosen initial guess. We illustrate this with a synthesis example in the following section.

Example 3.4 Dimensional Synthesis of PCDPMs for a Given Box and a Given Range of Orientations

Suppose we are given a prescribed rectangular WCW with lower-left and upper-right coordinates $\underline{\mathbf{p}} = [.4 \ \ .4]^T$ and $\overline{\mathbf{p}} = [.55 \ \ .55]^T$, respectively and the range of rotation angles is $-\pi/3 \leq \phi \leq \pi/3$. We want to find a PCDPM whose WCW within this given range of rotation angles includes this prescribed workspace. The assumed upper and lower bounds for the geometry of the mechanism are given in Table 3.7. The number of

Table 3.7: Upper and lower bounds on the geometry of the PCDPM of example 3.4.

$\underline{\mathbf{a}}^T$	$\overline{\mathbf{a}}^T$	$\underline{\mathbf{b}}^T$	$\overline{\mathbf{b}}^T$
$[0 \ \ 0]$	$[1 \ \ 1]$	$[-.2 \ \ -.2]$	$[.2 \ \ .2]$

cables is set to $m = 4$, which is the minimum necessary for a WCW to exist. In order to tighten the constraints on the variables defined in the previous section and obtain a

PCDPM with a larger WCW, we divide this prescribed box into $n = 9$ similar boxes with edges of 0.05 in the xy plane.

One of the most popular methods of finding local maxima to problem (3.46) is to use the standard Matlab solvers, which are called through the *fmincon* function. Unfortunately, we found this solver too slow when applied to the obtained formulation for the synthesis of PCDPMs. Also, as the function cannot accept sparse matrices, it often encounters memory errors, depending on the memory available on the computer and on the number of boxes n. In order to circumvent these problems, we decided instead to use our own specific Matlab implementation of the *penalty successive linear programming algorithm* (PSLP) [38] to solve the problem. The algorithm is in the class of SLP algorithms, which employ the l_1-norm i.e., the absolute value in the direction-finding subproblem, which becomes a linear program based on first-order Taylor series approximations of the objective and constraint functions. A brief explanation of this algorithm is reported in Appendix C. These linear-programming subproblems were solved using Matlab's *linprog* command with its *Large-Scale Algorithm* which exploits the sparsity pattern to improve speed and reduce memory cost. By successively solving this linear program, the PSLP algorithm converges towards a local maximum of the principal problem, which is defined over a hypercube-shaped trust region.

In order to solve the current example, we used the parameters of the PSLP algorithm that are proposed in [38]. The algorithm was implemented in Matlab 7.6.0 $R2008a$ on a PC with Intel(R) Core(TM)2 CPU 6400 @ 2.13GHz, with 4GB RAM memory. In order to find a better local optimum, the problem was solved repeatedly for 100 initial guesses, which were generated using uniformly distributed pseudo-random numbers produced by the *rand* function in Matlab. In order to ensure that the produced initial guesses cover well the feasible set, we used the following formulation to produce the initial geometry:

$$\mathbf{a}_i = \underline{\mathbf{a}} + \text{diag}(\overline{\mathbf{a}} - \underline{\mathbf{a}})\boldsymbol{\alpha}_i, \tag{3.47}$$
$$\mathbf{b}_i = \underline{\mathbf{b}} + \text{diag}(\overline{\mathbf{b}} - \underline{\mathbf{b}})\boldsymbol{\beta}_i, \quad i = 1, \dots, m,$$

where $\boldsymbol{\alpha_i} \in \mathbb{R}^2$ and $\boldsymbol{\beta_i} \in \mathbb{R}^2$ are the random numbers produced by the *rand* function of Matlab. Figure 3.12 shows the histogram of the obtained results for the generated points. As can be seen from this figure, 32% of the generated initial guesses end with an optimum scaling factor greater than 1, which means that the WCWs of the corresponding PCDPMs are guranteed to include the prescribed box for the given
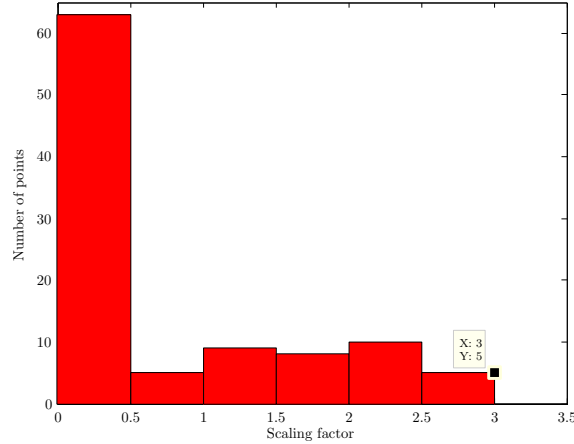
Figure 3.12: Distribution of the randomly generated initial points with the obtained scaling factors.

range of orientation angles. As for the remaining 68% initial guesses we cannot draw conclusions, but the prescribed box may yet be inside of the resulting WCW, as the proposed method always underestimates the WCW.

Two of the resulting robot geometries are shown in Fig. 3.13. Figure 3.13(a) corresponds to the best scaling factor, $s^\star = 2.8273$ and Fig. 3.13(b) is very close to the mechanisms reported in reference [25]. The corresponding scaled boxes and WCW cross sections are depicted in Fig. 3.14. As can be seen, the scaled boxes and, consequently, the prescribed boxes, are entirely inside the WCW of the mechanism obtained. The exact initial guess and final optimum are reported in Tables 3.8 and 3.9, respectively. For this example, it took 42 min to obtain the final solution by using a desktop computer equipped with an Intel(R) Core(TM)2 CPU 6400 @ 2.13GHz, and 4GB RAM. Figure 3.15 shows the evolution of the scaling factor during the solution procedure. Notice that the initial decrease in s is a result of the PSLSP algorithm first seeking to satisfy the constraints at the expense of the objective.

Table 3.8: Initial geometry of example 3.4.

i	$\mathbf{a}_{i,0}^T$	$\mathbf{b}_{i,0}^T$
1	$[0.4972 \quad 0.1391]$	$[0.1813 \quad -0.1943]$
2	$[0.5965 \quad 0.5021]$	$[-.0612 \quad -0.1840]$
3	$[0.1940 \quad 0.2865]$	$[-0.1971 \quad 0.1408]$
4	$[0.3583 \quad 0.2099]$	$[0.1447 \quad 0.0457]$
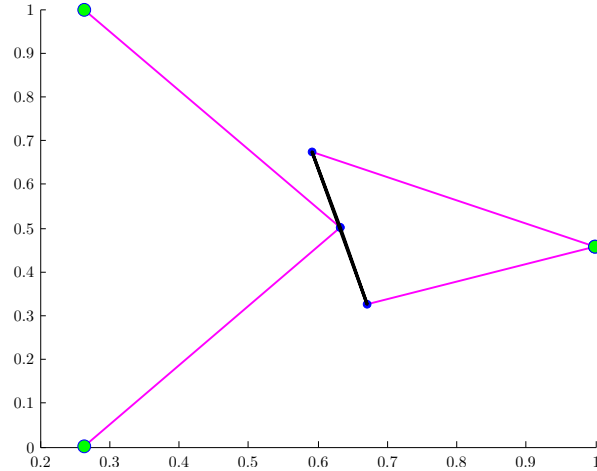
(a) Obtained PCDPM with the best scaling factor, $s^\star=2.8273$
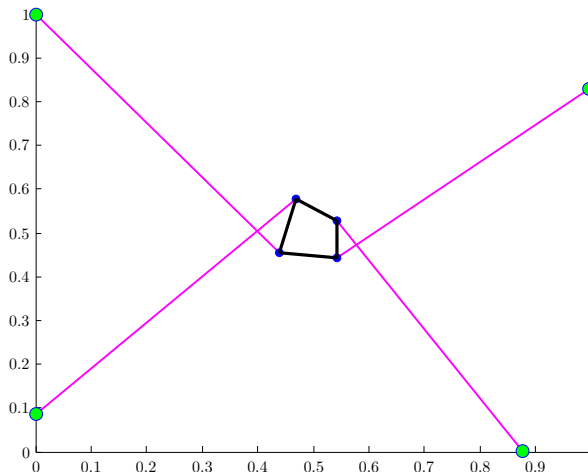
(b) Obtained PCDPM with the scaling factor, $s^\star=0.2752$

Figure 3.13: Two of the obtained PCDPMs.

Table 3.9: Final geometry of example 3.4.

i	$\mathbf{a}_{i,f}^T$	$\mathbf{b}_{i,f}^T$
1	$[0.2627 \quad 0.0000]$	$[0.0000 \quad 0.0000]$
2	$[1.0000 \quad 0.4566]$	$[0.0399 \quad -0.1748]$
3	$[1.0000 \quad 0.4566]$	$[-0.0399 \quad 0.1748]$
4	$[0.2627 \quad 1.0000]$	$[0.0000 \quad 0.0000]$

Example 3.5 Synthesis of a PCDPM for a Non-Rectangular Prescribed Workspace

Suppose we want to find the geometry of a PCDPM whose WCW for the given range of orientations $-\pi/6 \leq \phi \leq \pi/6$, includes the desired elliptic workspace $\mathcal{E}_d$ represented
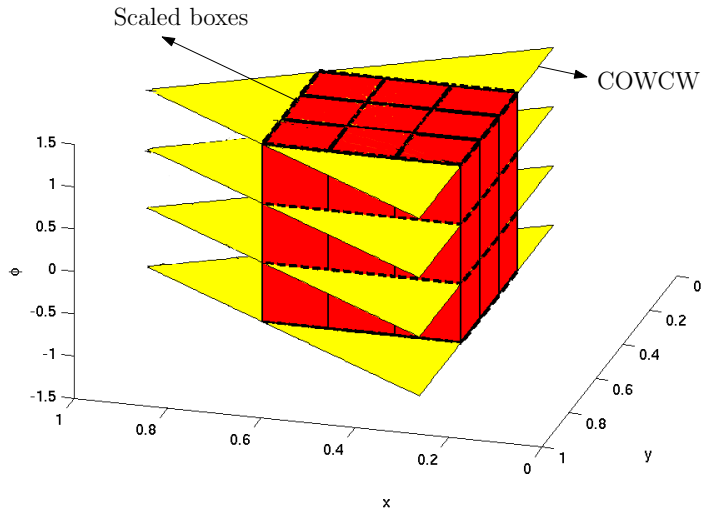
Figure 3.14: Scaled boxes and COWCWs for the orientations $\phi = -\pi/3, -\pi/9, \pi/9, \pi/3$.
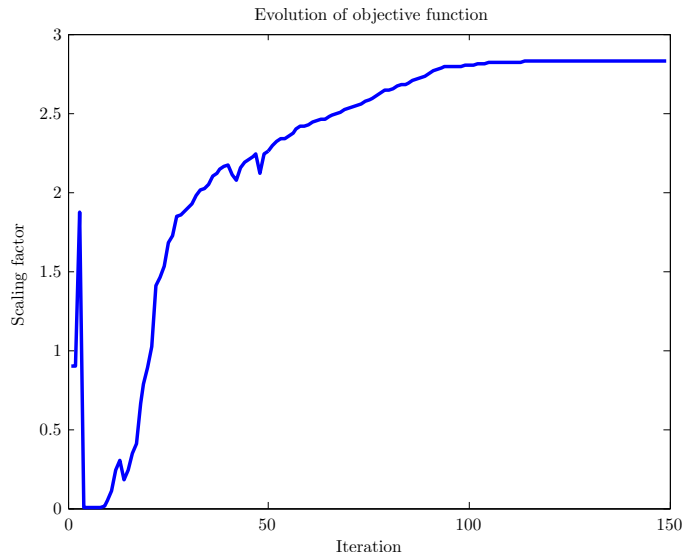
Figure 3.15: Evolution of scaling factor.

by $(x-3.5)^2/1.6^2 + (y-3)^2/1.1^2 \leq 1$. We approximate this prescribed WCW by means of interval analysis, as depicted in Fig. 3.16. In order to ensure that the multiple boxes will cover the entirety of the prescribed WCW, we overestimate the desired WCW with $\mathcal{E}_e$ represented by $(x-3.5)^2/1.9^2 + (y-3)^2/1.33^2 \leq 1$ whose corresponding certainly-inside boxes cover $\mathcal{E}_d$. For this estimation, we have $n = 32$ prescribed boxes and the selected lower and upper bounds for the base and moving platform anchor points are
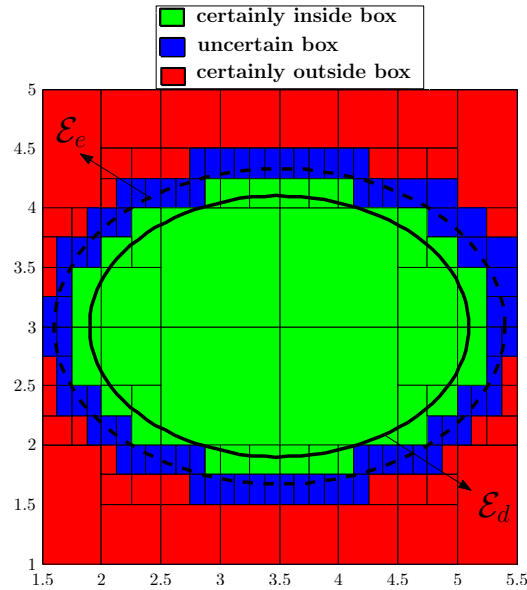
Figure 3.16: Approximated desired workspace with multiple boxes.

shown in Table 3.10. The number of cables is set to $m = 5$, and we solve this problem

Table 3.10: Upper and lower bounds on the geometry of the PCDPM for the prescribed workspace of example 3.5.

$\underline{\mathbf{a}}^T$	$\overline{\mathbf{a}}^T$	$\underline{\mathbf{b}}^T$	$\overline{\mathbf{b}}^T$
$\begin{bmatrix} 0 & 0 \end{bmatrix}$	$\begin{bmatrix} 6 & 5 \end{bmatrix}$	$\begin{bmatrix} -.5 & -.5 \end{bmatrix}$	$\begin{bmatrix} .5 & .5 \end{bmatrix}$

using the PSLP algorithm for 50 initial uniformly-distributed random points.

The best solution obtained using these initial guesses is $s^* = 1.3832$, and its corresponding geometry and COWCW for the angles $\phi = -\pi/6, 0, \pi/6$ are depicted in Fig. 3.17. Table 3.11 shows the coordinates of the attachment and anchor points corresponding to the initial guesses and its resulting solution.
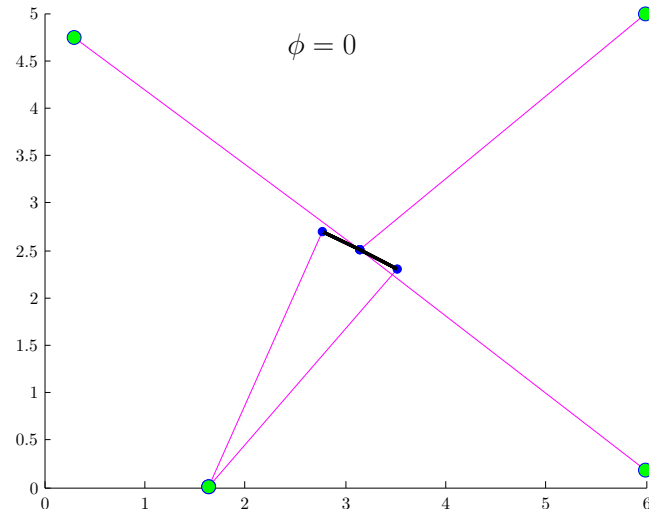
(a) The obtained PCDPM
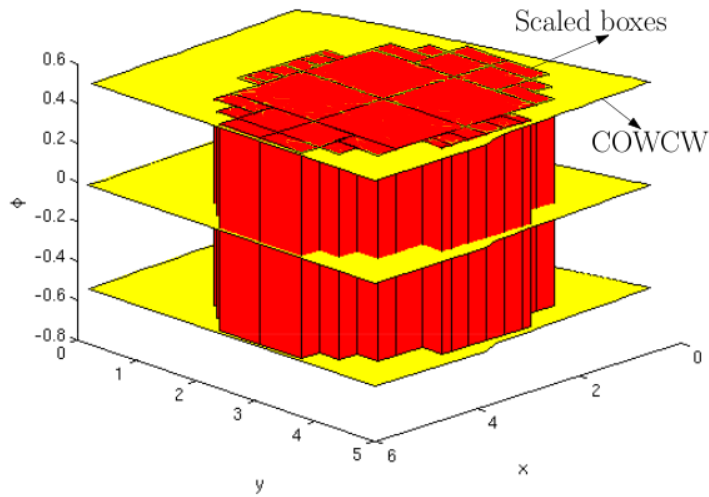
(b) COWCWs for the orientation angles $\phi = -\pi/6, 0, \pi/6$

Figure 3.17: The obtained PCDPM and its corresponding COWCW.

As can be seen from this figure the scaled boxes, and, consequently, the prescribed ellipse $\mathcal{E}_d$, are all inside the WCW of the obtained PCDPM for the provided range of orientations.

Table 3.11: Initial and final geometries of example 3.5.

i	$\mathbf{a}_{i,0}^T$	$\mathbf{b}_{i,0}^T$
1	[0.4884 0.3551]	[0.1656 0.2700]
2	[2.9599 2.2603]	[0.6799 0.5078]
3	[1.7818 1.3436]	[0.0239 0.8245]
4	[0.7605 0.4252]	[0.3723 0.3152]
5	[0.9550 3.8578]	[0.7498 0.1322]

i	$\mathbf{a}_{i,f}^T$	$\mathbf{b}_{i,f}^T$
1	[1.6382 0.0033]	[0.3774 $-$0.1935]
2	[5.9999 4.9995]	[0.0000 0.0000]
3	[5.9999 0.1784]	[0.0000 0.0000]
4	[1.6382 0.0033]	[$-$0.3774 0.1935]
5	[0.2906 4.7378]	[0.0000 0.0000]

3.6   Conclusions

A method for the dimensional synthesis of planar cable driven parallel mechanisms (PCDPMs) was proposed. To achieve this goal, an optimization problem was first introduced to verify whether a given pose is inside the wrench-closure workspace (WCW) of a given PCDPM. We then relaxed this problem over a box in the workspace, which led us to a sufficient condition for this box to be inside the COWCW of a given PCDPM. These mathematical conditions allowed the formulation of a nonlinear program in which the scale of the prescribed workspace is maximized while being constrained inside the PCDPM COWCW. The robot geometry being included in the decision variables of the nonlinear program, this optimization problem is the tool sought for the constant-orientation dimensional synthesis of PCDPMs. The value of the scaling factor at the optimum indicates whether the prescribed box is inside the COWCW. Solving the problem for different initial guesses may provide us with a larger scaling factor, and thus a larger COWCW. It was shown that the proposed approach can be applied to prescribed workspaces that cover several fixed orientations and that are not rectangular. We extended the results to the continous-orientation case, in which we seek geome-

tries of PCDPMs whose WCWs include a prescribed workspace within a given range of orientations. Finally, our intuition is that the same approach could be applied to the dimensional synthesis of conventional mechanisms.

Chapter 4

The Dimensional Synthesis Of Spatial Cable-Driven Parallel Mechanisms

In this chapter we extend the methods developed in the previous chapter for the dimensional synthesis of PCDPMs for the spatial cable-driven mechanisms. First, we recall the kinetostatic model and expressions for theses mechanisms and introduce a linear program to calculate their WCW. A relaxation of the introduced linear program provides a sufficient condition to verify whether a given six- dimensional box, i.e., a box covering point-positions and orientations, is inside or outside of the WCW of a given spatial CDPM. Then the geometry of the mechanism is considered as a set of optimization variables and scaling factor controlling the size of the prescribed box is used as the objective function, to be maximized. This leads us to a nonlinear program whose optima represent CDPMs whose WCWs include the prescribed box. The formulation is further extended to multiple boxes, which may represent an approximation of an irregularly-shaped prescribed workspace. The developed methods are illustrated through several examples.

4.1 Kinetostatic Model of Spatial Cable-Driven Parallel Mechanisms

Before searching for the geometry of a spatial parallel cable-driven mechanism for a prescribed workspace, we have to set up a standard mathematical description of the statics of such a mechanism, and more specifically, of its wrench-closure workspace. Such a spatial parallel cable-driven mechanism is schematically shown in Fig. 4.1. It consists of a moving platform (MP) that is connected by m cables to m fixed points.
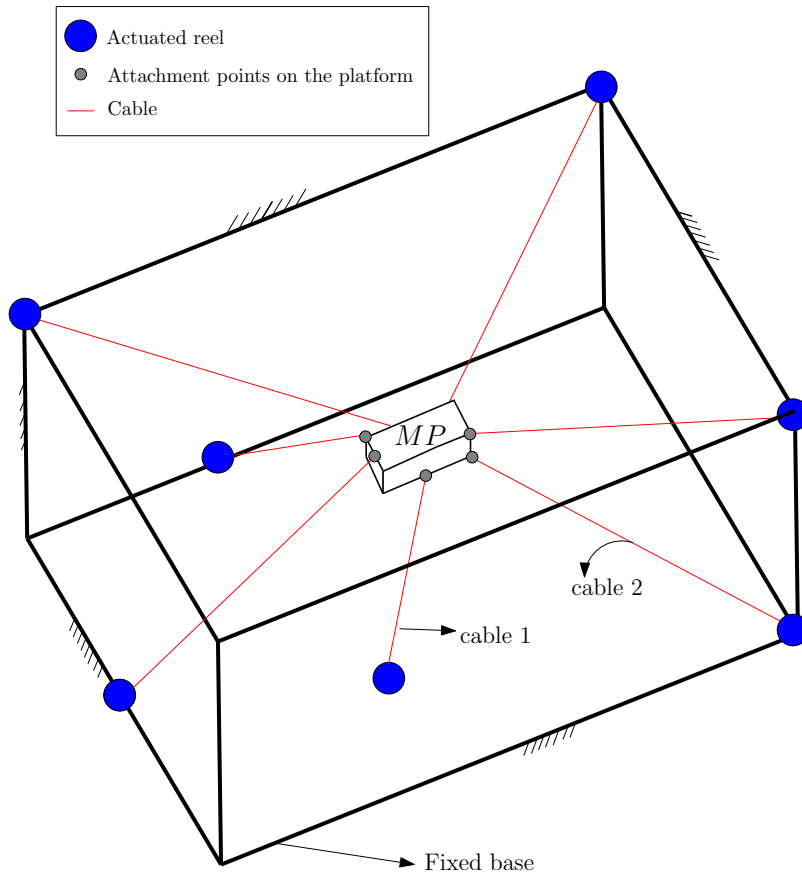
Figure 4.1: Sketch of a spatial cable-driven mechanism with 7 cables.

Alike the planar case, in order to analyze the motion of the MP, we have to consider two frames: the reference frame $\mathcal{A}$, which is fixed to the base, and the moving frame $\mathcal{B}$, which is attached to a reference point of the MP as depicted in Fig. 4.2. Cable i is attached to the MP at B_i, and winds at fixed point A_i around an actuated reel.

We use the same notation as that introduced in Chapter 2 for planar cable-driven
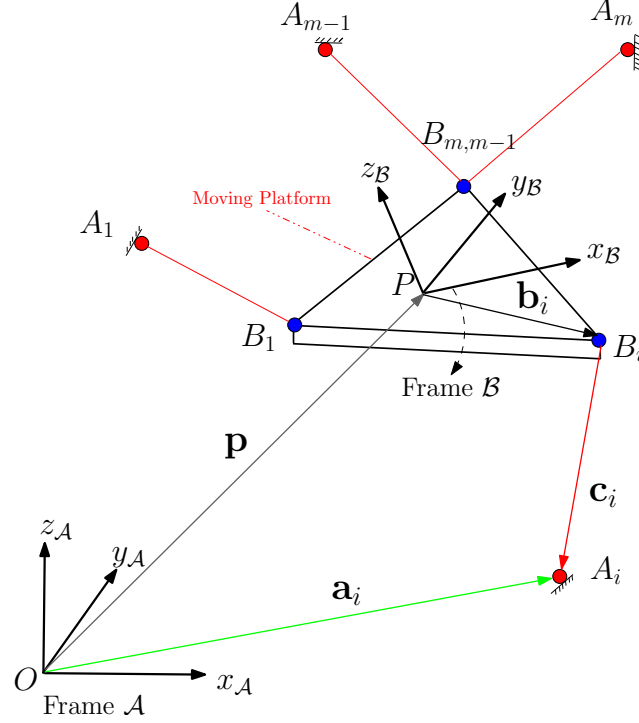
Figure 4.2: Notation used for the kinetostatic analysis of spatial cable-driven parallel mechanisms.

parallel mechanisms, namely:

- Vector $\mathbf{a}_i \in \mathbb{R}^3$ represents the position of the actuated reel A_i in the fixed frame $\mathcal{A}$;

- Vector $\mathbf{b}_i \in \mathbb{R}^3$ is a constant vector and represents the position of the attachment point B_i of the ith cable in frame $\mathcal{B}$;

- Vector $\mathbf{p} \in \mathbb{R}^3$, which is expressed in $\mathcal{A}$, represents the position of point P with respect to point O;

- Vector $\mathbf{c}_i$ points from B_i to A_i, and represents the length of the ith cable;

Frames $\mathcal{A}$ and $\mathcal{B}$ are connected via the rotation matrix $\mathbf{Q}$, which may be represented by three Euler angles. These angles can be any type of the twelve possible definitions of Euler angles [41]. Vector $\mathbf{c}_i$ representing the ith cable, is obtained as

$$\mathbf{c}_i = \mathbf{a}_i - \mathbf{p} - \mathbf{Q}\mathbf{b}_i. \tag{4.1}$$

The wrench applied at P, the origin of the moving frame, by the ith cable is

$$\mathbf{v}_i = [\ \mathbf{f}_i^T \quad \mathbf{n}_i^T\ ]^T \in \mathbb{R}^6, \tag{4.2}$$

where $\mathbf{f}_i$ and $\mathbf{n}_i$ are the force and moment about P produced by the ith cable on the MP. The moment applied by cable i is expressed as

$$\mathbf{n}_i = (\mathbf{Qb}_i) \times \mathbf{f}_i, \tag{4.3}$$

where symbol $\times$ represents the cross product of the two vector. In order to find a proper expression for the moments applied to the MP at reference point P, let us define the following matrices

$$\mathbf{E}_x = \begin{bmatrix} 0 & 1 & 0 \\ 0 & 0 & 1 \end{bmatrix}, \quad \mathbf{E}_y = \begin{bmatrix} 1 & 0 & 0 \\ 0 & 0 & 1 \end{bmatrix}, \quad \mathbf{E}_z = \begin{bmatrix} 1 & 0 & 0 \\ 0 & 1 & 0 \end{bmatrix} \quad \text{and} \quad \mathbf{E} = \begin{bmatrix} 0 & -1 \\ 1 & 0 \end{bmatrix}. \tag{4.4}$$

Hence, the moments applied by cable i on the MP are given by

$$\mathbf{n}_i = [\det(\mathbf{E}_x(\mathbf{Qb}_i), \mathbf{E}_x\mathbf{f}_i) \quad - \det(\mathbf{E}_y(\mathbf{Qb}_i), \mathbf{E}_y\mathbf{f}_i) \quad \det(\mathbf{E}_z(\mathbf{Qb}_i), \mathbf{E}_z\mathbf{f}_i)]^T \in \mathbb{R}^3, \tag{4.5}$$

$i = 1, \ldots, m$. Simplifying eq. (4.5) leads to

$$\mathbf{n}_i = \begin{bmatrix} (\mathbf{Qb}_i)^T\mathbf{H}_x\mathbf{f}_i & (\mathbf{Qb}_i)^T\mathbf{H}_y\mathbf{f}_i & (\mathbf{Qb}_i)^T\mathbf{H}_z\mathbf{f}_i \end{bmatrix}^T \tag{4.6}$$

where $\mathbf{H}_x = \mathbf{E}_x^T\mathbf{E}^T\mathbf{E}_x$, $\mathbf{H}_y = -\mathbf{E}_y^T\mathbf{E}^T\mathbf{E}_y$ and $\mathbf{H}_z = \mathbf{E}_z^T\mathbf{E}^T\mathbf{E}_z$.
These latter matrices are readily computed as,

$$\mathbf{H}_x = \begin{bmatrix} 0 & 0 & 0 \\ 0 & 0 & 1 \\ 0 & -1 & 0 \end{bmatrix}, \mathbf{H}_y = \begin{bmatrix} 0 & 0 & -1 \\ 0 & 0 & 0 \\ 1 & 0 & 0 \end{bmatrix}, \mathbf{H}_z = \begin{bmatrix} 0 & 1 & 0 \\ -1 & 0 & 0 \\ 0 & 0 & 0 \end{bmatrix}. \tag{4.7}$$

Since the exerted force is parallel to its corresponding cable, mathematical expressions for the force exerted by cable i is

$$\mathbf{f}_i = \frac{t_i}{l_i}\mathbf{c}_i, \tag{4.8}$$

where l_i, t_i are the length of cable i and the tension in that cable, respectively. Assuming that points A_i and B_i do not coincide, and substituting eqs. (4.8) and (4.6) in eq. (4.2), the wrench applied to the platform by cable i is $\mathbf{v}_i = \frac{t_i}{l_i}\mathbf{w}_i$, with $\mathbf{w}_i$ defined as

$$\mathbf{w}_i = \begin{bmatrix} \mathbf{c}_i^T & (\mathbf{Qb}_i)^T\mathbf{H}_x\mathbf{c}_i & (\mathbf{Qb}_i)^T\mathbf{H}_y\mathbf{c}_i & (\mathbf{Qb}_i)^T\mathbf{H}_z\mathbf{c}_i \end{bmatrix}^T. \tag{4.9}$$

Equation (2.5) shows that $\mathbf{w}_i$ is a function of both the geometric parameters of the mechanism and the orientation of MP. Note that t_i should always be non-negative for the cables to remain in tension. We define the wrench matrix and tension vector of the mechanism as

$$\mathbf{W} = \begin{bmatrix} \mathbf{w}_1 & \mathbf{w}_2 & \cdots & \mathbf{w}_m \end{bmatrix} \in \mathbb{R}^{6\times m} \text{ and } \mathbf{t} = \begin{bmatrix} \frac{t_1}{l_1} & \frac{t_2}{l_2} & \cdots & \frac{t_m}{l_m} \end{bmatrix}^T \in \mathbb{R}^m$$

respectively. In order to find a proper and compact expression of the wrench matrix, let us define

$$
\begin{aligned}
\mathbf{A} &\equiv \begin{bmatrix} \mathbf{a}_1 & \cdots & \mathbf{a}_m \end{bmatrix} \in \mathbb{R}^{3\times m}, \\
\mathbf{B} &\equiv \begin{bmatrix} \mathbf{b}_1 & \cdots & \mathbf{b}_m \end{bmatrix} \in \mathbb{R}^{3\times m}, \\
\mathbf{F} &\equiv \begin{bmatrix} (\mathbf{Q}\mathbf{b}_1)^T \mathbf{H}_x \mathbf{a}_1 & \cdots & (\mathbf{Q}\mathbf{b}_m)^T \mathbf{H}_x \mathbf{a}_m \\ (\mathbf{Q}\mathbf{b}_1)^T \mathbf{H}_y \mathbf{a}_1 & \cdots & (\mathbf{Q}\mathbf{b}_m)^T \mathbf{H}_y \mathbf{a}_m \\ (\mathbf{Q}\mathbf{b}_1)^T \mathbf{H}_z \mathbf{a}_1 & \cdots & (\mathbf{Q}\mathbf{b}_m)^T \mathbf{H}_z \mathbf{a}_m \end{bmatrix} \in \mathbb{R}^{3\times m}, \\
\mathbf{K} &\equiv \begin{bmatrix} (\mathbf{Q}\mathbf{b}_1)^T \mathbf{H}_x \mathbf{p} & \cdots & (\mathbf{Q}\mathbf{b}_m)^T \mathbf{H}_x \mathbf{p} \\ (\mathbf{Q}\mathbf{b}_1)^T \mathbf{H}_y \mathbf{p} & \cdots & (\mathbf{Q}\mathbf{b}_m)^T \mathbf{H}_y \mathbf{p} \\ (\mathbf{Q}\mathbf{b}_1)^T \mathbf{H}_z \mathbf{p} & \cdots & (\mathbf{Q}\mathbf{b}_m)^T \mathbf{H}_z \mathbf{p} \end{bmatrix} \in \mathbb{R}^{3\times m},
\end{aligned}
\tag{4.10}
$$

which allows us to rewrite $\mathbf{W}$ as

$$
\mathbf{W} \equiv \begin{bmatrix} \mathbf{A} - \mathbf{Q}\mathbf{B} - \mathbf{p}\mathbf{1}_m^T \\ \mathbf{F} - \mathbf{K} \end{bmatrix} \in \mathbb{R}^{6\times m}.
\tag{4.11}
$$

The static equilibrium equation for the moving platform may be expressed as

$$
\mathbf{W}\mathbf{t} + \mathbf{w}_P = \mathbf{0}_6,
\tag{4.12}
$$

in which $\mathbf{w}_P$ is the wrench applied on the MP at P, equivalent to all external forces and moments. These external loads may include gravity forces, for example. Now we can define the wrench closure workspace of CDPMs as follows.

Definition 1 *The Wrench-Closure Workspace (WCW) of a Generic Cable-Driven Parallel Mechanism*

The WCW of spatial parallel cable-driven mechanisms can be formally defined as the set of poses for which

$$
\forall \mathbf{w}_P \in \mathbb{R}^6, \ \exists \ \mathbf{t} \in \mathbb{R}^m \mid \mathbf{t} \succ \mathbf{0}_m \text{ and } \mathbf{W}\mathbf{t} + \mathbf{w}_P = \mathbf{0}_6,
$$

where the symbol $\succ$ denotes the strict componentwise inequality.

4.2 Verifying Whether a Pose Lies in the WCW of a CDPM

In order to verify whether a given pose is inside or outside of the WCW of a provided spatial CDPM, we need to solve the linear system of equations given by eq. (4.12). Alike eq. (2.7) for the planar CDPMs, letting $\mathbf{t}^\star$ be a solution of eq. (4.12), and $\mathbf{t}^\perp$ be a vector in the null space of $\mathbf{W}$, then

$$\mathbf{t} = \mathbf{t}^\star + \lambda \mathbf{t}^\perp, \lambda \in \mathbb{R}, \tag{4.13}$$

is also a solution of eq. (4.12).

For a strictly positive $\mathbf{t}^\perp$, we can add a sufficiently large positive scalar multiple λ of this vector to any particular solution $\mathbf{t}^\star$ of eq. (4.12) to obtain a cable-tension vector $\mathbf{t}$ with positive components. Now we can introduce the following theorem in order to see whether a given pose is inside the WCW of a spatial CDPM.

Theorem 3 *A given pose is inside the WCW of a CDPM if there exists a set $\mathbf{t}$ of tensions in the cables such that*

$$\mathbf{W}\mathbf{t} = \mathbf{0}_6, \quad \mathbf{t} \succ \mathbf{0}_m. \tag{4.14}$$

where $\mathbf{0}_6$ is the six-dimensional zero vector.

According to theorem 3, in order to calculate the WCW of a CDPM, we need to solve the feasibility problem (4.14) for each pose of the MP. Therefore, the WCW of a CDPM is the set of poses for which eq. (4.14) is satisfied. We may also use Stiemke's theorem [35] to verify whether a given pose is inside or outside of WCW. We recall this theorem for spatial CDPMs as follows.

Theorem 4 *The system of eq. (4.14) has no solution if and only if the following system of equations has a solution*

$$\mathbf{W}^T \boldsymbol{\lambda} \succeq \mathbf{0}_m, \tag{4.15}$$
$$\mathbf{W}^T \boldsymbol{\lambda} \neq \mathbf{0}_m.$$

where $\boldsymbol{\lambda} \in \mathbb{R}^6$.

In other words, a given pose of the MP lies outside the WCW if and only if eq. (4.15) admits a solution. Now, we can introduce the following linear program to calculate the wrench-closure workspace of a CDPM:

$$
\begin{aligned}
\text{minimize} \quad & 0, \\
\text{subject to} \quad & \mathbf{W}^T \boldsymbol{\lambda} \succeq \mathbf{0}_m, \\
& \mathbf{1}_m^T \mathbf{W}^T \boldsymbol{\lambda} = 1. \\
\text{over} \quad & \boldsymbol{\lambda} \in \mathbb{R}^6.
\end{aligned}
\tag{4.16}
$$

Problem (4.16), alike that of eq. (3.4), its counterpart for the planar cable-driven parallel mechanisms, yields 0 whenever the given pose is outside of the corresponding WCW and $+\infty$ otherwise. In other words, the given pose is outside of the WCW if the problem admits a feasible solution and inside if it does not. Hence, this equation can be used to calculate the WCW of a given CDPM by discretizing the examined region. This linear feasibility problem is the corner stone to the formulation of the dimensional synthesis of spatial cable-driven parallel mechanisms.

4.3 Verifying whether a Six-Dimensional Box Lies in the WCW of a Spatial Cable-Driven Parallel Mechanism

Let us now turn our attention to our main concern: the dimensional synthesis of CDPMs. Suppose we wish to find a condition to determine whether a given small six-dimensional box ,i.e, three-dimensions for the point-position and the remaining three for the orientation angles is completely inside the wrench-closure workspace of a given parallel cable-driven robot. Problem (4.16) can be turned into a phase-one problem by replacing the equality constraint with an inequality constraint and by maximizing a dummy variable δ_s. We formalize this by the following lemma:

Lemma 9 *Linear program WCW Membership Condition for a Six-Dimensional Pose*

$$
\begin{aligned}
\delta_s^* = maximize \quad & \delta_s, \\
subject\ to \quad & \mathbf{W}^T \boldsymbol{\lambda} \succeq \mathbf{0}_m, \\
& \mathbf{1}_m^T \mathbf{W}^T \boldsymbol{\lambda} \geq \delta_s, \\
over \quad & \boldsymbol{\lambda} \ and\ \delta_s.
\end{aligned}
\tag{4.17}
$$

Then, we have,

$$
\delta_s^* = \begin{cases} +\infty & \textit{if the pose lies outside of the WCW,} \\ 0 & \textit{otherwise.} \end{cases}
\tag{4.18}
$$

Proof. Proof of this lemma is the as same as the proof of lemma 6. □

Linear program 4.18 provides us with a good tool to calculate the constant-orientation WCW of a spatial CDPM by dicretizing the Cartesian space to several 3D points. The following example illustrates this.

Example 4.1. WCW of a Spatial Cable-Driven Mechanism

Figure 4.3 shows a sample spatial CDPM drawn from [42]. The parameters of this mechanism are given in Table 4.1

Table 4.1: Geometric parameters of the assumed CDPM.

i	$\mathbf{a}_i^T$	$\mathbf{b}_i^T$
1	[0 0 0]	[−0.15 − 0.1 − 0.05]
2	[1 0 1]	[0.15 − 0.1 − 0.05]
3	[1 1 0]	[0.15 0.1 − 0.05]
4	[0 1 0]	[−0.15 0.1 − 0.05]
5	[0 0 1]	[−0.15 − 0.1 0.05]
6	[1 0 1]	[0.15 − 0.1 0.05]
7	[1 1 1]	[0.15 0.1 0.05]
8	[0 1 1]	[−0.15 0.1 0.05]
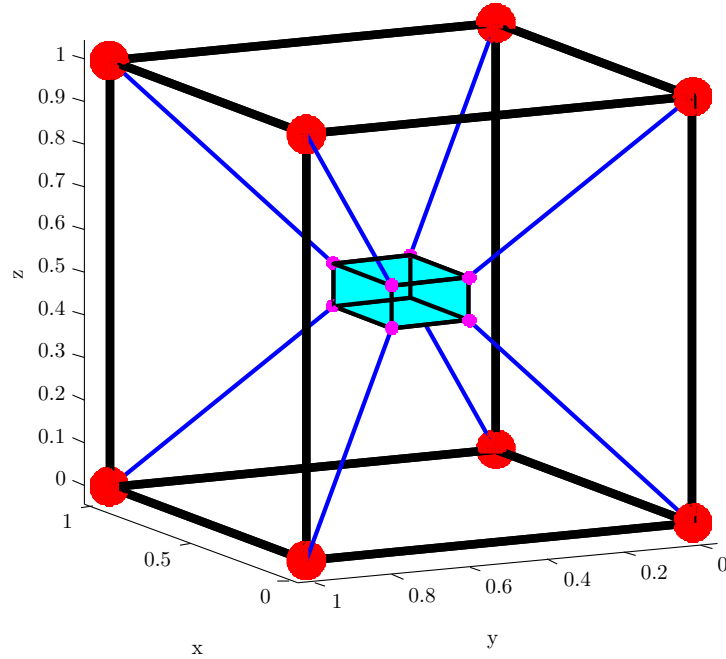
Figure 4.3: A spatial CDPM with eight cables ($\phi = 0\,rad, \theta = 0\,rad, \psi = 0\,rad$).

Discretizing the xyz space provides us with a set of 3D positions to be tested for their membership to the WCW based on the introduced linear program (4.17). Figure 4.4 shows the constant-orientation WCWs of the depicted robot, for various ZYZ type Euler angles, following ZYZ convention.

(a) $\phi = 2°, \theta = 0, \psi = 0$,

(b) $\phi = -2°, \theta = 0, \psi = 0$,

(c) $\phi = 4°, \theta = 0, \psi = 0$,

(d) $\phi = -4°, \theta = 0, \psi = 0$,
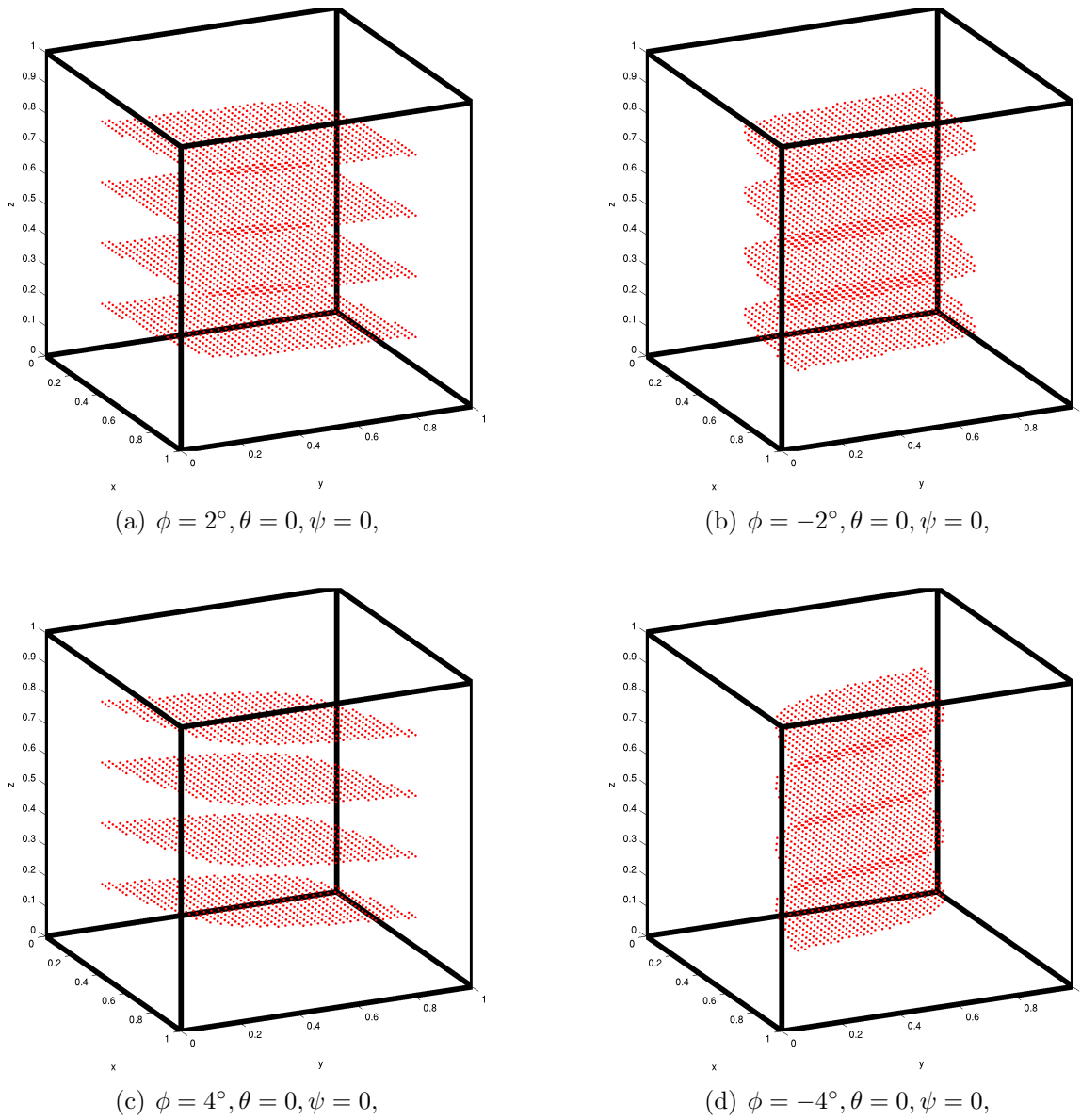
Figure 4.4: COWCWs of the CDPM depicted in Fig. 4.3, for various sets of ZYZ (ϕ, θ, ψ) Euler angles.

Consider now a six-dimensional box $\mathcal{B}_{\boldsymbol{\zeta}}$ with diagonally opposite corners $(\underline{\boldsymbol{\zeta}}, \underline{\mathbf{p}})$ and $(\overline{\boldsymbol{\zeta}}, \overline{\mathbf{p}})$, respectively, i.e., $\mathcal{B}_{\boldsymbol{\zeta}} = \{(\boldsymbol{\zeta}, \mathbf{p}) \in \mathbb{R}^3 \times \mathbb{R}^3 : \underline{\boldsymbol{\zeta}} \preceq \boldsymbol{\zeta} \preceq \overline{\boldsymbol{\zeta}}, \ \underline{\mathbf{p}} \preceq \mathbf{p} \preceq \overline{\mathbf{p}}\}$, and in which $\boldsymbol{\zeta} \in \mathbb{R}^3$ is a three dimensional vector whose elements represent the selected Euler angles. In order to find a necessary condition for $\mathcal{B}_{\boldsymbol{\zeta}}$ to be outside of the WCW, we substitute eq. (??) in problem (4.17), and we let $\mathbf{p}$ and $\boldsymbol{\zeta}$, become decision variables of

the problem, while confining them to $\mathcal{B}_\zeta$. This leads to

$$\text{maximize} \quad \delta_s,$$
$$\text{subject to} \quad \mathbf{A}^T\boldsymbol{\mu} - \mathbf{1}_m\mathbf{p}^T\boldsymbol{\mu} - \mathbf{B}^T\mathbf{Q}^T\boldsymbol{\mu} + \mathbf{F}^T\boldsymbol{\gamma} - \mathbf{K}^T\boldsymbol{\gamma} \succeq \mathbf{0}_m,$$
$$\mathbf{1}_m^T\mathbf{A}^T\boldsymbol{\mu} - m\mathbf{p}^T\boldsymbol{\mu} - \mathbf{1}_m^T\mathbf{B}^T\mathbf{Q}^T\boldsymbol{\mu} + \mathbf{1}_m^T\mathbf{F}^T\boldsymbol{\gamma} - \mathbf{1}_m^T\mathbf{K}^T\boldsymbol{\gamma} \geq \delta_s, \quad (4.19)$$
$$\underline{\boldsymbol{\zeta}} \preceq \boldsymbol{\zeta} \preceq \overline{\boldsymbol{\zeta}}, \ \underline{\mathbf{p}} \preceq \mathbf{p} \preceq \overline{\mathbf{p}},$$

where $\boldsymbol{\lambda} \equiv [\boldsymbol{\mu}^T \ \ \boldsymbol{\gamma}^T]^T$. Considering $\mathbf{p}$ and $\boldsymbol{\zeta}$ as optimization variables in (4.19) provides us a tool to find a necessary condition for $\mathcal{B}_\zeta$ to be outside of the WCW. If we let $\mathcal{W}$ represent the set of moving-platform that is necessarily met by any box $\mathcal{B}_\zeta$ such that $\mathcal{B}_\zeta \cap \mathcal{W} = \emptyset$.

In order to find explicit upper and lower bounds on the elements of the rotation matrix $\mathbf{Q}$, they are treated as interval variables. As an example, suppose that the rotation matrix $\mathbf{Q}$ is computed from (z, y, z) Euler angles ϕ, θ and ψ, namely,

$$\mathbf{Q} = \begin{bmatrix} \cos\theta\cos\phi\cos\psi - \sin\phi\sin\psi & -\cos\theta\cos\phi\sin\psi - \sin\phi\cos\psi & \sin\theta\cos\phi \\ \cos\theta\sin\phi\cos\psi + \cos\phi\sin\psi & -\cos\theta\sin\phi\sin\psi + \cos\phi\cos\psi & \sin\theta\sin\phi \\ -\sin\theta\cos\psi & \sin\theta\sin\psi & \cos\theta \end{bmatrix} \quad (4.20)$$

Then, for a given ranges of orientation angles $\underline{\theta} \leq \theta \leq \overline{\theta}$, $\underline{\phi} \leq \phi \leq \overline{\phi}$ and $\underline{\psi} \leq \psi \leq \overline{\psi}$, we have

$$\underline{c}_\phi \leq \cos(\phi) \leq \overline{c}_\phi, \quad \underline{s}_\phi \leq \sin(\phi) \leq \overline{s}_\phi,$$
$$\underline{c}_\theta \leq \cos(\theta) \leq \overline{c}_\theta, \quad \underline{s}_\theta \leq \sin(\theta) \leq \overline{s}_\theta, \quad (4.21)$$
$$\underline{c}_\psi \leq \cos(\psi) \leq \overline{c}_\psi, \quad \underline{s}_\psi \leq \sin(\psi) \leq \overline{s}_\psi.$$

Hence, the elements of the rotation matrix are interval variables, which are obtainable by interval arithmetics. Let us represent this by introducing the matrices $\underline{\mathbf{Q}}$ and $\overline{\mathbf{Q}}$, whose elements are the lower and upper bounds of the elements of the rotation matrix $\mathbf{Q}$, that is

$$\underline{\mathbf{Q}} \preceq \mathbf{Q} \preceq \overline{\mathbf{Q}}. \quad (4.22)$$

Hence eq. (4.19) can be relaxed as

$$\text{maximize} \quad \delta_s,$$
$$\text{subject to} \quad \mathbf{A}^T\boldsymbol{\mu} - \mathbf{1}_m\mathbf{p}^T\boldsymbol{\mu} - \mathbf{B}^T\mathbf{Q}^T\boldsymbol{\mu} + \mathbf{F}^T\boldsymbol{\gamma} - \mathbf{K}^T\boldsymbol{\gamma} \succeq \mathbf{0}_m,$$
$$\mathbf{1}_m^T\mathbf{A}^T\boldsymbol{\mu} - m\mathbf{p}^T\boldsymbol{\mu} - \mathbf{1}_m^T\mathbf{B}^T\mathbf{Q}^T\boldsymbol{\mu} + \mathbf{1}_m^T\mathbf{F}^T\boldsymbol{\gamma} - \mathbf{1}_m^T\mathbf{K}^T\boldsymbol{\gamma} \geq \delta_s, \quad (4.23)$$
$$\underline{\mathbf{Q}} \preceq \mathbf{Q} \preceq \overline{\mathbf{Q}}, \ \underline{\mathbf{p}} \preceq \mathbf{p} \preceq \overline{\mathbf{p}}$$

Notice that eq. (4.23) is the relaxed form of eq. (4.19) and these equations are not equivalent.

Considering the position vector $\mathbf{p}$ and rotation matrix $\mathbf{Q}$ as optimization variables, equation (4.23) provides us a non linear program whose global optimum indicates whether at least one pose of the box $\mathcal{B}_\zeta$ is outside of the WCW. Conversely, if the global optimum of this problem corresponds to $\delta_s = 0$, then the box $\mathcal{B}_\zeta$ is completely inside the WCW. Instead, alike the planar case studied in Chapter 3, we relax the non convex constraints of problem (4.23), to convex constraints over box $\mathcal{B}_\zeta$ which makes it easier for a pose to be excluded from the WCW.

Equation (4.23) includes the bilinear elements $\mathbf{p}^T\boldsymbol{\mu}$, $\mathbf{F}^T\boldsymbol{\gamma}$, and $\mathbf{Q}^T\boldsymbol{\mu}$, and the trilinear element $\mathbf{K}^T\boldsymbol{\gamma}$, in terms of $\boldsymbol{\mu}$, $\boldsymbol{\gamma}$, $\mathbf{Q}$ and $\mathbf{p}$. In order to eliminate the trilinear term appearing in problem (4.23) let us define the variable
$\mathbf{V} \equiv \begin{bmatrix} \mathbf{Q}_x^T\mathbf{p} & \mathbf{Q}_y^T\mathbf{p} & \mathbf{Q}_z^T\mathbf{p} \end{bmatrix} \in \mathbb{R}^{3\times3}$ where, $\mathbf{Q}_x = \mathbf{H}_x^T\mathbf{Q}$, $\mathbf{Q}_y = \mathbf{H}_y^T\mathbf{Q}$, and $\mathbf{Q}_z = \mathbf{H}_z^T\mathbf{Q}$. Upper and lower bounds are obtainable for the components of matrices $\mathbf{Q}_x$, $\mathbf{Q}_y$, $\mathbf{Q}_z$, as their components are directly those of the rotation matrix $\mathbf{Q}$. Consequently, we can obtain upper and lower bonds on the components of the matrix $\mathbf{V}$ by using interval arithmetics as they are the result of the multiplication of interval variables. We express this by the following equation:
$$\underline{\mathbf{V}} \preceq \mathbf{V} \preceq \overline{\mathbf{V}}. \tag{4.24}$$
Introducing this new variable enables us to rewrite the expressions of matrices $\mathbf{F}$ and $\mathbf{K}$ appearing in eq. (4.10) as
$$\mathbf{F} = \begin{bmatrix} (\mathbf{Q}_x\mathbf{b}_1)^T\mathbf{a}_1 & \cdots & (\mathbf{Q}_x\mathbf{b}_m)^T\mathbf{a}_m \\ (\mathbf{Q}_y\mathbf{b}_1)^T\mathbf{a}_1 & \cdots & (\mathbf{Q}_y\mathbf{b}_m)^T\mathbf{a}_m \\ (\mathbf{Q}_z\mathbf{b}_1)^T\mathbf{a}_1 & \cdots & (\mathbf{Q}_z\mathbf{b}_m)^T\mathbf{a}_m \end{bmatrix} \in \mathbb{R}^{3\times m}, \mathbf{K} = \mathbf{V}^T\mathbf{B}. \tag{4.25}$$
Substituting eq. (4.25) in problem (4.23) removes the trilinear element $\mathbf{K}^T\boldsymbol{\gamma}$ and changes it to a bilinear element in terms of $\mathbf{V}$ and $\boldsymbol{\gamma}$. Let us now separate the bilinear elements appearing in eq. (4.23) in terms of $\boldsymbol{\mu}$, $\boldsymbol{\gamma}$, $\mathbf{Q}$ $\mathbf{V}$ and $\mathbf{p}$ and define the new variables as follows:
$$\boldsymbol{\eta} \equiv \text{diag}(\boldsymbol{\mu})\mathbf{p} \in \mathbb{R}^3, \qquad \boldsymbol{\nu} \equiv \mathbf{Q}^T\text{diag}(\boldsymbol{\mu}) \in \mathbb{R}^3, \tag{4.26}$$
$$\boldsymbol{\Lambda} \equiv \text{diag}(\mathbf{I}_6\boldsymbol{\gamma})\mathbf{Q}_{xyz} \in \mathbb{R}^{6\times3}, \quad \boldsymbol{\Delta} \equiv \mathbf{V}\text{diag}(\boldsymbol{\gamma}) \in \mathbb{R}^{3\times3},$$

where $\mathbf{Q}_{xyz} = [\mathbf{Q}_x^T\mathbf{E}_x^T \quad \mathbf{Q}_y^T\mathbf{E}_y^T \quad \mathbf{Q}_z^T\mathbf{E}_z^T]^T \in \mathbb{R}^{6\times3}$, and $\mathbf{I}_6 = \begin{bmatrix} \mathbf{1}_2 & \mathbf{0}_2 & \mathbf{0}_2 \\ \mathbf{0}_2 & \mathbf{1}_2 & \mathbf{0}_2 \\ \mathbf{0}_2 & \mathbf{0}_2 & \mathbf{1}_2 \end{bmatrix} \in \mathbb{R}^{6\times3}$.

While the variables $\mathbf{p}$, $\mathbf{V}$ and $\mathbf{Q}$ are bounded, the variables $\boldsymbol{\mu}$ and $\boldsymbol{\gamma}$ are unbounded. Alike the planar case, for the sake of this analysis, let us assume the signs of $\boldsymbol{\mu}$ and $\boldsymbol{\gamma}$ to be known in advance, and let us label them

$$\boldsymbol{\sigma} \equiv \mathrm{sgn}(\boldsymbol{\mu}) \qquad \text{and} \qquad \boldsymbol{\tau} \equiv \mathrm{sgn}(\boldsymbol{\gamma}), \qquad (4.27)$$

where sgn represents the signum function. Knowing the signs of $\boldsymbol{\mu}$ and $\boldsymbol{\gamma}$ enables us to find the following bounds on the newly defined variables:

$$\mathrm{diag}(\boldsymbol{\sigma})\mathrm{diag}(\underline{\mathbf{p}})\boldsymbol{\mu} \preceq \mathrm{diag}(\boldsymbol{\sigma})\boldsymbol{\eta} \preceq \mathrm{diag}(\boldsymbol{\sigma})\mathrm{diag}(\overline{\mathbf{p}})\boldsymbol{\mu},$$
$$\underline{\mathbf{V}}\mathrm{diag}(\boldsymbol{\tau})\mathrm{diag}(\boldsymbol{\gamma}) \preceq \boldsymbol{\Delta}\mathrm{diag}(\boldsymbol{\tau}) \preceq \overline{\mathbf{V}}\mathrm{diag}(\boldsymbol{\tau})\mathrm{diag}(\boldsymbol{\gamma}),$$
$$\underline{\mathbf{Q}}^T\mathrm{diag}(\boldsymbol{\mu})\mathrm{diag}(\boldsymbol{\sigma}) \preceq \boldsymbol{\nu}\mathrm{diag}(\boldsymbol{\sigma}) \preceq \overline{\mathbf{Q}}^T\mathrm{diag}(\boldsymbol{\mu})\mathrm{diag}(\boldsymbol{\sigma}),$$
$$\mathrm{diag}(\mathbf{I}_6\boldsymbol{\tau})\mathrm{diag}(\mathbf{I}_6\boldsymbol{\gamma})\underline{\mathbf{Q}}_{xyz} \preceq \mathrm{diag}(\mathbf{I}_6\boldsymbol{\tau})\boldsymbol{\Lambda} \preceq \mathrm{diag}(\mathbf{I}_6\boldsymbol{\tau})\mathrm{diag}(\mathbf{I}_6\boldsymbol{\gamma})\overline{\mathbf{Q}}_{xyz} \qquad (4.28)$$

Treating $\boldsymbol{\tau}$ and $\boldsymbol{\sigma}$ as constants, the set formed by eq. (4.28) represents a closed convex polytope, which approximates the non-convex surfaces of eq. (4.26). Therefore, replacing the latter with the former, we obtain a *convex relaxation* of eq. (4.26). This approximation converges to the exact relationship as the size of box $\mathcal{B}_\zeta$ becomes infinitesimal. This is the reformulation-linearization technique (RLT) [36], and was introduced in Chapter 3.

Introducing the matrix $\mathbf{I}_E = \begin{bmatrix} \mathbf{E}_x^T & \mathbf{E}_y^T & \mathbf{E}_z^T \end{bmatrix} \in \mathbb{R}^{3\times 6}$ and substituting the newly defined variables in eq. (4.23) enables us to write the relaxed form of equation (4.23) as

maximize $\qquad \delta_s,$

subject to $\qquad \mathbf{A}^T\boldsymbol{\mu} - \mathbf{B}^T\boldsymbol{\nu}\mathbf{1}_3 - \mathbf{1}_m\mathbf{1}_3^T\boldsymbol{\eta} + \mathrm{diag}(\mathbf{A}^T\mathbf{I}_E\boldsymbol{\Lambda}\mathbf{B}) - \mathbf{B}^T\boldsymbol{\Delta}\mathbf{1}_3 \succeq \mathbf{0}_m,$

$\qquad \mathbf{1}_m^T\mathbf{A}^T\boldsymbol{\mu} - \mathbf{1}_m^T\mathbf{B}^T\boldsymbol{\nu}\mathbf{1}_3 - m\mathbf{1}_3^T\boldsymbol{\eta} + \mathbf{1}_m^T\mathrm{diag}(\mathbf{A}^T\mathbf{I}_E\boldsymbol{\Lambda}\mathbf{B}) - \mathbf{1}_m^T\mathbf{B}^T\boldsymbol{\Delta}\mathbf{1}_3 \geq \delta_s,$

$\qquad \mathrm{diag}(\boldsymbol{\sigma})\mathrm{diag}(\underline{\mathbf{p}})\boldsymbol{\mu} \preceq \mathrm{diag}(\boldsymbol{\sigma})\boldsymbol{\eta} \preceq \mathrm{diag}(\boldsymbol{\sigma})\mathrm{diag}(\overline{\mathbf{p}})\boldsymbol{\mu},$

$\qquad \underline{\mathbf{V}}\mathrm{diag}(\boldsymbol{\tau})\mathrm{diag}(\boldsymbol{\gamma}) \preceq \boldsymbol{\Delta}\mathrm{diag}(\boldsymbol{\tau}) \preceq \overline{\mathbf{V}}\mathrm{diag}(\boldsymbol{\tau})\mathrm{diag}(\boldsymbol{\gamma}), \qquad (4.29)$

$\qquad \underline{\mathbf{Q}}^T\mathrm{diag}(\boldsymbol{\mu})\mathrm{diag}(\boldsymbol{\sigma}) \preceq \boldsymbol{\nu}\mathrm{diag}(\boldsymbol{\sigma}) \preceq \overline{\mathbf{Q}}^T\mathrm{diag}(\boldsymbol{\mu})\mathrm{diag}(\boldsymbol{\sigma}),$

$\qquad \mathrm{diag}(\mathbf{I}_6\boldsymbol{\tau})\mathrm{diag}(\mathbf{I}_6\boldsymbol{\gamma})\underline{\mathbf{Q}}_{xyz} \preceq \mathrm{diag}(\mathbf{I}_6\boldsymbol{\tau})\boldsymbol{\Lambda} \preceq \mathrm{diag}(\mathbf{I}_6\boldsymbol{\tau})\mathrm{diag}(\mathbf{I}_6\boldsymbol{\gamma})\overline{\mathbf{Q}}_{xyz},$

$\qquad \boldsymbol{\sigma} = \mathrm{sgn}(\boldsymbol{\mu}) \qquad \text{and} \qquad \boldsymbol{\tau} = \mathrm{sgn}(\boldsymbol{\gamma}).$

The only non-convex constraints in problem (4.29) are the last two equalities. However, these inequalities yield exactly 64 possible combinations of $\boldsymbol{\sigma}$ and $\boldsymbol{\tau}$, which are

the solutions to

$$\text{diag}(\boldsymbol{\sigma})^2 = \mathbf{1}_{3\times 3} \qquad \text{and} \qquad \text{diag}(\boldsymbol{\tau})^2 = \mathbf{1}_{3\times 3}. \qquad (4.30)$$

Let us label these solutions $\boldsymbol{\sigma}_j$ and $\boldsymbol{\tau}_j$, $j = 1, \ldots, 64$. As a result, the solution to problem (4.29) is the maximum of the outcomes of the 64 linear programs. Introducing the function vec() as

$$\text{vec}() : \mathbb{R}^{p\times q} \longrightarrow \mathbb{R}^{pq}, \quad \text{vec}(\mathbf{U}) = \begin{bmatrix} \mathbf{u}_1 & \mathbf{u}_2 & \ldots & \mathbf{u}_p \end{bmatrix}^T \in \mathbb{R}^{pq}, \qquad (4.31)$$
$$\forall \mathbf{U} \in \mathbb{R}^{p\times q}, \quad \mathbf{U} = \begin{bmatrix} \mathbf{u}_1^T & \mathbf{u}_2^T & \ldots & \mathbf{u}_p^T \end{bmatrix}^T, \ \mathbf{u}_i \in \mathbb{R}^{1\times q}, \ i = 1, \ldots, p.$$

enables us to represent these linear programs by the following lemma

Lemma 10 *Sufficient Condition for a 3D Box to Lie Inside the WCW of a Spatial Cable-Driven Parallel Mechanism within a Given Range of Orientation Angles Consider the 64 distinct linear programs*

$$\begin{aligned} \text{maximize} \quad & \delta_{s,j}, \\ \text{subject to} \quad & \mathbf{G}_j \boldsymbol{\xi}_j \preceq \mathbf{0}_{m+79} \\ & j = 1, \ldots, 64, \end{aligned} \qquad (4.32)$$

where
$$\mathbf{G}_j \equiv \begin{bmatrix} \mathbf{g}^T & 1 \\ \mathbf{R}_j^T & \mathbf{0}_{m+78} \end{bmatrix} \in \mathbb{R}^{(m+79)\times 46}, \ \mathbf{R}_j \text{ and vector } \mathbf{g} \text{ are given in Appendix D, and}$$
$$\boldsymbol{\xi}_j = \begin{bmatrix} \boldsymbol{\mu}_j^T & \boldsymbol{\gamma}_j^T & \boldsymbol{\eta}_j^T & \text{vec}(\boldsymbol{\nu}_j)^T & \text{vec}(\boldsymbol{\Delta}_j)^T & \text{vec}(\boldsymbol{\Lambda}_j)^T & \delta_{s,j} \end{bmatrix}^T \in \mathbb{R}^{46}. \text{ Then, the given box}$$
$\mathcal{B}_\zeta = \{(\boldsymbol{\zeta}, \mathbf{p}) \in \mathbb{R}^3 \times \mathbb{R}^3 : \underline{\boldsymbol{\zeta}} \preceq \boldsymbol{\zeta} \preceq \overline{\boldsymbol{\zeta}}, \ \underline{\mathbf{p}} \preceq \mathbf{p} \preceq \overline{\mathbf{p}}\}$ *is fully inside the WCW if all of the problems (4.32), $j = 1, \ldots, 64$, yield zero.*

Proof. The proof is similar to that of lemma 7. $\square$

Hence, problem (4.32) provides a sufficient condition for a 3D box to lie completely inside the WCW within a given range of orientation angles. This condition may be used to compute a *contracted* WCW, namely, a subset of the Cartesian workspace that is guaranteed to lie inside the WCW. The following example illustrates the concept of the contracted WCW in the case of spatial CDPMs.

Example 4.2 The Contracted WCW of a Spatial Cable-Driven Parallel Mechanism

Consider again the CDPM depicted in Fig. 4.3. We calculated the real wrench closure workspace of this mechanism by discretizing the examined region into several points, and by applying eq. (4.16) in example 4.1. Using the same procedures with several 3D boxes instead of points and applying eq. (4.32), instead of eq. (4.16) we calculate the contracted WCW of this mechanism within a given range of orientation angles. We divide the Cartesian space into three-dimensional boxes, each box covering the interval $[-0.03 \quad -0.03 \quad -0.03]^T$ rad $\leq \boldsymbol{\zeta} \leq [0.03 \quad 0.03 \quad 0.03]^T$ rad in the rotation workspace ,i.e., the workspace specified by ZYZ Euler angles. In the Cartesian space, each box has an edge of length 0.02 along the x, y and z axes. We solve problem (4.32) for each of these 3D boxes, and keep only those for which the maximum is 0. We obtain the contracted WCW, which is shown in Figs. (4.5), along with cross-sections of the exact COWCWs. This contracted WCW is the common WCW of the constant-orientation WCWs (COWCWs) corresponding to each orientations within the given range. Smaller boxes would have led to a closer estimate of the WCW, as the convex relaxation (4.28) then forms a tighter approximation of (4.26). Also, notice that dividing the rotation workspace accompanying with dividing the Cartesian workspace can provide even tighter bounds on the convex relaxation of eq. (4.28), but it increases the size of the corresponding linear program and may make the formulation more complicated for our main concern of finding a formulation for the dimensional synthesis of spatial CDPMs. However this could be the main goal of the future works.
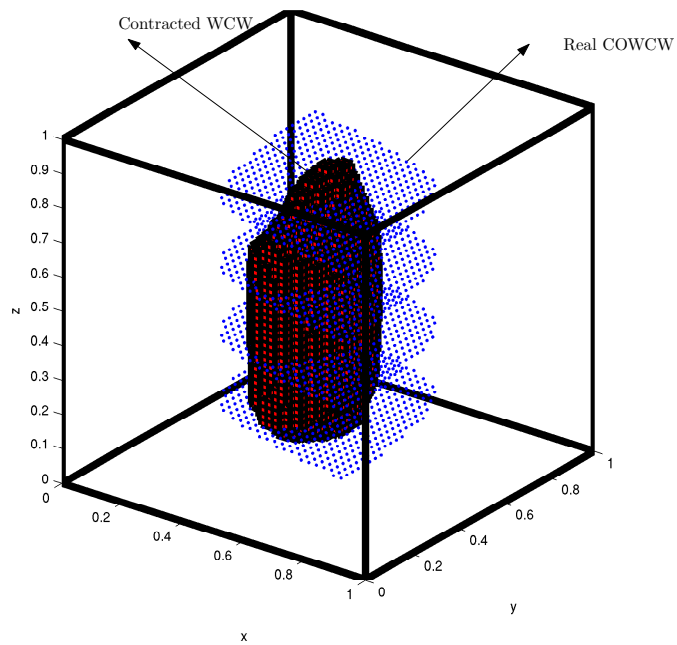
(a) $\phi = -0.03\, rad, \theta = -0.03\, rad, \psi = -0.03\, rad$
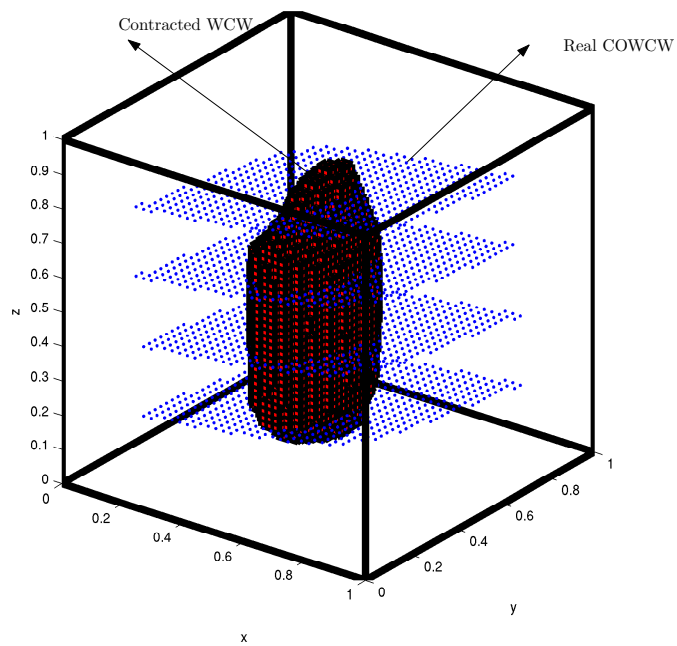
(b) $\phi = 0.03\, rad, \theta = 0.03\, rad, \psi = 0.03\, rad$

Figure 4.5: The contracted and the real COWCW of a spatial CDPM.

As they were obtained in problem (4.32), the inequality constraints can always be satisfied by choosing $\boldsymbol{\xi}_j = \mathbf{0}_{46}$. For the purpose of later assembling them, we would like these constraints to be feasible only if a given box is fully inside the WCW. To this end, we compute the Lagrange dual [37] of problem (4.32). Let us start by writing the Lagrangian of problem (4.32),

$$L(\mathbf{x}_j, \boldsymbol{\xi}_j) = \mathbf{x}_j^T(\mathbf{G}_j\boldsymbol{\xi}_j) - \delta_{s,j}, \tag{4.33}$$

where $\mathbf{x}_j \in \mathbb{R}_+^{m+46}$ is the vector of Lagrange multipliers and $\mathbb{R}_+$ represents the non-negative real numbers. Hence, the Lagrange dual of our problem is that of maximizing $\theta_j(\mathbf{x}_j)$, where

$$\theta_j(\mathbf{x}_j) = \inf_{\boldsymbol{\xi}_j} L(\mathbf{x}_j, \boldsymbol{\xi}_j), \tag{4.34}$$

Considering $\delta_{s,j} = \mathbf{e}_{46}^T\boldsymbol{\xi}_j$, where $\mathbf{e}_{46} = [\mathbf{0}_{45}^T \quad 1]^T \in \mathbb{R}^{46}$, and substituting eq. (4.33) into eq. (4.34) gives

$$\theta_j(\mathbf{x}_j) = \inf_{\boldsymbol{\xi}_j} (\mathbf{x}_j^T\mathbf{G}_j - \mathbf{e}_{46}^T)\boldsymbol{\xi}_j. \tag{4.35}$$

Clearly,

$$\theta(\mathbf{x}_j) = \begin{cases} 0 & \text{if } \mathbf{G}_j^T\mathbf{x}_j = \mathbf{e}_{46}, \\ -\infty & \text{otherwise.} \end{cases} \tag{4.36}$$

Hence, the dual problem of problem (4.32) can be stated as the following feasibility problem:

$$\begin{aligned} \text{maximize} \quad & 0, \\ \text{subject to} \quad & \mathbf{G}_j^T\mathbf{x}_j - \mathbf{e}_{46} = \mathbf{0}_{46}, \\ & \mathbf{x}_j \succeq \mathbf{0}_{m+79}, \\ \text{over} \quad & \mathbf{x}_j. \end{aligned} \tag{4.37}$$

The last equality constraint of this linear program implies $x_{j,1} = 1$, where $x_{j,1}$ represents the first element of the Lagrange multiplier $\mathbf{x}_j$. Substituting this in eq. (4.37) eliminates $x_{j,1}$ as a variable and reduces the number of equality constraints from 46 to 45, which yields,

$$\begin{aligned} \text{maximize} \quad & 0, \\ \text{subject to} \quad & \mathbf{R}_j\mathbf{y}_j + \mathbf{g} = \mathbf{0}_{45}, \\ & \mathbf{y}_j \succeq \mathbf{0}_{m+78}, \\ \text{over} \quad & \mathbf{y}_j, \end{aligned} \tag{4.38}$$

where $\mathbf{y}_j \in \mathbb{R}_+^{m+78}$ represents the vector of Lagrange multipliers after eliminating the last equality constraint of eq. (4.37).

Problem (4.38) is equivalent to its primal problem (4.32) but is feasible when the corresponding problem (4.32) is zero and infeasible when the primal is unbounded. These correspond to cases 3 and 1, respectively, of the primal-dual relationships enumerated in Chapter 3. In order to verify whether a given box $\mathcal{B}_\zeta$ is inside the WCW of a given spatial CDPM for a given range of orientation angles, we may combine all these linear programs into one for $j = 1, \ldots, 64.$. Alike problem (3.20), this is done by summing the objective values of these problems while considering all of their constraints together as follows:

$$
\begin{aligned}
\text{maximize} \quad & 0, \\
\text{subject to} \quad & \mathbf{R}_j \mathbf{y}_j + \mathbf{g} = \mathbf{0}_{45}, \qquad j = 1, \ldots, 64, \\
& \mathbf{y}_j \succeq \mathbf{0}_{m+78}, \quad j = 1, \ldots, 64, \\
\text{over} \quad & \mathbf{y}_j, \qquad\qquad\qquad j = 1, \ldots, 64.
\end{aligned}
\tag{4.39}
$$

Notice that eq. (4.38) represents 64 linear programs while eq. (4.39) represents only one, but with 64 times more variables and constraints. Equation (4.39) may now be regarded as a single feasibility problem of 2880 equality constraints and $64(m + 78)$ non-negative variables. If there is a feasible solution to this problem, then the given box $\mathcal{B}_\zeta$ is inside the WCW. Having this information, we can now turn our attention to the problem of the synthesis of spatial cable-driven parallel mechanisms.

4.4 A Formulation for the Problem of Synthesizing a Spatial CDPM

We start from problem (4.39) in order to solve the dimensional synthesis of CDMPs. Suppose we are interested in finding a CDPM geometry whose WCW contains a given box $\mathcal{B}_\zeta$ within a given range of orientation angles. In order to solve this problem, we

introduce the nonlinear feasibility problem

satisfy $\quad \mathbf{R}_j \mathbf{y}_j + \mathbf{g} = \mathbf{0}_{45}, \quad j = 1, \ldots, 64,$ $\qquad (4.40)$

$$\mathbf{y}_j \succeq \mathbf{0}_{m+78}, \quad j = 1, \ldots, 64,$$

$$\underline{\mathbf{a}} \preceq \mathbf{a}_i \preceq \overline{\mathbf{a}}, \ \ \underline{\mathbf{b}} \preceq \mathbf{b}_i \preceq \overline{\mathbf{b}}, \ \ i = 1, \ldots, m,$$

over $\quad \mathbf{y}_j \in \mathbb{R}^{m+78}, \ j = 1, \ldots, 64, \ \mathbf{a}_i \in \mathbb{R}^3, \ \mathbf{b}_i \in \mathbb{R}^3, \ i = 1, \ldots, m,.$

Here, $\underline{\mathbf{a}}$, $\overline{\mathbf{a}}$, $\underline{\mathbf{b}}$ and $\overline{\mathbf{b}}$ are lower and upper bounds on the positions of the base and MP attachments points, which would otherwise be drawn to infinity during the solution process. Any solution to problem (4.40) yields a CDPM geometry whose WCW is guaranteed to include the prescribed box $\mathcal{B}_\zeta$. However, the absence of a solution to this problem does not imply that there is no possible CDPM geometry containing $\mathcal{B}_\zeta$. Moreover, the failure to obtain a solution from this feasibility problem does not provide any information regarding a *good* but *not perfect* geometry. For this reason, in the next section, we add an objective function over the constraints, which is thought to be more attractive to the designer.

4.4.1 Adjoining an Objective Function to the Feasibility Problem (4.40)

Suppose we look for the geometry of a CDPM whose WCW includes a prescribed box $\mathcal{B}_\zeta$. Alike the planar case introduced in Section 3.3.1, if we use a scaled version of $\mathcal{B}_\zeta$ in problem (4.40) and can find a CDPM geometry whose WCW allows for a scaling factor above one, then the original problem is solved. Hence, we must consider the scaling factor as an objective function to be maximized. If, at the optimum point, this factor is smaller than one, then the designer is left with the best infeasible solution.

Since the prescribed box has six dimensions and includes point-position and orientation intervals, we suggest to set the priority on one of the two sets of components so as to preserve the dimensional homogeneity of the problem. Hence, we restrict the problem to that of finding a CDPM with a large WCW for a given range of orientation angles. In other words, we consider the prescribed six-dimensional box as Cartesian product of two three-dimensional boxes, one covering point-position, the other covering the Euler angles. We then maximize the size of point-position box while keeping the size of the orientation box constant.

This scaling process is depicted in Fig. 4.6 for a prescribed six dimensional box $\mathcal{B}_\varsigma$, which is split in two point-position and orientation boxes. Figure 4.6(a) shows the scaled point-position box $\mathcal{B}'_p$ with dashed lines in pale yellow, which is the scaled image of the smaller point-position box $\mathcal{B}_p$ with solid lines in orange. Figure **??** shows the orientation box $\mathcal{B}_o$ whose size remains unchanged. The scaling factor is s and the position of the scaling point is represented by $\mathbf{p}_c$. From this figure, we obtain the

(a) Scaled point-positional box and its corresponding parameters

(b) Orientation box
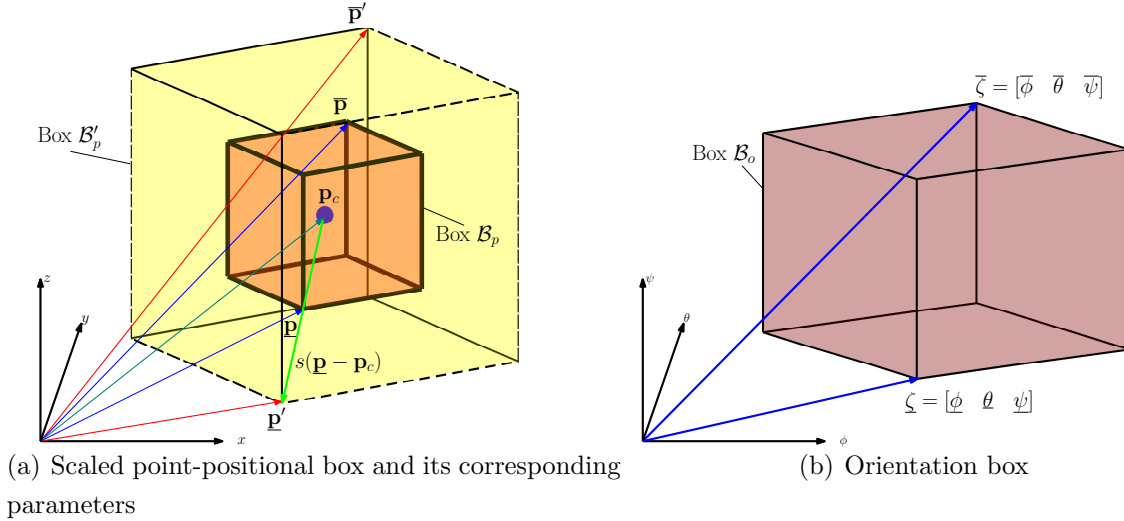
Figure 4.6: Representing the six-dimensional prescribed box as the Cartesian product of two three-dimensional boxes.

coordinates of the lower-left-front and upper-right-back vertices of the scaled box $\mathcal{B}'_p$ as

$$\underline{\mathbf{p}}' = \mathbf{p}_c + s(\underline{\mathbf{p}} - \mathbf{p}_c) \ \text{ and } \ \overline{\mathbf{p}}' = \mathbf{p}_c + s(\overline{\mathbf{p}} - \mathbf{p}_c), \tag{4.41}$$

respectively. If we consider the centroid of the box as the scaling point, then $\mathbf{p}_c = \frac{1}{2}(\overline{\mathbf{p}} + \underline{\mathbf{p}})$. Introducing this objective function enables us to develop a nonlinear program for the dimensional synthesis of CDPMs.

4.4.2 A Nonlinear Program for the Dimensional Synthesis of CDPMs

We now turn the feasibility problem (4.40) into a nonlinear program where $\mathbf{R}'_j$ is obtained by substituting $\overline{\mathbf{p}}'$ and $\underline{\mathbf{p}}'$ for $\overline{\mathbf{p}}$ and $\underline{\mathbf{p}}$, respectively, in the expression of $\mathbf{R}_j$ given in problem (4.32). Moreover, to ensure that $\underline{\mathbf{p}}'$ and $\overline{\mathbf{p}}'$ remain the lower-left-front and

upper-right-back corners of the scaled 3D positional box, we constrain the scaling factor s to non-negative real numbers. Hence, the corresponding nonlinear program to solve the synthesis of CDPMs for a prescribed box $\mathcal{B}_\zeta$ is

$$
\begin{aligned}
\text{maximize} \quad & s \\
\text{subject to} \quad & \mathbf{R}'_j \mathbf{y}_j + \mathbf{g} = \mathbf{0}_{45}, \\
& \underline{\mathbf{p}}' - \mathbf{p}_c - s(\underline{\mathbf{p}} - \mathbf{p}_c) = \mathbf{0}_3, \\
& \overline{\mathbf{p}}' - \mathbf{p}_c - s(\overline{\mathbf{p}} - \mathbf{p}_c) = \mathbf{0}_3, \\
& \underline{\mathbf{a}} \preceq \mathbf{a}_i \preceq \overline{\mathbf{a}}, \ \ \underline{\mathbf{b}} \preceq \mathbf{b}_i \preceq \overline{\mathbf{b}}, \ \ i = 1, \ldots, m, \\
& \mathbf{y}_j \succeq \mathbf{0}_{m+78}, \ \ j = 1, \ldots, 64, \\
& s \geq 0, \\
\text{over} \quad & \mathbf{y}_j \in \mathbb{R}^{m+78}, \ \ \mathbf{a}_i \in \mathbb{R}^3, \ \ \mathbf{b}_i \in \mathbb{R}^3, \ \ s \in \mathbb{R}.
\end{aligned}
\tag{4.42}
$$

We illustrate problem (4.42) with a synthesis example in the following section.

Example 4.3 The Dimensional Synthesis of a CDPM for a Prescribed Three-Dimensional Box

Suppose we look for a spatial CDPM whose WCW contains a three-dimensional prescribed box within a given range of orientations. The lower-left-front and upper-right-back coordinates of this box are $\underline{\mathbf{p}} = [0.4 \quad 0.4 \quad 0.4]^T$ and $\overline{\mathbf{p}} = [0.6 \quad 0.6 \quad 0.6]^T$, respectively. This box is required to lie inside the WCW of a spatial CDPM within $\frac{-\pi}{12}\mathbf{1}_3 \preceq \boldsymbol{\zeta} \preceq \frac{\pi}{12}\mathbf{1}_3$ where $\boldsymbol{\zeta} = [\phi \quad \theta \quad \psi]^T$ represents ZYZ Euler angles. The number of cables is set to 7 which is the minimum required for a WCW to exist. The geometry of the CDPM is constrained inside the bounds reported in Table 4.2. In order to

Table 4.2: Bounds on the geometry of the sought spatial CDPM.

$\underline{\mathbf{a}}^T$	$\overline{\mathbf{a}}^T$	$\underline{\mathbf{b}}^T$	$\overline{\mathbf{b}}^T$
$[0 \quad 0 \quad 0]$	$[1 \quad 1 \quad 1]$	$[-0.2 \quad -.2 \quad -0.2]$	$[0.2 \quad .2 \quad 0.2]$

solve the nonlinear program (4.42) associated with this example, we implemented the PSLP method [38] in Matlab. This method was introduced in Chapter 3 and a brief explanation of it is reported in Appendix C. We use the "*Large-scale*" algorithm of the *Linprog* function in Matlab to solve the direction-finding subproblems of the PSLP method. The required initial guess is uniformly-distributed pseudo-random , produced by the *rand* function in Matlab. In order to ensure that the produced initial guesses

cover well the feasible set, we use the following formulation to produce the initial geometry, this formulation being the counterpart of eq. (3.47):

$$\mathbf{a}_i = \underline{\mathbf{a}} + \mathrm{diag}(\overline{\mathbf{a}} - \underline{\mathbf{a}})\boldsymbol{\alpha}_i, \tag{4.43}$$
$$\mathbf{b}_i = \underline{\mathbf{b}} + \mathrm{diag}(\overline{\mathbf{b}} - \underline{\mathbf{b}})\boldsymbol{\beta_i}, \quad i = 1, \ldots, m,$$

where $\boldsymbol{\alpha_i} \in \mathbb{R}^3$ and $\boldsymbol{\beta_i} \in \mathbb{R}^3$ are pseudo-random numbers produced by *rand* function of Matlab. Applying the PSLP method to problem (4.42) with the initial geometry reported in Table 4.3 yields the mechanism depicted in Fig. 4.7. The coordinates describing the geometry of this CDPM are reported in Table 4.4.

Table 4.3: The initial CDPM geometry in example 4.3.

i	$\mathbf{a}_{i,0}^T$	$\mathbf{b}_{i,0}^T$
1	$[0.7195 \quad 0.9388 \quad 0.0529]$	$[-0.0660 \quad -0.0621 \quad 0.0492]$
2	$[0.5544 \quad 0.2530 \quad 0.4870]$	$[-0.0489 \quad -0.1087 \quad -0.0920]$
3	$[0.8436 \quad 0.1315 \quad 0.9629]$	$[0.1859 \quad -0.0882 \quad -0.1333]$
4	$[0.8422 \quad 0.8157 \quad 0.4625]$	$[0.0238 \quad 0.0821 \quad -0.0163]$
5	$[0.3223 \quad 0.7279 \quad 0.2520]$	$[-0.1676 \quad 0.1788 \quad -0.1051]$
6	$[0.2353 \quad 0.1533 \quad 0.9439]$	$[-0.1835 \quad -0.0044 \quad 0.1826]$
7	$[0.1222 \quad 0.5299 \quad 0.1280]$	$[0.1904 \quad 0.1273 \quad -0.0582]$

An optimum scaling factor of $s^* = 1.5663$ is obtained after 44 minutes of calculation time on a computer equipped by Intel(R) Core(TM) i7-2600 CPU @3.40GHz and 8 GB of RAM memory. Figure 4.8 shows the evolution of the objective during the calculation. Notice that, PSLP is a penalty based method and during the solution procedure we may increase the penalty parameter as it must be at least as large as the absolute value of any Lagrange multiplier associated with equality and inequality constraints. Increasing the penalty parameter gives the priority to find a feasible solution rather than of maximizing the objective. Hence, the objective may not increase monotonically during the solution procedure.

Since the optimum value is greater than one, the scaled box and the prescribed one are both inside the WCW of the obtained mechanism, within the given range of orientation angles. This is confirmed in Fig. 4.9, as the scaled box in dashed lines and prescribed box in solid lines are both located inside the COWCWs of the resulting spatial CDPM, which are represented by cloud of points. Notice that we only show constant-orientation WCW of the resulting CDPM, because a six-dimensional WCW

Table 4.4: The optimum CDPM geometry in example 4.3.

i	$\mathbf{a}_{i,f}^T$			$\mathbf{b}_{i,f}^T$		
1	[1.0000	1.0000	0.5632]	[0.0000	0.0000	0.0000]
2	[0.0006	0.4487	1.0000]	[0.0000	0.0000	0.0000]
3	[0.9961	0.0000	0.5402]	[0.0834	-0.0297	-0.0710]
4	[0.9961	0.0000	0.5402]	[-0.0833	0.0297	0.0710]
5	[0.0849	0.6725	0.0005]	[-0.0491	-0.0031	0.0001]
6	[0.3174	0.0093	0.0072]	[0.0000	0.0000	0.0000]
7	[0.0849	0.6725	0.0005]	[0.0492	0.0031	-0.0001]

cannot be represented directly. On the right side of Fig. 4.9, we display the cable-cable interference regions of the corresponding MP orientations, although they were not taken into account in the proposed synthesis method. These regions were obtained by using the algorithm proposed in [43]. According to this algorithm, two cables that have a common attachment point either on the fixed base or on the moving platform do not collide. Interestingly, with the CDPM geometry obtained, several pairs of cables are in this situation. More precisely,the pairs of points $\{\mathbf{a}_{3,f}, \mathbf{a}_{4,f}\}$ and $\{\mathbf{a}_{5,f}, \mathbf{a}_{7,f}\}$ coincide on the fixed base and the triplet $\{\mathbf{b}_{1,f}, \mathbf{b}_{2,f}, \mathbf{b}_{6,f}\}$ coincide on the moving platform, as shown in Table 4.4. Hence, although the obtained mechanism is not free of interferences, it has relatively few interference regions for this reason. Moreover, the location of the attachment points on the edges of the MP limits the interferences between the cables and the end-effector [44].

The formulation developed in this section is only applicable to rectangular prescribed workspaces. In order to cover irregularly-shaped workspaces, one would need a set of boxes. Moreover, the performance of the method, depends on the size of the prescribed box, as smaller boxes lead to better approximations of the WCW. On the contrary, when the prescribed box becomes too large, problem (4.42) may not admit any feasible solution even though, in practice, some exist. Hence, accounting for multiple boxes presents some interest, and is the subject of the following section.
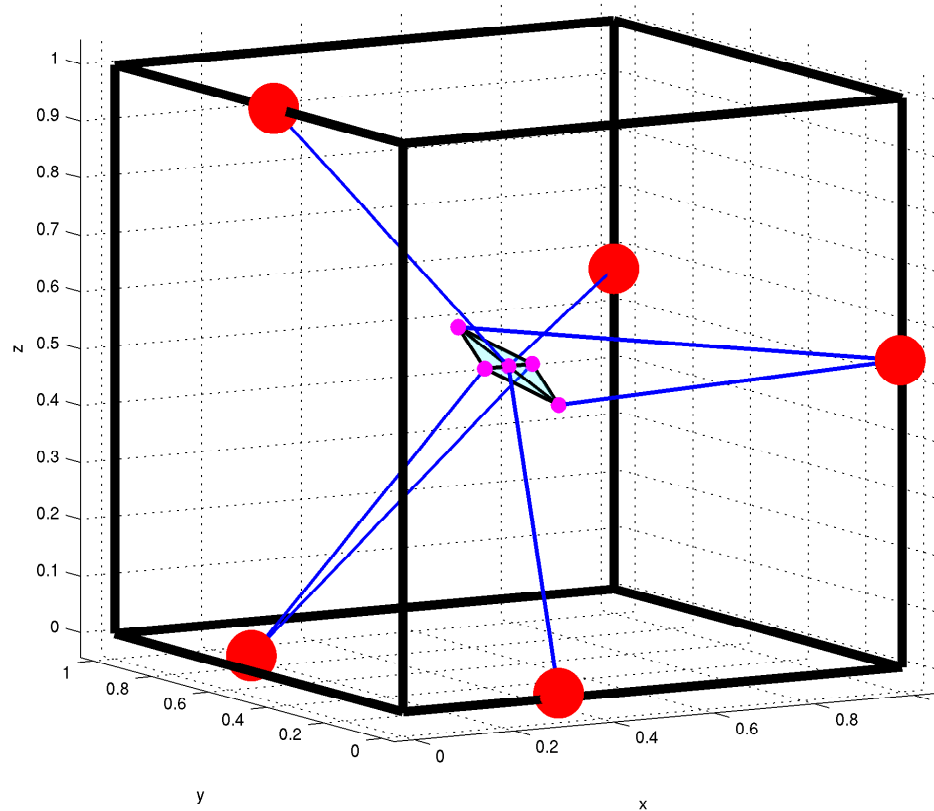
(a) 3D view, $\phi = 0$, $\theta = 0$, $\psi = 0$
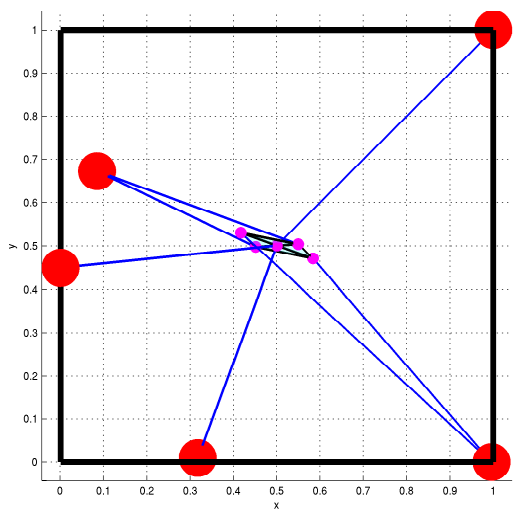
(b) Top view, $\phi = 0$, $\theta = 0$, $\psi = 0$
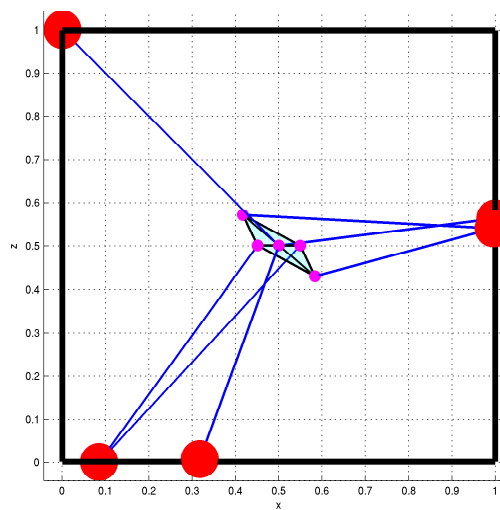
(c) Side view $\phi = 0$, $\theta = 0$, $\psi = 0$

Figure 4.7: A resulting CDPM with seven cables.
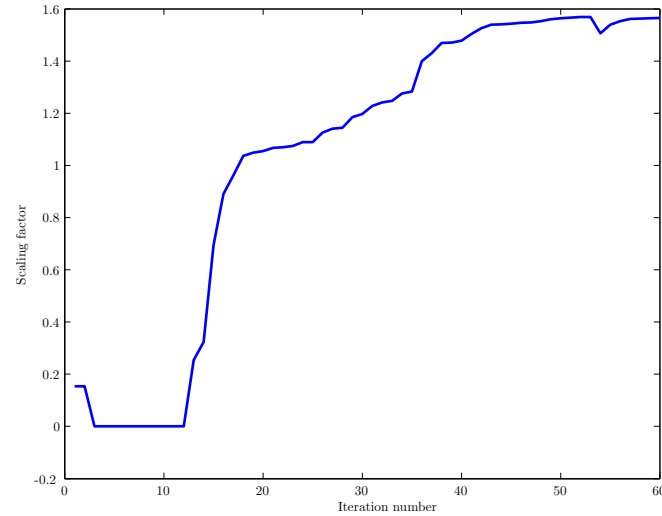
Figure 4.8: Evolution of the objective of example 4.3.

4.5 The Dimensional Synthesis of CDPMs for Multiple Prescribed Boxes and Non-Rectangular Workspaces

Splitting a prescribed box into several smaller boxes provides tighter bounds on the variables defined in problem (4.32) as the bounds on the position vector $\mathbf{p}$ become tighter. This generally leads to a CDPM with a larger WCW compared to that obtained for a single large prescribed box. In order to solve the dimensional synthesis problem for a prescribed workspace composed of multiple boxes, the formulation (4.42) can be developed to include several boxes. This is done by considering the constraints corresponding to each box while attempting to maximize a common scaling factor s with respect to a common scaling point, which may be the centroid of the prescribed
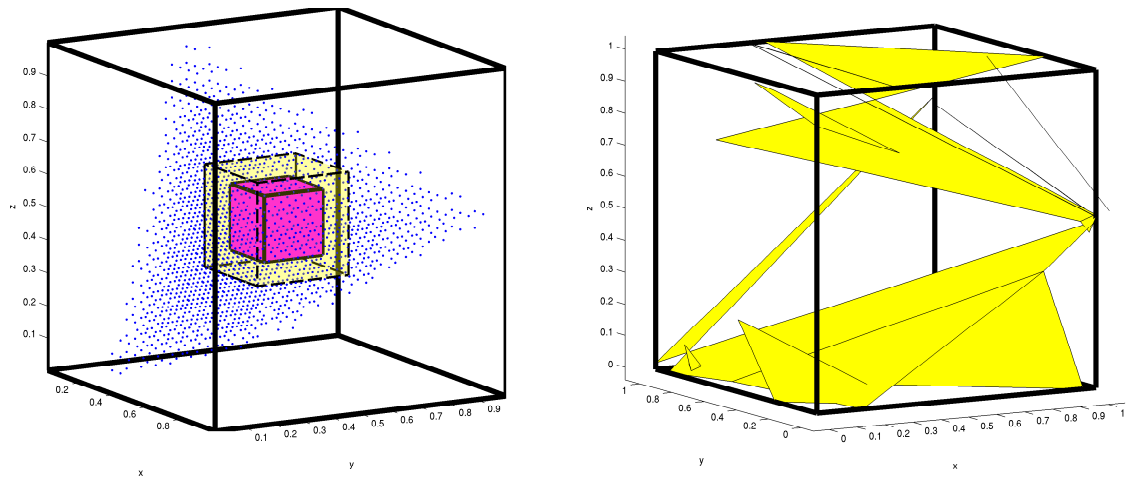
(a) $\phi = -\pi/12\,rad, \theta = -\pi/12\,rad, \psi = -\pi/12\,rad$
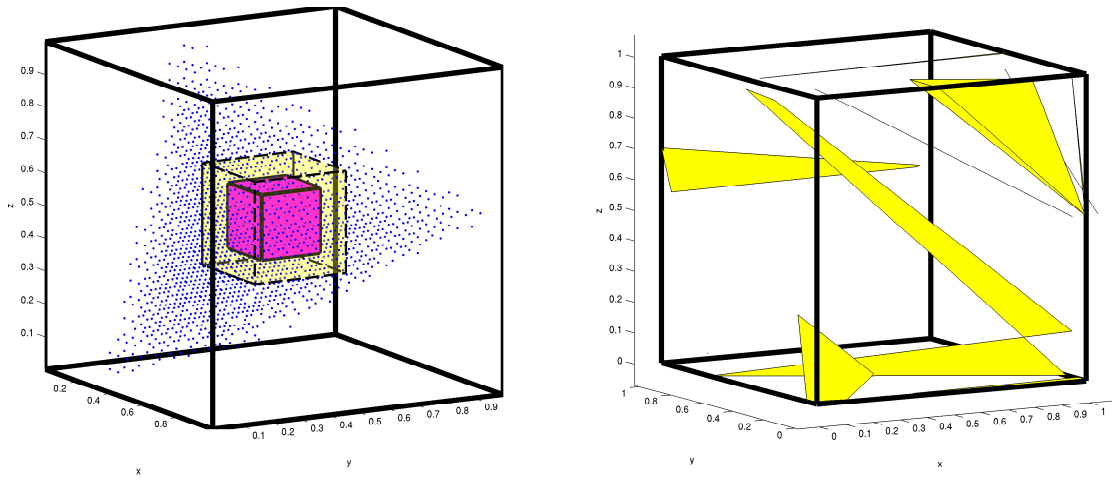
(b) $\phi = 0\,rad, \theta = 0\,rad, \psi = 0\,rad$
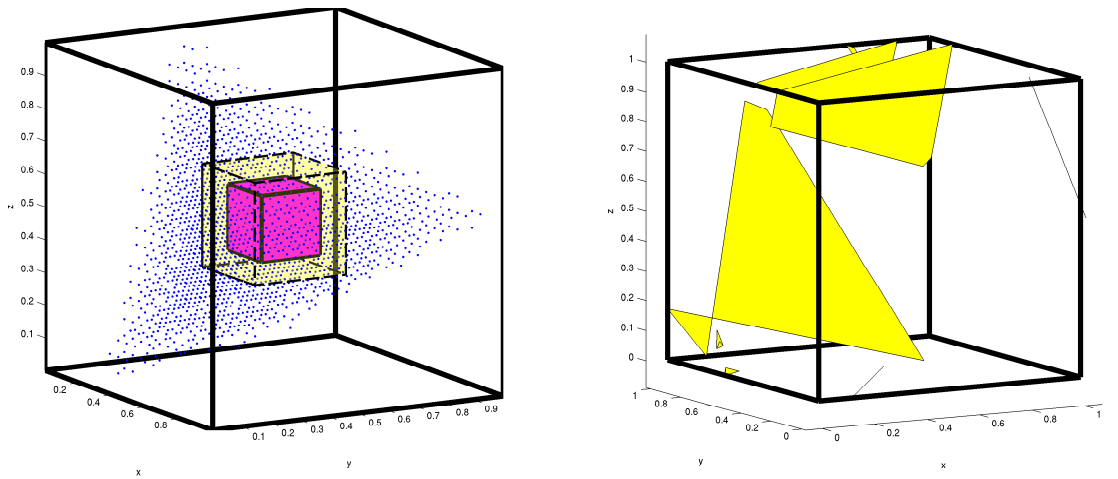
(c) $\phi = \pi/12\,rad, \theta = \pi/12\,rad, \psi = \pi/12\,rad$

Figure 4.9: COWCWs of the CDPM of example 4.2 and the corresponding cable-cable interferences regions.

set of boxes. The corresponding formulation is

$$
\begin{aligned}
\text{maximize} \quad & s \\
\text{subject to} \quad & \mathbf{R}_{k,j}\mathbf{y}_{k,j} + \mathbf{g} = \mathbf{0}_{45}, \\
& \underline{\mathbf{p}}'_k - \mathbf{p}_c - s(\underline{\mathbf{p}}_k - \mathbf{p}_c) = \mathbf{0}_3, \\
& \overline{\mathbf{p}}'_k - \mathbf{p}_c - s(\overline{\mathbf{p}}_k - \mathbf{p}_c) = \mathbf{0}_3, \\
& \underline{\mathbf{a}} \preceq \mathbf{a}_i \preceq \overline{\mathbf{a}}, \ \ \underline{\mathbf{b}} \preceq \mathbf{b}_i \preceq \overline{\mathbf{b}}, \ \ i = 1, \ldots, m, \\
& s \geq 0, \\
& \mathbf{y}_{k,j} \succeq \mathbf{0}_{m+78}, \ \ j = 1, \ldots, 64, \ \ k = 1 \ldots n, \\
\text{over} \quad & \mathbf{y}_{k,j} \in \mathbb{R}^{m+78}, \ \ \mathbf{a}_i \in \mathbb{R}^3, \ \ \mathbf{b}_i \in \mathbb{R}^3, \ s \in \mathbb{R},
\end{aligned}
\tag{4.44}
$$

where n is the number of boxes. Notice that we must consider the lower-left-front corner $\underline{\mathbf{p}}'_k$ and the upper-right-back corner $\overline{\mathbf{p}}'_k$ of each three-dimensional box to construct the matrix $\mathbf{R}_{k,j}$. This forms a nonlinear program with $64n(m+78)+6m+1$ variables, $2886n$ equality constraints, and $64n(m+78)+12m+1$ inequality constraints. Evidently, depending on the number of boxes required, this problem has a high potential of becoming a large-scale nonlinear program. Nevertheless, problem 4.44 provides us with a tool to find a CDPM whose WCW includes a prescribed three-dimensional workspace composed of multiple boxes within a given range of orientations. We illustrate this formulation with the following example.

Example 4.4 The Dimensional Synthesis of a CDPM for a Prescribed Three-Dimensional Workspace Composed of Multiple Boxes

Let us reconsider the prescribed box of example 4.3 and divide it to 4 equally sized boxes. These boxes are obtained by dividing the prescribed box along the y and z axes. We keep the upper and lower bounds on the geometry as reported on Table 4.2, and the ranges of the Euler angles and the number of cables are also the as same as in example 4.3. Depending on the initial point, we obtain different mechanisms two of which are represented in this example.

Figure 4.10 shows the CDPM resulting from a randomly chosen initial guess and the application of the PSLP method to problem 4.44. The corresponding initial and final geometries are reported in Tables 4.5 and (4.6), respectively. The scaling factor s^* at the optimum point equals 1.5898, which is slightly larger than the scaling factor obtained in example 4.3. Figure 4.11 shows the evolution of the scaling factor for this

optimization process. Using the same machine mentioned in previous example, it took eight hours and 47 minutes to obtain this result.

Table 4.5: Initial geometric parameters of example 4.4.

i	$\mathbf{a}_{i,0}^T$			$\mathbf{b}_{i,0}^T$		
1	[0.9690	0.9178	0.4683]	[−0.1988	0.1279	− 0.0475]
2	[0.0638	0.1057	0.5077]	[0.0662	− 0.0737	− 0.0043]
3	[0.2365	0.7545	0.4688]	[−0.0563	− 0.1111	− 0.1354]
4	[0.1437	0.5582	0.4022]	[−0.1894	− 0.0877	− 0.1913]
5	[0.4330	0.6551	0.4869]	[−0.0676	− 0.1327	0.1083]
6	[0.2424	0.0505	0.0663]	[0.0666	− 0.1153	− 0.0809]
7	[0.8958	0.0958	0.9464]	[−0.1167	0.1026	− 0.0304]

Table 4.6: Geometric parameters of the obtained CDPM of figure4.10.

i	$\mathbf{a}_{i,f}^T$			$\mathbf{b}_{i,f}^T$		
1	[1.0000	1.0000	0.4940]	[0.0000	0.0000	0.0000]
2	[0.1691	0.3729	1.0000]	[0.0000	0.0000	0.0000]
3	[0.0028	0.9996	0.2484]	[−0.0263	− 0.0036	− 0.0476]
4	[0.1650	0.2071	0.0000]	[−0.1287	0.0326	− 0.1416]
5	[0.0028	0.9996	0.2484]	[0.0263	0.0036	0.0476]
6	[0.1650	0.2071	0.0000]	[0.1232	− 0.0312	0.1356]
7	[1.0000	0.0001	0.6008]	[0.0000	0.0000	0.0000]

Different COWCWs of the obtained geometry and their corresponding cable-cable interferences regions are depicted in Fig. 4.12. Once more, the obtained mechanism has coinciding attachment points on the fixed base and on the moving platform, leading again to relatively few cable-cable interference regions.

Another interesting result computed using the same approach is depicted in Fig. 4.13. This CDPM was obtained from randomly chosen initial guess while keeping the initial geometry as same as the values reported in Table 4.5. In other words, we change the Lagrange multipliers, $\mathbf{y}_{k,j,0}$ while keeping the initial geometry same as that of Table 4.5. The detailed values of the obtained geometry is reported in Table 4.7. As can be seen from Fig. 4.13 and Table 4.7, two of the seven cables i.e., cables 2 and 4, are almost coincident, and we may end up with an *under constrainted* CDPM rather than a fully constrained one. Indeed, if the points $B_1, \ldots, B_5$ coincide while B_1, B_6 and B_7
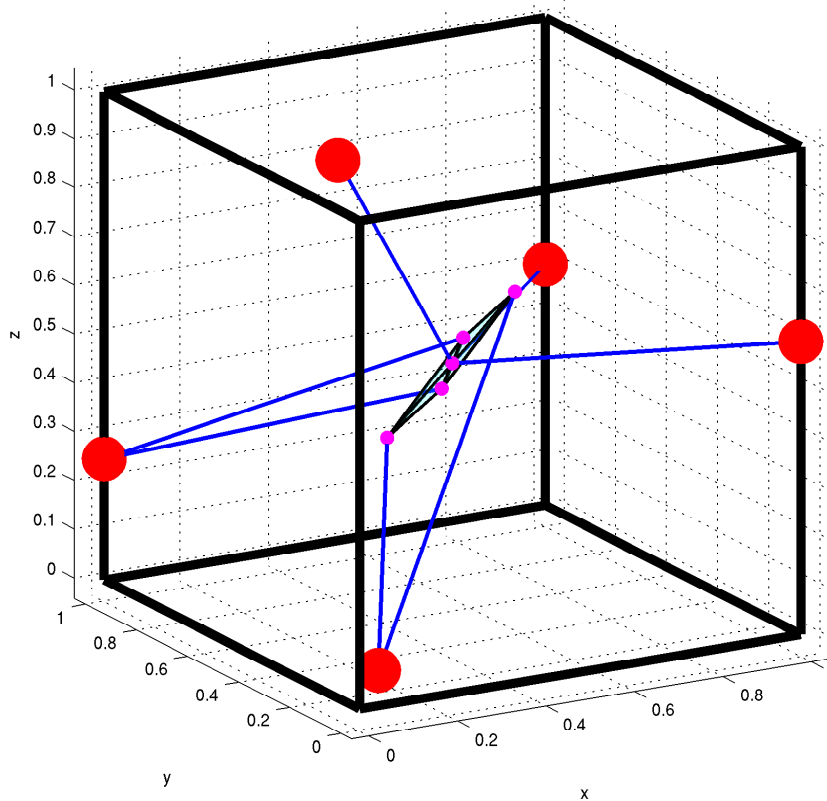
(a) 3D view, $\phi = 0$, $\theta = 0$, $\psi = 0$
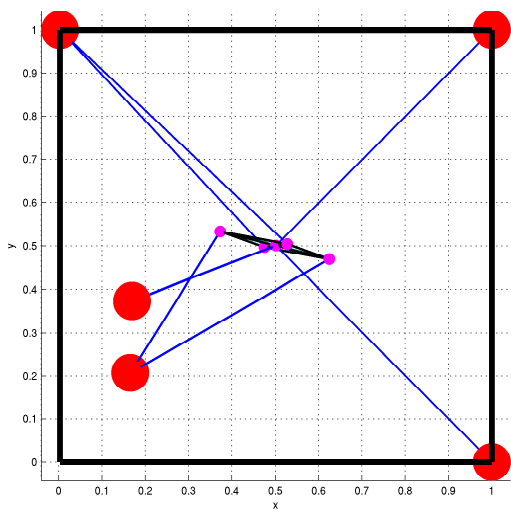
(b) Top view, $\phi = 0$, $\theta = 0$, $\psi = 0$
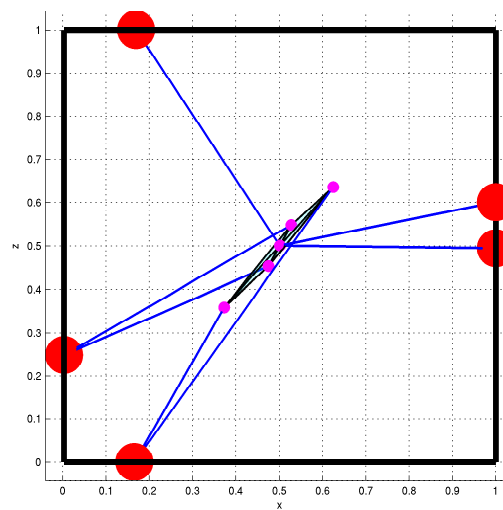
(c) Side view $\phi = 0$, $\theta = 0$, $\psi = 0$

Figure 4.10: First optimum CDPM with seven cables for example 4.4.
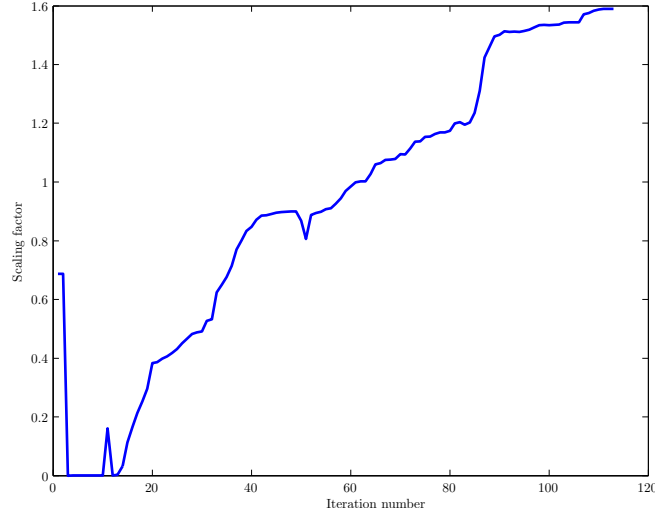
Figure 4.11: Evolution of the objective of example 4.4 for the first solution.

are collinear, then the cables cannot balance a pure moment about the line through $B_1, B6, B_7$.

Table 4.7: Geometric parameters of the CDPM obtained in figure 4.13.

i	$\mathbf{a}_{i,f}^T$			$\mathbf{b}_{i,f}^T$		
1	[0.2206	0.9195	1.0000]	[0.0000	0.0000	0.0000]
2	[1.0000	0.0000	0.4048]	[0.0000	0.0000	0.0000]
3	[0.0000	0.0399	0.4434]	[0.0000	0.0000	0.0000]
4	[1.0000	0.0000	0.4038]	[0.0000	0.0000	0.0000]
5	[0.5001	0.8828	1.0000]	[0.0000	0.0000	0.0000]
6	[0.5446	0.9999	0.0824]	[0.1432	-0.0614	0.1456]
7	[0.5446	0.9999	0.0824]	[-0.1432	0.0614	-0.1456]

The value of the optimum objective corresponding to this result is $s^* = 1.4387$ and its evolution through the optimization is shown in Fig. 4.14. Figure 4.15 shows the COWCWs of the resulting CDPM, along with the corresponding cable-cable interference regions. Interestingly, this mechanism has even less interference regions than the the other two obtained previously.

Since a prescribed workspace may have an irregular shape, and the main challenge of the synthesis problem consists in finding a CDPM whose WCW contains such an arbitrary workspaces. Here the strategy is to estimate this prescribed workspace with multiple three-dimensional boxes. Alike the planar case, we use interval analysis as a

(a) $\phi = -\pi/12\,rad, \theta = -\pi/12\,rad, \psi = -\pi/12\,rad$

(b) $\phi = 0\,rad, \theta = 0\,rad, \psi = 0\,rad$

(c) $\phi = \pi/12\,rad, \theta = \pi/12\,rad, \psi = \pi/12\,rad$

Figure 4.12: COWCWs of the first resulting CDPM of example 4.4 and the corresponding cable-cable interferences regions.
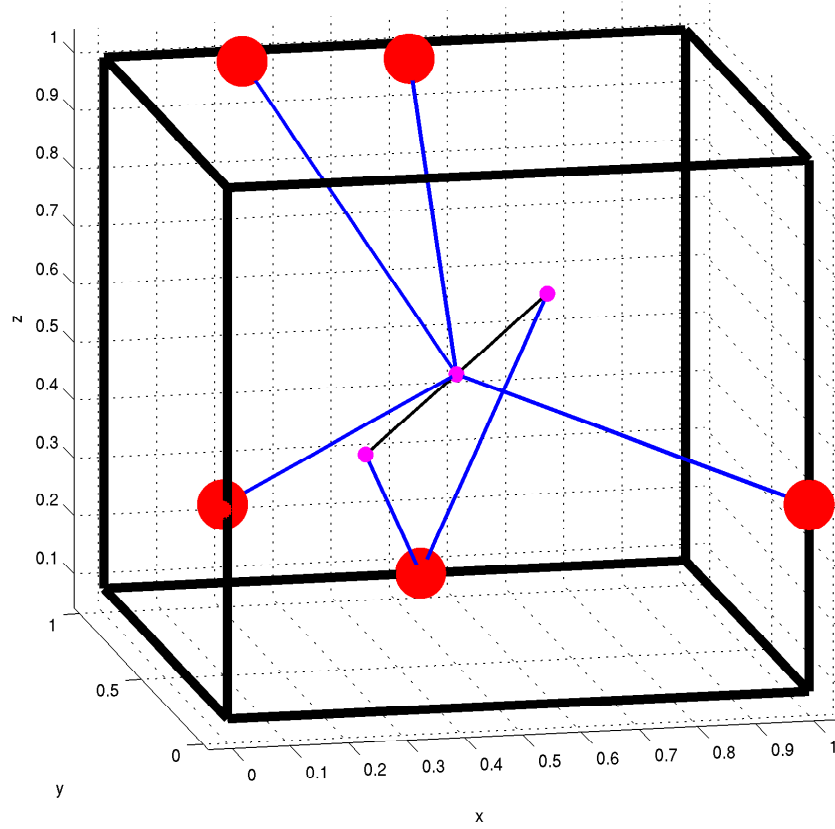
(a) 3D view, $\phi = 0$, $\theta = 0$, $\psi = 0$
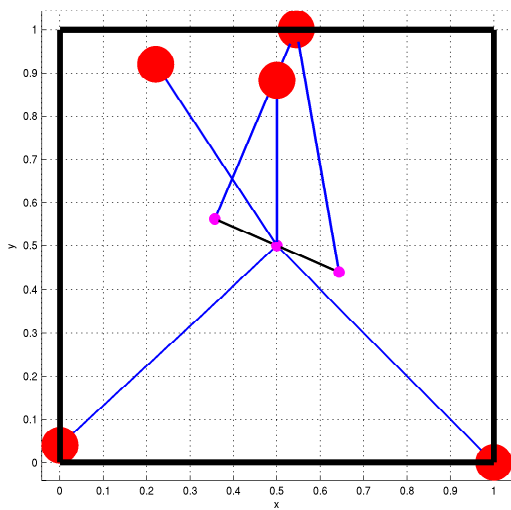
(b) Top view, $\phi = 0$, $\theta = 0$, $\psi = 0$
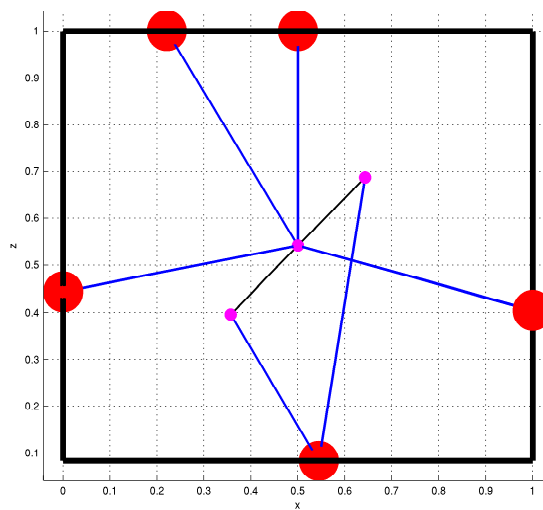
(c) Side view $\phi = 0$, $\theta = 0$, $\psi = 0$

Figure 4.13: Second optimum with six cables for example 4.4.
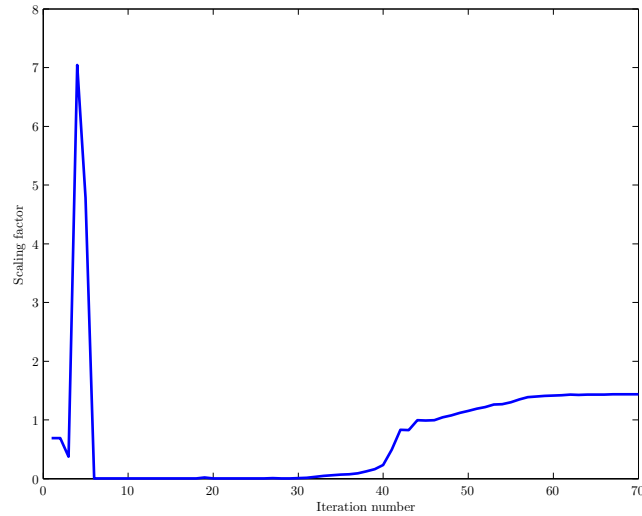
Figure 4.14: Evolution of the objective of example 4.4 for the second solution.

tool to over-estimate the prescribed workspace with a set of such boxes. The procedure is the same as the one we used to estimate the planar prescribed workspaces in Chapter 3. For the sake of conciseness, we avoid reexplaining it here, and rather refer the reader to example 3.3. Once the appropriate set of boxes has been computed, nonlinear program (4.44) can be directly applied to solve the dimensional synthesis of CDPMs. We illustrate this with the following example.
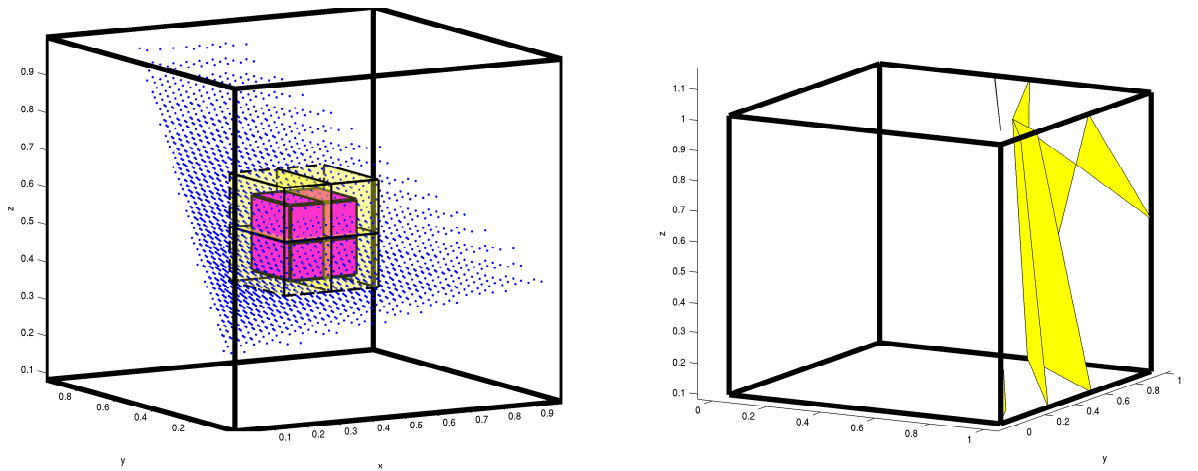
(a) $\phi = -\pi/12\,rad, \theta = -\pi/12\,rad, \psi = -\pi/12\,rad$
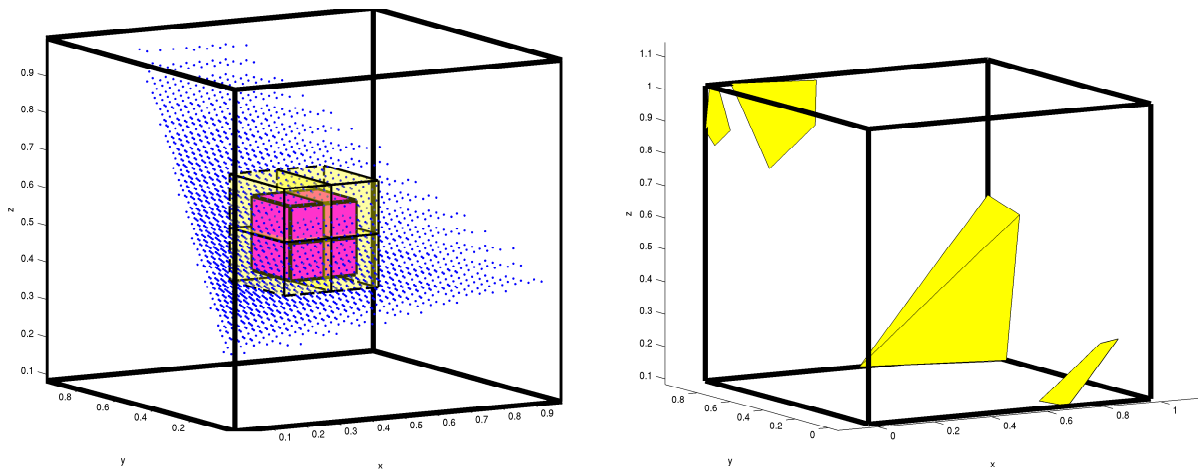
(b) $\phi = 0\,rad, \theta = 0\,rad, \psi = 0\,rad$

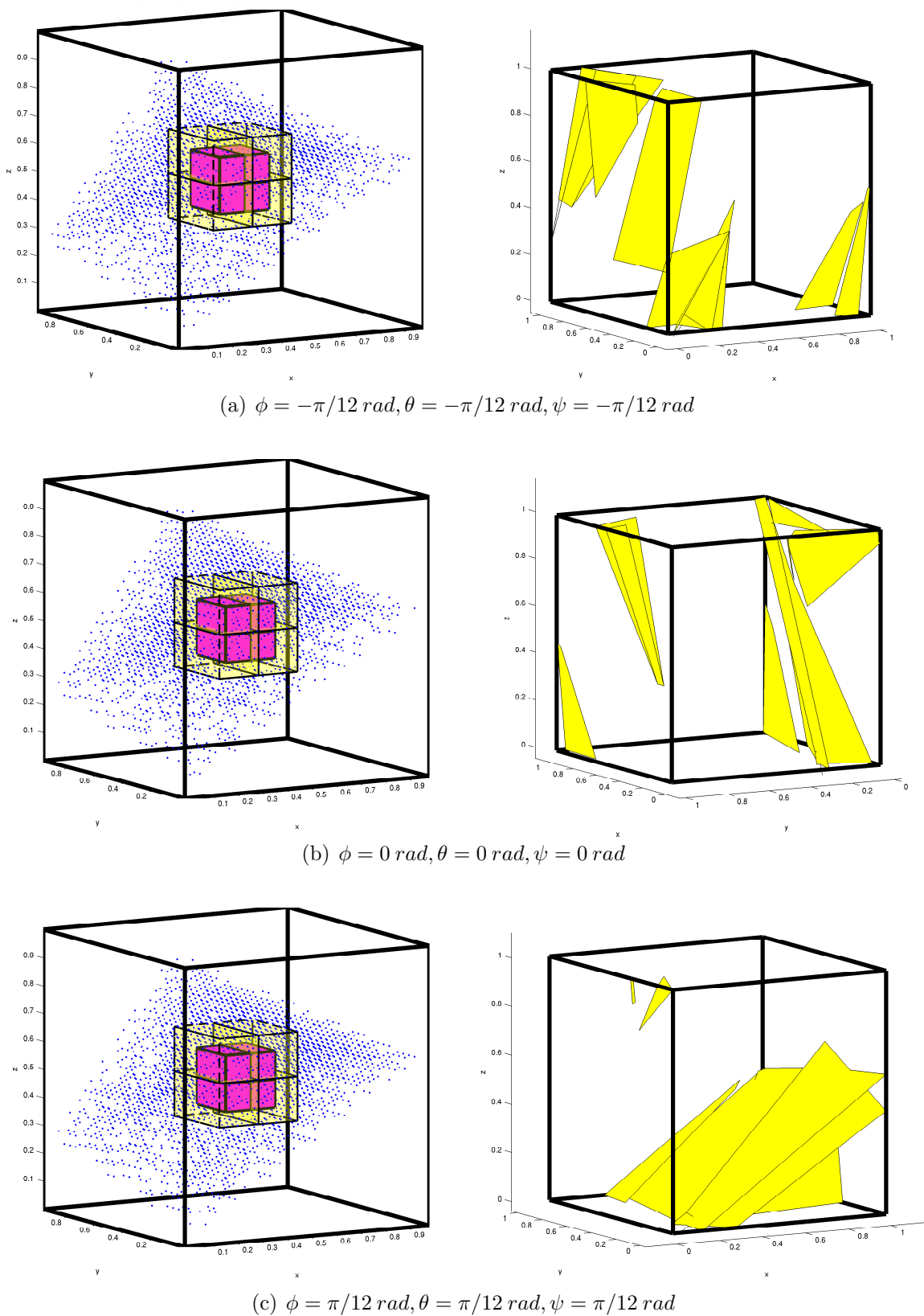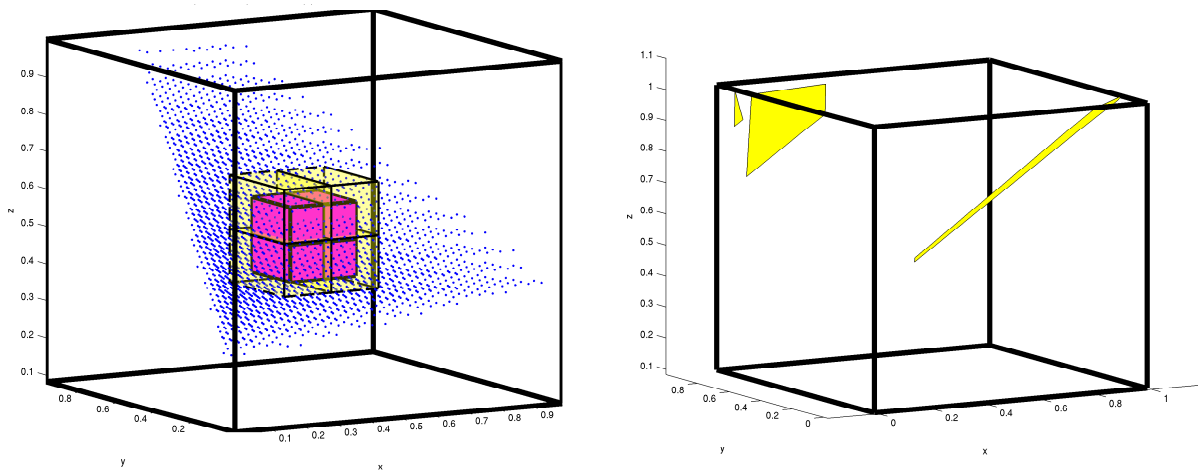(c) $\phi = \pi/12\,rad, \theta = \pi/12\,rad, \psi = \pi/12\,rad$

Figure 4.15: COWCWs of the second resulting CDPM of example 4.4 and the corresponding cable-cable interference regions.

Example 4.5 The Dimensional Synthesis of a CDPM for a Prescribed Irregular Three-Dimensional Workspace

Suppose that we seek for a CDPM whose WCW includes a prescribed workspace with the shape of a unit ball represented by $(x-2)^2 + (y-2)^2 + (z-2)^2 = 1$ within the same orientation range as in the previous example. We set the number of cables to eight and the geometry of the CDPM is bounded within the values provided in Table 4.8.

Table 4.8: Bounds on the geometry of the spatial CDPM of example 4.5.

$\underline{\mathbf{a}}^T$	$\overline{\mathbf{a}}^T$	$\underline{\mathbf{b}}^T$	$\overline{\mathbf{b}}^T$
$[0 \quad 0 \quad 0]$	$[5 \quad 5 \quad 5]$	$[-0.5 \quad -.5 \quad -0.5]$	$[0.5 \quad .5 \quad 0.5]$

A good approximation of this sphere is depicted in Fig. 4.17. Such an approximation includes 54 boxes, and cover the entire sphere.

However, applying problem 4.44 for these multiple boxes requires solving a nonlinear program with 308273 variables and 155844 equality constraints. So as to give the reader an idea of the size of the direction finding sub-problem of the PSLP method, this means solving a linear program with 587825 variables, 308321 inequality constraints and 161280 equality constraints at each iteration. Evidently, this requires a high-performance computer with a strong CPU and a large amount of memory. Instead, we elect to use a rough approximation of this prescribed workspace by only 16 boxes as depicted in Fig. 4.17.

For such approximation, we have to solve the corresponding nonlinear program with 88113 variables and 46176 equality constraints. In each iteration of the direction finding subproblem of the PSLP method, we must solve a linear program with 167985 variables and 88161 inequality constraints and 46080 equality constraints. Unfortunately, *linprog*, the built-in linear program solver of Matlab, is relatively slow to solve such large scale problems, and requires large amounts of memory. Instead, we resort to *IBM ILOG CPLEX* version 12.3 [45] integrated with Matlab, through which we call its linear program solver *CPLEXLP*. This solver is capable of parallel optimization via shared memory parallelism and enjoys good memory-management properties. We use the concurrent optimizer [46] of this solver which runs the dual simplex, the primal simplex,
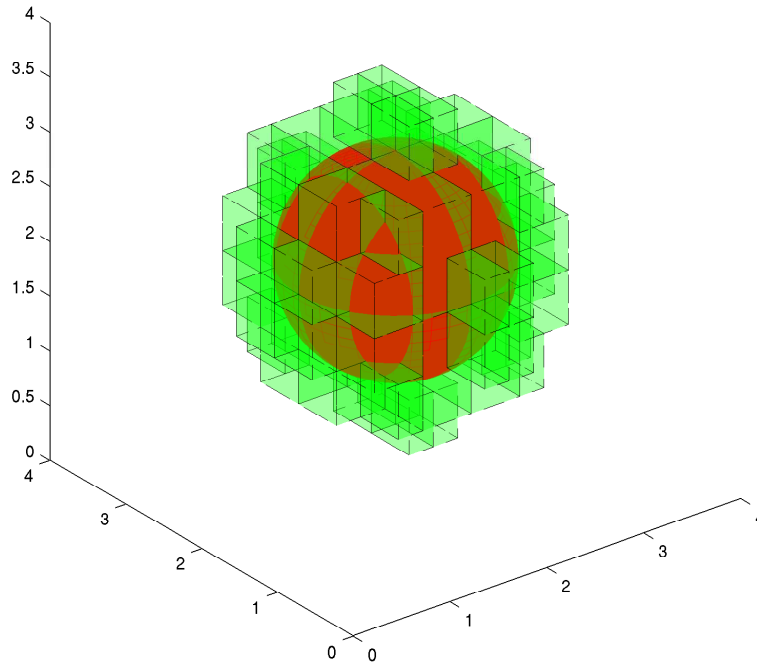
Figure 4.16: A good approximation of the unit ball with 54 boxes.

and barrier methods in parallel on different microprocessors and terminates as soon as the first method finishes.

The mechanism depicted in Fig. 4.18 is the CDPM obtained by applying the PSLP method to problem (4.44) while using CPLEXLP as linear program solver during the solution procedure and with the initial geometry reported on Table 4.9.

The coordinate values of the final geometry are reported in Table 4.10, and the evolution of the objective is shown in Fig. 4.19. The optimum objective value for this example is $s^* = 0.1319$ and the corresponding COWCWs and their cable-cable interference regions are shown in Fig. 4.20. This figure shows that the corresponding COWCWs cover the scaled boxes, depicted with dashed lines, which are smaller than the prescribed boxes, depicted with solid line. Using the same machine mentioned in example 4.3, it took twelve hours and 59 minutes to obtain this result. Although we
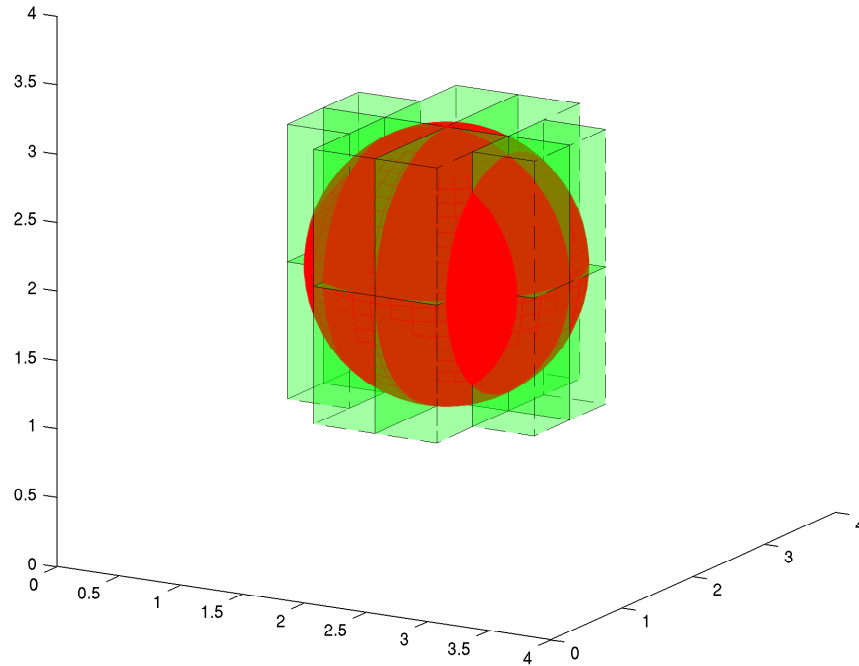
Figure 4.17: A rough approximation of the unit ball with 16 boxes.

Table 4.9: Initial geometric parameters of example 4.5.

i	$\mathbf{a}_{i,0}^T$			$\mathbf{b}_{i,0}^T$		
1	[4.4545	3.1258	3.5588]	[-0.0530	-0.0917	-0.1943]
2	[4.3631	2.6244	1.0961]	[0.3497	-0.4420	-0.2606]
3	[3.0892	4.1774	0.4404]	[0.2094	0.2531	-0.0391]
4	[1.2424	4.3662	3.4800]	[0.3146	-0.0028	-0.1019]
5	[1.7157	3.6551	2.4686]	[0.4722	0.2395	0.1641]
6	[3.8849	2.2735	1.8958]	[-0.0092	0.4212	-0.3672]
7	[2.5938	2.8668	0.6995]	[0.3914	0.4546	-0.0284]
8	[1.0909	3.7087	0.0040]	[-0.4818	0.2894	-0.1322]

ended with a scaling factor smaller than one, notice that we are left with a CDPM design which is not perfect but nevertheless seems to cover the major part of the prescribed boxes with its corresponding COWCWs. Notice that using CPLEX integrated

Table 4.10: Geometric parameters of the CDPM shown in Fig. 4.18.

i	$\mathbf{a}_{i,f}^{T}$	$\mathbf{b}_{i,f}^{T}$
1	$[5.0000 \quad 1.9522 \quad 4.9169]$	$[-0.2193 \quad -0.5000 \quad -0.3040]$
2	$[5.0000 \quad 0.3122 \quad 0]$	$[-0.1917 \quad -0.4566 \quad 0.1850]$
3	$[1.6660 \quad 5.0000 \quad 1.8937]$	$[0.4380 \quad 0.4980 \quad 0.1310]$
4	$[0 \quad 4.5004 \quad 5.0000]$	$[-0.4392 \quad -0.5000 \quad -0.3456]$
5	$[0.0422 \quad 0.0000 \quad 5.0000]$	$[0.4341 \quad 0.4940 \quad 0.4274]$
6	$[0 \quad 0.0000 \quad 0.1995]$	$[0.1515 \quad 0.2452 \quad -0.5000]$
7	$[5.0000 \quad 2.7841 \quad 0.9454]$	$[0.1645 \quad 0.4831 \quad 0.0893]$
8	$[0.0000 \quad 2.0421 \quad 0.0000]$	$[-0.3498 \quad -0.4354 \quad 0.2662]$

in Matlab enabled us to do the computation for this example in a reasonable time, while Matlab built-in function *linprog* is not capable of doing such calculation with the aforesaid machine. Also, increasing the number of boxes or changing the initial guess may lead to results different from the optimum scaling factor reported here. But based on our experience, this may require several days of calculation and ending up with an optimum scaling factor that is very close to zero. The reported result in this example is the best we obtained among the different examples we tried. However, interested readers may try to find a better result.
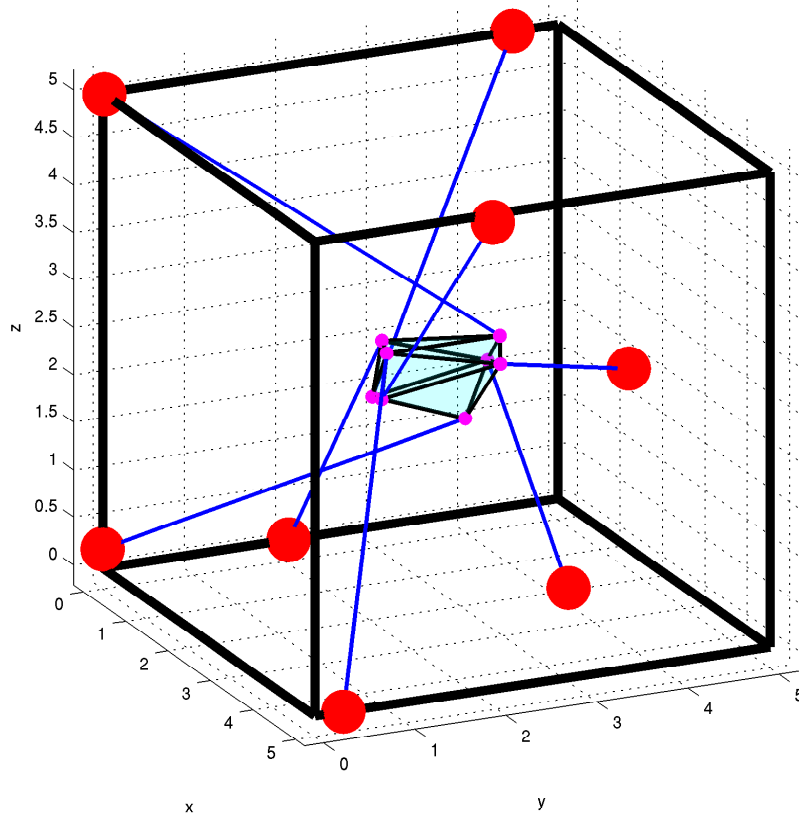
(a) 3D view, $\phi = 0$, $\theta = 0$, $\psi = 0$
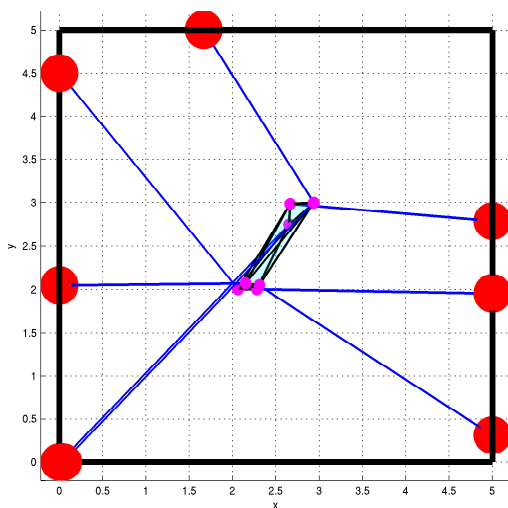
(b) Top view, $\phi = 0$, $\theta = 0$, $\psi = 0$
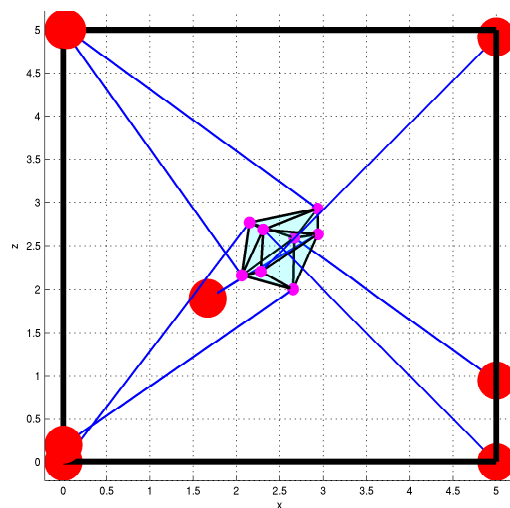
(c) Side view, $\phi = 0$, $\theta = 0$, $\psi = 0$

Figure 4.18: The resulting CDPM for example 4.5.
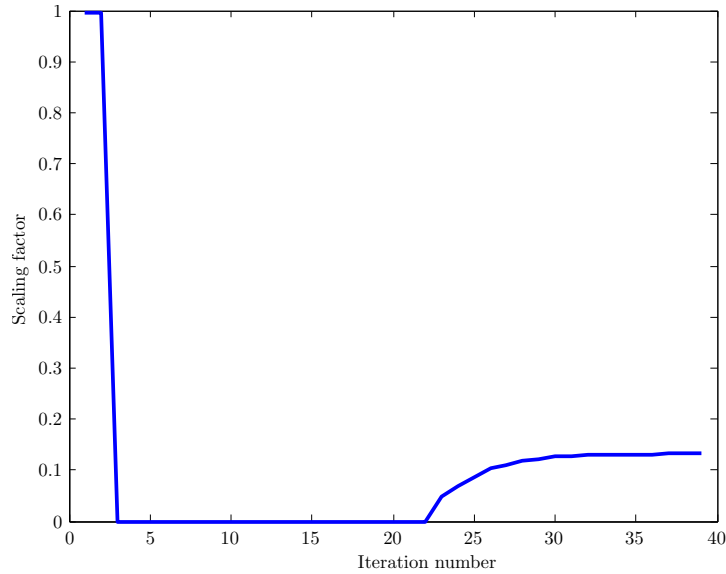
Figure 4.19: Evolution of the objective of example 4.5.

4.6 Conclusion

An algorithm for the dimensional synthesis of spatial cable-driven parallel mechanisms was proposed. We extended the results obtained in Chapter 3 for planar cable-driven parallel mechanisms to formulate the dimensional synthesis of CDPMs. We formally defined the WCW of spatial CDPMs and introduced a linear program to compute the WCW of such mechanisms. This linear program provided us a foundation to find a formulation to determine whether a six-dimensional box, within the space of point-positions and Euler angles, is inside or outside of the WCW of a given CDPM. As in the planar case, considering the pose of the moving platform as optimization variables turned this linear program into a nonlinear program whose global solution determines whether the box lies completely inside of the WCW. The global optimum being difficult to find, we resorted to multiple-convex linear relaxations of this nonlinear program in order to find a computable sufficient condition for the prescribed box to be inside of the WCW. These linear programs are infeasible whenever the box is inside the WCW. Hence we calculated the duals of these optimization problems to end up with linear programs that are feasible whenever the prescribed box is inside the WCW. Combining all of these linear programs and considering the geometry of the CDPM as optimization variables lead us to a nonlinear feasibility problem. Any solution to this problem if it exists, provides a CDPM whose WCW is guaranteed to include a prescribed six-dimensional box. However, failure to find such a solution does not
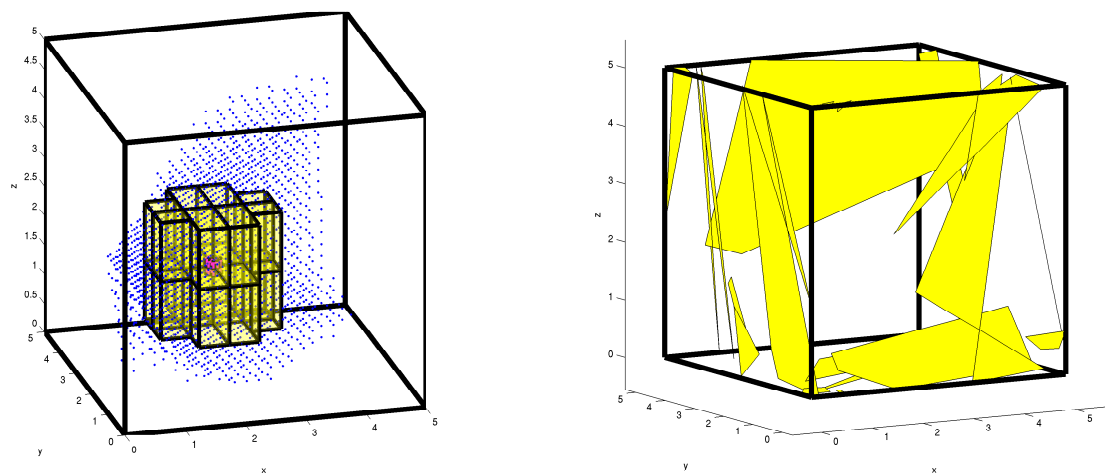
(a) $\phi = -\pi/12\ rad, \theta = -\pi/12\ rad, \psi = -\pi/12\ rad$
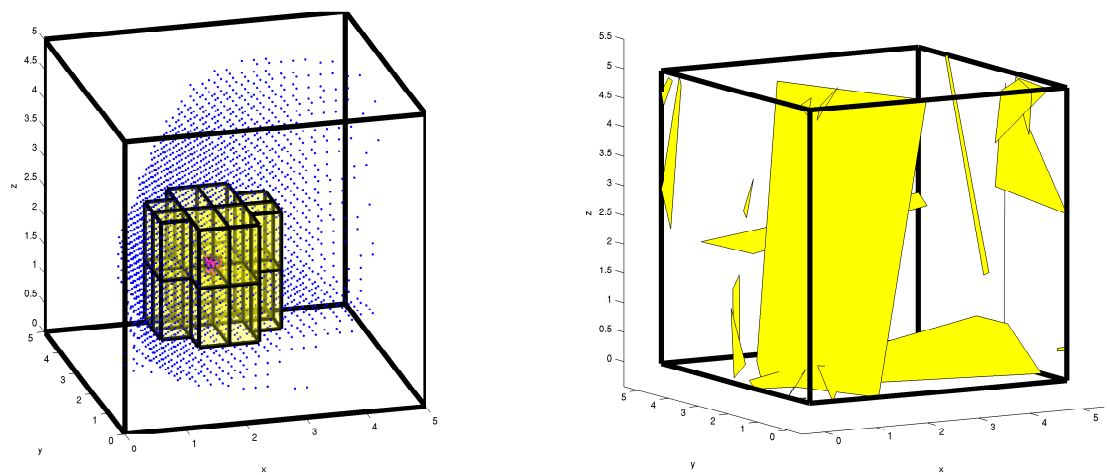
(b) $\phi = 0\ rad, \theta = 0\ rad, \psi = 0\ rad$
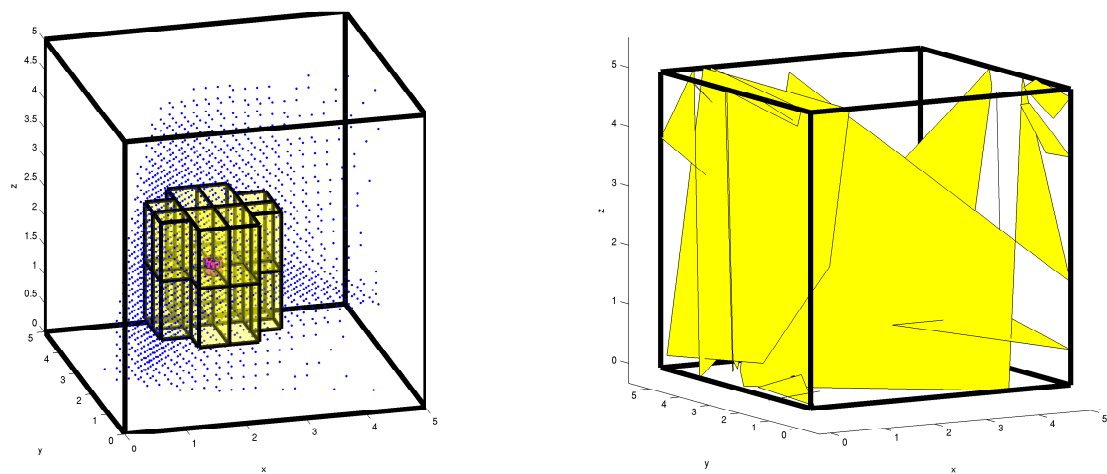
(c) $\phi = \pi/12\ rad, \theta = \pi/12\ rad, \psi = \pi/12\ rad$

Figure 4.20: COWCWs of the resulting CDPM of example 4.5 and the corresponding cable-cable interferences regions.

provide any information about a good but not perfect geometry. Hence, alike the planar case, we introduced an objective function and changed the feasibility problem into a nonlinear program. In fact, we considered the prescribed six-dimensional box as two three-dimensional boxes in the space of point-positions and Euler angles, and scaled only the first of the two, leaving the second constant. Evidently, depending on the application one could also give priority to the box of Euler angles by introducing its scaling factor as the objective to be maximized. Splitting the prescribed box into several boxes refines the relaxations and generally leads to better solutions. Hence, we extended the formulation obtained for one prescribed box to multiple prescribed boxes. The obtained formulation is applicable to irregular shapes approximated by multiple three-dimensional boxes. However, the resulting optimization problems quickly fall into the large scale category, as they consist of many variables and constraints. Solving such problems is always a challenge and may require an advanced solver and several hours of computation time. We illustrated the effectiveness of the proposed algorithm by some examples throughout the chapter.

Chapter 5

Conclusions

In this chapter, the results obtained in the previous chapters are summarized, the contributions are highlighted, and future possible work is suggested.

5.1 Summary of the Thesis

In this thesis, a systematic study was conducted on the dimensional synthesis of cable-driven parallel mechanisms (CDPMs). The dimensional synthesis of CDPMs consists in finding the geometry or design of a CDPM whose wrench-closure workspace (WCW) contains a prescribed workspace. Compared to the analysis problem, which is that

of finding the WCW of an existing CDPM, the synthesis problem is generally more difficult. In this study, we developed a formulation which led us to find different designs of CDPMs whose WCWs include prescribed workspaces.

In chapter one, cable-driven parallel mechanisms and their characteristics, including their advantages, disadvantages, and applications, were introduced. We reviewed the classification of these mechanisms based on their numbers of cables and degrees of freedom, which was followed by an overview of the relevant literature.

In Chapter 2, the analysis of planar cable-driven parallel mechanisms (PCDPMs) was investigated as a requisite to our main concern, their dimensional synthesis. We recalled the kineto-static model of PCDPMs, which provided the basic mathematical expressions for the synthesis problem. We showed that the concept of workspace is different for CDPMs compared with conventional parallel mechanisms, due to the nature of cables, which always have to be in tension in order to apply a force on the main platform. Consequently, we introduced the concept of the wrench matrix and formally defined the wrench-closure workspace (WCW) of CDPMs. We introduced a linear program to calculate the WCW of PCDPMs. We pushed further the analysis and, showed that there are relationships between the boundaries of the constant-orientation WCW (COWCW) of PCDPMs and the oriented area concept. We already knew that the boundaries of COWCWs of PCDPMs are formed by segments of conic sections. The equations of these conic sections are represented by three by three determinants, which are constructed by different combinations of the three selected columns of the wrench matrix. We showed that the the equations of these conic sections are related to the geometry of the triangles made by the corresponding triplets of fixed and moving attachment points of the mechanism. We proved that whenever the two triangles have the opposite orderings of vertices then the conic section is a hyperbola. For the case in which the two triangles have the same ordering, we developed a graphical algorithm to identify the type of the corresponding conic section. The algorithm is based on some interesting properties of parabolas. We showed that the developed algorithm can be applied to find the type of singularity curves of $3R\underline{P}R$ planar parallel mechanisms as well, because of the similarities between the Jacobin matrix of a $3R\underline{P}R$ planar parallel robots and wrench matrix of a PCDPMs. We hope that the results reported in this chapter can lead to the development of a graphical method for tracing the boundaries of the constant orientation wrench-closure workspace of a given planar parallel cable-driven mechanism.

In Chapter 3, we focused on the dimensional synthesis of planar cable-driven parallel mechanisms. In order to find a basic formulation, we began with the simpler case of the constant-orientation dimensional synthesis. In other words, we proposed a method for finding a PCDPM whose WCW includes a prescribed constant-orientation workspace. To this end, we used Stiemke's theorem to introduce a linear program which is feasible if and only if a given pose is outside of the WCW. The relaxation of this linear program over a box of constant-orientation workspace led us to eight distinct linear programs whose optimal solutions determine whether a given box is inside of the COWCW of the provided PCDPM. The relaxation is based on the Reformulation-Linearization Technique (RLT) which changes non-convex constraints into convex constraints. The resulting linear programs are feasible whenever the examined box is outside of the COWCW. Based on this relaxation, we introduced the contracted COWCW concept by which the COWCW is underestimated with a set of boxes, its size depending on the size of the approximating boxes. Since, we were interested in finding a convex problem which is feasible whenever the examining box is inside the COWCW, we computed the duals of these eight distinct linear programs. Assembling these dual linear programs and including the geometry of the PCDPM in the decision variables provided us a nonlinear feasibility problem for the synthesis of these mechanisms. The solutions to this problem, if they exist, provide us with a PCDPM whose COWCW includes the prescribed box. On the other hand, the absence of such solutions gives no information, even though a feasible solution may exist, having been discovered by the relaxation. For this reason, we appended our feasibility problem with the scaling factor of the prescribed box, as the objective function to be maximized. This led us to a nonlinear program, which is the formulation sought for the dimensional synthesis of CDPMs. Maximizing this objective function and obtaining optimum scaling factor greater or equal to one then guarantees that the prescribed box is included in the COWCW of the obtained PCDPM. Otherwise, we are left generally with a good but not perfect geometry of a PCDPM.

Since the main challenge here is to design a robot whose workspace includes a prescribed workspace of irregular shape, we proposed to use interval analysis to approximate such irregular shapes with multiple boxes. Hence, we adapted the aforesaid nonlinear program so that it takes into account n prescribed boxes. Solutions to the resulting formulation provide PCDPMs whose COWCW contains the prescribed set of boxes. We also showed that the developed nonlinear program can be applied to find the geometry of a PCDPM whose COWCWs defined at several orientations contain a

prescribed workspace.

The developed formulations in the first part of Chapter 3 are restricted to constant-orientation workspaces. In practice, we look for designs of PCDPMs which are capable of operating within a continous range of orientations. In order to accommodate this more general case, we included the orientation angle of the main platform as a variable in our calculations. Hence, we considered a three dimensional box whose first and second dimensions represent the position of a point, while the third represents the orientation angle. We converted from the linear program obtained through the Stiemkie's theorem to verify the WCW. This problem was relaxed over a 3D box in the workspace to find a necessary condition which determines whether the box is inside the WCW of the provided PCDPM within a given range of orientation angles. This led to a nonlinear program whose optimum value equals to zero when the given 3D box is inside the WCW of the provided PCDPM. Since finding the global optimum is a difficult task, we resorted to convex relaxation over this three-dimensional box. This led us to eight distinct linear programs, which provided sufficient conditions for the prescribed box to lie inside the WCW within a given range of orientations. This allowed us to compute the contracted WCW, which is a subset of the Cartesian space that is guaranteed to lie inside the WCW.

As in the case of the constant-orientation dimensional synthesis, we calculated the dual of these eight distinct linear program to find a linear program which is feasible whenever a prescribed three-dimensional box lies inside the WCW. Considering the geometry of the PCDPM as optimization variables, led us to a nonlinear feasibility problem whose solutions are feasible PCDPM designs. However, the failure to obtain such solutions does not imply that there is no PCDPM design whose WCW includes the prescribed box. In order to find those designs, we used the same objective function introduced for the constant-orientation synthesis problem of PCDPMs, thus turning the feasibility problem into a nonlinear program. If the value of the objective function at the optimum point is greater or equal to one then we obtain a PCDPM for which the WCW includes the prescribed box. Developing this nonlinear program for multiple boxes, which may represent an approximation of the prescribed workspace, yields a nonlinear program for the dimensional synthesis of PCDPMs. This nonlinear program can be a medium or large scale problem, depending on the numbers of cables and prescribed boxes. Therefore, solving this optimization problem is a challenge, which was overcome by resorting to Penalty Sequential Linear Programming (PSLP). The

effectiveness of the developed algorithms for the dimensional synthesis of PCDPMS were illustrated through Chapter 3 via several examples.

In general, planar robots have limited applications compared with their spatial counterparts. Cable-driven parallel robots are no exception, and for this reason, we investigated the dimensional synthesis of spatial cable driven mechanisms in Chapter 4. The approach towards a proper formulation for the dimensional synthesis of these mechanisms was similar to that of the planar case. We recalled the kinetostatic of spatial CDPMs and introduced a formulation for the wrench matrix of these mechanisms. We formally defined the WCW of spatial CDPMs and introduced a linear program by which one can verify the WCW membership of a given MP pose. Considering the point-position vector and the rotation matrix as optimization variables of this linear program yields a nonlinear program whose global solution over a six-dimensional box to be out side of the WCW. In fact, this 6 dimensional box may be viewed as the Cartesian product of two three-dimensional boxes associated respectively with point-position and orientation of the MP. An unbounded nonlinear program indicates that at least one pose of the prescribed box is not inside the WCW, while ending up with zero as the global optimum means that the box is completely inside the WCW.

Since finding the global optimum is very difficult in general, we relaxed the non convex constraints of this nonlinear program into convex constraints over the prescribed box thus making it easier for a pose to be excluded from the WCW. To this end we had to introduce sixty-four distinct linear programs, which represented a us linear sufficient condition for a six-dimensional box to lie inside the WCW of a spatial CDPM. Alike for planar CDPMs, we showed the effect of this relaxation over the WCW by introducing the contracted WCW.

Calculating the dual of these distinct linear programs and including the geometry of the CDPM among the optimization variables lead to a nonlinear feasibility problem. The solutions to this nonlinear feasibility problem, if they exist provides designs of CDPMs whose WCWs include the prescribed six-dimensional box. Alike the planar case, we turned this feasibility problem to a nonlinear program by introducing an objective function. This objective function is the scaling factor of the prescribed box. We showed that the WCW of the obtained CDPM is guaranteed to include the prescribed six-dimensional box whenever this scaling factor is equal to or greater than one. Interestingly, we observed that the CDPMs resulting from this synthesis method exhibit

relatively small interferences regions, as some of their attachment points coincide. We extended this formulation to compute designs of CDPMs to prescribed six-dimensional workspaces approximated by multiple boxes. The resulting nonlinear program for the dimensional synthesis of spatial CDPMs is generally a large scale problem, depending on the numbers of cables and boxes. Solving such a problem remains a challenge and requires high-performance algorithms and computers. This has led us to use the IBM Cplex solver integrated with Matlab to solve the direction-finding subproblems of the PSLP algorithm. The effectiveness of the developed algorithms were illustrated by implementing them in Matlab and applying them to several examples.

5.2   Contributions

The contributions of this thesis to the literature of cable-driven parallel mechanisms are highlighted below.

We revealed hidden geometric properties of the boundaries of the constant-orientation wrench-closure workspace of planar cable-driven parallel mechanisms. We showed that there is a relationship between the boundaries of COWCWs of PCDPMs and the concept of oriented area concept. We introduced a graphical algorithm to verify the types of conic sections forming the boundaries of COWCWs of PCDPMs. This algorithm applied to find the type of singularity curve of $3R\underline{P}R$ planar parallel robot as well.

Applying the convex relaxation techniques to the dimensional synthesis of cable-driven parallel mechanisms was reported for the first time in this thesis. These techniques allow for a formulation for the dimensional synthesis of planar and spatial cable-driven parallel mechanisms. It is believed that these techniques may be suitable for synthesizing conventional parallel mechanisms as well. Indeed, these manipulators are limited by their singularity regions, which are represented by polynomial equality constraints. Relaxing these equality constraints over a box in the workspace provides a set of convex constraints that, when satisfied, are sufficient for a box to be free of singularities. However, the effectiveness of these methods must be compared with currently available methods.

Implementing the developed algorithms in Matlab via computer codes and func-

tions enables the designers to perform the dimensional synthesis in practice.Structural synthesis may be solved through these codes as well, by varying the number of cables, once the dimensional synthesis solved.

5.3   Future Works

This thesis provides a foundation for the following topics, which may deserve some attention in the future. In this thesis we gave priority to the point-position rather than orientation during the development of the formulation for the dimensional synthesis of CDPMs. However, depending on the application, we may require a CDPM which is capable of operating in wide ranges of orientations. Introducing a multiobjective function including scaling factors for both the point-position and orientation boxes seems to be a good method of turning the obtained feasibility problem into a nonlinear program. The effect of this proposed method may be greater when synthesizing spatial CDPMs, as the orientation workspace has three dimensions and suffers from coarser relaxations of its constraints than planar case. However, this may increase the size of the problem, which is already in the large-scale category.

Including a kinematic sensitivity index in the objective function may result in a CDPM design whose WCW is guaranteed to include a prescribed workspace, but also enjoys good kinematic properties.

Considering the number of cables as optimization variables, may lead to develop a formulation for the dimensional and structural synthesis of CDPMs simultaneously. The resulting formulation will be a mixed integer nonlinear program, the solution of which is even more challenging.

Considering the cable interference problem during the prescribed-workspace synthesis is another interesting topic. This may be done by introducing the inequality constraints that guarantee a minimum distance between the cables, and adding them to the constraints of the developed nonlinear programs.

Applying the procedures presented in this thesis for wrench feasible concept may lead us to designs of CDPMs whose wrench feasible workspaces include a prescribed

workspace. This is more interesting from a practical point of view, as tensions in cables are limited to maximum possible tensions due to their limited strength.

Finally, finding the global optimum for the developed optimization problems will lead to the best possible design of CDPMs. Applying the branch and bound method [38] may result achieving such a global optimum.

Bibliography

[1] Ryu J. H. *Parallel Manipulators, New Developments*. I-Tech Education and Publishing, Vienna, Austria, 2008.

[2] E. Stump and V. Kumar. Workspaces of cable-actuated parallel manipulators. *ASME Journal of Mechanical Design*, 128(1):159–167, 2006.

[3] A. T. Riechel, P. Bosscher, H. Lipkin, and I. Ebert-Uphoff. Concept paper: Cable-driven robots for use in hazardous environments. In 10th *Int. Top. Meeting Robot. Remote Syst. Hazardous Environ.*, Gainesville, FL, USA, Mar.2004.

[4] Albus J. S. Williams II R. L. and Bostelman R. V. Self-contained automated construction deposition system. *Automation in Construction*, 13:393–407, 2004.

[5] Cone L. Skycam: An aerial robotic system. *BYTE,October*, pages 122–132, 1985.

[6] Ryu J. C. Oh S. R. and Agrawal S. K. Dynamics and control of a helicopter carrying a payload using a cable-suspended robot. *ASME Journal of Mechanical Design*, 128(5):1113–1121, 2006.

[7] P. Bosscher, R. L. Williams, and M. Tummino. A concept for rapidly deployable cable robot search and rescue systems. In *ASME IDETC/CIE*, Long Beach , CA, USA, Sep.2005.

[8] SkyCam. (2007).[Online]. Available: www.skycam.tv.

[9] P. H. Borgstrom, N. P. Borgstrom, M. J. Stealey, B. Jordan, and G. S. Sukhatme. Design and implementation of NIMS3D, a 3-d cabled robot for actuated sensing applications. *IEEE Transactions on Robotics*, 25(2):325–339, 2009.

[10] P. H. Borgstrom, B. J. Jordan, M. J. Stealey, G. S. Sukhatme, and W. J. Kaiser M.A. Batalin. Nims-pl: A cable-driven robot with self-calibration capabilities. *IEEE Transactions on Robotics*, 25(5):1005–1015, 2009.

[11] C. Gosselin, R. Poulin, and D. Laurendeau. A planar parallel 3-dof cable-driven haptic interface. In *12th World Multi-Conference on Systemics, Cybernetics and Informatics*, pages 266–271, Orlando, Florida, USA, 2008.

[12] Robert L. Williams II. Cable-suspended haptic interface. *THE INTERNATIONAL JOURNAL OF VIRTUAL REALITY*, 3(3):13–20, 1998.

[13] Norton L. *Design Of Machinery*. Mc Graw Hill, 2007.

[14] Merlet J.P. Optimal design of robots. In *Robotics: Science and Systems I*, Boston, USA, 2005.

[15] R. Kurtz and V. Hayward. Dexterity measure for tendon actuated parallel mechanisms. In *IEEE Int. Conf. Adv. Robot.*, pages 1141–1146, Pisa, Italy, 1991.

[16] A. Ming and T. Higuchi. Study on multiple degree-of-freedom positioning mechanism using wires (part 1)—concept, design and control. *Int. J. Jpn. Soc. Precision Eng.*, 28(2):131–138, 1994.

[17] Clément Gosselin, Simon Lefrançois, and Nathaniel Zoso. Underactuated cable-driven robots: Machine, control and suspended bodies. In *Brain, Body and Machine*, volume 83, pages 311–323. Springer Berlin / Heidelberg, 2010.

[18] C. B. Pham, S. H. Yeo, G. Yang, M. S. Kurbanhusen, and I.-M. Chen. Force-closure workspace analysis of cable-driven parallel mechanisms. *Mech. and Mach. Theory*, 41:53–69, 2006.

[19] A. Fattah and S. Agrawal. On the design of cable-suspended planar parallel robots. *ASME J. Mech. Des.*, 127(5):1021–1028, 2005.

[20] A. T. Riechel and I. Ebert-Uphoff. Force-feasible workspace analysis for underconstrained, point-mass cable robots. In *IEEE internatlonal Conference on Robotics & Automation*, pages 4956–4962, New Orleans, LA, USA, 2004.

[21] D. McColl and L. Notash. Extension of antipodal theorem to workspace analysis of planar wire-actuated manipulators. In *Proc. 5th IFToMM Int. Workshop*, pages 9–16, 2009.

[22] M. Gouttefarde, D. Daney, and J. P. Merlet. Interval-analysis-based determination of the wrench-feasible workspace of parallel cable-driven robots. *IEEE Transactions on Robotics*, 27(1):1–13, 2011.

[23] J. Pusey, A. Fattah, and S. Agrawal. Design and workspace analysis of a 6-6 cable-suspended parallel robot. *Mechanism and Machine Theory*, 39(7):761–778, 2004.

[24] A. M. Hay and J. A. Snyman. Optimization of a planar tendon-driven parallel manipulator for a maximal dextrous workspace. *Engineering Optimization*, 37(3):217–236, 2005.

[25] M. Gouttefarde. *Analyse de l'espace des pose polyvalente des mécanisms parallèles entraînés par câbles.* PhD thesis, Faculté des études supérieures, Université Laval, Québec, Canada, 2005.

[26] Gouttefarde M. and Gosselin C. On the properties and the determination of the wrench-closure workspace of planar parallel cable-driven mechanisms. In *ASME International Design Engineering Technical Conferences*, pages 337–346, Salt Lake City, Utah, USA, 2004.

[27] Gouttefarde M. and Gosselin C. Analysis of the wrench-closure workspace of planar parallel cable driven mechanisms. *IEEE Transactions on Robotics*, 22(3):434–445, 2006.

[28] Damien Chablat, Phillippe Wenger, and Ilian A Bonev. Self motions of special 3-rpr planar parallel robot. In *Mechanisms and Motion*, Advances in Robot Kinematics series, pages 221–228, Dordrecht, The Netherlands, 2006. Springer.

[29] M. L. Husty and C. Gosselin. On the singularity surface of planar 3-rpr parallel mechanisms. *Mech. Based Design of Structures and Machines*, 36(4):411–435, 2008.

[30] T. Graham R. Roberts and T. Lippitt. On the inverse kinematics, statics, and fault tolerance of cable-suspended robots. *J. Rob. Syst.*, 15(10):581–597, 1998.

[31] J. Sefrioui and C. Gosselin. On the quadratic nature of the singularity curves of planar three-degree-of-freedom parallel manipulators. *Mech. Mach. Theory*, 30(4):533–551, 1995.

[32] Müller Ch. and Wallner J. Oriented mixed area and discrete minimal surfaces. *Discrete and Computational Geometry*, 43(2):303–320, 2010.

[33] Dörrie H. *100 Great Problems of Elementary Mathematics*. Dover Publications, NY, 1965.

[34] R.B. Nelsen. *Proof Without Words*. The Mathematical Association of America, USA, 1993.

[35] G. Dantzig and M. Thapa. *Linear Programming: Theory and Extensions*. Springer, USA, 2003.

[36] H. Sherali and C.H. Tuncbilek. A reformulation-convexification approach for solving nonconvex quadratic programming problems. *J. Global Optimization*, 7:1–31, 1995.

[37] S. Boyd and L. Vandenberghe. *Convex Optimization*. Cambridge University Press, Cambridge, UK., 2004.

[38] M. Bazarra, H. Sherali, and C. Shetty. *Nonlinear Programming*. Wiley Interscience, New Jersy, US, 2006.

[39] D. Dubé and P. Cardou. Tracer rapidement l'espace des poses polyvalentes (EPP) d'un manipulateur parallèle plan à entraînement par câbles sous Matlab. In *REPARTI Workshop*, 2010.

[40] Micael J. Cloud Ramon E. Moore, R. Baker Kearfott. *Introduction to INTERVAL ANALYSIS*. Siam, USA, 2009.

[41] John J. Craig. *Introduction to Robotics*. Pearson Education International, USA, 2005.

[42] Pham C. B., Yeo S. H., Yang G., and Chen I-Ming. Workspace analysis of fully restrained cable-driven manipulators. *Robotics and Autonomous Systems*, 57:901–912, 2009.

[43] S. Perreault, , P. Cardou, C. M. Gosselin, and M.J.D. Otis. Geometric determination of the interference-free constant-orientation workspace of parallel cable-driven mechanism. *ASME Journal of Mechanisms and Robotics*, 2(3):paper 031016, 2010.

[44] P. Lafourcade. *Étude des manipulateurs parallèles à câble, conception d'une suspension active pour soufflerie*. PhD thesis, Ecole Nationale Superieur de l'Aéronautique et de l'Espace, Toulouse, France, 2004.

[45] *http://www-01.ibm.com/software/integration/optimization/cplex-optimizer*.

[46] IBM, USA. *IBM ILOG CPLEX User's Manual for CPLEX*, 2009.

Appendix A

The Gradients Corresponding to Problem (3.25)

As we mentioned in example 3.2, we may provide with gradients of the nonlinear objective and constraints for the "trust-region-reflective" algorithm in order to accelerate the calculations. In this appendix, we report the symbolic expressions of these gradients.

A.1 Linear and Nonlinear Constraints Appearing in Problem (3.25)

In order to accelerate the calculations of problem (3.25), we can specify the gradients of corresponding nonlinear constraints thorough the required function of nonlinear constraints for *fmincon*. Hence, regarding the vector of optimization variables as $\mathbf{x}_{opt} = [\mathbf{y}_{k,j}^T \quad \mathbf{a}_1^T \cdots \mathbf{a}_m^T \quad \mathbf{b}_1^T \cdots \mathbf{b}_m^T \quad s]^T \in \mathbb{R}^{8n(m+8)}$, we split matrix $\mathbf{R}_{k,j}$ into a linear matrix $\mathbf{R}_{k,j,l}$ and a nonlinear matrix $\mathbf{R}_{k,j,nl}$ as follows.

$$\mathbf{R}_{k,j,l} \equiv \begin{bmatrix} \mathbf{1}_2\mathbf{1}_m^T & \mathbf{0}_4^T & -\mathrm{diag}(\boldsymbol{\sigma}_j) & \mathrm{diag}(\boldsymbol{\sigma}_j) \end{bmatrix} \in \mathbb{R}^{2\times(m+8)},$$

$$\mathbf{R}_{k,j,nl} \equiv \begin{bmatrix} -(\mathbf{A}-\mathbf{QB})^T & -\mathbf{f} & \mathbf{B}^T\mathbf{Q}^T\mathbf{E}^T \\ \mathbf{0}_{2\times2} & \sigma_{0,j}\underline{\mathbf{p}} & -\sigma_{0,j}\mathbf{1}_{2\times2} \\ \mathbf{0}_{2\times2} & -\sigma_{0,j}\overline{\mathbf{p}} & \sigma_{0,j}\mathbf{1}_{2\times2} \\ \mathrm{diag}(\boldsymbol{\sigma}_j)\mathrm{diag}(\underline{\mathbf{p}}) & \mathbf{0}_2 & \mathbf{0}_{2\times2} \\ -\mathrm{diag}(\boldsymbol{\sigma}_j)\mathrm{diag}(\overline{\mathbf{p}}) & \mathbf{0}_2 & \mathbf{0}_{2\times2} \end{bmatrix}^T \in \mathbb{R}^{5\times(m+8)}. \qquad (\text{A-1})$$

This allows us to split, the equality constraints of problem (3.25) into linear and non-linear equations as

$$\mathbf{R}_{k,j,l}\mathbf{y}_{k,j} + \mathbf{g}_l = \mathbf{0}_2, \qquad (\text{A-2})$$

$$\mathbf{R}_{k,j,nl}\mathbf{y}_{k,j} + \mathbf{g}_{nl} = \mathbf{0}_3, k = 1,\dots,n, \quad j = 1,\cdots,8 \qquad (\text{A-3})$$

where $\mathbf{g}_{nl} \equiv \begin{bmatrix} -\mathbf{1}_m^T(\mathbf{A}-\mathbf{QB})^T & -\mathbf{1}_m^T\mathbf{f} & \mathbf{1}_m^T\mathbf{B}^T\mathbf{Q}^T\mathbf{E}^T \end{bmatrix}^T \in \mathbb{R}^5$ and $\mathbf{g}_l \equiv m\mathbf{1}_2$.

Clearly, the Jacobian matrices of the linear equations are $\mathbf{R}_{k,j,l}^T$. Let us now we can calculate the corresponding gradients of eq. (A-3).

A.2 Gradients of Nonlinear Equality Constraints of Problem (3.25)

In order to calculate the gradients of the nonlinear equality constraints appearing in problem (3.25) let us define the function vec() as follows

$$\mathrm{vec}() : \mathbb{R}^{p\times q} \longrightarrow \mathbb{R}^{pq}, \quad \mathrm{vec}(\mathbf{U}) = \begin{bmatrix} \mathbf{u}_1 & \mathbf{u}_2 & \dots & \mathbf{u}_p \end{bmatrix}^T \in \mathbb{R}^{pq},$$

$$\forall \mathbf{U} \in \mathbb{R}^{p\times q}, \quad \mathbf{U} = \begin{bmatrix} \mathbf{u}_1^T & \mathbf{u}_2^T & \dots & \mathbf{u}_p^T \end{bmatrix}^T, \ \mathbf{u}_i \in \mathbb{R}^{1\times q}, \ i = 1,\dots,p.$$

Then, the Jacobian matrix of the nonlinear equality constraints appearing in problem (3.25) is given by

$$\nabla\mathbf{H} = \begin{bmatrix} \mathbf{H}_1 & \mathbf{0}_{(8(m+8))\times40} & \cdots & \mathbf{0}_{(8(m+8))\times40} \\ \mathbf{0}_{(8(m+8))\times40} & \mathbf{H}_2 & \cdots & \mathbf{0}_{(8(m+8))\times40} \\ \vdots & \vdots & \ddots & \vdots \\ \mathbf{0}_{(8(m+8))\times40} & \mathbf{0}_{(8(m+8))\times40} & \cdots & \mathbf{H}_n \\ \mathbf{N}_1 & \mathbf{N}_2 & \cdots & \mathbf{N}_n \end{bmatrix} \in \mathbb{R}^{(8n(m+8)+4m+1)\times40n},$$

where

$$\mathbf{H}_k \equiv \begin{bmatrix} \mathbf{R}_{k,1,nl}^T & \mathbf{0}_{(m+8)\times 5} & \cdots & \mathbf{0}_{(m+8)\times 5} \\ \mathbf{0}_{(m+8)\times 5} & \mathbf{R}_{k,2,nl}^T & \cdots & \mathbf{0}_{(m+8)\times 5} \\ \vdots & \vdots & \ddots & \vdots \\ \mathbf{0}_{(m+8)\times 5} & \mathbf{0}_{(m+8)\times 5} & \cdots & \mathbf{R}_{k,8,nl}^T \end{bmatrix} \in \mathbb{R}^{8(m+8)\times 40},$$

$$\mathbf{N}_k \equiv \begin{bmatrix} \mathbf{G}_{k,1} & \cdots & \mathbf{G}_{k,8} \end{bmatrix} \in \mathbb{R}^{(4m+1)\times 40},$$

$$\mathbf{G}_{k,j} \equiv \begin{bmatrix} -\mathbf{I}_{k,j} & -\mathrm{vec}(\mathrm{diag}(\mathbf{t}_{k,j})\mathbf{B}^T\mathbf{Q}_k^T\mathbf{E}^T) & \mathbf{0}_{2m\times 2} \\ \mathbf{I}_{k,j} & -\mathrm{vec}(\mathrm{diag}(\mathbf{t}_{k,j})\mathbf{A}^T\mathbf{E}\mathbf{Q}_k) & \mathbf{I}_{k,j}\mathbf{E}\mathbf{Q}_k \\ \mathbf{h}_{k,j} & \mathbf{u}_{k,j} & \mathbf{0}_2^T \end{bmatrix} \in \mathbb{R}^{(4m+1)\times 5},$$

and

$$\mathbf{I}_{k,j} \equiv \mathrm{diag}(\mathrm{vec}(\mathbf{t}_{k,j}\mathbf{1}_2^T))\mathbf{I}_\nabla,$$

$$\mathbf{t}_{k,j} \equiv (\mathbf{1}_m + \mathbf{I}_t\mathbf{y}_{k,j}),$$

$$\mathbf{I}_t \equiv \begin{bmatrix} \mathbf{1}_{m\times m} & \mathbf{0}_{m\times 8} \end{bmatrix} \in \mathbb{R}^{m\times(m+8)},$$

$$\mathbf{I}_\nabla \equiv \begin{bmatrix} \mathbf{1}_{2\times 2} & \mathbf{1}_{2\times 2} & \cdots & \mathbf{1}_{2\times 2} \end{bmatrix}^T \in \mathbb{R}^{2m\times 2}, \tag{A-4}$$

$$\mathbf{h}_{k,j} \equiv -\mathrm{diag}(\boldsymbol{\sigma}_j)(\mathrm{diag}(\overline{\mathbf{p}} - \mathbf{p}_c)\mathbf{I}_{\overline{d}}\ \mathbf{y}_{k,j} - \mathrm{diag}(\underline{\mathbf{p}} - \mathbf{p}_c)\mathbf{I}_{\underline{d}}\ \mathbf{y}_{k,j})^T,$$

$$\mathbf{I}_{\underline{d}} \equiv \begin{bmatrix} \mathbf{0}_{2\times m} & \mathbf{0}_{2\times 4} & \mathbf{1}_{2\times 2} & \mathbf{0}_{2\times 2} \end{bmatrix} \in \mathbb{R}^{2\times(m+8)},$$

$$\mathbf{I}_{\overline{d}} \equiv \begin{bmatrix} \mathbf{0}_{2\times m)} & \mathbf{0}_{2\times 6} & \mathbf{1}_{2\times 2} \end{bmatrix} \in \mathbb{R}^{2\times(m+8)},$$

$$\mathbf{u}_{k,j} \equiv -\sigma_{0,j}((\overline{\mathbf{p}} - \mathbf{p}_c)^T\mathbf{I}_{\overline{e}}\ \mathbf{y}_{k,j} - (\underline{\mathbf{p}} - \mathbf{p}_c)^T\mathbf{I}_{\underline{e}}\ \mathbf{y}_{k,j}),$$

$$\mathbf{I}_{\underline{e}} \equiv \begin{bmatrix} \mathbf{0}_{2\times m} & \mathbf{1}_{2\times 2} & \mathbf{0}_{2\times 6} \end{bmatrix} \in \mathbb{R}^{2\times(m+8)},$$

$$\mathbf{I}_{\overline{e}} \equiv \begin{bmatrix} \mathbf{0}_{2\times(m+2)} & \mathbf{0}_{2\times 2} & \mathbf{1}_{2\times 2} & \mathbf{0}_{2\times 4} \end{bmatrix} \in \mathbb{R}^{2\times(m+8)}.$$

Appendix B

The Matrix and Vector Appearing in Problem (3.46)

In this appendix, we present the expressions of matrix $\mathbf{U}_j$ and vector $\mathbf{h}_j$, which appear in eq. (3.46). In order to accelerate the solution of problem (3.46) via a gradient method, we also calculate the corresponding gradients of the nonlinear constraints in this problem.

B.1 The Expressions of Matrix $\mathbf{U}_j$ and Vector $\mathbf{h}_j$

The expressions of matrix $\mathbf{U}_j \in \mathbb{R}^{15 \times (m+24)}$ and vector $\mathbf{h}_j \in \mathbb{R}^{15}$ are given as follows:

$$\mathbf{h} \equiv \begin{bmatrix} 0 & -\mathbf{1}_m^T\mathbf{u} & -\mathbf{1}_m^T\mathbf{v} & -\mathbf{1}_m^T\mathbf{A}^T & m\mathbf{1}_2^T & \mathbf{1}_m^T\mathbf{B}^T & \mathbf{1}_m^T\mathbf{B}^T\mathbf{E}^T & \mathbf{1}_m^T\mathbf{B}^T\mathbf{E}^T & -\mathbf{1}_m^T\mathbf{B}^T \end{bmatrix}^T,$$

$$\mathbf{U}_j \equiv$$

$$\begin{bmatrix}
\mathbf{0}_{m\times1} & -\mathbf{u} & -\mathbf{v} & -\mathbf{A}^T & \mathbf{1}_m\mathbf{1}_2^T & \mathbf{B}^T & \mathbf{B}^T\mathbf{E}^T & \mathbf{B}^T\mathbf{E}^T & -\mathbf{B}^T \\
\mathbf{0}_{2\times1} & \mathbf{0}_{2\times1} & \mathbf{0}_{2\times1} & \mathrm{diag}(\boldsymbol{\sigma}_j)\mathrm{diag}(\underline{\mathbf{p}}) & -\mathrm{diag}(\boldsymbol{\sigma}_j) & \mathbf{0}_{2\times2} & \mathbf{0}_{2\times2} & \mathbf{0}_{2\times2} & \mathbf{0}_{2\times2} \\
\mathbf{0}_{2\times1} & \mathbf{0}_{2\times1} & \mathbf{0}_{2\times1} & -\mathrm{diag}(\boldsymbol{\sigma}_j)\mathrm{diag}(\overline{\mathbf{p}}) & \mathrm{diag}(\boldsymbol{\sigma}_j) & \mathbf{0}_{2\times2} & \mathbf{0}_{2\times2} & \mathbf{0}_{2\times2} & \mathbf{0}_{2\times2} \\
\mathbf{0}_{2\times1} & \mathbf{0}_{2\times1} & \mathbf{0}_{2\times1} & \underline{c}\,\mathrm{diag}(\boldsymbol{\sigma}_j) & \mathbf{0}_{2\times2} & -\mathrm{diag}(\boldsymbol{\sigma}_j) & \mathbf{0}_{2\times2} & \mathbf{0}_{2\times2} & \mathbf{0}_{2\times2} \\
\mathbf{0}_{2\times1} & \mathbf{0}_{2\times1} & \mathbf{0}_{2\times1} & -\overline{c}\,\mathrm{diag}(\boldsymbol{\sigma}_j) & \mathbf{0}_{2\times2} & \mathrm{diag}(\boldsymbol{\sigma}_j) & \mathbf{0}_{2\times2} & \mathbf{0}_{2\times2} & \mathbf{0}_{2\times2} \\
\mathbf{0}_{2\times1} & \mathbf{0}_{2\times1} & \mathbf{0}_{2\times1} & \underline{s}\,\mathrm{diag}(\boldsymbol{\sigma}_j) & \mathbf{0}_{2\times2} & \mathbf{0}_{2\times2} & -\mathrm{diag}(\boldsymbol{\sigma}_j) & \mathbf{0}_{2\times2} & \mathbf{0}_{2\times2} \\
\mathbf{0}_{2\times1} & \mathbf{0}_{2\times1} & \mathbf{0}_{2\times1} & -\overline{s}\,\mathrm{diag}(\boldsymbol{\sigma}_j) & \mathbf{0}_{2\times2} & \mathbf{0}_{2\times2} & \mathrm{diag}(\boldsymbol{\sigma}_j) & \mathbf{0}_{2\times2} & \mathbf{0}_{2\times2} \\
\sigma_{0,j}\underline{\boldsymbol{\alpha}} & \mathbf{0}_{2\times1} & \mathbf{0}_{2\times1} & \mathbf{0}_{2\times2} & \mathbf{0}_{2\times2} & \mathbf{0}_{2\times2} & \mathbf{0}_{2\times2} & -\sigma_{0,j}\mathbf{1}_{2\times2} & \mathbf{0}_{2\times2} \\
-\sigma_{0,j}\overline{\boldsymbol{\alpha}} & \mathbf{0}_{2\times1} & \mathbf{0}_{2\times1} & \mathbf{0}_{2\times2} & \mathbf{0}_{2\times2} & \mathbf{0}_{2\times2} & \mathbf{0}_{2\times2} & \sigma_{0,j}\mathbf{1}_{2\times2} & \mathbf{0}_{2\times2} \\
\sigma_{0,j}\underline{\boldsymbol{\beta}} & \mathbf{0}_{2\times1} & \mathbf{0}_{2\times1} & \mathbf{0}_{2\times2} & \mathbf{0}_{2\times2} & \mathbf{0}_{2\times2} & \mathbf{0}_{2\times2} & \mathbf{0}_{2\times2} & -\sigma_{0,j}\mathbf{1}_{2\times2} \\
-\sigma_{0,j}\overline{\boldsymbol{\beta}} & \mathbf{0}_{2\times1} & \mathbf{0}_{2\times1} & \mathbf{0}_{2\times2} & \mathbf{0}_{2\times2} & \mathbf{0}_{2\times2} & \mathbf{0}_{2\times2} & \mathbf{0}_{2\times2} & \sigma_{0,j}\mathbf{1}_{2\times2} \\
\sigma_{0,j}\underline{c} & -\sigma_{0,j} & 0 & \mathbf{0}_{1\times2} & \mathbf{0}_{1\times2} & \mathbf{0}_{1\times2} & \mathbf{0}_{1\times2} & \mathbf{0}_{1\times2} & \mathbf{0}_{1\times2} \\
-\sigma_{0,j}\overline{c} & \sigma_{0,j} & 0 & \mathbf{0}_{1\times2} & \mathbf{0}_{1\times2} & \mathbf{0}_{1\times2} & \mathbf{0}_{1\times2} & \mathbf{0}_{1\times2} & \mathbf{0}_{1\times2} \\
\sigma_{0,j}\underline{s} & 0 & -\sigma_{0,j} & \mathbf{0}_{1\times2} & \mathbf{0}_{1\times2} & \mathbf{0}_{1\times2} & \mathbf{0}_{1\times2} & \mathbf{0}_{1\times2} & \mathbf{0}_{1\times2} \\
-\sigma_{0,j}\overline{s} & 0 & \sigma_{0,j} & \mathbf{0}_{1\times2} & \mathbf{0}_{1\times2} & \mathbf{0}_{1\times2} & \mathbf{0}_{1\times2} & \mathbf{0}_{1\times2} & \mathbf{0}_{1\times2}
\end{bmatrix}^T.$$

B.2 The Gradients of the Nonlinear Constraints of Problem (3.46)

In order to find an optimal solution to problem (3.46) through a gradient method, such as the PSLP algorithm we calculate the gradients of the nonlinear constraints of this problem. Hence, upon defining the vector of optimization variables as $\mathbf{x}_{opt} = [\mathbf{y}_{k,j}^T \quad \mathbf{a}_1^T \cdots \mathbf{a}_m^T \quad \mathbf{b}_1^T \cdots \mathbf{b}_m^T \quad s]^T \in \mathbb{R}^{8n(m+24)+6m+1}$, we separate the linear and nonlinear appearing terms in matrix $\mathbf{U}_{k,j}, \ j = 1,\ldots,8, \quad k = 1,\cdots,n$, which yields

138

$$\mathbf{U}_{k,j,nl} \equiv \begin{bmatrix} \mathbf{A}^T & \mathbf{B}^T & \mathbf{B}^T\mathbf{E}^T & \mathbf{B}^T\mathbf{E}^T & \mathbf{B}^T & \mathbf{u} & \mathbf{v} \\ -\mathrm{diag}(\boldsymbol{\sigma}_j)\mathrm{diag}(\underline{\mathbf{p}}'_k) & \mathbf{0}_{2\times2} & \mathbf{0}_{2\times2} & \mathbf{0}_{2\times2} & \mathbf{0}_{2\times2} & \mathbf{0}_2 & \mathbf{0}_2 \\ \mathrm{diag}(\boldsymbol{\sigma}_j)\mathrm{diag}(\overline{\mathbf{p}}'_k) & \mathbf{0}_{2\times2} & \mathbf{0}_{2\times2} & \mathbf{0}_{2\times2} & \mathbf{0}_{2\times2} & \mathbf{0}_2 & \mathbf{0}_2 \\ -\underline{c}\,\mathrm{diag}(\boldsymbol{\sigma}_j) & -\mathrm{diag}(\boldsymbol{\sigma}_j) & \mathbf{0}_{2\times2} & \mathbf{0}_{2\times2} & \mathbf{0}_{2\times2} & \mathbf{0}_2 & \mathbf{0}_2 \\ \overline{c}\,\mathrm{diag}(\boldsymbol{\sigma}_j) & \mathrm{diag}(\boldsymbol{\sigma}_j) & \mathbf{0}_{2\times2} & \mathbf{0}_{2\times2} & \mathbf{0}_{2\times2} & \mathbf{0}_2 & \mathbf{0}_2 \\ -\underline{s}\,\mathrm{diag}(\boldsymbol{\sigma}_j) & \mathbf{0}_{2\times2} & -\mathrm{diag}(\boldsymbol{\sigma}_j) & \mathbf{0}_{2\times2} & \mathbf{0}_{2\times2} & \mathbf{0}_2 & \mathbf{0}_2 \\ \overline{s}\,\mathrm{diag}(\boldsymbol{\sigma}_j) & \mathbf{0}_{2\times2} & \mathrm{diag}(\boldsymbol{\sigma}_j) & \mathbf{0}_{2\times2} & \mathbf{0}_{2\times2} & \mathbf{0}_2 & \mathbf{0}_2 \\ \mathbf{0}_{2\times2} & \mathbf{0}_{2\times2} & \mathbf{0}_{2\times2} & -\sigma_{0,j}\mathbf{1}_{2\times2} & \mathbf{0}_{2\times2} & \mathbf{0}_2 & \mathbf{0}_2 \\ \mathbf{0}_{2\times2} & \mathbf{0}_{2\times2} & \mathbf{0}_{2\times2} & \sigma_{0,j}\mathbf{1}_{2\times2} & \mathbf{0}_{2\times2} & \mathbf{0}_2 & \mathbf{0}_2 \\ \mathbf{0}_{2\times2} & \mathbf{0}_{2\times2} & \mathbf{0}_{2\times2} & \mathbf{0}_{2\times2} & \sigma_{0,j}\mathbf{1}_{2\times2} & \mathbf{0}_2 & \mathbf{0}_2 \\ \mathbf{0}_{2\times2} & \mathbf{0}_{2\times2} & \mathbf{0}_{2\times2} & \mathbf{0}_{2\times2} & -\sigma_{0,j}\mathbf{1}_{2\times2} & \mathbf{0}_2 & \mathbf{0}_2 \\ \mathbf{0}_2^T & \mathbf{0}_2^T & \mathbf{0}_2^T & \mathbf{0}_2^T & \mathbf{0}_2^T & \sigma_{0,j} & 0 \\ \mathbf{0}_2^T & \mathbf{0}_2^T & \mathbf{0}_2^T & \mathbf{0}_2^T & \mathbf{0}_2^T & -\sigma_{0,j} & 0 \\ \mathbf{0}_2^T & \mathbf{0}_2^T & \mathbf{0}_2^T & \mathbf{0}_2^T & \mathbf{0}_2^T & 0 & \sigma_{0,j} \\ \mathbf{0}_2^T & \mathbf{0}_2^T & \mathbf{0}_2^T & \mathbf{0}_2^T & \mathbf{0}_2^T & 0 & -\sigma_{0,j} \end{bmatrix}^T \quad \text{and}$$

$$\mathbf{U}_{k,j,l} \equiv \begin{bmatrix} \mathbf{0}_m^T & \mathbf{0}_2^T & \mathbf{0}_2^T & \mathbf{0}_8^T & \sigma_{0,j}\underline{\boldsymbol{\alpha}}_k^T & -\sigma_{0,j}\overline{\boldsymbol{\alpha}}_k \\ \mathbf{1}_2\mathbf{1}_m^T & -\mathrm{diag}(\boldsymbol{\sigma}_j) & \mathrm{diag}(\boldsymbol{\sigma}_j) & \mathbf{0}_{8\times2} & \mathbf{0}_{2\times2} & \mathbf{0}_{2\times2} \end{bmatrix}$$
$$\begin{bmatrix} \sigma_{0,j}\underline{\boldsymbol{\beta}}_k^T & -\sigma_{0,j}\overline{\boldsymbol{\beta}}_k^T & \sigma_{0,j}\underline{c} & -\sigma_{0,j}\overline{c} & \sigma_{0,j}\underline{s} & -\sigma_{0,j}\overline{s} \\ \mathbf{0}_{2\times2} & \mathbf{0}_{2\times2} & \mathbf{0}_2 & \mathbf{0}_2 & \mathbf{0}_2 & \mathbf{0}_2 \end{bmatrix}^T \tag{B-1}$$

which leads us to rewrite the equality constraints of problem (3.46) as

$$\mathbf{U}_{k,j,l}\mathbf{y}_{k,j} + \mathbf{h}_l = \mathbf{0}_3, \tag{B-2}$$
$$\mathbf{U}_{k,j,nl}\mathbf{y}_{k,j} + \mathbf{h}_{nl} = \mathbf{0}_{12}, \quad k=1,\dots,n, \quad j=1,\dots,8, \tag{B-3}$$

where

$$\mathbf{h}_l = [0 \quad m\mathbf{1}_2^T]^T \in \mathbb{R}^3$$
$$\mathbf{h}_{nl} = \left[-\mathbf{1}_m^T\mathbf{u} \quad -\mathbf{1}_m^T\mathbf{v} \quad -\mathbf{1}_m^T\mathbf{A}^T \quad \mathbf{1}_m^T\mathbf{B}^T \quad \mathbf{1}_m^T\mathbf{B}^T\mathbf{E}^T \quad \mathbf{1}_m^T\mathbf{B}^T\mathbf{E}^T \quad -\mathbf{1}_m^T\mathbf{B}^T\right]^T \in \mathbb{R}^{12}$$

Then, the Jacobian matrix of eq. (B-3) is given by

$$\nabla\mathbf{H} = \begin{bmatrix} \mathbf{H}_1 & \mathbf{0}_{(8(m+24))\times96} & \cdots & \mathbf{0}_{(8(m+24))\times96} \\ \mathbf{0}_{(8(m+24))\times96} & \mathbf{H}_2 & \cdots & \mathbf{0}_{(8(m+24))\times96} \\ \vdots & \vdots & \ddots & \vdots \\ \mathbf{0}_{(8(m+24))\times96} & \mathbf{0}_{(8(m+24))\times96} & \cdots & \mathbf{H}_n \\ \mathbf{N}_1 & \mathbf{N}_2 & \cdots & \mathbf{N}_n \end{bmatrix} \in \mathbb{R}^{(8n(m+24)+4m+1)\times96n},$$

where

$$\mathbf{H}_k = \begin{bmatrix} \mathbf{R}_{k,1,nl}^T & \mathbf{0}_{(m+24)\times 12} & \cdots & \mathbf{0}_{(m+24)\times 12} \\ \mathbf{0}_{(m+24)\times 12} & \mathbf{R}_{k,2,nl}^T & \cdots & \mathbf{0}_{(m+24)\times 12} \\ \vdots & \vdots & \ddots & \vdots \\ \mathbf{0}_{(m+24)\times 12} & \mathbf{0}_{(m+24)\times 12} & \cdots & \mathbf{R}_{k,8,nl}^T \end{bmatrix} \in \mathbb{R}^{8(m+24)\times 96}, \qquad \text{(B-4)}$$

$$\mathbf{N}_k \equiv [\mathbf{G}_{k,1} \quad \cdots \quad \mathbf{G}_{k,8}] \in \mathbb{R}^{(4m+1)\times 96}, \qquad \text{(B-5)}$$

and

$$\mathbf{G}_{k,j} \equiv \begin{bmatrix} \mathbf{I}_{k,j} & \mathbf{0}_{2m\times 2} & \mathbf{0}_{2m\times 2} & \mathbf{0}_{2m\times 2} & \mathbf{0}_{2m\times 2} \\ \mathbf{0}_{2m\times 2} & \mathbf{I}_{k,j} & \mathbf{I}_{k,j}\mathbf{E}^T & \mathbf{I}_{k,j}\mathbf{E}^T & \mathbf{I}_{k,j} \\ \mathbf{h}_{k,j} & \mathbf{0}_2^T & \mathbf{0}_2^T & \mathbf{0}_2^T & \mathbf{0}_2^T \end{bmatrix} \qquad \text{(B-6)}$$

$$\begin{matrix} \text{vec}(\text{diag}(\mathbf{t}_{k,j})\mathbf{B}^T\mathbf{E}^T) & -\text{vec}(\text{diag}(\mathbf{t}_{k,j})\mathbf{B}^T) \\ \text{vec}(\text{diag}(\mathbf{t}_{k,j})\mathbf{A}^T\mathbf{E}) & -\text{vec}(\text{diag}(\mathbf{t}_{k,j})\mathbf{A}^T) \\ 0 & 0 \end{matrix} \Bigg] \in \mathbb{R}^{(4m+1)\times 12},$$

in which

$$\mathbf{I}_{k,j} \equiv \text{diag}(\text{vec}(\mathbf{t}_{k,j}\mathbf{1}_2^T))\mathbf{I}_\nabla,$$

$$\mathbf{t}_{k,j} \equiv (\mathbf{1}_m + \mathbf{I}_t\mathbf{y}_{k,j}),$$

$$\mathbf{I}_t \equiv [\mathbf{1}_{m\times m} \quad \mathbf{0}_{m\times 24}] \in \mathbb{R}^{m\times(m+24)}, \qquad \text{(B-7)}$$

$$\mathbf{I}_\nabla \equiv \begin{bmatrix} \mathbf{1}_{2\times 2} & \mathbf{1}_{2\times 2} & \cdots & \mathbf{1}_{2\times 2} \end{bmatrix}^T \in \mathbb{R}^{2m\times 2},$$

$$\mathbf{h}_{k,j} \equiv \text{diag}(\boldsymbol{\sigma}_j)(\text{diag}(\bar{\mathbf{p}}_k - \mathbf{p}_c)\mathbf{I}_{\bar{d}}\ \mathbf{y}_{k,j} - \text{diag}(\underline{\mathbf{p}}_k - \mathbf{p}_c)\mathbf{I}_{\underline{d}}\ \mathbf{y}_{k,j})^T,$$

$$\mathbf{I}_{\underline{d}} \equiv [\mathbf{0}_{2\times m} \quad \mathbf{1}_{2\times 2} \quad \mathbf{0}_{2\times 22}] \in \mathbb{R}^{2\times(m+24)} \text{ and } \mathbf{I}_{\bar{d}} \equiv [\mathbf{0}_{2\times(m+2)} \quad \mathbf{1}_{2\times 2} \quad \mathbf{0}_{2\times 20}] \in \mathbb{R}^{2\times(m+24)}.$$

Appendix C

Penalty Successive Linear Programming (PSLP) Algorithm

Sequential Linear Programming (SLP) is a method to solve nonlinear programs in which at each iteration, a direction-finding linear program is formulated based on first-order Taylor series approximations to the objective and constraint functions, in addition to appropriate step bounds or trust region restrictions on the direction components.

The Penalty Successive Linear Programming (PSLP) algorithm is a special class of algorithm of SLP, which employs the l_1-norm penalty function as the direction-finding problem itself, rather than as only a merit function, and enjoys good robustness and convergence properties. In this appendix we explain the method very briefly. For more details, see reference [38].

C.1 A general Nonlinear Program

The problem we consider is of the form

$$P : \text{minimize} \quad f(\mathbf{x})$$
$$\text{subject to} \quad g_i(\mathbf{x}) \le 0 \ \ i = 1, \ldots, n_g,$$
$$h_i(\mathbf{x}) = 0 \ \ i = 1, \ldots, n_h,$$
$$\mathbf{A}\mathbf{x} \preceq \mathbf{b}, \tag{C-1}$$
$$\mathbf{A}_e\mathbf{x} = \mathbf{b}_e,$$

where all functions are assumed to be continuously differentiable, and the latter two sets of constraints represent the linear constraints. Now, let $F_E(\mathbf{x})$ be the l_1-norm or absolute-value, exact penalty function of eq. (C-1), namely, for a penalty parameter $\mu_p > 0$,

$$F_E(\mathbf{x}) = f(\mathbf{x}) + \mu_p \left[\sum_{i=1}^{n_g} \max\{0, g_i(\mathbf{x})\} + \sum_{i=1}^{n_h} |h_i(\mathbf{x})| \right] \tag{C-2}$$

Accordingly, consider the following linearly constrained penalty problem PP:

$$PP : \text{minimize} \quad F_E(\mathbf{x}),$$
$$\text{subject to} \quad \mathbf{A}\mathbf{x} \preceq \mathbf{b}, \tag{C-3}$$
$$\mathbf{A}_e\mathbf{x} = \mathbf{b}_e.$$

Substituting y_i for $\max\{0, g_i(\mathbf{x})\}, i = 1, \ldots, n_g$, and writing $h_i(\mathbf{x})$ as the difference $z_i^+ - z_i^-$ of two nonnegative variables, where $|h_i(\mathbf{x})| = z_i^+ - z_i^-$, for $i = 1, \ldots, n_h$ we can rewrite eq. (C-3) without non differentiable terms as follows:

$$PP : \text{minimize} \quad f(\mathbf{x}) + \mu_p \left[\sum_{i=1}^{n_g} y_i + \sum_{i=1}^{n_h} (z_i^+ - z_i^-) \right]$$
$$\text{subject to} \quad y_i \ge g_i(\mathbf{x}), \quad i = 1, \ldots, n_g,$$
$$z_i^+ - z_i^- = h_i(\mathbf{x}), \quad i = 1, \ldots, n_h, \tag{C-4}$$
$$\mathbf{A}\mathbf{x} \preceq \mathbf{b},$$
$$\mathbf{A}_e\mathbf{x} = \mathbf{b}_e,$$
$$y_i \ge 0 \quad i = 1, \ldots, n_g,,$$
$$z_i^+ \text{ and } z_i^- \ge \quad 0 \ i = 1, \ldots, n_h.$$

Equation (C-4) is equivalent to eq. (C-3) and may also be viewed as an optimization problem in the variable $\mathbf{x}$.

In order to solve problem PP, consider a current iterate $\mathbf{x}_k$ and a trust region or step-bound vector $\boldsymbol{\Delta}_k$ with the same dimensions as $\mathbf{x}$. Then, the linearization of PP, given by eq. (C-3) combined with imposed trust region step bound on the variation of $\mathbf{x}$ about $\mathbf{x}_k$ leads to

$$
\begin{aligned}
LP : \text{Minimize} \quad F_{EL}(\mathbf{x}) &= f(\mathbf{x}_k) + \nabla f(\mathbf{x}_k)^T(\mathbf{x} - \mathbf{x}_k) \\
&+ \mu_p\Big[\sum_{i=1}^{n_g} \max\{0, g_i(\mathbf{x}_k) + \nabla g_i(\mathbf{x}_k)^T(\mathbf{x} - \mathbf{x}_k)\} \\
&+ \sum_{i=1}^{n_h} |h_i(\mathbf{x}_k) + \nabla h_i(\mathbf{x}_k)^T)(\mathbf{x} - \mathbf{x}_k)|\Big]
\end{aligned}
$$
(C-5)

$$
\begin{aligned}
\text{subject to} \quad &\mathbf{Ax} \preceq \mathbf{b}, \\
&\mathbf{A}_e\mathbf{x} = \mathbf{b}_e, \\
&-\boldsymbol{\Delta}_k \preceq \mathbf{x} - \mathbf{x}_k \preceq \boldsymbol{\Delta}_k.
\end{aligned}
$$

Similar to eq. (C-4), this can be restated as the following *linear programming problem*, where we have also used $\mathbf{x} = \mathbf{x}_k + \mathbf{d}$ and have dropped the constant $f(\mathbf{x}_k)$ from the objective function:

$$
\begin{aligned}
\text{LP}(\mathbf{x}_k, \mathbf{d}_k) : \text{Minimize} \quad &\nabla f(\mathbf{x}_k)^T(\mathbf{x} - \mathbf{x}_k) + \mu_p\Big[\sum_{i=1}^{n_g} y_i + \sum_{i=1}^{n_h}(z_i^+ - z_i^-)\Big], \\
\text{subject to} \quad &y_i \geq g_i(\mathbf{x}_k) + \nabla g_i(\mathbf{x}_k)^T\mathbf{d}, \quad i = 1, \ldots, n_g, \\
&z_i^+ - z_i^- = h_i(\mathbf{x}_k) + \nabla h_i(\mathbf{x}_k)^T\mathbf{d} \quad i = 1, \ldots, n_h, \\
&\mathbf{A}(\mathbf{x}_k + \mathbf{d}) \preceq \mathbf{b}, \\
&\mathbf{A}_e(\mathbf{x}_k + \mathbf{d}) = \mathbf{b}_e, \\
&-\boldsymbol{\Delta}_k \preceq \mathbf{d} \preceq \boldsymbol{\Delta}_k \\
&y_i \geq 0, \quad i = 1, \ldots, n_g, \quad z_i^+ \text{and} \quad z_i^- \geq 0 \quad i = 1, \ldots, n_h.
\end{aligned}
$$
(C-6)

The linear program $\text{LP}(\mathbf{x}_k, \mathbf{d}_k)$ given by eq. (C-6) is the direction-finding subproblem that yields an optimal solution $\mathbf{d}_k$, say, along with the accompanying values of $y_i, i = 1, \ldots, n_g$, and $z_i^+, z_i^-, \quad i = 1, \ldots, n_h$, which are given as follows

$$
\begin{aligned}
y_i &= \max\{0, g_i(\mathbf{x}_k) + \nabla g_i(\mathbf{x}_k)^T\mathbf{d}_k\}, \quad i = 1, \ldots, n_g, \\
z_i^+ &= \max\{0, h_i(\mathbf{x}_k) + \nabla h_i(\mathbf{x}_k)^T\mathbf{d}_k\}, \quad i = 1, \ldots, n_h, \\
z_i^- &= \max\{0, -[h_i(\mathbf{x}_k) + \nabla h_i(\mathbf{x}_k)^T\mathbf{d}_k]\}, \quad i = 1, \ldots, n_h,
\end{aligned}
$$
(C-7)

so that $z_i^+ + z_i^- = |h_i(\mathbf{x}_k) + \nabla h_i(\mathbf{x}_k)^T)\mathbf{d}_k|, i = 1, \ldots, n_h$.

The decision whether to accept or to reject the new iterate $\mathbf{x}_k + \mathbf{d}_k$ and the adjustment of the step bounds $\boldsymbol{\Delta}_k$ is made based on the ratio R_k of the actual decrease ΔF_{E_k} in the penalty function F_E, to the decrease ΔF_{EL_k} predicted by its linearized version F_{EL_k}, provided that the latter is nonzero. A summary of the PSLP algorithm is provided below.

C.2 Summary of the Penalty Successive Linear Programming (PSLP) Algorithm

Initialization Set the iteration counter $k = 1$, and select a starting solution $\mathbf{x_1}$, along with the trust region vector $\boldsymbol{\Delta}_k \succ 0$. Let $\boldsymbol{\Delta}_{LB} \succ 0$ be some small lower bound tolerance on $\boldsymbol{\Delta}_k$. Additionally, select a suitable value of the penalty parameter μ_p. Choose values for the scalars $0 < \rho_0 < \rho_1 < \rho_2 < 1$ to be used in the trust region ratio test, and for the step bound adjustment multiplier $\beta \in (0, 1)$. (Typically, $\rho_0 = 10^{-6}, \rho_1 = .25, \rho_2 = .75$, and $\beta = .5$.)

Step 1: Linear Programming Subproblem Solve the linear program $\text{LP}(\mathbf{x}_k, \mathbf{d}_k)$ to obtain an optimum $\mathbf{d}_k$. Compute the actual and predicted decreases, $\Delta F_{E_k} = F_E(\mathbf{x}_k) - F_E(\mathbf{x}_k + \mathbf{d}_k)$ and $\Delta F_{EL_k} = F_{EL}(\mathbf{x}_k) - F_{EL}(\mathbf{x}_k + \mathbf{d}_k)$. If $\Delta F_{EL_k} = 0$ then stop. Otherwise, compute the ratio $R_k = \dfrac{\Delta F_{E_k}}{\Delta F_{EL_k}}$. If $R_k < \rho_0$, then the penalty function has either worsened or its improvement is insufficient. Hence, reject the current solution, shrink the $\boldsymbol{\Delta}_k$ to $\beta\boldsymbol{\Delta}_k$, and repeat this step. On the other hand, if $R_k > \rho_0$, then proceed to Step 2.

Step 2: New Iterate and Adjustment of Step Bounds Let $\mathbf{x}_{k+1} = \mathbf{x}_k + \mathbf{d}_k$. If $\rho_0 < R_k < \rho_1$ then shrink the $\boldsymbol{\Delta}_k$ to $\boldsymbol{\Delta}_{k+1} = \beta\boldsymbol{\Delta}_k$, since the penalty function has not improved sufficiently. If $\rho_1 < R_k < \rho_2$, then retain $\boldsymbol{\Delta}_{k+1} = \boldsymbol{\Delta}_k$. On the other hand, if $R_k >_\rho 2$, amplify the trust region by letting $\boldsymbol{\Delta}_{k+1} = \boldsymbol{\Delta}_k/\beta$. In all cases, replace $\boldsymbol{\Delta}_{k+1}$ with $\max\{\boldsymbol{\Delta}_{k+1}$ and $\boldsymbol{\Delta}_{LB}\}$, where $\max\{.\}$ is taken componentwise. Increase k by 1 and go to **Step 1**.

Appendix D

Matrix $\mathbf{R}_j$ and Vector g Appearing in Eq. (4.32)

In this appendix, we present the expressions of the matrix $\mathbf{R}_j$ and vector $\mathbf{g}$ appearing in eq. (4.32). Moreover, in order to solve problem (4.32) via a gradient -based method, we must calculate the derivative of the nonlinear constraints in this problem. This appendix presents these gradients as well.

D.1 Expressions of Matrix $\mathbf{R}_j$ and Vector g

The vector $\mathbf{g} \in \mathbb{R}^{45}$ and the matrix $\mathbf{R}_j \in \mathbb{R}^{45 \times (m+78)}$ appearing in eq. (3.14) are

$$\mathbf{g} \equiv \begin{bmatrix} -\mathbf{1}_m^T \mathbf{A}^T & \mathbf{0}_3^T & m\mathbf{1}_3^T & \mathbf{1}_m^T \mathbf{B}^T \mathbf{I}_9^T & \mathbf{1}_m^T \mathbf{B}^T \mathbf{I}_9^T & -\mathbf{1}_m^T \mathbf{I}_\Lambda \end{bmatrix}^T \in \mathbb{R}^{45},$$

$$\mathbf{R}_j \equiv \begin{bmatrix}
-\mathbf{A}^T & \mathbf{0}_{m\times 3} \\
-\mathrm{diag}(\boldsymbol{\sigma}_j)\mathrm{diag}(\overline{\mathbf{p}}) & \mathbf{0}_{3\times 3} \\
\mathrm{diag}(\boldsymbol{\sigma}_j)\mathrm{diag}(\underline{\mathbf{p}}) & \mathbf{0}_{3\times 3} \\
-\mathrm{diag}(\mathrm{vec}(\overline{\mathbf{Q}}^T\mathrm{diag}(\boldsymbol{\sigma}_j)))\mathbf{I}_\sigma & \mathbf{0}_{9\times 3} \\
\mathrm{diag}(\mathrm{vec}(\underline{\mathbf{Q}}^T\mathrm{diag}(\boldsymbol{\sigma}_j)))\mathbf{I}_\sigma & \mathbf{0}_{9\times 3} \\
\mathbf{0}_{9\times 3} & -\mathrm{diag}(\mathrm{vec}(\overline{\mathbf{V}}\mathrm{diag}(\boldsymbol{\tau}_j)))\mathbf{I}_\sigma \\
\mathbf{0}_{9\times 3} & \mathrm{diag}(\mathrm{vec}(\underline{\mathbf{V}}\mathrm{diag}(\boldsymbol{\tau}_j)))\mathbf{I}_\sigma \\
\mathbf{0}_{18\times 3} & -\mathrm{diag}(\mathrm{vec}(\mathrm{diag}(\mathbf{I}_6\boldsymbol{\tau}_j)\overline{\mathbf{Q}}_{xyz})\mathbf{I}_\tau \\
\mathbf{0}_{18\times 3} & \mathrm{diag}(\mathrm{vec}(\mathrm{diag}(\mathbf{I}_6\boldsymbol{\tau}_j)\underline{\mathbf{Q}}_{xyz})\mathbf{I}_\tau
\end{bmatrix}$$

$$\begin{bmatrix}
\mathbf{1}_m\mathbf{1}_3^T & \mathbf{B}^T\mathbf{I}_9^T & \mathbf{B}^T\mathbf{I}_9^T & -\mathbf{I}_\Lambda \\
\mathrm{diag}(\boldsymbol{\sigma}_j) & \mathbf{0}_{3\times 9} & \mathbf{0}_{3\times 9} & \mathbf{0}_{3\times 18} \\
-\mathrm{diag}(\boldsymbol{\sigma}_j) & \mathbf{0}_{3\times 9} & \mathbf{0}_{3\times 9} & \mathbf{0}_{3\times 18} \\
\mathbf{0}_{9\times 3} & \mathrm{diag}(\mathbf{I}_\sigma\boldsymbol{\sigma}_j) & \mathbf{0}_{9\times 9} & \mathbf{0}_{9\times 18} \\
\mathbf{0}_{9\times 3} & -\mathrm{diag}(\mathbf{I}_\sigma\boldsymbol{\sigma}_j) & \mathbf{0}_{9\times 9} & \mathbf{0}_{9\times 18} \\
\mathbf{0}_{9\times 3} & \mathbf{0}_{9\times 9} & \mathrm{diag}(\mathbf{I}_\sigma\boldsymbol{\tau}_j) & \mathbf{0}_{9\times 18} \\
\mathbf{0}_{9\times 3} & \mathbf{0}_{9\times 9} & -\mathrm{diag}(\mathbf{I}_\sigma\boldsymbol{\tau}_j) & \mathbf{0}_{9\times 18} \\
\mathbf{0}_{18\times 3} & \mathbf{0}_{18\times 9} & \mathbf{0}_{18\times 9} & \mathrm{diag}(\mathbf{I}_\tau\boldsymbol{\tau}_j) \\
\mathbf{0}_{18\times 3} & \mathbf{0}_{18\times 9} & \mathbf{0}_{18\times 9} & -\mathrm{diag}(\mathbf{I}_\tau\boldsymbol{\tau}_j)
\end{bmatrix}^T,$$

where

$$\mathbf{I}_9 = \begin{bmatrix}
\mathbf{1}_3 & \mathbf{0}_3 & \mathbf{0}_3 \\
\mathbf{0}_3 & \mathbf{1}_3 & \mathbf{0}_3 \\
\mathbf{0}_3 & \mathbf{0}_3 & \mathbf{1}_3
\end{bmatrix} \in \mathbb{R}^{9\times 3},$$

$$\mathbf{I}_\Lambda = \begin{bmatrix}
(\mathrm{vec}(\mathbf{E}_x\mathbf{a}_1\mathbf{b}_1^T))^T & (\mathrm{vec}(\mathbf{E}_y\mathbf{a}_1\mathbf{b}_1^T))^T & (\mathrm{vec}(\mathbf{E}_z\mathbf{a}_1\mathbf{b}_1^T))^T \\
\vdots & \vdots & \vdots \\
(\mathrm{vec}(\mathbf{E}_x\mathbf{a}_m\mathbf{b}_m^T))^T & (\mathrm{vec}(\mathbf{E}_y\mathbf{a}_m\mathbf{b}_m^T))^T & (\mathrm{vec}(\mathbf{E}_z\mathbf{a}_m\mathbf{b}_m^T))^T
\end{bmatrix} \in \mathbb{R}^{m\times 18},$$

$$\mathbf{I}_\sigma = \begin{bmatrix} \mathbf{1}_{3\times 3} & \mathbf{1}_{3\times 3} & \mathbf{1}_{3\times 3} \end{bmatrix}^T \in \mathbb{R}^{9\times 3},$$

$$\mathbf{I}_\tau = \begin{bmatrix}
\mathbf{1}_6 & \mathbf{0}_6 & \mathbf{0}_6 \\
\mathbf{0}_6 & \mathbf{1}_6 & \mathbf{0}_6, \\
\mathbf{0}_6 & \mathbf{0}_6 & \mathbf{1}_6
\end{bmatrix} \in \mathbb{R}^{18\times 3}.$$

D.2   Gradients of the Nonlinear Constraints Appearing in Eq. (4.44)

In order to find a locally optimum solution to problem (4.44) through a gradient based descending method, like PSLP algorithm, we must calculate the gradients of the non-linear constraints of this problem. Hence, upon defining the vector of optimization variables as $\mathbf{x}_{opt} = [\mathbf{y}_{k,j}^T \quad \mathbf{a}_1^T \cdots \mathbf{a}_m^T \quad \mathbf{b}_1^T \cdots \mathbf{b}_m^T \quad s]^T \in \mathbb{R}^{64n(m+78)+6m+1}$, we separate the linear and nonlinear terms appearing in matrices $\mathbf{R}_{k,j}, j = 1, \ldots, 8, \quad k = 1, \cdots, n$, which leads to the following new matrices

$$\mathbf{R}_{k,j,nl} \equiv \begin{bmatrix} -\mathbf{A}^T & \mathbf{B}^T\mathbf{I}_9^T & \mathbf{B}^T\mathbf{I}_9^T & -\mathbf{I}_\Lambda \\ -\text{diag}(\boldsymbol{\sigma}_j)\text{diag}(\overline{\mathbf{p}}_k') & \mathbf{0}_{3\times9} & \mathbf{0}_{3\times9} & \mathbf{0}_{3\times18} \\ \text{diag}(\boldsymbol{\sigma}_j)\text{diag}(\underline{\mathbf{p}}_k') & \mathbf{0}_{3\times9} & \mathbf{0}_{3\times9} & \mathbf{0}_{3\times18} \\ -\text{diag}(\text{vec}(\overline{\mathbf{Q}}^T\text{diag}(\boldsymbol{\sigma}_j)))\mathbf{I}_\sigma & \text{diag}(\mathbf{I}_\sigma\boldsymbol{\sigma}_j) & \mathbf{0}_{9\times9} & \mathbf{0}_{9\times18} \\ \text{diag}(\text{vec}(\underline{\mathbf{Q}}^T\text{diag}(\boldsymbol{\sigma}_j)))\mathbf{I}_\sigma & -\text{diag}(\mathbf{I}_\sigma\boldsymbol{\sigma}_j) & \mathbf{0}_{9\times9} & \mathbf{0}_{9\times18} \\ \mathbf{0}_{9\times3} & \mathbf{0}_{9\times9} & \text{diag}(\mathbf{I}_\sigma\boldsymbol{\tau}_j) & \mathbf{0}_{9\times18} \\ \mathbf{0}_{9\times3} & \mathbf{0}_{9\times9} & -\text{diag}(\mathbf{I}_\sigma\boldsymbol{\tau}_j) & \mathbf{0}_{9\times18} \\ \mathbf{0}_{18\times3} & \mathbf{0}_{18\times9} & \mathbf{0}_{18\times9} & \text{diag}(\mathbf{I}_\tau\boldsymbol{\tau}_j) \\ \mathbf{0}_{18\times3} & \mathbf{0}_{18\times9} & \mathbf{0}_{18\times9} & -\text{diag}(\mathbf{I}_\tau\boldsymbol{\tau}_j) \end{bmatrix}^T \in \mathbb{R}^{39\times(m+78)},$$

$$\mathbf{R}_{k,j,l} \equiv \begin{bmatrix} \mathbf{0}_{m\times3} & \mathbf{1}_m\mathbf{1}_3^T \\ \mathbf{0}_{3\times3} & \text{diag}(\boldsymbol{\sigma}_j) \\ \mathbf{0}_{3\times3} & -\text{diag}(\boldsymbol{\sigma}_j) \\ \mathbf{0}_{9\times3} & \mathbf{0}_{9\times3} \\ \mathbf{0}_{9\times3} & \mathbf{0}_{9\times3} \\ -\text{diag}(\text{vec}(\overline{\mathbf{V}}_k\text{diag}(\boldsymbol{\tau}_j)))\mathbf{I}_\sigma & \mathbf{0}_{9\times3} \\ \text{diag}(\text{vec}(\underline{\mathbf{V}}_k\text{diag}(\boldsymbol{\tau}_j)))\mathbf{I}_\sigma & \mathbf{0}_{9\times3} \\ -\text{diag}(\text{vec}(\text{diag}(\mathbf{I}_6\boldsymbol{\tau}_j)\overline{\mathbf{Q}}_{xyz}))\mathbf{I}_\tau & \mathbf{0}_{18\times3} \\ \text{diag}(\text{vec}(\text{diag}(\mathbf{I}_6\boldsymbol{\tau}_j)\underline{\mathbf{Q}}_{xyz}))\mathbf{I}_\tau & \mathbf{0}_{18\times3} \end{bmatrix}^T \in \mathbb{R}^{6\times(m+78)}.$$

This allows us to split the equality constraints appearing in eq. (4.44) into linear and nonlinear equality constraints as follows:

$$\mathbf{R}_{k,j,l}\mathbf{y}_{k,j} + \mathbf{g}_l = \mathbf{0}_6, \tag{D-1}$$

$$\mathbf{R}_{k,j,nl}\mathbf{y}_{k,j} + \mathbf{g}_{nl} = \mathbf{0}_{39}. \tag{D-2}$$

The Jacobian matrix of the nonlinear equality constraints of problem (4.44) is given by:

$$\nabla\mathbf{H} = \begin{bmatrix} \mathbf{H}_1 & \mathbf{0}_{64(m+78)\times 2496} & \cdots & \mathbf{0}_{64(m+78)\times 2496} \\ \mathbf{0}_{64(m+78)\times 2496} & \mathbf{H}_2 & \cdots & \mathbf{0}_{64(m+78)\times 2496} \\ \vdots & \vdots & \ddots & \vdots \\ \mathbf{0}_{64(m+78)\times 2496} & \mathbf{0}_{64(m+78)\times 2496} & \cdots & \mathbf{H}_n \\ \mathbf{N}_1 & \mathbf{N}_2 & \cdots & \mathbf{N}_n \end{bmatrix} \in \mathbb{R}^{(64n(m+78)+6m+1)\times 2496n}, \quad \text{where}$$

$$\tag{D-3}$$

$$\mathbf{H}_k = \begin{bmatrix} \mathbf{R}_{k,1,nl}^T & \mathbf{0}_{(m+78)\times 39} & \cdots & \mathbf{0}_{(m+78)\times 39} \\ \mathbf{0}_{(m+78)\times 39} & \mathbf{R}_{k,2,nl}^T & \cdots & \mathbf{0}_{(m+78)\times 39} \\ \mathbf{0}_{(m+78)\times 39} & \mathbf{0}_{(m+78)\times 39} & \cdots & \mathbf{0}_{(m+78)\times 39} \\ \vdots & \vdots & \ddots & \vdots \\ \mathbf{0}_{(m+78)\times 39} & \mathbf{0}_{(m+78)\times 39} & \cdots & \mathbf{R}_{k,64,nl}^T \end{bmatrix} \in \mathbb{R}^{64(m+78)\times 2496},$$

$$\mathbf{N}_k = \begin{bmatrix} \mathbf{G}_{k,1} & \cdots & \mathbf{G}_{k,64} \end{bmatrix} \in \mathbb{R}^{(6m+1)\times 2496},$$

$$\mathbf{G}_{k,j} \equiv \begin{bmatrix} -\mathbf{I}_{k,j} & \mathbf{0}_{3m\times 9} & \mathbf{0}_{3m\times 9} & -\text{diag}(\text{vec}(\mathbf{t}_{k,j}\mathbf{1}_3^T))\mathbf{U}_b \\ \mathbf{0}_{3m\times 3} & \mathbf{I}_{k,j}\mathbf{I}_9^T & \mathbf{I}_{k,j}\mathbf{I}_9^T & -\text{diag}(\text{vec}(\mathbf{t}_{k,j}\mathbf{1}_3^T))\mathbf{U}_a \\ \mathbf{h}_{k,j} & \mathbf{0}_9^T & \mathbf{0}_9^T & \mathbf{0}_{18}^T \end{bmatrix} \in \mathbb{R}^{(6m+1)\times 39},$$

$$\mathbf{I}_{k,j} \equiv \text{diag}(\text{vec}(\mathbf{t}_{k,j}\mathbf{1}_3^T))\mathbf{I}_{3m},$$

$$\mathbf{t}_{k,j} \equiv (\mathbf{1}_m + \mathbf{I}_t\mathbf{y}_{k,j}), \tag{D-4}$$

$$\mathbf{I}_t \equiv \begin{bmatrix} \mathbf{1}_{m\times m} & \mathbf{0}_{m\times 78} \end{bmatrix} \in \mathbb{R}^{m\times(m+78)},$$

$$\mathbf{I}_{3m} \equiv \begin{bmatrix} \mathbf{1}_{3\times 3} & \ldots & \mathbf{1}_{3\times 3} \end{bmatrix}^T \in \mathbb{R}^{3m\times 3},$$

$$\mathbf{h}_{k,j} = (\text{diag}(\boldsymbol{\sigma}_j)(\text{diag}(\underline{\mathbf{p}}_k - \mathbf{p}_c)\mathbf{I}_{\underline{d}}\ \mathbf{y}_{k,j} - \text{diag}(\overline{\mathbf{p}}_k - \mathbf{p}_c)\mathbf{I}_{\overline{d}}\ \mathbf{y}_{k,j}))^T, \tag{D-5}$$

$$\mathbf{I}_{\overline{d}} \equiv \begin{bmatrix} \mathbf{0}_{3\times m} & \mathbf{1}_{3\times 3} & \mathbf{0}_{3\times 72} \end{bmatrix} \in \mathbb{R}^{3\times(m+78)},$$

$$\mathbf{I}_{\underline{d}} \equiv \begin{bmatrix} \mathbf{0}_{3\times(m+3)} & \mathbf{1}_{3\times 3} & \mathbf{0}_{3\times 69} \end{bmatrix} \in \mathbb{R}^{3\times(m+78)}.$$

The expressions of matrices $\mathbf{U}_a$ and $\mathbf{U}_b$ are

$$\mathbf{U}_b \equiv \begin{bmatrix} \mathbf{e}_2\mathbf{b}_1^T & \mathbf{e}_3\mathbf{b}_1^T & \mathbf{e}_1\mathbf{b}_1^T & \mathbf{e}_3\mathbf{b}_1^T & \mathbf{e}_1\mathbf{b}_1^T & \mathbf{e}_2\mathbf{b}_1^T \\ \vdots & \vdots & \vdots & \vdots & \vdots & \vdots \\ \mathbf{e}_2\mathbf{b}_m^T & \mathbf{e}_3\mathbf{b}_m^T & \mathbf{e}_1\mathbf{b}_m^T & \mathbf{e}_3\mathbf{b}_m^T & \mathbf{e}_1\mathbf{b}_m^T & \mathbf{e}_2\mathbf{b}_m^T \end{bmatrix} \in \mathbb{R}^{3m\times 18}, \tag{D-6}$$

$$\mathbf{U}_a \equiv \begin{bmatrix} \mathbf{A}_y & \mathbf{A}_z & \mathbf{A}_x & \mathbf{A}_z & \mathbf{A}_x & \mathbf{A}_y \end{bmatrix} \in \mathbb{R}^{3m\times 18},$$

where $\mathbf{A}_x = \operatorname{diag}(\operatorname{vec}(\mathbf{A}^T\mathbf{e}_1\mathbf{1}_3^T))\mathbf{I}_{3m}, \quad \mathbf{A}_y = \operatorname{diag}(\operatorname{vec}(\mathbf{A}^T\mathbf{e}_2\mathbf{1}_3^T))\mathbf{I}_{3m}, \quad \mathbf{A}_z = \operatorname{diag}(\operatorname{vec}(\mathbf{A}^T\mathbf{e}_3\mathbf{1}_3^T))\mathbf{I}_{3m}$ and $\mathbf{e}_i, i = 1, \ldots, 3$, represents the canonical base vectors of $\mathbb{R}^3$.